Syntheses and Complexes of Heterocyclic Ligands

A thesis submitted in partial fulfilment
of the requirements for the Degree
of
Doctor of Philosophy in Chemistry
at the
University of Canterbury
by

Ian G. Phillips

University of Canterbury, Christchurch, New Zealand

1995

Abstract.

Nine new bidentate chelating heterocyclic ligands, namely 4,4'-bis-t-butyl-2,2'-bipyrimidine (**41**), 2,2'-bi-(5S,8R)-5,6,7,8-tetrahydro-8,9,9-trimethyl-5,8-methanoquinazoline (**42**), 2,4-bis-(1-pyrazolyl)pyrimidine (**53**), 1-methyl-2-(2-pyridinyl)perimidine (**94**), 2-(2-pyrimidinyl)perimidine (**95**), 2,6-bis-[6-(2-pyridinyl)-4-pyrimidinyl]pyridine (**110**), 2,6-bis-(1-pyrazolyl)-1,5-naphthyridine (**132**), 2,2'-bis-(1-pyrazolyl)-4,4'-bipyridine (**144**) and 2,2'-bis-(3,5-dimethyl-1-pyrazolyl)-4,4'-bipyridine (**145**), have been prepared and characterised by NMR spectroscopy and mass spectrometry and, in some cases, by elemental analyses. X-Ray crystal structures have been determined for the two 4,4'-bipyridine derivatives, **144** and **145**. A new synthesis for the known ligand 4,4'-dimethyl-2,2'-bipyrimidine (**40**) is also reported.

The coordination chemistry of the above ligands, the known bridging ligand 2,2':4',4":2",2"'-quaterpyridine (**25**) and two known compounds, 2-(2-pyridinyl)perimidine (**93**) and 4,6-bis-(2-pyridinyl)pyrimidine (**109**), has been investigated. Complexes with the metals copper(I), palladium(II) and molybdenum(0) are described for some of the ligands, including an X-ray crystal structure for the palladium(II) complex of **94**. The majority of the complexes described are of ruthenium(II). These include monoruthenium complexes $\{RuBL(L)_2^{2+}$ with BL=bidentate chelating ligand and L=4,4'-bipyridine (bpy) or 4,4'-dimethyl-2,2'-bipyridine (dmb)$\}$, biruthenium complexes $\{(L)_2Ru(\mu\text{-}BL)Ru(L')_2^{4+}$ with μ-BL=doubly bidentate bridging ligand and L=bpy or dmb and L'=bpy or dmb$\}$ and tetraruthenium complexes $\{Ru[(\mu\text{-}BL)Ru(bpy)_2]_3^{8+}\}$. ^1H NMR spectroscopy, electronic absorption spectroscopy and cyclic voltammetry have been used to study the nature of the metal-ligand and metal-metal interactions in these complexes. With the seven different bridging ligands (**40**, **109**, **110**, **25**, **144** , **145** and **132**), the metal-metal distance in the biruthenium complexes has been varied systematically, in the order shown, resulting in a general trend of increasing metal-metal distance and decreasing metal-metal interaction

Table of Contents

Chapter 1

Introduction

Introduction

Aromatic nitrogen heterocycles represent an important class of ligands for transition metal coordination chemistry.[1] On the basis of ring size aromatic nitrogen heterocycles may be divided into two main groups, namely six-membered azines (e.g. pyridine) and five-membered azoles (e.g. pyrazole). The azines are π-deficient with relatively low lying π* orbitals and hence form stable complexes with transition metals due to metal-ligand back-bonding from the metal d-orbitals to the π system of the ligand, whilst the five-membered azines are π-excessive π-donors and can also form anionic ligands by deprotonation of acidic N-H groups in the free ligand. Heterocycles can also have more than one nitrogen atom in six-membered (diazines, triazines etc) rings and five-membered (diazoles, triazoles etc) rings and in general these ligands have quite different electronic properties from those of pyridine.[1,2,3]

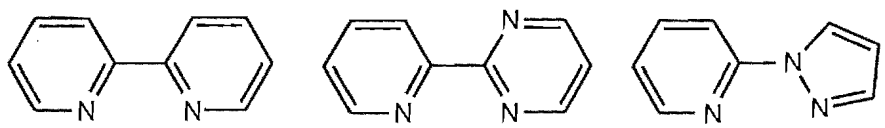

1 **2** **3**

Figure 1.1

2,2'-Bipyridine (bpy, **1**) (Figure 1.1) was synthesised over 100 years ago[4] and is the most well studied chelating heterocyclic ligand. This ligand has been used extensively in preparative and analytical chemistry because of the stable complexes it forms with transition metals.[5] In particular there has been a thorough examination of the redox and photophysical properties of the complex $Ru(bpy)_3^{2+}$, with emphasis on the electron-transfer processes involved in the photochemical decomposition of water.[6-9] This has led to the synthesis of many new complexes in which one or more of the bpy ligands in the complex is replaced by a different chelating ligand with one or more azole or azine rings. Such ligands form complexes with properties which depend markedly on the choice of ligand, and in this manner it is possible to tune the ground and excited-state properties of the complex by the appropriate choice of ligand.[6] For example, recent studies of the complexes of **2**[10] and **3**[11,12,13] (Figure 1.1) have shown that replacement of a pyridine of **1** with a pyrazole or a pyrimidine ring results in significant changes in the physicochemical properties of the complexes, relative to those of $Ru(bpy)_3^{2+}$. Thus metal-ligand interactions are governed by the specific metal and ligand involved and many such ligands are available.[1,2,3]

Many aromatic nitrogen heterocycles have more than one nitrogen atom per ring. Ligands of this class which possess multiple coordination sites are potentially capable of bridging more than one metal centre and, in recent years, there has been much interest in binuclear and multinuclear complexes incorporating one or more of these ligands in a bridging mode. Complexes of this type can exhibit metal-metal interactions in the form of energy or electron transfer, magnetic coupling and intervalence transfer and the study of these compounds has been important in developing our understanding of these processes.[14] These interactions are mediated by the bridging aromatic heterocycle, with communication between the metal centres generally taking place via the π system of the ligand. In general, the electronic coupling between the metal centres varies strongly with the distance between the metals and is dependent on the nature of the ligand, on the degree of conjugation between the metals, and the charge and π-donor/acceptor properties of the bridging ligand. Binuclear and multinuclear complexes of this type have also been used to model important bio-inorganic systems, such as metalloproteins, and there is much interest in their role as molecular components in the construction of supramolecular assemblies.[3] Components with suitable redox potentials and/or excited state levels are fundamental building blocks for the design of photochemical molecular devices capable of performing important functions such as information storage, solar energy conversion and multielectron catalysis.[15,16]

Electron transfer is an important process in supramolecular assemblies and many studies have been directed toward intramolecular electron transfer by the use of different bridges between the metal ions in binuclear and multinuclear complexes. The most common bridging ligands are those that coordinate to both metal centres in a monodentate manner, such as pyrazine (**4**) in the well studied mixed-valence Creutz-Taube complex $[(NH)_5Ru(\mathbf{4})Ru(NH)_5]^{5+}$.[17,18] In this complex two ruthenium atoms are bridged by pyrazine which has relatively low energy π* orbitals and hence is an excellent π-acceptor of metal d-orbital electron density, facilitating strong π-communication across the short bridge.

Bidentate coordination of bridging ligands is desirable because of the chelate effect on complex stability and the enhanced metal dπ-bridging ligand pπ-metal dπ electronic interaction.[19] Numerous binucleating ligands that coordinate in a bidentate manner to both metal centres have been used to bridge metals in both homobinuclear, heterobinuclear and polynuclear complexes.[3] Much attention is presently focused on systems based on $(N\text{-}N)_2M\text{-}\mu L\text{-}M(N\text{-}N)_2^{n+}$ incorporating a doubly bidentate aromatic heterocycle as the bridging ligand (μL) between two metals M, more often of the second or third transition row (in particular, Ru(II) and Os(II)), each with two

additional N-N bidentate ligands. This choice of ligands is understandable given the useful excited-state and redox properties of the $M(bpy)_3^{n+}$ complexes.[6,8] The following discussion gives an overview of the most well known doubly bidentate binucleating ligands, with particular reference to the degree of metal-metal communication that they facilitate. Mention is also made of related complexes containing a doubly tridentate bridging ligand and tridentate peripheral ligands, which may also have a role to play as molecular components in the design of nanomachines.[20]

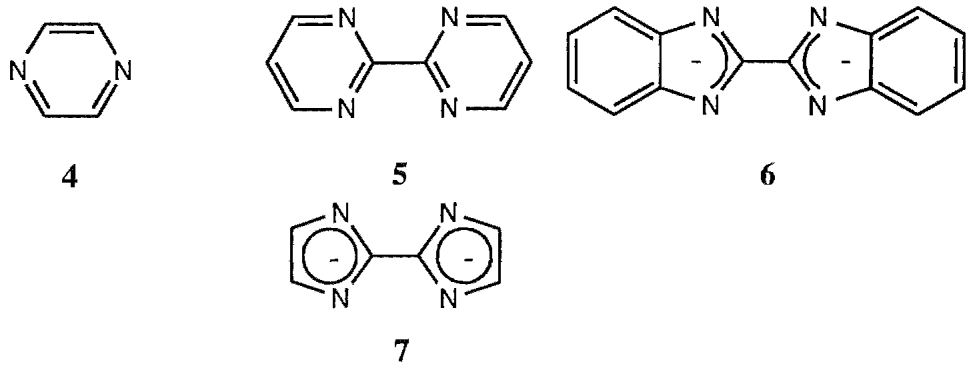

4 **5** **6**

7

Figure 1.2

The most well studied doubly bidentate chelating bridging ligand is 2,2'-bipyrimidine (**5**).[3] Numerous homo- and heterobinuclear complexes in which the π-acceptor **5** bridges two metals have been reported, with ruthenium complexes being particularly well studied.[21-59] The short inter-metal separation (5.5Å) in such complexes facilitates relatively strong metal-metal interactions with the possibility of direct d-orbital overlap contributing to this interaction. In comparison, complexes in which metals are bridged by 2,2'-bibenzimidazolate (**6**) and 2,2'-biimidazolate (**7**)[60-62] dianions have a similar coordination geometry and inter-metal separation. A wide range of metals have been bridged by these ligands in both homobimetallic[63-76] and heterobimetallic complexes.[77-81] Ruthenium, osmium, cobalt, and nickel complexes of **6** have been shown to be more stable and to exhibit a stronger metal-metal interaction than similar complexes of **5**.[72] This has been attributed to the superior donor properties of these ligands, which are π-donors, and to the reduction in electrostatic repulsion between the positive metal centres when bridged by the dianionic forms of **6** and **7**.

Stronger interactions are possible in complexes where the bridging ligand (Figure 1.3) allows for a shorter inter-metal separation than in complexes of **5**. This is apparent in the dicopper and other heterobimetallic complexes of 3,6-bis-(2-pyridinyl)-pyridazine (**8**) where strong interactions such as antiferromagnetic exchange occur.[82-92] The inter-metal separation is typically 3.35Å in complexes of **8** and the related ligands **9** and **10**.[93-96] In binuclear complexes of six-membered chelate ligands, such as the dicopper complex of **11**, the inter-metal separation is

shorter (2.99-3.22Å) due to the greater conformational flexibility which is possible in six-membered chelating ligands.[97-102] The inter-metal separation can be increased to 4.0Å by replacement of the central pyridazine ring with an azole ring as in binuclear copper and nickel complexes of **12**, **13** and **14**.[103-106] However, the same short inter-metal separation is not observed in homo-and heterobinuclear bis(2,2'-bipyridine) ruthenium(II), iridium(I) and rhodium(I) complexes of the triazole **14** in which steric restraints force the ligand to adopt N1,N4 coordination in the bridging mode rather than N1-N2 coordination.[107-113] Thus of the ligands in Figure 1.3 only **14** has been shown to form binuclear ruthenium(II) complexes.

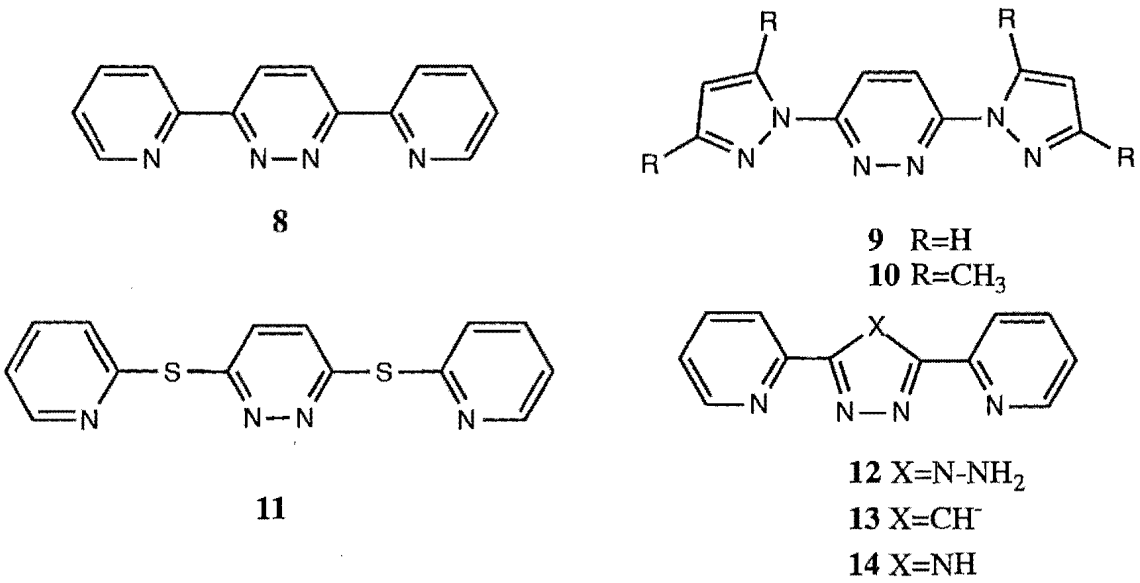

Figure 1.3

Chelating bridging ligands that contain a pyrazine ring which is able to bridge two metals in a similar manner to the pyrazine bridge in the Creutz-Taube complex, but with the advantage of enhanced complex stability and electronic interactions due to the chelate effect, have been much studied in recent years (Figure 1.4). 2,3-Bis-(2-pyridinyl)-pyrazine (**15**)[114] and 2,5-bis-(2-pyridinyl)-pyrazine (**16**)[115] are the most well used of these binucleating ligands and many complexes of **15**[15,22-24,114,116-139] and **16**[29-33,119,127,131,133] have been prepared. Ruthenium and osmium complexes, in particular, have been shown to exhibit strong metal-metal interactions despite the greater inter-metal separation (6.7-6.9Å) relative to binuclear complexes of **5**. This is not surprising given that pyrazine is an excellent π-acceptor of metal d-orbital electron density, thus permitting π-communication between the metals. In particular, **15** has been used extensively in the preparation of supramolecular polynuclear Ru(II) or Os(II) complexes.[15,124,125,131-133,136,137] Included in Figure 1.4 are other structurally related ligands which have been employed as binucleating ligands. Binuclear complexes of **17**,[117,140] **18**[25,26,117,129,130,134,135,141,142] **19**[129,130,134,135] and **20**[19,143-145] have been reported and

exhibit strong metal-metal interactions similar to **15** and **16**. Similarly, binuclear complexes of **21** show strong metal-metal interactions.[29-34,146-150] The use of related substituted pyrimidines as bridging ligands has been much less common with binuclear complexes of only 4,6-bis-(1-pyrazolyl)-pyrimidine (**22**) and its 3,5-dimethylpyrazolyl analogue (**23**) being reported.[96,151]

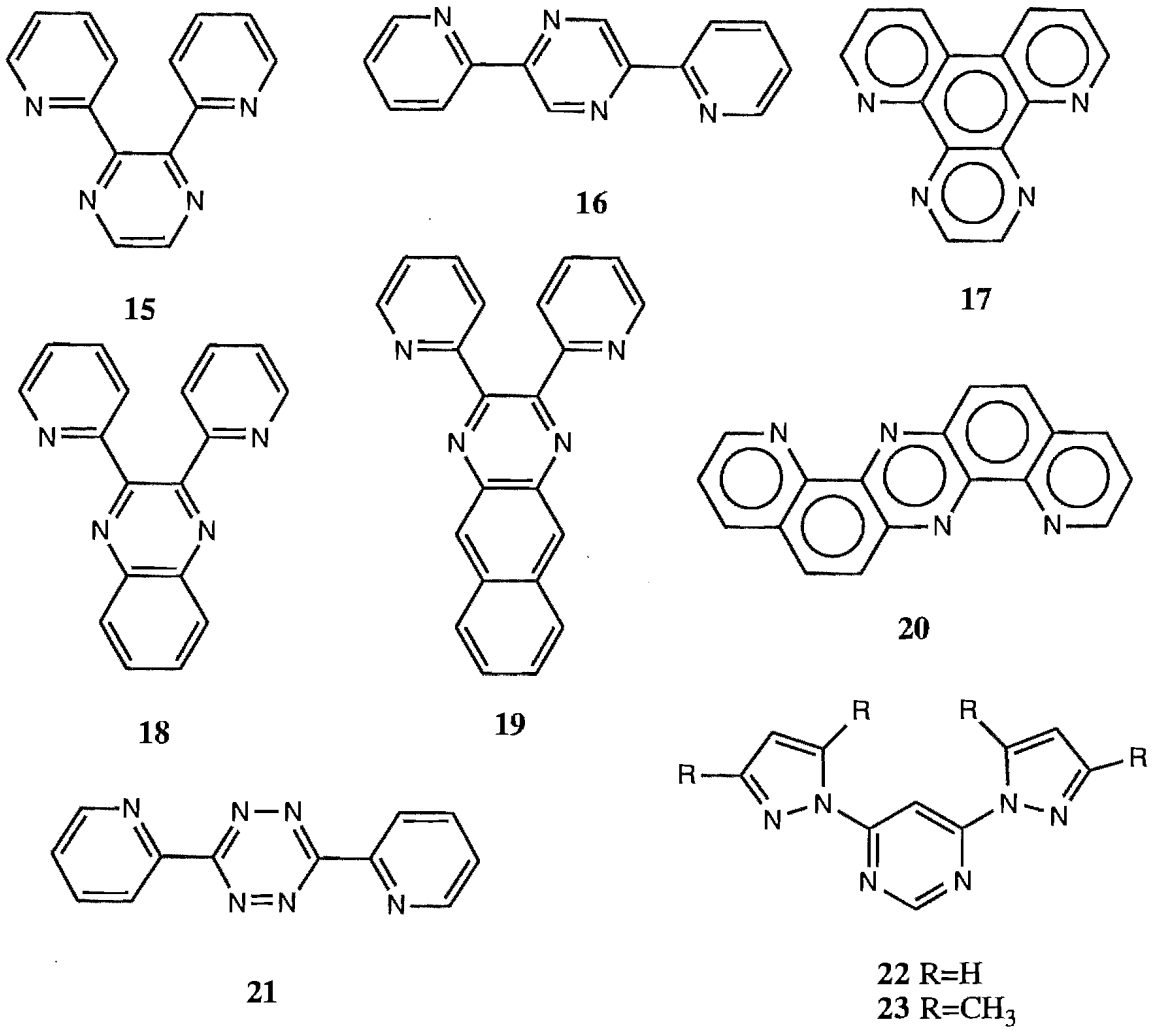

Figure 1.4

The ligand 2,6-bis-(2-pyridinyl)-benzodiimidazole (**24**) (Figure 1.5) is an excellent example of a bridging ligand which increases the distance between the metals whilst maintaining the rigid and well defined orientation of the metals that exists in the complexes of the ligands discussed thus far. The bridging ligand **24** can still facilitate electronic communication through its π-network, as has been shown in the diruthenium(II) complex of **24** which exhibits a weaker metal-metal interaction than the diruthenium complexes of **5**, **15** etc, where the metals are much closer together.[152]

The ability of the π-network of the bridging ligand to mediate metal-metal interactions is lessened in the biruthenium complex of the ligand 2,2':4',4":2",2"'-quaterpyridine (**25**). Rotation about the 4,4'-inter-ring bond reduces the conjugation within the π-network of the bridge

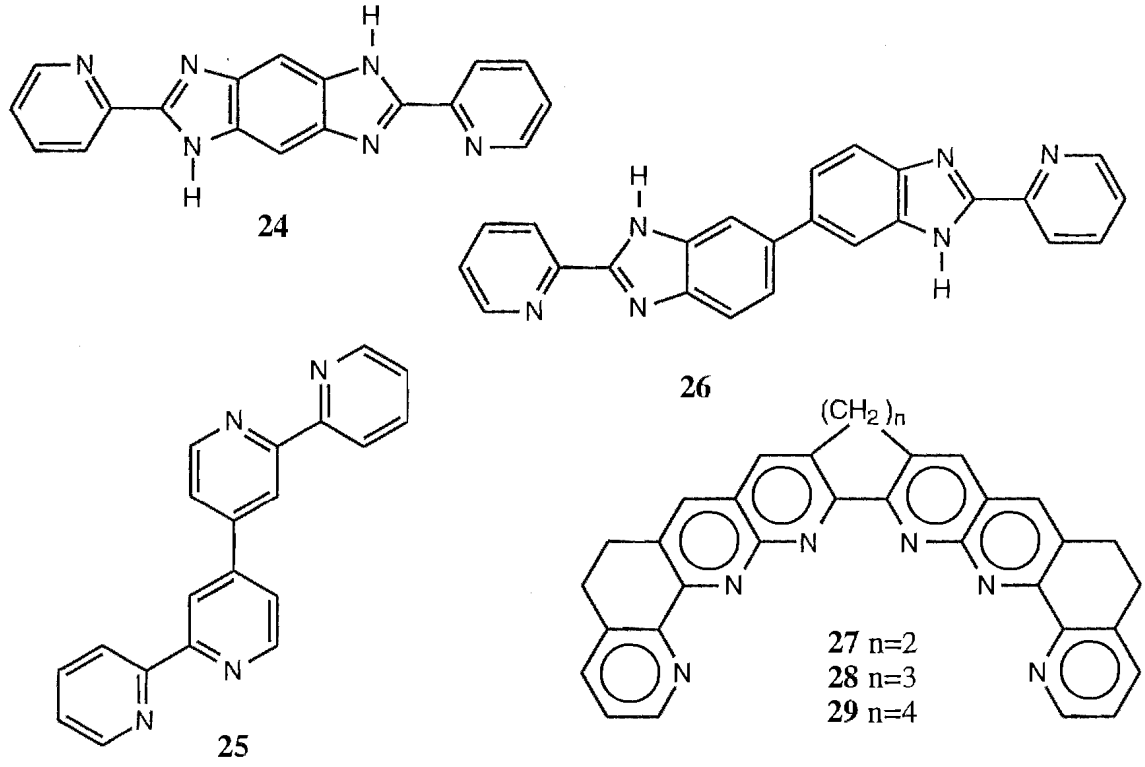

Figure 1.5

and, with the greater inter-metal separation, complexes of **25** show a weak but detectable interaction.[153] Similarly, in binuclear complexes of 2,2'-bis-(2-pyridinyl)-6,6'-bibenzimidazole (**26**) there is free rotation about the 6,6' inter-ring bond.[154-156] This accounts for the weaker metal-metal interaction in the diruthenium complex of **26**, relative to the diruthenium complex of its ring fused analogue **24**.

Considerable latitude in the proximity of the metals in binuclear complexes can also be achieved by the inclusion of flexible groups between bipyridine-like units in the bridging ligand such as in the polyaza shaped ligands **27-29**. Binuclear bis-(2,2'-bipyridine)ruthenium complexes of **27-29** have been shown to behave much like their independent mononuclear components.[157,158]

Numerous other bridging ligands incorporating flexible tethers or spacers are known, many of which have been shown to form homonuclear and heteronuclear supramolecular helical complexes with numerous metals (Figure 1.6).[159] For example, the ligand **30** has been shown by X-ray crystallography to form a triple helical structure with octahedral cobalt(II) in the complex $[Co_2(\mathbf{30})_3][ClO_4]_4$,[160] whilst double helical structures and even a trefoil knot have been observed in the tetrahedral metal complexes of a number of oligobipyridine/oligophenanthroline ligands, which contain a linking spacer group such as **31**.[161-164] The oligopyridines **32** and **33** have also been used in helical self-assemblies with a number of different metals.[159] More recently a large

bidentate-tridentate-bidentate segmental ligand has been shown to exhibit strict self-assembly of supramolecular complexes with a number of different metals. This ligand incorporates pyridylbenzimidazole fragments structurally related to **26**.[165]

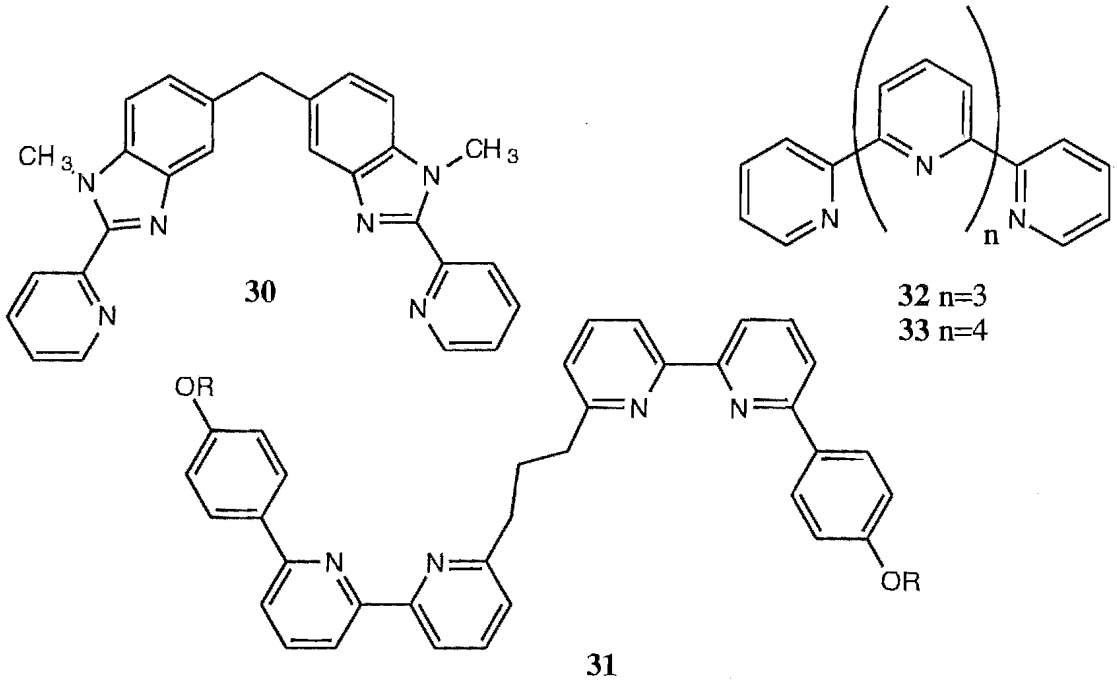

Figure 1.6

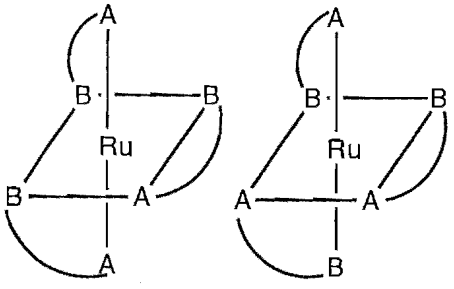

Meridonal (mer) Facial (fac)

Figure 1.7

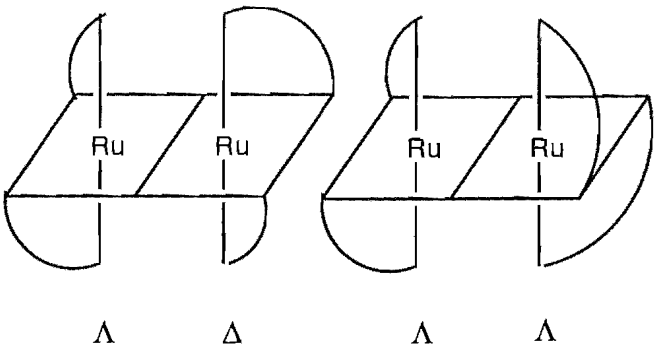

(≡ΔΔ)

Figure 1.8

An important aspect of bidentate chelation to octahedral metals is the potential for the formation of stereo or geometric isomers. For homoleptic complexes of symmetrical bidentate ligands such as $Ru(bpy)_3^{2+}$ only the two enantiomeric Δ and Λ forms exist, but in homoleptic complexes with an unsymmetrical ligand meridonal (mer) and facial (fac) isomers are possible (Figure 1.7). Binuclear complexes exist as two diastereoisomers, the ΔΔ/ΛΛ racemic form and the ΔΛ meso form (Figure 1.8). Such diastereoisomers were first distinguished in the ^1H NMR spectrum of $(bpy)_2Ru(\mathbf{16})Ru(bpy)_2^{4+}$.[32] The early studies of $(bpy)_2Ru(\mathbf{5})Ru(bpy)_2^{4+}$ did not address this aspect of the complex, since the isomers are indistinguishable by electrochemical or electronic absorption studies, although the preparation and ^1H NMR spectrum of optically pure

ΛΛ–$(phen)_2Ru(\mathbf{5})Ru(phen)_2^{4+}$ (phen=1,10-phenanthroline) has been described.[166] More recently both diastereoisomers have been identified and separated in biruthenium complexes bridged by **5** and with non identical terminal ligands.[167]

Recently a number of ligands have been described which coordinate in a tridentate manner to both metal centres.[20,168-171] In particular polymetallic ruthenium(II) and osmium(II) complexes have been prepared using tridentate terpyridine type ligands **34-36** and with terpyridine (**37**) terminal ligands (Figure 1.9).[20,171] These rod-like complexes exhibit a decreasing metal-metal interaction in the order n=0,1,2 corresponding to inter-metal separations of 11, 15.5 and 20Å respectively and have important applications to long range electron transfer in photochemical supramolecular devices. A result of the tridentate coordination of the ligands in octahedral complexes of **34-36** is the absence of the geometric and/or optical isomerism seen in bidentate complexes. For this reason some researchers[20] have proposed that tridentate rod like complexes are more suitable building blocks in the controlled design of advanced materials. However, with bidentate ligands there exists the possibility of assembling advanced materials in more than one dimension and with a greater variety of structures.

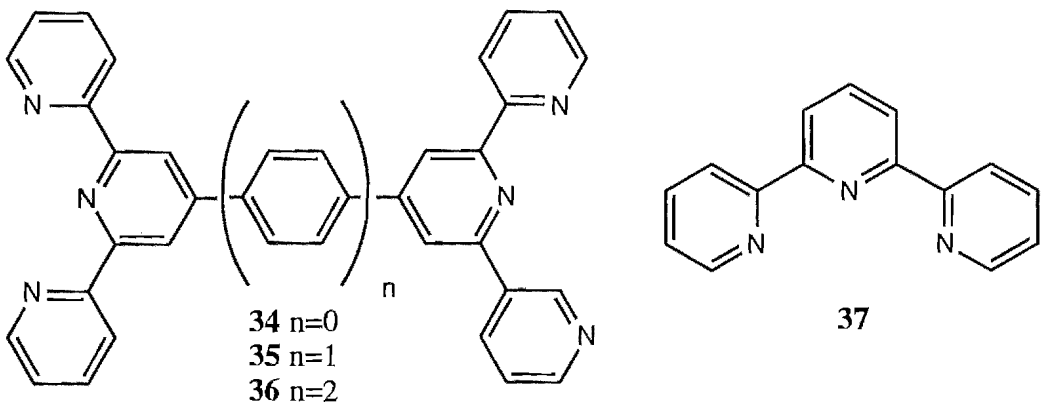

Figure 1.9

The present work describes studies of new and known compounds which can be used as bidentate ligands, with particular emphasis on the role of these compounds as doubly bidentate binucleating ligands. Included are the syntheses and attempted syntheses of a number of such ligands and their mono, bi, and multinuclear complexes, particularly of ruthenium(II). All the complexes described are five-membered chelates. In the binuclear complexes a general trend of increasing metal-metal distance and hence decreasing metal-metal interaction will be revealed. This was achieved by synthesising a range of ligands that successively increase the inter-metal separation in their binuclear complexes.

Ligands and complexes are characterised by nuclear magnetic resonance spectroscopy, with assignments based on a combination of one and two dimensional correlation techniques. High resolution mass spectrometry and elemental analysis are also used to characterise the ligands and complexes. Cyclic voltammetry and UV/VIS absorption spectroscopy of the ruthenium(II) complexes and some molybdenum(0) complexes are also discussed. These techniques reveal the energy of electron transfer processes in the complexes and the degree of metal-metal interaction in the binuclear complexes. The X-ray crystal structures of one complex and two ligands are also included.

Chapter 2

2,2'-Bipyrimidine Ligands and Complexes.

2,2'-Bipyrimidine Ligands and Complexes.

2.1. Introduction.

As mentioned in chapter 1, the most well studied doubly bidentate binucleating ligand is the commercially available ligand 2,2'-bipyrimidine (bpm, **5**). Many homo- and heteronuclear complexes of bpm have been described[21-59] including X-ray crystal structures of a dicobalt(II),[50] a diiron(II),[51] a distannacarborane[52] and several copper(II)[53-55] complexes. In these structures the metal-metal separation is typically 5.5Å, thus facilitating relatively strong metal-metal interactions mediated by the bridging ligand.

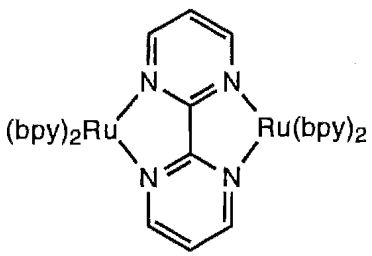

38

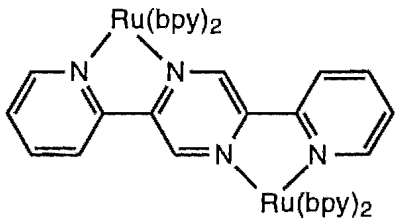

39

Figure 2.1

Many ruthenium(II) complexes of bpm have been studied,[25,26,32,33,35-38] including mixed valence examples[32] and a tetranuclear complex with a central ruthenium(II) core surrounded by three bridging bpm ligands.[26,35] The biruthenium(II) complex $(bpy)_2Ru(\mathbf{5})Ru(bpy)_2^{4+}$ (**38**) (Figure 2.1) is the earliest example of a binuclear complex containing a doubly bidentate bridging ligand and was first described by Hunziker and Ludi.[35] The complex has been the subject of several spectroscopic and electrochemical studies[25,35,36,46,172-174] which have indicated a strong interaction between the ruthenium(II) atoms. More recently the complete assignment of the eight individual reduction steps has been achieved.[175] However, these studies have failed to detect the stereoisomerism of **38** (c.f. Figure 1.8), since the electrochemical and spectroscopic differences between the diastereoisomers are very small. Meso (ΔΛ) and racemic (ΔΔ/ΛΛ) forms have been shown, by ^1H NMR spectroscopy, to exist in the related complex $(bpy)_2Ru(\mathbf{16})Ru(bpy)_2^{4+}$ (**39**).[32] Similar ^1H NMR studies of **38** have not been reported for binuclear complexes of **5**, with the exception of a reported preparation[166] of optically pure ΛΛ-$Ru(phen)_2bpmRu(phen)_2^{4+}$ from optically pure Λ-$[Ru(phen)_2(py)_2]^{2+}$ and rac-$Ru(phen)_2Cl_2$ (phen=1,10-phenanthroline, py=pyridine). However, Keene and Reitsma[167] have now shown that the diastereoisomers of

complexes of the type $[(L_t)_2Ru(L_b)Ru(L_t')_2]$ {L_b=bpm or 2,3-bis-(2-pyridinyl)pyrazine and L_t, L_t' are typically bpy, phen or tmbpy (3,3',4,4'-tetramethyl-2,2'bipyridine), with $L_t \neq L_t'$} can be both distinguished by ^1H NMR and separated by sephadex ion-exchange chromatography.

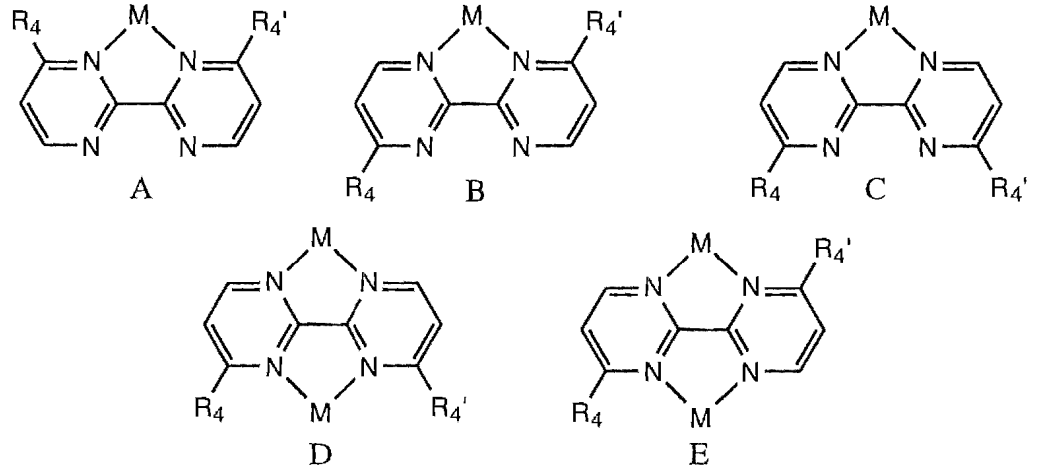

Figure 2.2

Substituted 2,2'-bipyrimidine ligands as mono and binucleating ligands have been less well studied. In general, up to three different bidentate coordination modes would be possible for a symmetrically disubstituted bipyrimidine ligand on coordination to a metal. Which mode of coordination is used is likely to depend on the size of the substituent and the coordination geometry of the metal. Figure 2.2 shows these modes of coordination in the isomers A, B and C for a mononuclear complex and D and E for a homobinuclear complex. The coordination geometry of tetrahedral metals is such that only two ligands may be coplanar. Hence metals such as copper(I) would not be expected to significantly restrict the coordination mode and conformation of the ligand. However, octahedral metals, such as ruthenium(II), and square-planar metals such as palladium(II), have four coplanar ligands and would be expected to restrict the mode of ligand coordination. This is shown in Figure 2.2 where coordination through N3-N3' (A) gives rise to the most sterically demanding environment for the metal whereas coordination through N1-N3' (B) or N1-N1' (C) is less so. Such octahedral mononuclear complexes could be expected to be a mixture of the transoid isomer, B, and cisoid isomer, C, with C becoming the only isomer observed as the size of the R4/R4' substituent increases. It follows that a binuclear octahedral complex is likely to have the ligand in the transoid conformation, as in E, and this complex must form by the coordination of a second metal to B. A large R4/R4' group thus restricts the ligand to mononuclear complexes since coordination of an octahedral metal to isomer C cannot occur.

An early report of the complex **38**[36] also described the absorption and luminescence spectroscopy and the electrochemical oxidations of structurally related complexes of the ligand 4,4'-dimethyl-2,2'-bipyrimidine (**40**) (Figure 2.3). In this chapter we describe a new synthesis of the binucleating ligand **40** and include a study of its coordination chemistry with tetrahedral copper(I), octahedral molybdenum(0) and square-planar palladium(II), followed by a more detailed spectroscopic and electrochemical study of its ruthenium(II) complexes. It will be shown that the coordination chemistry of **40** conforms to the general pattern of stereoisomerism proposed above (Figure 2.2). The synthesis of two new substituted bipyrimidine ligands, **41** and **42** (Figure 2.3), of which **42** is chiral, and a study of their ruthenium(II), palladium(II) and molybdenum(0) complexes is also described. The larger R groups of **41** and **42** will be shown to restrict the ligand to mononuclear octahedral coordination.

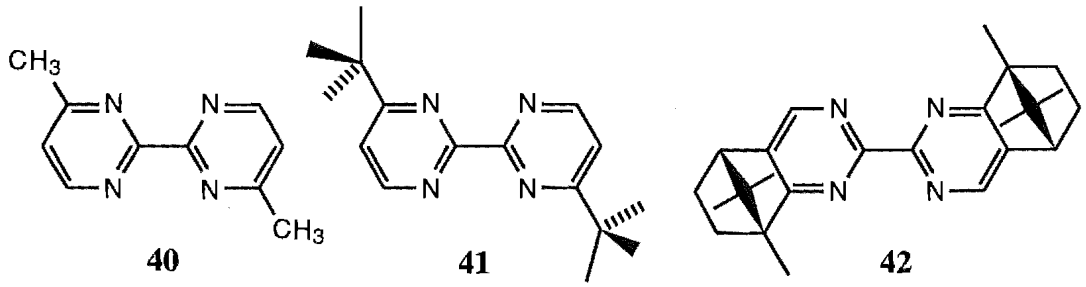

Figure 2.3

Bidentate ligands which contain azole rings have been the subject of recent study.[176] Ruthenium(II) complexes of bidentate ligands incorporating an azole ring with two (**43**),[11-13] three (**44**),[177,178] or four (**45**)[176] nitrogens have shown that the azole ring causes significant changes in the physicochemical properties of the complex in comparison to the more widely used $Ru(bpy)_3^{2+}$ (Figure 2.4). In the case of **44** and **45** the presence of an acidic N-H proton allows additional pH control of the properties of the complex, since the deprotonated and protonated forms of the ligand have very different electronic properties.[176-178]

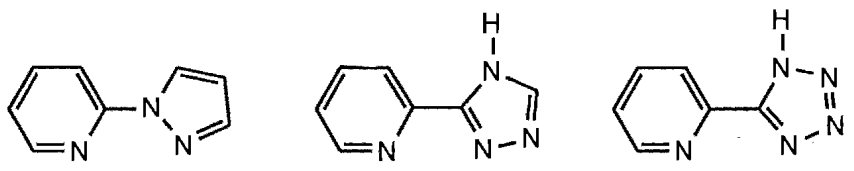

Figure 2.4

Planar tridentate terheteroaromatic analogues of 2,2':6',2''-terpyridine (terpy, **37**) are less common, although recently the syntheses and complexes of **46**[179] and **47**[180,181] (Figure 2.5) have been reported in which the pyrazole rings have a significant effect on the absorption spectra and electrochemical properties relative to terpy. In these complexes the first reduction potential and the energy of the MLCT absorption were both increased, reflecting the higher energies of the π*-LUMO of the ligands relative to $Ru(terpy)_2^{2+}$.

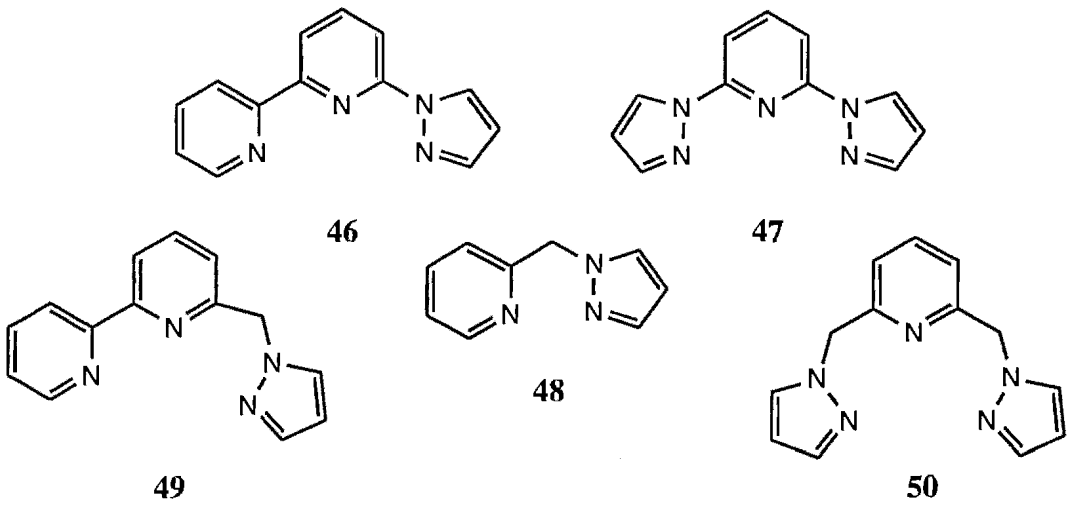

Figure 2.5

Bidentate and tridentate ligands which incorporate methylene bridges between the azole and azine rings such as in the ligands **48**,[182,183] **49**[179] and **50**[184-186] (Figure 2.5), have also been described in recent years. Such ligands form a six membered chelate ring on coordination to a metal which has additional conformational flexibility, since such six-membered rings exist in a boat conformation.[187] The methylene bridge also prevents the possibility of conjugation between the component heterocyclic rings.

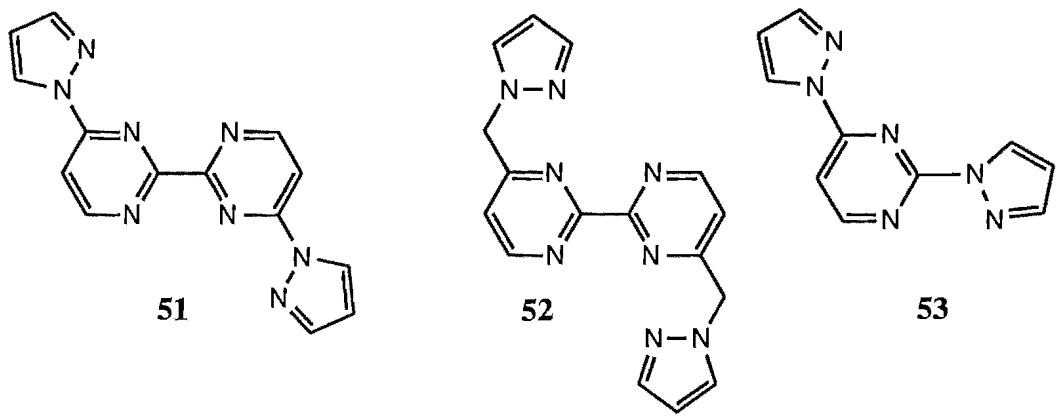

Figure 2.6

Complexes of the ligands **51** (Figure 2.6) should show similar interesting properties to **43-47**. Two attempted syntheses of **51**, which has the potential to exhibit bis-tridentate coordination, are described. A brief discussion of the attempted synthesis of its methylene

bridged analogue **52** is also included. Although both syntheses were unsuccessful the new ligand **53**, which was the major product of the attempted synthesis of **51**, is described, along with a detailed study of its ruthenium(II) complexes.

2.2 Results and Discussion

The first ligand investigated was **40**, the synthesis of which is outlined in Scheme 2.1. The method for converting commercially available 2-amino-4-methylpyrimidine (**54**) to a mixture of 2-chloro-4-methylpyrimidine (**56**) and 2-hydroxy-4-methylpyrimidine (**55**) (step I) using $NaNO_2$ in conc HCl at -10°C was derived from diazotization of the related compound 2-amino-4-(t-butyl)pyrimidine (see later).[188] The mixture of **55** and **56** was then separated by radial chromatography on silica. Chlorination of **55** in refluxing $POCl_3$ afforded additional **56** which was purified in a similar manner. In step II the catalyst $Ni^0(PPh_3)_2$ was prepared *in situ* in deoxygenated DMF at 50°C from $NiCl_2$ and PPh_3. Purified **56** was then coupled by the red Ni^0 catalyst to produce the desired ligand **40** in reasonable yield. Nasielski *et al.* have used this method to couple other heteroaryl halides.[189] The previous synthesis[36] of **40** involved the coupling of 2-bromo-4-methylpyrimidine using a copper catalyst.

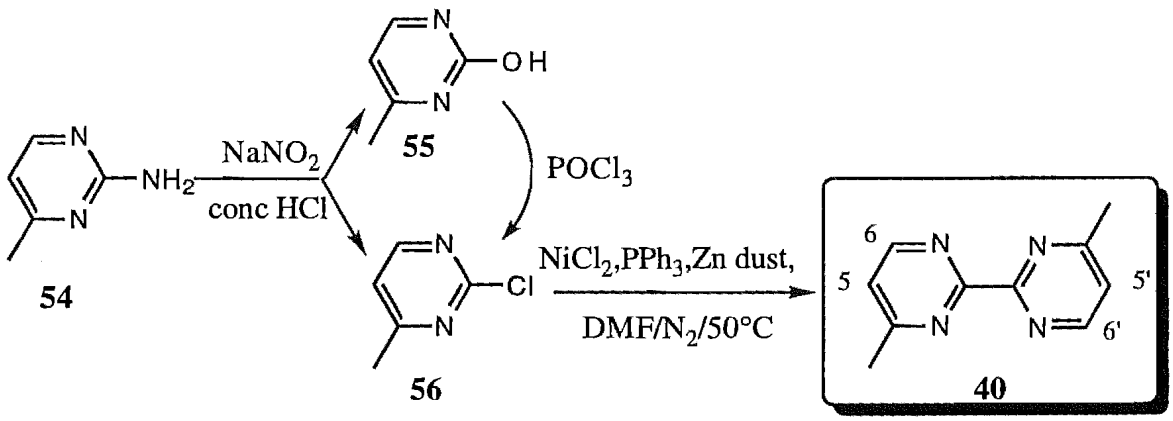

Scheme 2.1

The ^1H and ^{13}C NMR spectra of **40** were obtained in $CDCl_3$, CD_3CN and DMSO-d_6. Two aromatic doublets are observed in the ^1H NMR spectrum of **40** corresponding to H5 and H6. The more upfield doublet was assigned to H5, given that in a pyrimidine ring the 5-position is more electron rich than the 6-position. Similarly, C5 and C6 were assigned in the ^{13}C NMR spectrum of **40** whilst C4 and C2 were distinguished on the basis that C2 has the greater downfield shift relative to **56** on substitution by a pyrimidinyl group.

As discussed in 2.1 the formation of binuclear complexes of **40** with tetrahedral metals is expected to be facile. The ligand **5** has been shown to bridge two tetrahedral Cu(I) atoms in a

binuclear complex[190] and we have found that **40** forms an analogous complex. The reaction of **40** with two equivalents of a copper(I) solution and four equivalents of triphenylphosphine gave a yellow complex which was shown by elemental analysis to be the binuclear complex **57** (Scheme 2.2). The ^1H spectrum of **57** showed that the two pyrimidine rings are equivalent as are all the triphenylphosphine ligands. This supports the structure shown in Scheme 2.2, in which the bridging ligand is transoid (N1-N3', N1'-N3) and all the auxiliary ligands are related by the C_{2h} symmetry of the complex. The contrasting cisoid structure of **57** would have C_{2v} symmetry and hence two non-equivalent triphenylphosphine ligands.

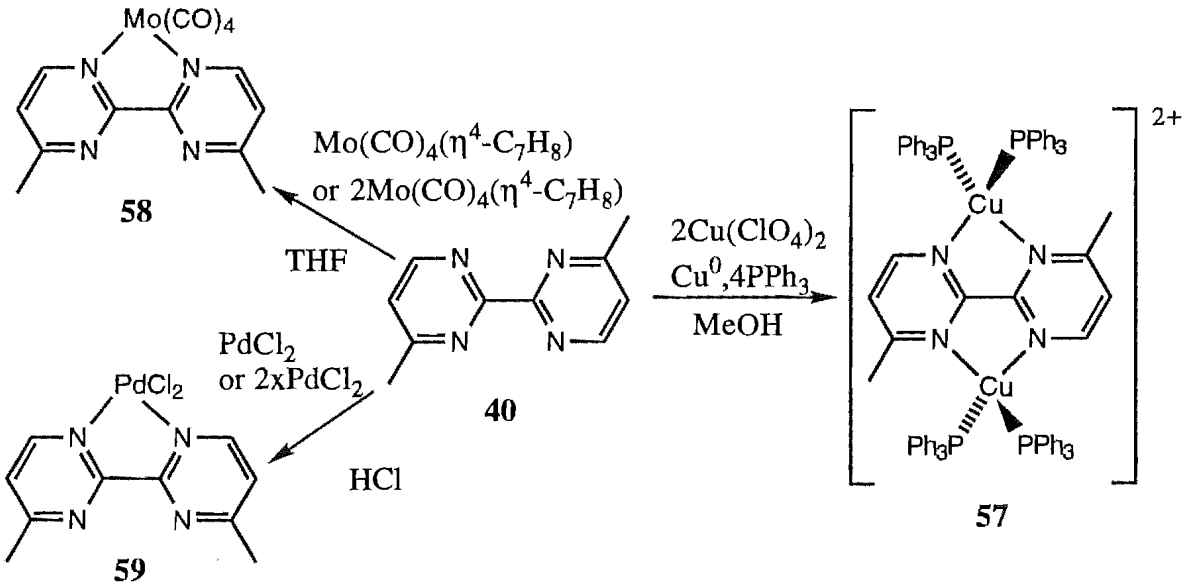

Scheme 2.2

Having demonstrated that **40** forms a binuclear complex with tetrahedral Cu(I), its coordination chemistry with molybdenum(0) and palladium(II) was investigated. The mononuclear molybdenum(0) complex **58** (Scheme 2.2) was prepared by reacting one equivalent of the complex $Mo(CO)_4(\eta^4\text{-}C_7H_8)$ with **40**. The complex $Mo(CO)_4(\eta^4\text{-}C_7H_8)$ has been used previously to prepare structurally related complexes.[44,191] The ^1H NMR spectrum of **58** in $CDCl_3$ indicated a symmetrical complex in which the ligand most probably coordinates to molybdenum(0) in the N1-N1' mode, since N3-N3' coordination would be more sterically demanding. This assumption is supported by the reaction of **40** with two equivalents of $Mo(CO)_4(\eta^4\text{-}C_7H_8)$, which gave the same mononuclear complex. The ^1H NMR spectrum of **58** showed evidence of dissociation to the free ligand after only a few minutes in solution. The complex was also unstable in the solid state and hence, no elemental analysis was obtained.

The reaction of **40** with one equivalent of $PdCl_2$ in conc HCl gave a yellow complex which was shown by elemental analysis to be mononuclear. The ^1H NMR spectrum of the

complex in DMSO-d_6 shows two doublets corresponding to H5 and H6. This indicates that the ligand coordinates symmetrically to palladium(II), therefore excluding transoid N1-N3' coordination. Furthermore, the reaction of **40** with two equivalents of $PdCl_2$ also gave the same mononuclear complex. This implies that the complex has the structure **59** (Scheme 2.2), in which the ligand again coordinates in the N1-N1' mode with a non-coordinated N3-N3', which is too sterically demanding to allow coordination of a second palladium(II). The lack of N3-N3' coordination contrasts with the sterically hindered coordination mode observed in the molybdenum(0) complex of 6,6'-dimethyl-2,2'-bipyridine, for which an X-ray structure has recently been determined.[192] However in the latter case the ligand is forced to coordinate in this mode, because there are only two nitrogens which can chelate to molybdenum(0).

Table 2.1 ^{1}H NMR Chemical Shifts[a] and Coordination Induced Shifts[b] of **40** and **59**.

	4-CH_3	H5	H6
59	2.82	7.95	9.24
40	2.66	7.61	8.91
CIS[b]	0.16	0.34	0.33

[a] For deuterated dimethylsulphoxide solutions. [b] CIS = $\delta_{complex}$-δ_{ligand}.

When a ligand forms a transition metal complex, subtle or even dramatic differences in the NMR spectra of the ligand and complex are observed. For example, in the ^{1}H NMR spectrum of **40** and **59** (Table 2.1) the H5, H6 and 4-CH_3 protons are shifted downfield from their positions in the spectrum of the free ligand by 0.34, 0.33 and 0.16ppm, respectively. These downfield shifts are described as coordination induced shifts (CIS=$\delta_{complex}$-δ_{ligand}) and they reflect the σ-donation of electron density from the ligand to the metal and, also for H6, the deshielding effect of the nearby chlorine atom. Previously, a number of factors have been identified which contribute to the sign and magnitude of CIS values in ruthenium(II) complexes. These include ligand-to-metal σ donation (analogous to the palladium(II) complex **59**), metal-to-ligand π back donation, chelation imposed conformational changes, coordinative disruption of inter-ring conjugation and interligand through-space ring-current anisotropy effects.[11,176,179,193] The contribution of these factors to the CIS values of the series of complexes $L_2Ru(\mathbf{40})(RuL_2)_n$ (L=2,2-bipyridine (bpy) or L=4,4'-dimethyl-2,2'-bipyridine (dmb), n=0,1) is included in the discussion which follows.

The reaction of **40** with one equivalent of bis-(2,2'-bipyridine)-dichlororuthenium(II) in 3:1 ethanol/water afforded, in good yield, the complex $Ru(\mathbf{40})(bpy)_2^{2+}$ which was isolated as a hexafluorophosphate salt and characterised by FAB mass spectrometry (Scheme 2.3). Elemental analyses for this compound, and others to be described, were often unreliable due to traces of

NH_4PF_6 or ruthenium(III) impurities and the formation of metal carbides in the analysis process. Other workers have reported similar problems with structurally related complexes.[194] In anticipation that the ^1H NMR spectrum of Ru(**40**)$(bpy)_2^{2+}$ might be difficult to assign, the complex Ru(**40**)$(dmb)_2^{2+}$ (Scheme 2.3) was prepared by an analogous procedure from **40** and bis-(4,4'-dimethyl-2,2'-bipyridine)-dichlororuthenium(II) and characterised by FAB mass spectrometry. Previously the preparation of a related $RuL(dmb)_2^{2+}$ complex has been found to assist in the assignment of the L ligand in the ^1H NMR spectra of the complexes.[176] The replacement of the bpyH4 protons (8ppm) with methyl groups (2.6ppm), and the subsequent removal of ^3J and ^4J coupling associated with bpyH4, considerably simplifies the spectra. An alternative procedure for simplifying the overlapping ^1H NMR spectra of ruthenium(II) complexes completely eliminates the bpy signals by replacing the bpy ligands with fully deuterated bpy ligands (d_8-bpy).[195] However, apart from the prohibitive cost of d_8-bpy, this technique sacrifices the information contained in the chemical shifts of the bpy protons.

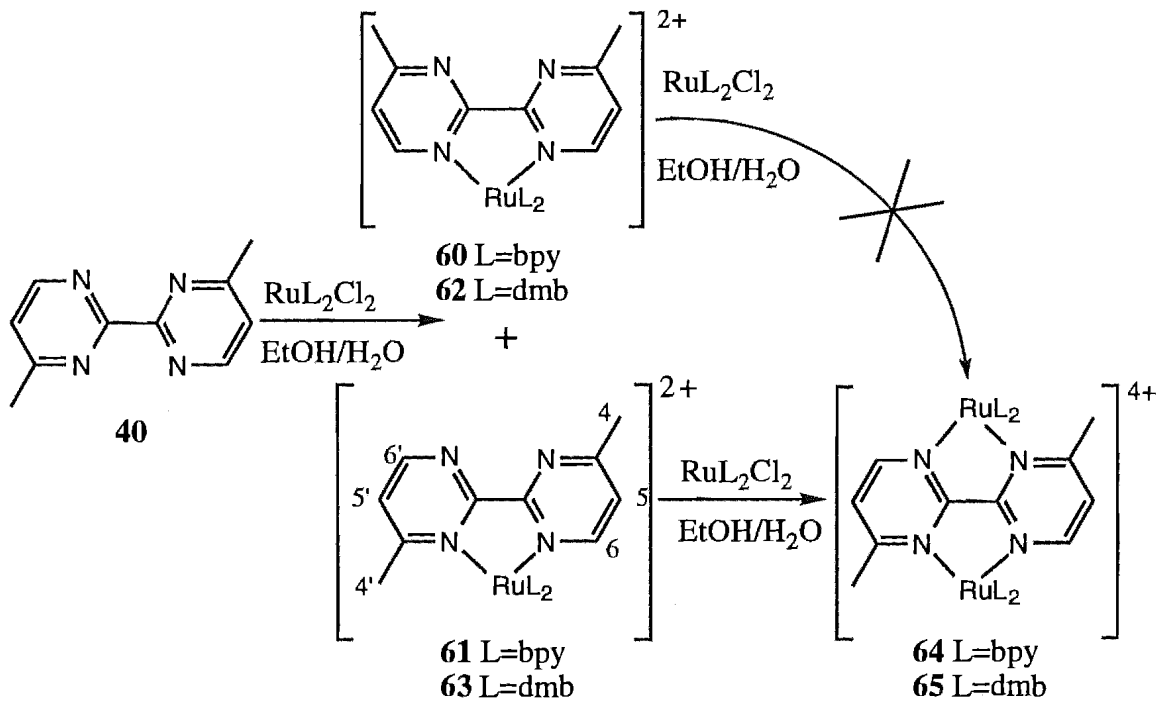

Scheme 2.3

By examination of its ^1H NMR spectrum, the complex Ru(**40**)$(bpy)_2^{2+}$ was found to exist as a 1:1 mixture of the symmetrical (**60**) and unsymmetrical (**61**) isomers (Scheme 2.3). Similarly, a 1:1 mixture of (**62**) and (**63**) is observed for Ru(**40**)$(dmb)_2^{2+}$ (Scheme 2.3). The ^1H NMR spectra of the mixtures, herein referred to as **60/61**, for the mixture of **60** and **61**, and **62/63**, for the mixture of **62** and **63**, are shown in Figure 2.7 and summarised in Table 2.2.

In the symmetrical isomer both pyrimidine rings and the bpy ligands are equivalent, whereas in the unsymmetrical isomer all six rings are non-equivalent. Hence, the ^{1}H NMR spectrum of **60/61** (top of Figure 2.7) consists of 30 non-equivalent aromatic protons, 10 corresponding to **60** and 20 corresponding to **61**. Not shown are the three methyl singlets, in a 6:3:3 ratio, corresponding to 4-CH_3 of **60** and the 4-CH_3 and 4'-CH_3 of **61**. These were easily assigned from their relative integrals and with the methyl groups of **61** differentiated on the basis that 4'-CH_3 is shielded by a pyridine ring and therefore exhibits a large negative CIS. The assignment of the aromatic protons of **60/61** is more difficult, since some of the signals of **60** and **61** overlap with each other and the bpyH5 signals in the region 7.38-7.56ppm. Despite this, the protons H6(**60**) and H6(**61**) and H6'(**61**) can be distinguished by their multiplicity in the spectrum and assigned from their observed CIS values. In this case H6'(**61**) exhibits a downfield shift (8.99ppm) due to the net positive effect of ligand-to-metal σ donation and metal-to-ligand π back donation, whilst H6(**60**) and H6(**61**) (at 7.87 and 7.70ppm, respectively) are shifted upfield as a result of interligand through-space ring-current anisotropy.

The spectrum of **62/63** was then used to assign the three H5 protons of **60/61**. The spectrum of **62/63** (bottom of Figure 2.7) consists of 24 non-equivalent aromatic protons, 8 corresponding to **62**, and 16 corresponding to **63**. Unlike the spectrum of **60/61**, the signals for H5/H6(**62**), H5/H5'/H6/H6'(**63**) and the dmbH6's are all clearly visible in the spectrum of **62/63**.

The protons H5(**62**) and H5/H5'(**63**) were assigned by correlation to the H6(**62**) and H6/H6'(**63**) signals using the homonuclear 2D COSY spectrum shown in Figure 2.8. Correlation of the doublet H6(**62**) at 7.86ppm to the doublet at 7.42ppm locates H5(**62**), thus completely assigning the pyrimidine spin system of **62** and hence, by comparison, of **60**. Similarly, H5'(**63**) can be assigned to the doublet at 7.52ppm by its correlation to the H6'(**63**) doublet at 8.97ppm, whilst H5(**63**) is located at 7.37ppm by correlation to the H6(**63**) at 7.68ppm. Hence, **61** can be assigned by comparison with **63**. The advantage of the dmb substitution is evident from this last assignment, since H5(**61**) is completely overlapped by the bpyH5 signals in the spectrum of **60/61**.

The assignment of the dmb pyridine ring spin systems (excluding methyl groups), but not the individual rings in the complex, is also possible using a COSY spectrum (Figure 2.8). For example, the dmbH6 at 7.90ppm shows a correlation to the H5 proton at 7.34ppm which in turn exhibits a long-range coupling to the H3 singlet at 8.41ppm. In contrast, complete assignment of

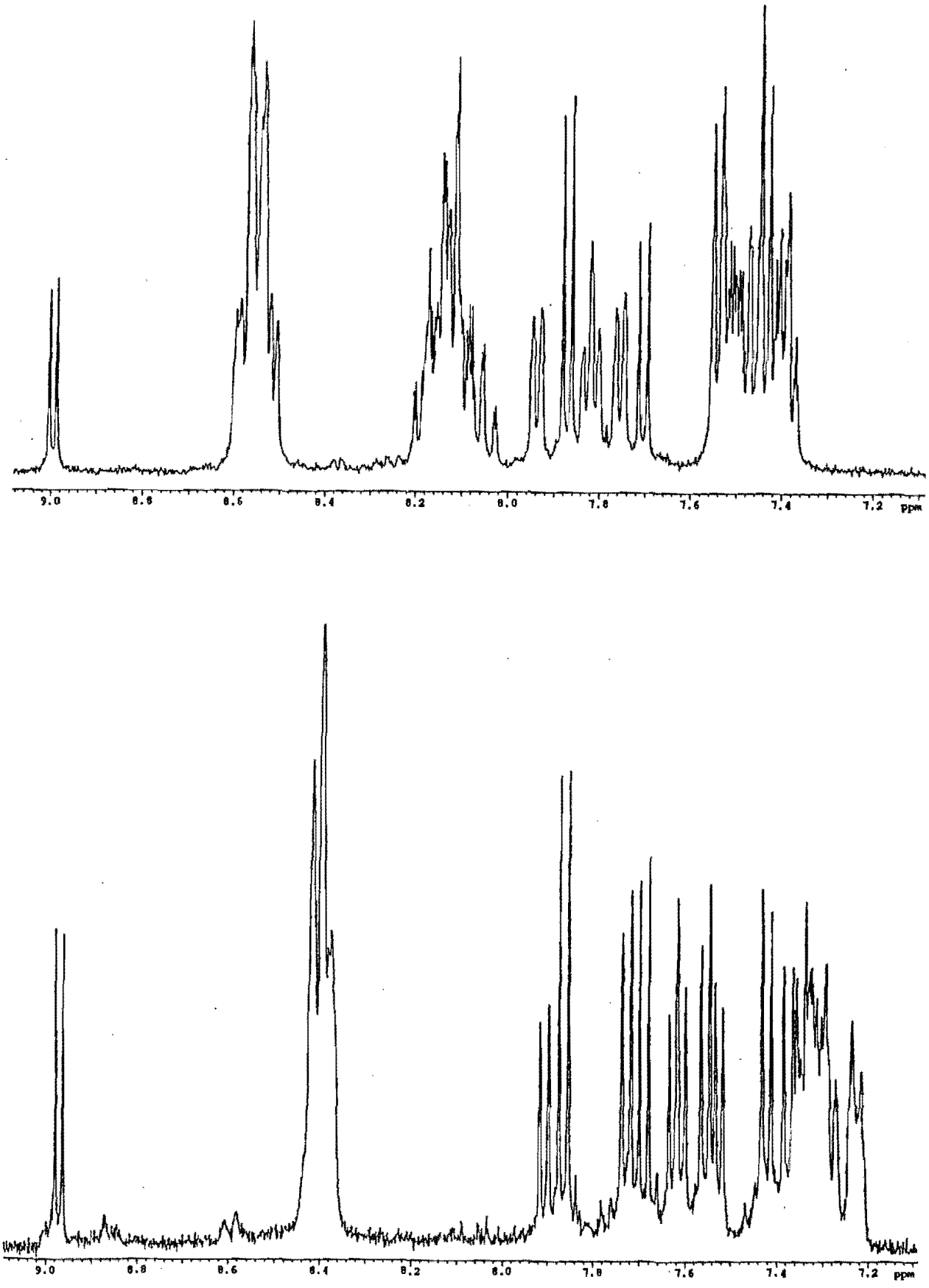

Figure 2.7 ^{1}H NMR Spectra of **60/61** (top), **62/63** (bottom).

the bpy pyridine ring spin systems was prevented by the closely spaced H4bpy protons in the spectrum of **60/61**, although the bpy protons were located using a similar COSY spectrum to that shown in Figure 2.8.

Figure 2.8 also shows the ^{1}H NMR spectrum of the symmetrical isomer **62**. The reaction of **62/63** with one equivalent of $Ru(dmb)_2Cl_2$ gave a 1:1 mixture of the biruthenium(II) complex **65** and unreacted **62**, the latter of which is too sterically demanding for N3-N3' coordination of a second ruthenium(II) (Scheme 2.3). Similarly **64** and unreacted **60** were obtained from the reaction of **60/61** with $Ru(bpy)_2Cl_2$. In both cases, the mixture of the binuclear and symmetrical mononuclear complexes was separated on C-25 sephadex. The ^{1}H NMR spectra of **60** and **62**, once determined, provided confirmation of our previous assignments. The binuclear complexes are discussed in detail later.

Table 2.2 ^{1}H NMR Chemical Shifts[a] and Coordination Induced Shifts[b] for $Ru(\mathbf{40})L_2^{2+}$.

	Ligand=**40**						Ligand=L			
	4-CH_3	H5	H6	4'-CH_3	H5'	H6'	H3	H4	H5	H6
40	2.64	7.42	8.83							
60	2.77	7.44	7.87	-	-	-	8.55	8.14	7.49	7.93
CIS[b]	+0.13	+0.02	-0.96	-	-	-	8.55	8.11	7.45	7.75
61	2.76	7.40	7.70	1.90	7.54	8.99	8.53[d]	8.06[d]	7.39[d]	7.83[d]
							8.54[d]	8.13[d]	7.40[d]	7.81[d]
CIS[b]	+0.12	-0.02	-1.13	-0.74	+0.12	+0.16	8.58[d]	8.16[d]	7.41[d]	7.54[d]
							8.59[d]	8.17[d]	7.51[d]	7.46[d]
62	2.77	7.42	7.86	-	-	-	8.39	2.59[c]	7.29	7.72
CIS[b]	+0.13	+0.00	-0.97	-	-	-	8.39	2.58[c]	7.31	7.55
63	2.76	7.37	7.68	1.90	7.52	8.97	8.41	2.61[c]	7.34	7.90
							8.41	2.60[c]	7.33	7.62
CIS[b]	+0.12	-0.05	-0.95	-0.74	+0.10	+0.17	8.37	2.56[c]	7.22	7.60
							8.37	2.54[c]	7.22	7.34

[a] For deuterated acetonitrile solutions. [b] CIS = $\delta_{complex}$-δ_{ligand}. [c] Methyl group [d] Not assigned.

The ^{1}H NMR chemical shifts and CIS values for **60-63** are summarised in Table 2.2. Small differences are observed between the ligand signals of the two mixtures, which can be attributed to the electron donating effect of the methyl groups of the dmb ligands. The small CIS values for all H5 and H6' protons of the ligands indicates the presence of strong metal-to-ligand π back-donation into the low lying π^* orbitals of the ligand, which reduces the strong positive CIS effect of ligand-to-metal σ donation. The other important CIS effects have already been discussed.

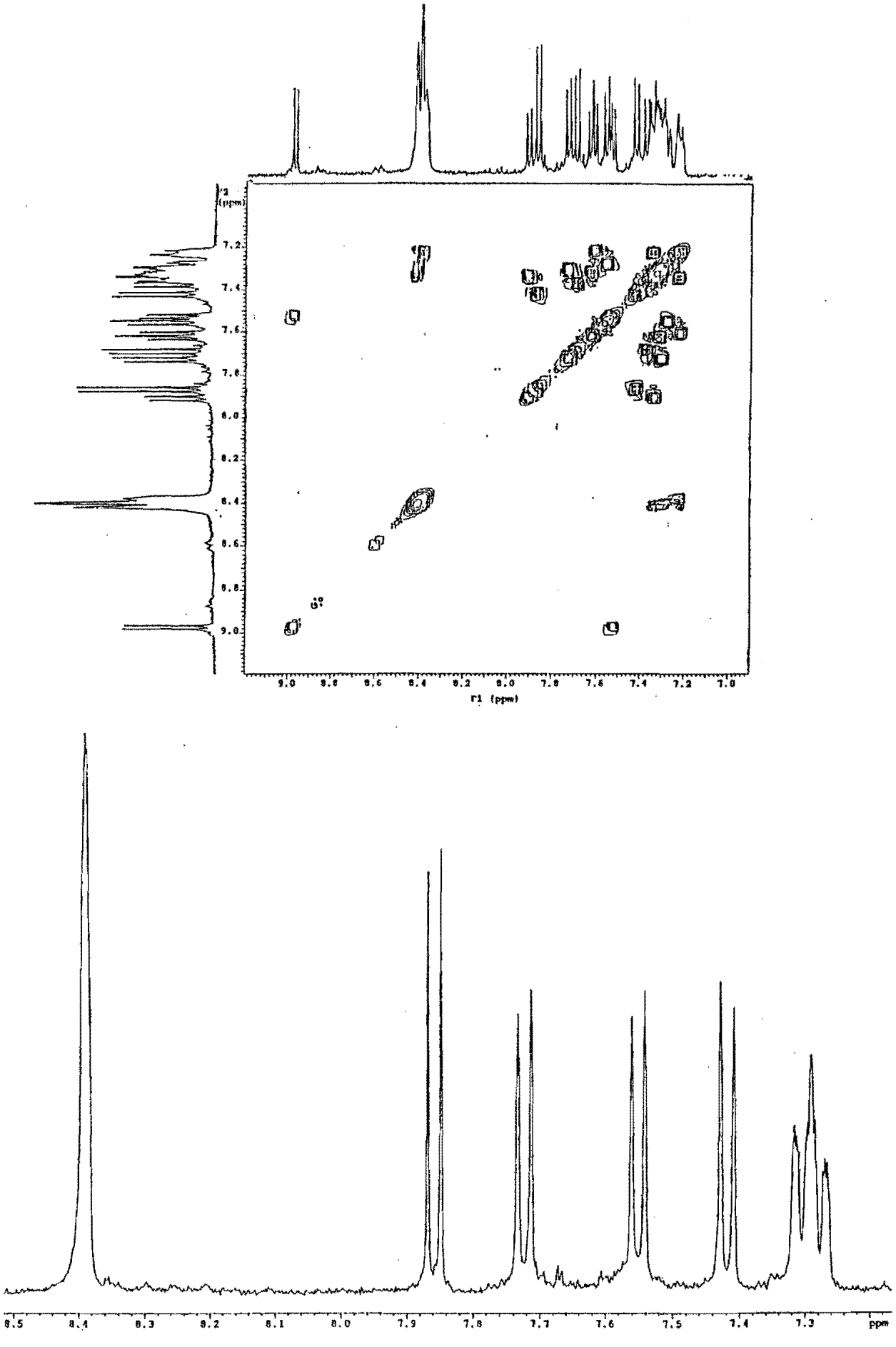

Figure 2.8 2D COSY Spectrum (top) of **62/63** and ^{1}H NMR Spectrum of **62** (bottom).

The UV/VIS spectra of **60/61** and its dmb equivalent **62/63** consist of strong ligand ntred absorptions at λ<300nm and a MLCT absorption at λ>400nm. The spectrum of **60/61** is good agreement with that previously reported by Wilson *et al.*,[36] with the maxima for both)mplexes appearing at 438nm. Unsymmetrical absorptions in this region of the spectrum :present a combination of low energy transitions (dπ-π*(**40**)) from the metal (HOMO) to the π* rbitals (LUMO) of **40** and slightly higher energy transitions (dπ-π*bpy) from the metal to the py π* orbitals (SUMO). The dπ-π*(**40**) transition of **60/61** is undoubtedly at higher energy han the dπ-π*(**5**) transition of Ru(**5**)$(bpy)_2^{2+}$ due to destabilisation of the ligand π* orbitals by he electron donating methyl groups. In **62/63** this transition appears as a shoulder at lower :nergy (482nm) as a result of additional metal d orbital destabilisation by the dmb methyl groups.

Wilson *et al.* have described the oxidations of **60/61**.[36] In this study we describe the complete electrochemistry (oxidations and reductions) of **60/61**, the new complex **62/63** and the ligand **40** (reductions). The cyclic voltammograms of **60/61** and **62/63** are shown in Figure 2.9, whilst Table 2.3 summarises the redox potentials of these and related complexes.

The complex mixture **60/61** exhibits a reversible one electron oxidation at +1.28V and three reversible one electron reductions at -1.19, -1.56 and -1.81V. A fourth irreversible one electron reduction is also observed at -2.17V. In comparison the mixture **62/63** exhibits a one electron oxidation at +1.19V and four similar reductions at -1.20, -1.65, -1.87 and -2.17V.

Destabilisation of the metal d orbitals (HOMO) by the electron donating methyl groups of **40**, as described above, makes **60/61** and **62/63** easier to oxidise (Table 2.3) than Ru(**5**)$(bpy)_2^{2+}$. Also, the introduction of methyl groups in the dmb substituted complex **62/63** further increases the ease of oxidation by 0.09V relative to **60/61**. It has been previously noted for structurally related complexes that methyl groups decrease oxidation potentials by approximately 0.025V per methyl group.[180]

The first reduction potentials of **60/61** (1.19V) and **62/63** (1.20V) were both assigned to the reduction of **40** since the π* orbitals of **40** are at lower energy than those of bpy, as shown by the reductions of the free ligands at -2.00V for **40** and -2.18V[10] for bpy. Both complexes are therefore harder to reduce than Ru(**5**)$(bpy)_2^{2+}$ again reflecting the π* orbital destabilisation of **40** (complex-LUMO) by the methyl groups, and which is mirrored by the free ligand reductions for **40** and **5** (-1.80V).[10] Subsequent reductions can be readily assigned to the bpy or dmb ligands except the fourth reduction, which again is constant for **60/61** and **61/62** and therefore most likely to be a second irreversible reduction of the ligand **40**. The $\Delta E_{ox\text{-}red}$ values in Table 2.3

Table 2.3. Absorption Maxima[a] and Redox Potentials[b].

Complex	λ	E_{ox}	E_{red1}	E_{red2}	E_{red3}	E_{red4}	$\Delta E_{ox\text{-}red}$
$Ru(\mathbf{5})(bpy)_2^{2+}$	422,480sh	+1.40	-1.02	-1.45	c	c	2.42
60/61	438	+1.28	-1.19	-1.56	-1.81	-2.17[d]	2.47
62/63	438,482sh	+1.19	-1.20	-1.65	-1.87	-2.17[d]	2.40

[a] In nanometres. [b] In volts vs SCE in acetonitrile. [c] Not observed. [d] Irreversible.

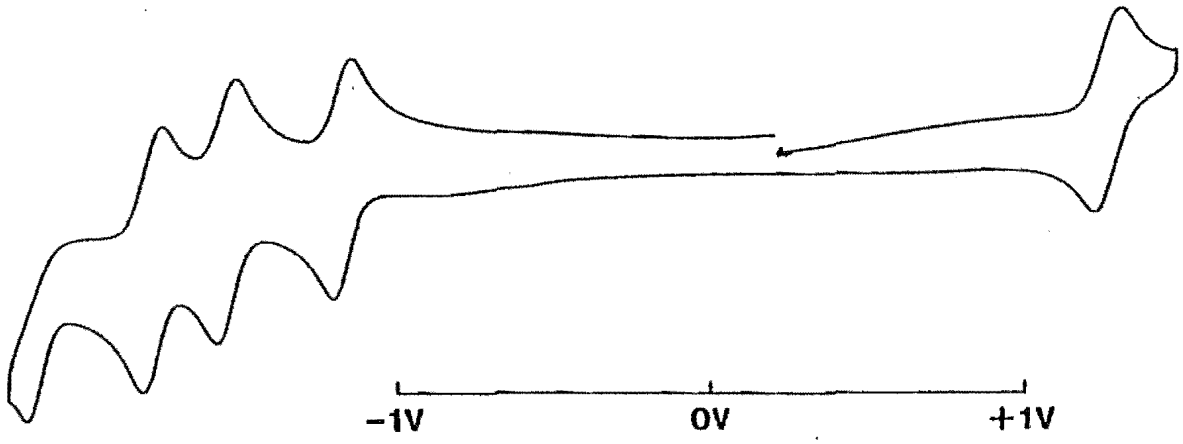

Cyclic Voltammogram for **60/61**

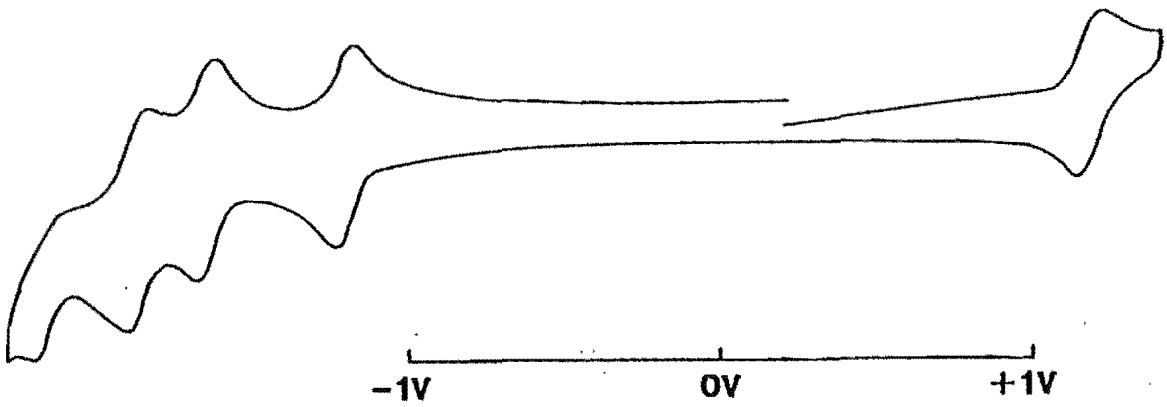

Cyclic Voltammogram for **62/63**

Figure 2.9.

reflect the HOMO-LUMO energy gap in the complexes and are consistent with the lowest energy MLCT absorptions of the complexes for which the same orbitals are involved.[6] The value of 2.47V for **60/61** is larger than the value for $Ru(\mathbf{5})(bpy)_2^{2+}$ (2.42V) for the reasons described above, but smaller for **62/63** (2.40V) reflecting the additional metal d orbital destabilisation of the electron donating dmb ligands.

The reactions of one equivalent of $Ru(bpy)_2Cl_2$ with **60/61** and one equivalent of $Ru(dmb)_2Cl_2$ with **62/63** gave mixtures of symmetrical mononuclear and binuclear ruthenium(II) complexes **60/64** and **62/65** (Scheme 2.3). Separations of the mixtures are facile on ion-

exchange C-25 sephadex by simply eluting with 0.1M NaCl to remove the dication followed by 0.5M NaCl to remove the tetracation. Once purified by chromatography, the binuclear complexes **64** and **65** were characterised by mass spectrometry.

As already discussed biruthenium(II) complexes which contain two $Ru(bpy)_2^{2+}$ units bridged by a doubly bidentate ligand should exists as two diastereoisomers, *viz.* the meso ($\Lambda\Delta$) and racemic ($\Lambda\Lambda/\Delta\Delta$) forms (Figure 1.8, chapter 1). Such isomerism has been detected by ^1H NMR for the biruthenium(II) complexes of 2,5-bis-(2-pyridinyl)pyrazine[32] and more recently, 2,2'-bipyrimidine.[167] In such cases the two diastereoisomers are generally observed in a 1:1 ratio.

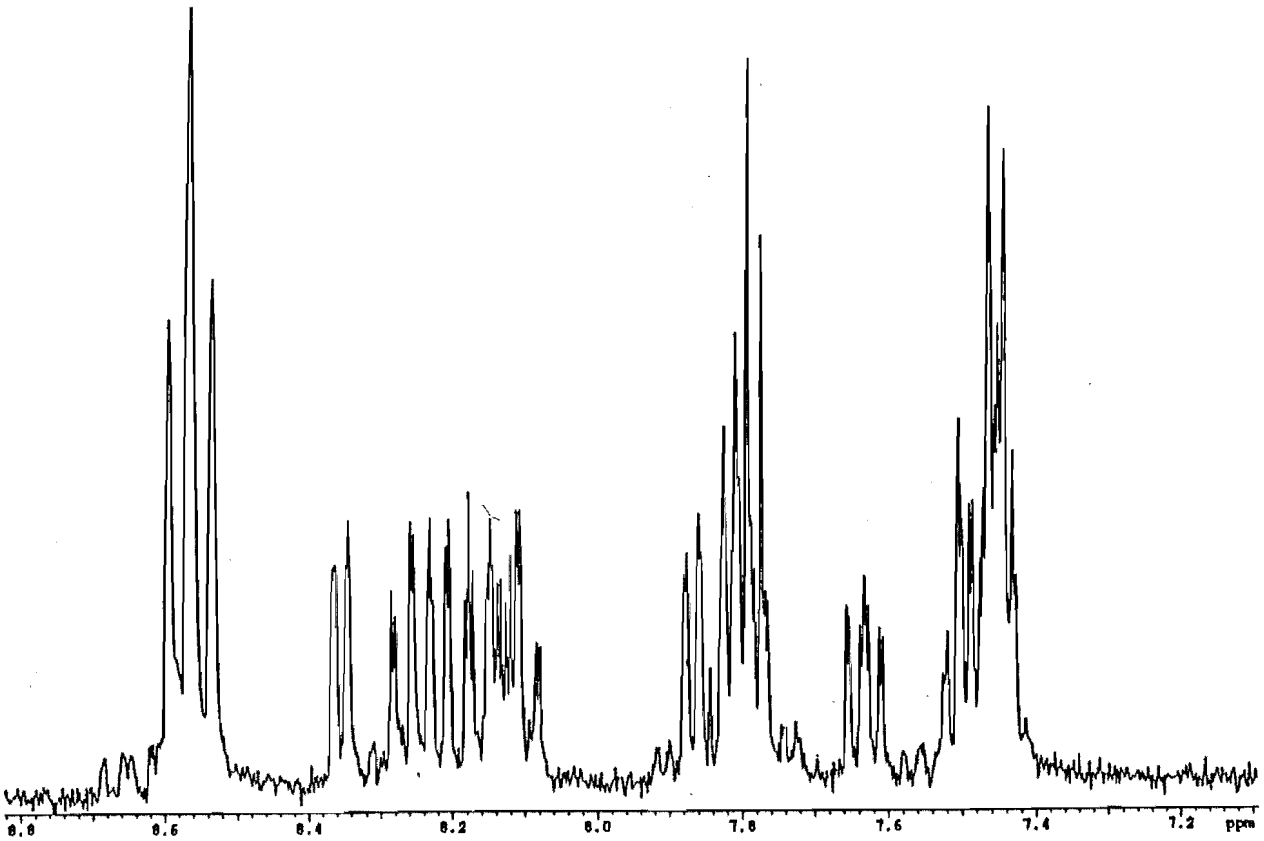

Figure 2.10 ^1H NMR Spectrum of **64**.

For the complex **64** we have found this ratio ranges from 4:1 to 5:1. Figure 2.10 shows the aromatic region of the ^1H NMR spectrum for **64** after several fractional recrystallisations from ether/acetonitrile. As a result of the coordination of a second $Ru(bpy)_2$ unit, the downfield H6' of **61** disappears in the ^1H NMR spectrum of **64**, since both pyrimidine rings are now equivalent, a result of the C_2 symmetry of **64**. The bridging ligand protons H5 and H6 can be easily distinguished and were assigned by comparison with the spectra of **60/61**. These two protons exhibit coordination induced shifts of +0.04 and -1.05ppm, respectively, for reasons already described.

One dimensional total correlation spectroscopy (1D TOCSY)[196,197] can often allow dramatic spectral simplification by editing a complex ^{1}H NMR spectrum into a set of simpler subspectra,[198] thus allowing isolation of individual spin systems. The method requires at least one multiplet to be sufficiently isolated that it can be inverted by a selective 180° pulse; the magnetization of this inverted spin then propagates through the network of spins coupled to it.[198] In this research we have found this technique particularily useful for isolating multiplets which are overlapped by other signals and hence allowing assignment of the spin systems of individual aromatic rings.

All the bpy protons in the spectrum of **64** were located using 1D TOCSY spectra (Figure 2.11). Trace I, II and III show the effect of irradiating the bpyH3 multiplet and allowing the magnetization to propagate further through the spin system. At 0.02s (Trace I) the bpyH4 signals are prominent, whilst signals for bpyH5 and bpyH6 are developing. With increasing mixing time, signals for bpyH5 (trace II-0.04s) and bpyH6 (trace III-0.08s) predominate. The traces clearly show the large spread of signals for the bpy protons, particularly for bpyH6.

Table 2.4 ^{1}H NMR Chemical shifts[a] and Coordination Induced Shifts[b] for **64** and **65**

	4-CH_3	H5	H6	H3	H4	H5	H6
64 (ΔΛ)	1.95	7.46	7.78	8.55	8.21	7.63	7.87
CIS[b]	-0.69	+0.04	-1.105	8.55	8.26	7.79	8.35
				8.58	8.11	7.45	7.51
				8.58	8.15	7.47	7.82
65 (ΔΛ)	1.94	7.42	7.75	8.43	2.68[c,d]	7.46	8.15
CIS[b]	-0.70	+0.00	-1.08	8.43[d]	2.58[c,d]	7.62[d]	7.66[d]
				8.39[d]	2.64[c,d]	7.28[d]	7.62[d]
				8.39[d]	2.67[c,d]	7.32[d]	7.31[d]

[a] For deuterated acetonitrile solutions. [b] CIS=$\delta_{complex}$-δ_{ligand}. [c] Methyl group. [d] Spin system not assigned.

In some cases where a proton is well isolated the individual rings can be assigned. For example, by irradiating the bpyH5 at 7.63ppm (trace IV), signals for bpyH3, bpyH4 and bpyH6 develop with extended mixing time (trace IV, V and VI). Similar subspectra for a second pyridine spin system can be obtained by irradiating the bpyH6 at 8.35ppm. This proton is the most downfield of all the bpyH6 protons and its unique chemical shift implies that the major diastereoisomer is the meso form (ΛΔ) (see Figure 1.8). Molecular models show that this proton is deshielded (relative to the racemic form (ΛΛ/ΔΔ)) by through-space anisotropy effects. This effect has recently been observed for structurally related complexes of **5**.[167] The spin systems for the other two non-equivalent bpy pyridine rings were assigned by a 2D COSY spectrum. The

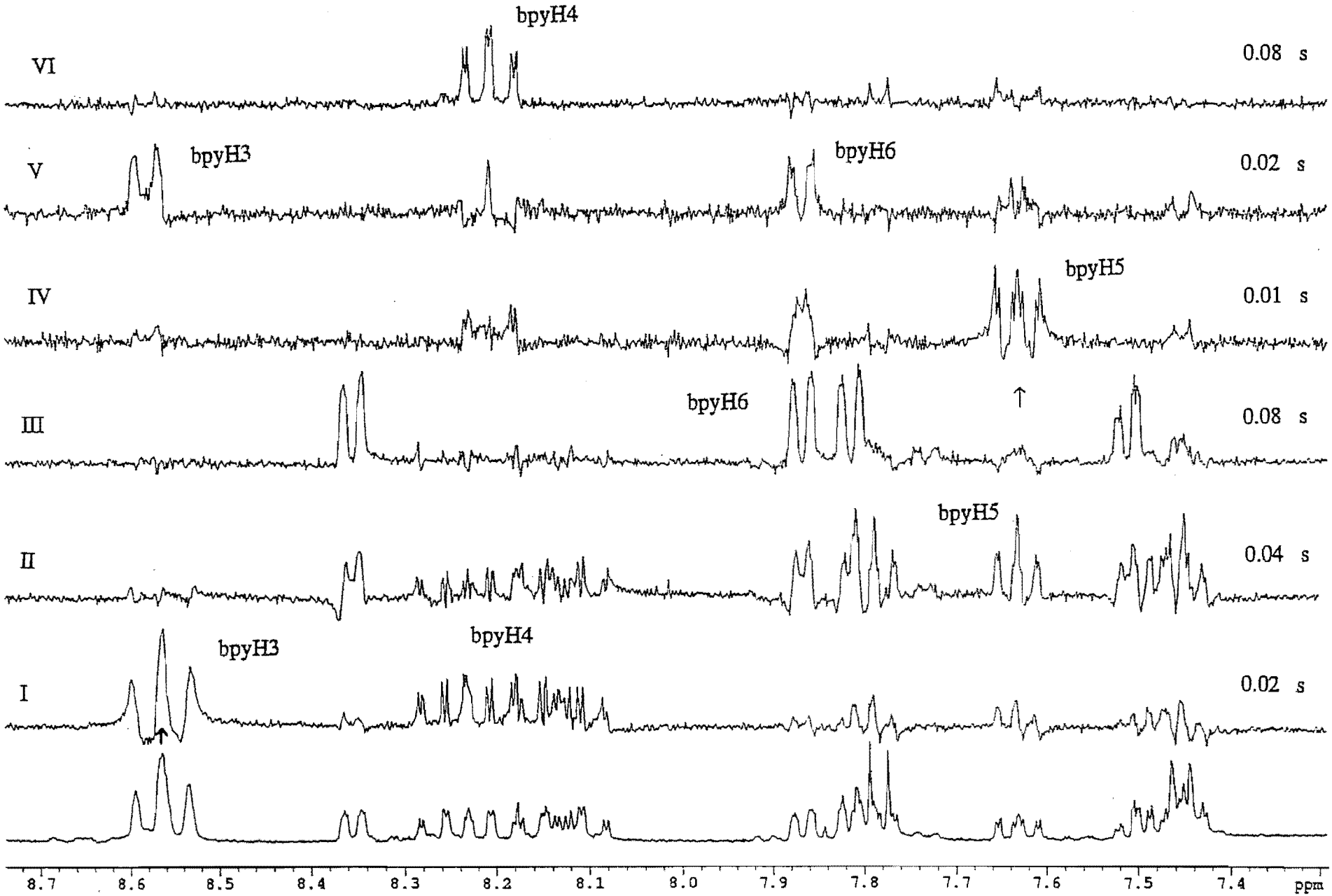

Figure 2.11 1D TOCSY Spectra of **64**.

minor racemic form (ΛΛ/ΔΔ) was not isolated in pure form but its ^{1}H NMR spectrum was tentatively assigned from the mixture.

The meso form (ΛΔ) was also found to be the major isomer for **65** in a 3:1 ratio with the racemic form (ΛΛ/ΔΔ), but neither could be separated by fractional recrystallisation. The meso form was assigned by 1D TOCSY spectra in an analogous manner to **64**, with the racemic form being tentatively assigned from the mixture of the diastereoisomers. The ^{1}H NMR chemical shifts of the major isomers of **64** and **65** are summarised in Table 2.4.

The UV/VIS spectra of **64** and **65** are summarised in Table 2.5. The spectrum of **64** was found to be in agreement with that previously described by Wilson *et al.*[36] Below 300nm both complexes display strong ligand centred transitions. The lowest energy absorptions of **64** and **65** can be assigned as a MLCT transition into the bridging ligand (dπ-π*(**40**)). The large red shift of these MLCT absorptions, relative to the monoruthenium(II) complexes, has been observed for bi-ruthenium complexes of related ligands, including **5**[35,36,37], and 2,3-bis-(2-pyridinyl)pyrazine (2,3-dpp-**15**),[116,126] and is attributed to a lowering of the π* orbitals of the bridging ligand by coordination of the second $Ru(bpy)_2^{2+}$. Similarly, the weaker shoulders at 544nm in **64** and 558nm in **65** have been detected in other binuclear complexes and numerous explanations have been offered for these weaker transitions.[30,33] The higher energy absorptions around 412nm for **64** has been previously assigned as a dπ–π*bpy with the observed blue shift relative to the mononuclear complex rationalised by assuming a small additional electrostatic energy required to remove the optical electron from one Ru^{2+} ion to an adjacent bpy and thus further from the other Ru^{2+}.[36] This blue shift is also observed for the dπ-dmbπ* transition of **65**, whilst the dmb electron donating methyl groups also lower the dπ-π*(**40**) transition (596nm) further by metal d orbital destabilisation.

Table 2.5. Absorption Maxima[a] and Redox Potentials[b] for **38**, **64** and **65**..

	λ	E_{ox2}	E_{ox1}	E_{red1}	E_{red2}	E_{red3}	E_{red4}	$\Delta E_{ox\text{-}red}$
38	411,545sh,594	+1.69	+1.53	-0.41	-1.08	c	c	1.94
64	412,544sh,578	+1.68	+1.48	-0.55	-1.21	-1.63[d]	c	2.03
65	414,558sh,596	+1.59	+1.39	-0.59	-1.25	-1.72[d]	-2.17	1.98

[a] In nanometres. [b] In volts vs SCE in acetonitrile. [c] Not observed. [d] Two electrons

Ligand bridged binuclear complexes such as **64** and **65** also show metal-metal interactions which are mediated by the π-system of the bridging ligand and depend on the metal-metal distance, the extent of conjugation between the coordination sites and the charge and π-donor/acceptor properties of the bridging ligand. Molecular modelling studies using

CHEM3D-PLUS found the inter-metal separation of the two complexes to be 5.6Å, which is comparable with the inter-metal separation observed in bipyrimidine bridged complexes.[50-55] On this basis **64**, **65** and **38** would be expected to exhibit similar metal-metal interactions.

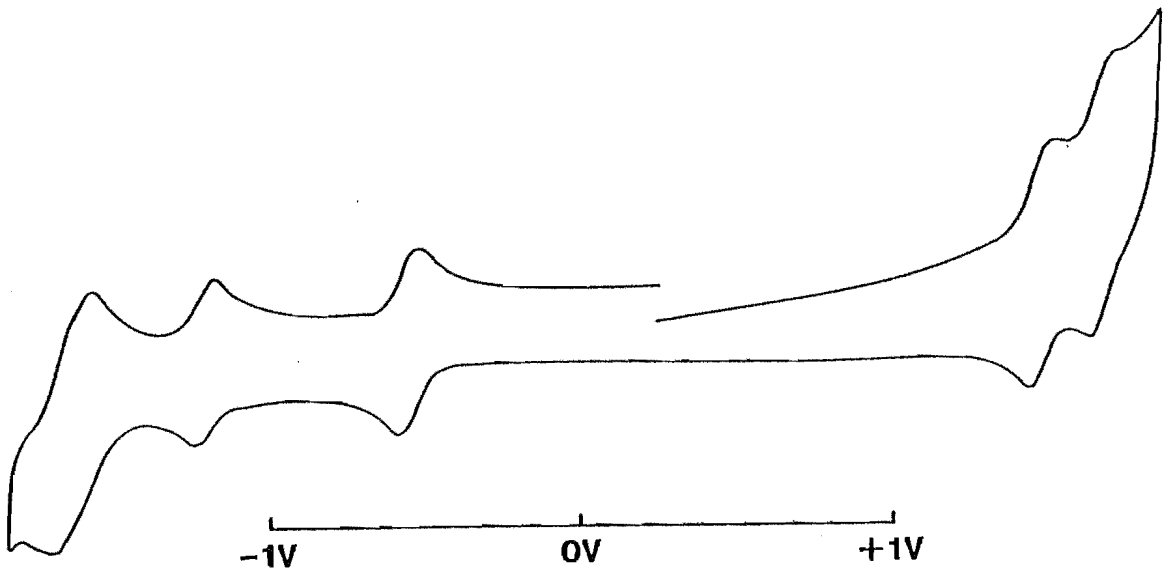

Figure 2.12 Cyclic Voltammogram of **64**.

The degree of metal-metal interaction can be shown in the splitting of the metal-based oxidation potentials ($\Delta E_{1/2}$), which is illustrated in the cyclic voltammogram of **64** (Figure 2.12) and in Table 2.5, which summarises the electrochemistry of **64** and **65**. For the binuclear complex **64** the metal-based oxidations are split into two reversible oxidations, with E_{ox1}=1.48V and E_{ox2}=1.68V ($\Delta E_{1/2}$=200mV), indicating a strong interaction. The splitting of oxidation potentials of binuclear complexes is an indication of the stability of the mixed valence intermediate $(bpy)_2$Ru(II)(**40**)Ru(III)$(bpy)_2^{5+}$.[18] In related complexes this has been attributed to strong back-donation by the electron-rich ruthenium(II) into the bridging ligand π^* orbitals (LUMO) causing an increase in ligand field strength at the other coordination centre,[199] thus lowering the reduction potential for the ruthenium(III) fragment and increasing the difference between both potentials.[32,33] The reduction potential of the Ru(III) fragment or the mixed valence Ru(II)Ru(III) state, equates with the first oxidation, E_{ox1}, in Table 2.5. For **64** this potential is 50mV lower than for the related complex $[Ru(bpy)_2]_2(\mathbf{5})^{4+}$ (**38**) (1.53V); thus in **64** there is a stronger metal-metal interaction ($\Delta E_{1/2}$=200mV) than in **38** ($\Delta E_{1/2}$=160mV). The greater electron density electron at the π^* LUMO of the bridge, which is due to the electron donating methyl groups of **40**, accounts for this additional stabilisation of the Ru(II)/Ru(III) state of **64**. This is consistent with the work of Kaim *et al.*, who have demonstrated conclusively, for a group of structurally related binuclear complexes, that the electron density at the coordination centres in

the LUMO of the bridging π ligand correlates with K_c.[32,33] Like $\Delta E_{1/2}$, the comproportionation constant K_c is a measure of the stability of the mixed valence state and is related to $E_{1/2}$ by the equation $K_c=\exp[\Delta E_{1/2}\ (mV)/25.69mV]$. In **65** the dmb ligands cause the oxidation at each metal centre (Table 2.5) to be ≈100mV less than the same oxidations of **64**, for reasons already described.

The coordination of a second polarizing $Ru(bpy)_2^{2+}$ fragment constitutes a strong perturbation to the π system of the bridging ligand[33] and thus decreases the electron density of **40**. The reduction of the bridging ligand in **64** and **65**, which is represented by the first reversible one electron reductions at -0.55 and -0.59V respectively (Table 2.5), is therefore easier than reduction of **40** in the corresponding monoruthenium(II) complexes. This result is reflected in the large red shift of the lowest energy MLCT of **64** and **65** (Table 2.5). The second reversible reduction of **64** and **65** is attributed to a second one electron reduction of the bridging ligand. Successive reductions of the terminal ligands occur at more negative potentials with closely spaced reductions often appearing as two-electron waves. For example, the third and fourth reductions of **64** (Figure 2.12) appear as one reversible two-electron wave ΔEp=140mV.

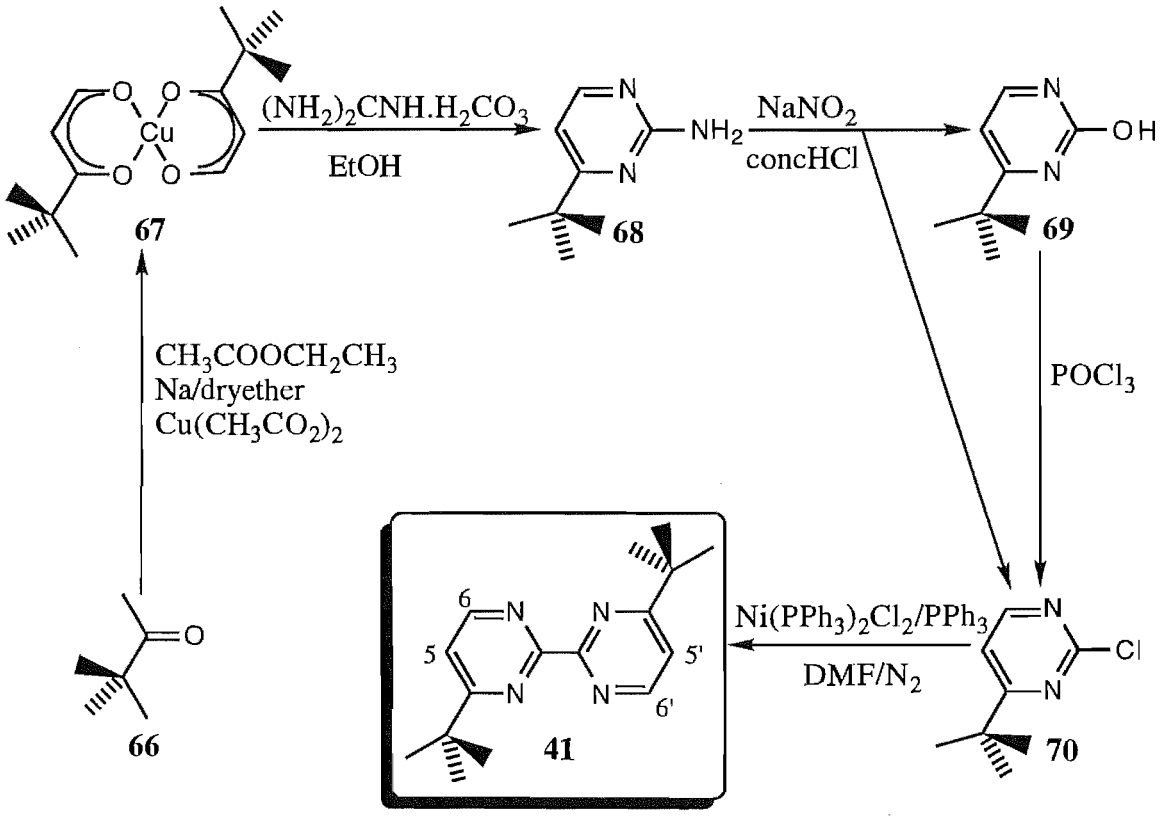

Scheme 2.4

The second ligand investigated was **41** and Scheme 2.4 details its synthesis from pinacolone (**66**) in which the first three steps are known literature procedures.[200,201,188] In an

analogous manner to that used in the synthesis of **40**, the side product **69** was chlorinated in refluxing $POCl_3$ to yield additional **70**. The compound $Ni^0(PPh_3)_2$ was generated from the reduction of $Ni^{II}(PPh_3)_2Cl_2$[202] by Zn in oxygen free DMF and used to couple **70** to give **41** in low yield. This method has been used to couple related heteroaryl halides.[153,203,194] The related coupling method successfully used in the synthesis of **40** was completely ineffective at coupling **70**, whilst the coupling reaction in Scheme 2.4 was found to be very irreproducible.

The ligand **41** was characterised by mass spectrometry and its ^1H and ^{13}C NMR spectra assigned by comparison with the related ligand **40**. A study of the coordination chemistry of **41** was begun by synthesising a monomolybdenum(0) complex (Scheme 2.5). Reaction of **41** with either one or two equivalents of $Mo(CO)_4(\eta^4\text{-}C_7H_8)$ gave the same red complex which was shown by ^1H NMR spectroscopy to have the structure **71** in which the ligand exhibits symmetrical N1-N1' coordination to molybdenum(0), similar to **58**. Hence the large substituents of **41** have significantly restricted the choice of coordination sites for octahedral metals. Like **58**, the complex **41** was also unstable and therefore no elemental analysis was obtained.

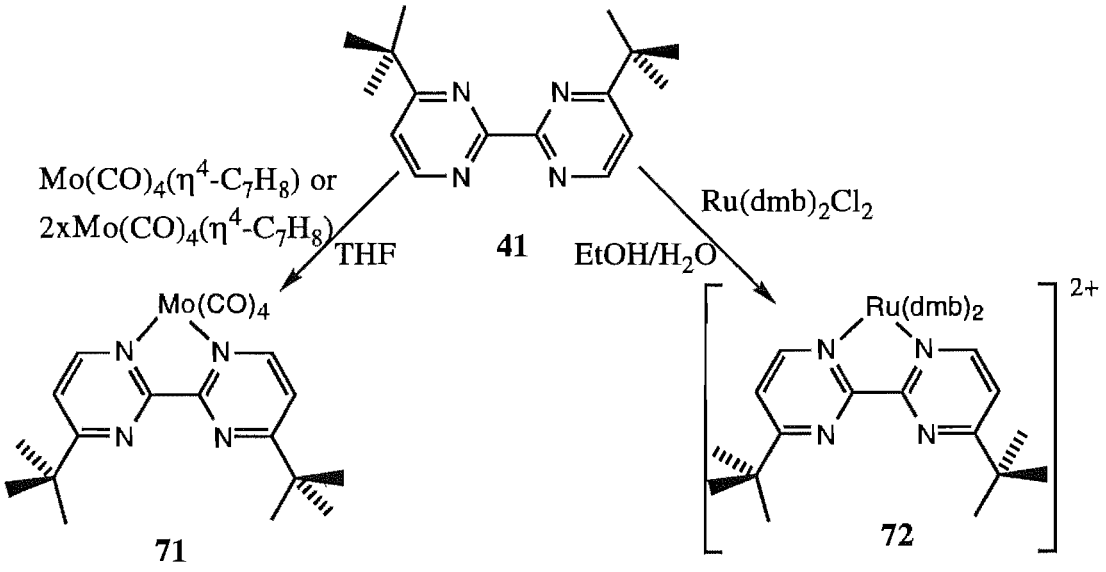

Scheme 2.5

The reaction of **41** with one equivalent of $Ru(dmb)_2Cl_2$ gave, in good yield, a red complex which was isolated as a hexafluorophosphate salt. This complex was shown by mass spectrometry to be mononuclear and from its ^1H NMR spectrum was assigned the structure **72**, in which the octahedral metal occupies the most sterically accessible N1-N1' coordination sites. The ^1H NMR spectrum was readily assigned by comparison with the spectrum of **60**. The ^{13}C NMR spectrum of **72** was assigned by comparison with the ^{13}C NMR spectra of related complexes.[11] Thus, unlike the corresponding reaction of **40**, which gave a mixture of isomers **62/63**, the ligand **41** gave a single complex as a result of the greater steric demand of the t-butyl substituents.

In the UV/VIS spectrum of **72** the unsymmetrical absorption (λ>400nm) is a combination of a higher energy dπ-π*(dmb) MLCT (442nm) and a lower energy dπ-π*(**41**) MLCT, which shows up as a shoulder (480nm). This behaviour is similar to that observed in the UV/VIS spectrum of **62/63**. Analogous to **62/63**, the cyclic voltammogram of **72** consists of a reversible one-electron oxidation (1.17V), reversible reduction of **41** (-1.23V), two successive reversible dmb reductions (-1.68 and -1.90V) and finally irreversible reduction of **41** (-2.11V). The slight increase in the ease of oxidation and decrease in the ease of reduction, relative to **62/63**, reflects the differences in the electron donating abilities of the t-butyl and methyl groups.

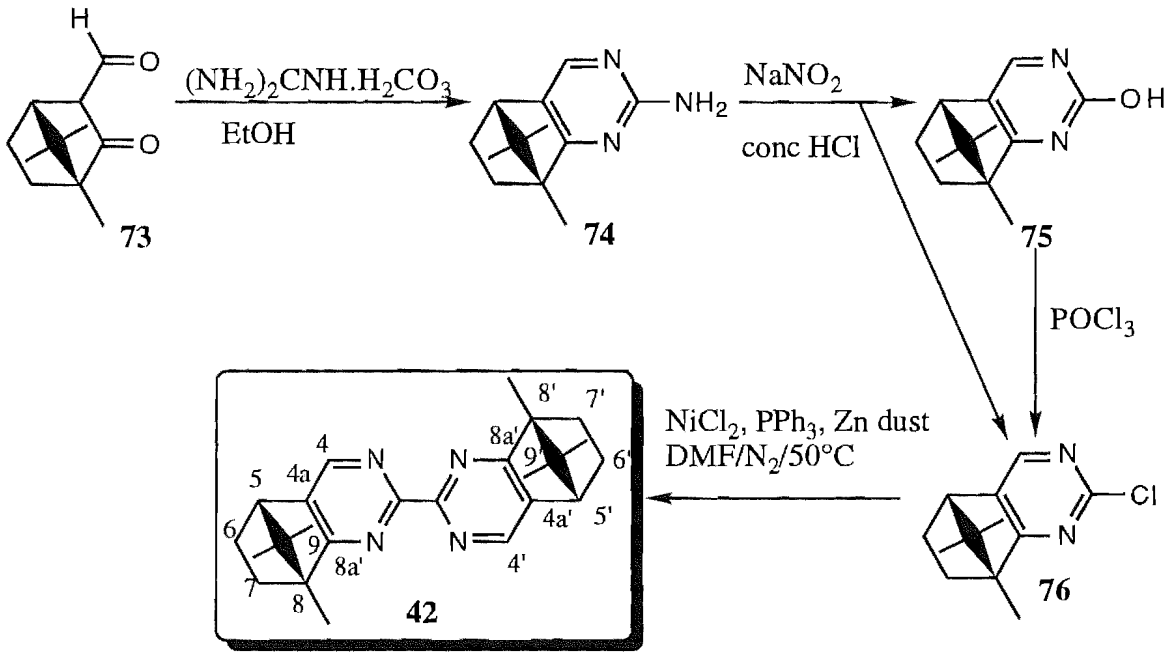

Scheme 2.6

The synthesis of a third disubstituted bipyrimidine, **42**, is shown in Scheme 2.6. The amine **74** was formed by heating formyl camphor (**73**) with guanidine carbonate at 120° in the first step. The diazotization method described in Schemes 2.1 and 2.4 was then applied to **74** to give a mixture of **75** and **76** which were separated by chromatography on silica. Additional **76** was obtained from **75** in refluxing $POCl_3$. The coupling of **76** to give **42** was found to be more successful than the coupling of **70** (Scheme 2.4), and was accomplished using *in situ* generated $Ni^0(PPh_3)_2$[189] as described above for the synthesis of **40**.

The ligand **42** was characterised by mass spectrometry and its ^1H and ^{13}C NMR spectra were assigned by comparison with the spectra of **40** and related chiral ligands containing a camphor group.[204]

Reaction of **42** with one equivalent of $PdCl_2$ in hot HCl gave a yellow complex which was characterised by elemental analysis (Scheme 2.7). Although the complex was found to be

insoluble in common NMR solvents, its structure is most likely **77** given the large size of the camphor substituents. The proposed structure **77** is supported by the observed structure of the mono-molybdenum(0) complex **78**, which was prepared from reaction of **42** with either one or two equivalents of $Mo(CO)_4(\eta^4\text{-}C_7H_8)$. The ^1H NMR spectrum of **78** indicated the symmetrical mononuclear structure shown. Again no elemental analysis of **78** was obtained because of the instability of the complex.

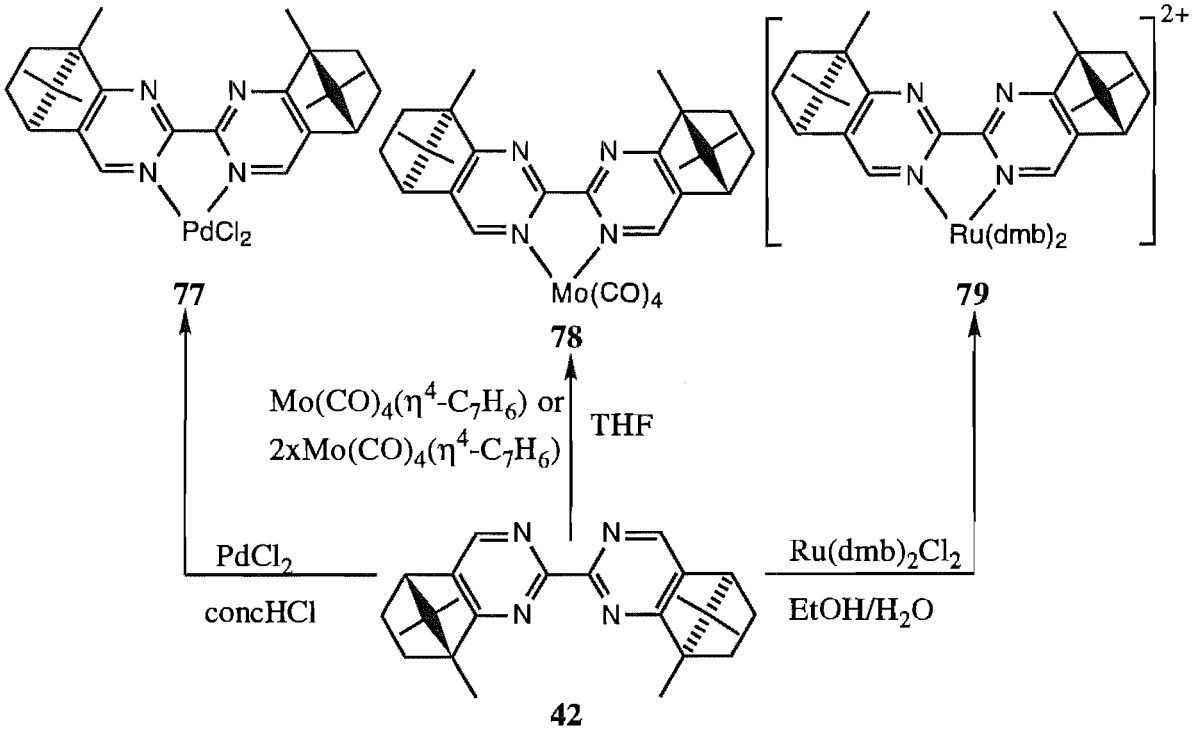

Scheme 2.7

The ruthenium(II) complex **79** was prepared by reaction of **42** with one equivalent of $Ru(dmb)_2Cl_2$ and isolated as a red hexafluorophosphate salt. Analysis by mass spectrometry confirmed that this complex was mononuclear, whilst the symmetrical N1-N1' coordination shown was confirmed by the ^1H and ^{13}C NMR spectra which were assigned by comparison with the spectra of **62**, **72**, and with the spectra of related free ligands[204] and complexes.[11]

For a complex of the form $RuL(dmb)_2^{2+}$ with an achiral bidentate ligand L, the Δ and Λ forms are enantiomeric and hence equivalent in the ^1H NMR spectrum. As a consequence of the chirality of **42**, the Δ and Λ forms of the complex **79** are diastereoisomeric and therefore distinguished in the ^1H NMR spectrum (Figure 2.13). For example, the H4 protons of the diastereoisomers are observed as two singlets at 7.65 and 7.68ppm. Only the two most upfield singlets could be unambiguously assigned to the Δ and Λ forms. In this case the Δ-syn-9-CH_3 proton (0.36ppm) is positioned above a pyridine ring and more shielded relative to the Λ-syn-9-

CH_3 proton (0.77ppm) which is coplanar to a pyridine ring. The complete assignment of the ^1H NMR spectrum of the mixture of diastereoisomers of **79** can only be achieved by physical separation of the Δ and Λ forms. No attempt was made to separate these diastereoisomers.

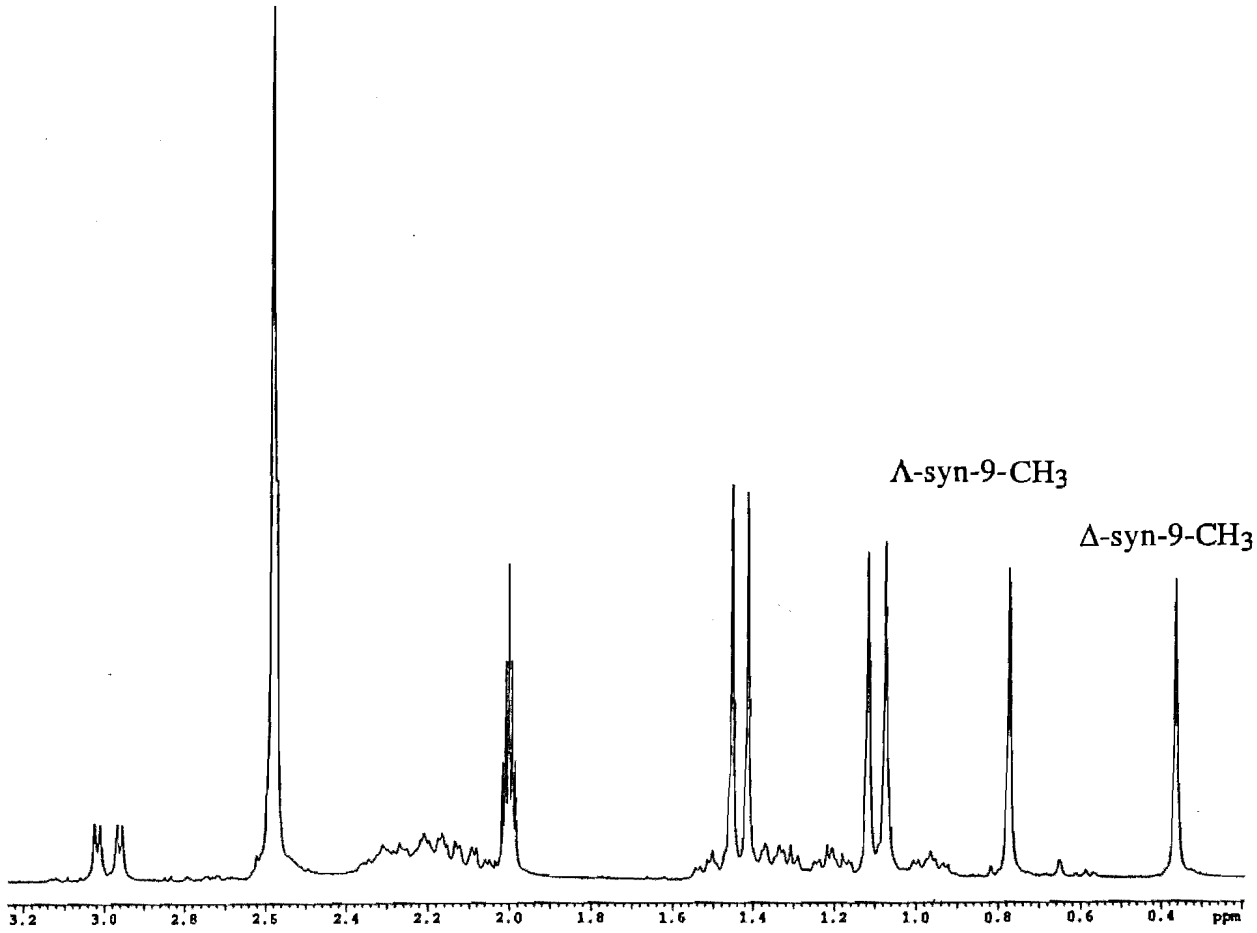

Figure 2.13 ^1H NMR Spectrum of **79**.

The complex **79** exhibits an absorption centred around 456nm, which is at lower energy and appears more symmetrical than those of **62/63** and **72**, with no shoulder corresponding to dπ-π*(**42**) visible at lower energy. Again, as seen previously, this absorption is probably a combination of MLCT transitions into the ligand **42** and the dmb ligands.

The cyclic voltammogram of **79** comprises a reversible one-electron oxidation (1.12V) and three reversible one-electron reductions (-1.39, -1.69 and -1.92V). The fourth irreversible reduction, seen in the voltammograms of **62/63** and **72**, was not observed for this complex. This complex is slightly easier to oxidise than **62/63** and **72** but harder to reduce, which reflects increased metal d orbital destabilisation and even greater destabilisation of the π* orbitals of **42** by having one more substituent per pyrimidine ring relative to **40** and **41**.

A heterobinuclear complex was also synthesised (Scheme 2.8). Treatment of the complex **79**, in dichloromethane, with one equivalent of $HgCl_2$, in acetone, gave a red solid, the ^1H NMR

spectrum of which showed very small differences in chemical shift relative to the ^{1}H NMR spectrum of **79**. This is interpreted in terms of a heterobinuclear complex **80**, with tetrahedral N3-N3' coordination of mercury and octahedral N1-N1' coordination of ruthenium(II) to the bridging ligand. However, **80** gave an unsatisfactory elemental analysis due to the presence of mercury salt impurities whilst mass spectrometry of **80** was inconclusive, due to the extreme lability of the Hg-N bond.

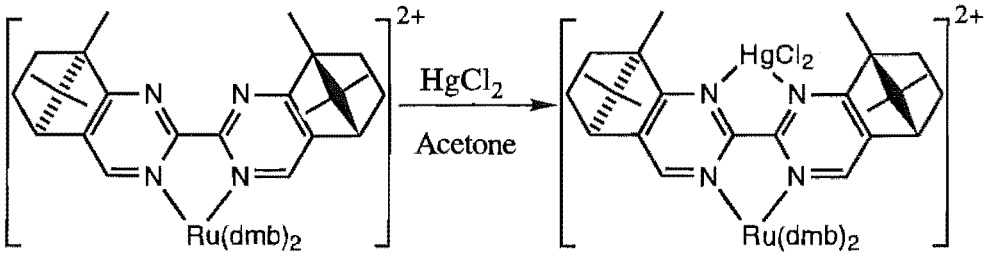

79 **80**

Scheme 2.8

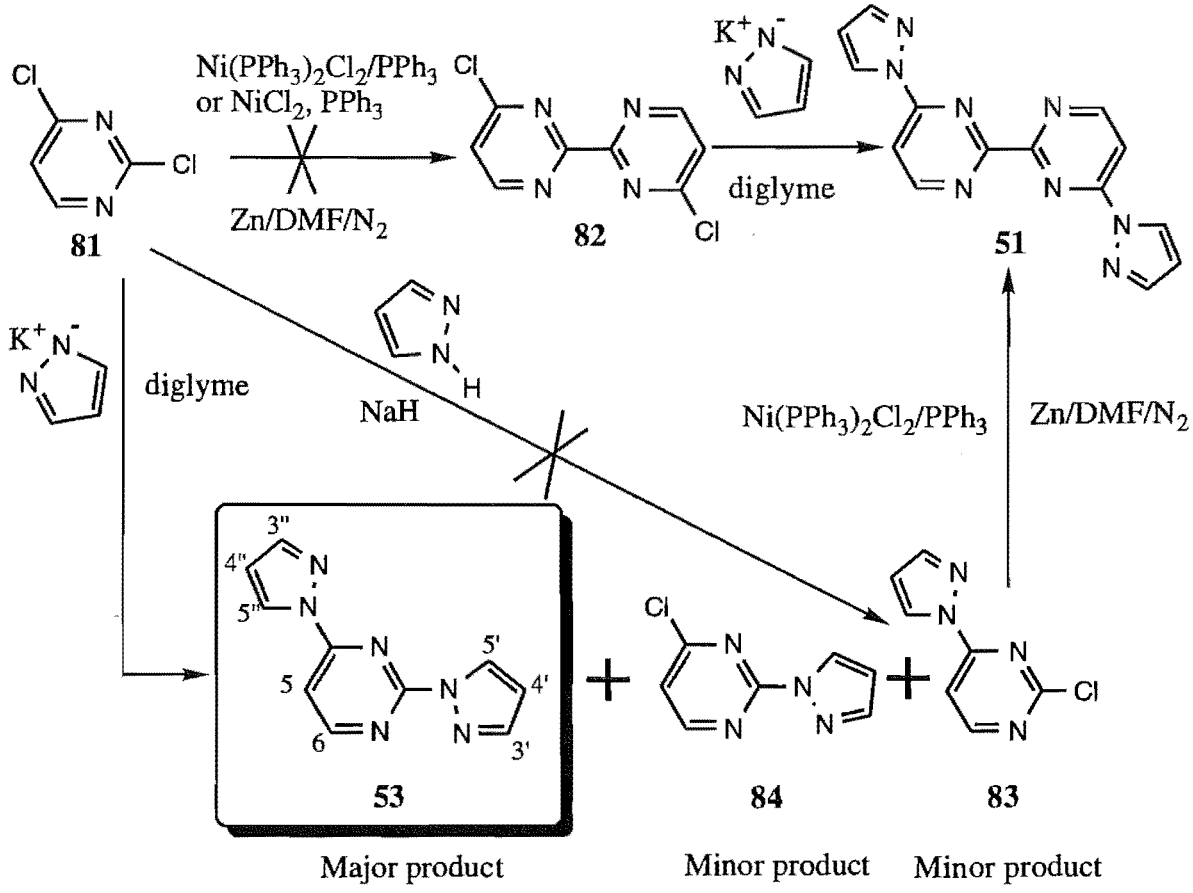

Scheme 2.9

The quaterheterocycle **51** was the next ligand to be investigated, for which two possible synthetic routes were envisaged. It was hoped that the coupling of 2,4-dichloropyrimidine (**81**) using $Ni^0(PPh_3)_2$ would produce 4,4'-dichloro-2,2'-bipyrimidine (**82**) (Scheme 2.9), which

could then be reacted with two equivalents of potassium pyrazolate to give **51**. However all attempts to couple **81** using the $Ni^{II}(PPh_3)_2Cl_2$ precursor or by generating $Ni^0(PPh_3)_2$ *in situ* from $NiCl_2$ and PPh_3 were unsuccessful. Alternatively (Scheme 2.9), we intended to synthesise 2-chloro-4-(1-pyrazolyl)pyrimidine (**83**) by reaction of **81** with one equivalent of potassium pyrazolate followed by $Ni^0(PPh_3)_2$ catalysed coupling of **83** to give **51**.

The potassium pyrazolate salt was prepared by reacting pyrazole with potassium in dry DMF at 70°C and reacted with **81** under reflux. Analysis of the crude reaction mixture by ^1H NMR indicated a complex mixture of products which was then separated by radial chromatography on silica. The major product from this reaction was found to be 2,4-bis-(1-pyrazolyl)pyrimidine (**53**), whilst the desired product 2-chloro-4-(1-pyrazolyl)pyrimidine **83** was obtained in very low yield. Presumably substitution of the first chlorine with a pyrazole activates the second chlorine toward substitution. Additionally, the structural isomer of **83**, 4-chloro-2-(1-pyrazolyl)pyrimidine (**84**), was also obtained in very low yield.

Alternative preparations in which **81** was reacted with pyrazole and NaH in either glyme, THF or acetone also failed to give **83**. Because of these failures and the low yield of **83** in Scheme 2.9, the synthesis of **51** was abandoned.

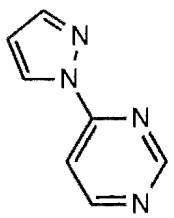

85

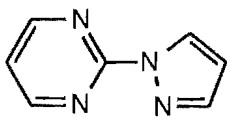

86

The two structural isomers, **83** and **84**, were characterised by mass spectrometry and distinguished by their ^1H NMR spectra in $CDCl_3$. For both compounds the pyrazole ring can be easily assigned given that the H4' proton is a doublet of doublets and of the two doublets, H3' and H5', H3' has a smaller coupling constant to H4' than does H5'. Of the two pyrimidine ring protons, the more electron deficient H6 proton was assigned to the downfield doublet. There exists a significant difference in the chemical shift of the H5 proton which is at 7.25ppm in **84** but is further downfield at 7.87ppm in **83** and these were assigned by comparison with the spectra of the related known ligands **85** and **86**.[205] In this case the H5 (7.87ppm) of **85** has the same chemical shift as H5 (7.87ppm) of **83**, whilst the H5 (7.25ppm) of **84** is 0.06ppm downfield of H5 (7.19ppm) of **86**, due to the effect of the chlorine in the 4-position.

To synthesise **52**, the methylene bridged analogue of **51**, the methyl groups of **40** needed to be functionalised. However, attempts at the radical bromination of **40** using light initiated or dibenzoyl peroxide initiated N-bromosuccinamide were unsuccessful. Given this result and the unsuccessful attempts at oxidation and brominations of **40**, reported in a contemporary paper,[206] the synthesis of **52** was also abandoned.

The major product **53** of the above reaction is, however, a potentially useful ligand, which was characterised by mass spectrometry and ^{1}H and ^{13}C NMR spectroscopy. In the ^{1}H NMR (CD_3CN) spectrum of **53**, H5 (7.84ppm) and H6 (8.83ppm) were easily located, whilst the pyrazole ring systems were assigned by homonuclear decouplings of the pyrazole H4 protons. This, however, did not assign the position of each pyrazole ring system on the pyrimidine ring. No nOe could be observed from either of the pyrazole H5's to the pyrimidine H5, nor could the long-range C4 to H5" or C2-H5' couplings be detected in an HMBC experiment. However, the ^{13}C NMR spectrum of **53** was assigned by comparison with the ^{13}C NMR spectra of **85** and **86**.[205] This result enabled assignment of the pyrazole rings protons in the ^{1}H NMR spectrum by correlation to the pyrazole carbons using a 2D HMQC spectrum. In this manner, the pyrazole ring system with the lowest chemical shifts for each proton was assigned as H3', H4' and H5' (Table 2.6). The ^{13}C NMR spectrum was assigned by correlation to the ^{1}H NMR spectrum in an HMQC experiment.

The coordination chemistry of **53** with ruthenium(II) was investigated by preparing the complexes **87** and **88** in an analogous manner to the ruthenium(II) complexes already described (Scheme 2.10). The complexes were obtained, in good yields, as yellow solids and characterised by mass spectrometry.

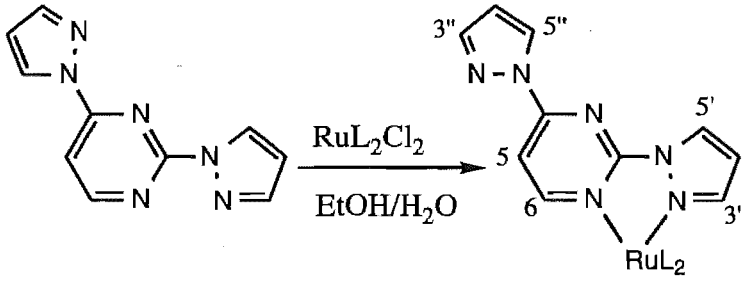

53 **87** L=bpy
88 L=dmb

Scheme 2.10

The ^{1}H NMR spectrum (Figure 2.14) of **87** consists of 24 non-equivalent protons some of which are overlapping. The ruthenium(II) coordinates through the most accessible N1-N2' nitrogens of the ligand, which was confirmed by the absence of an nOe from H5" to H5. Any

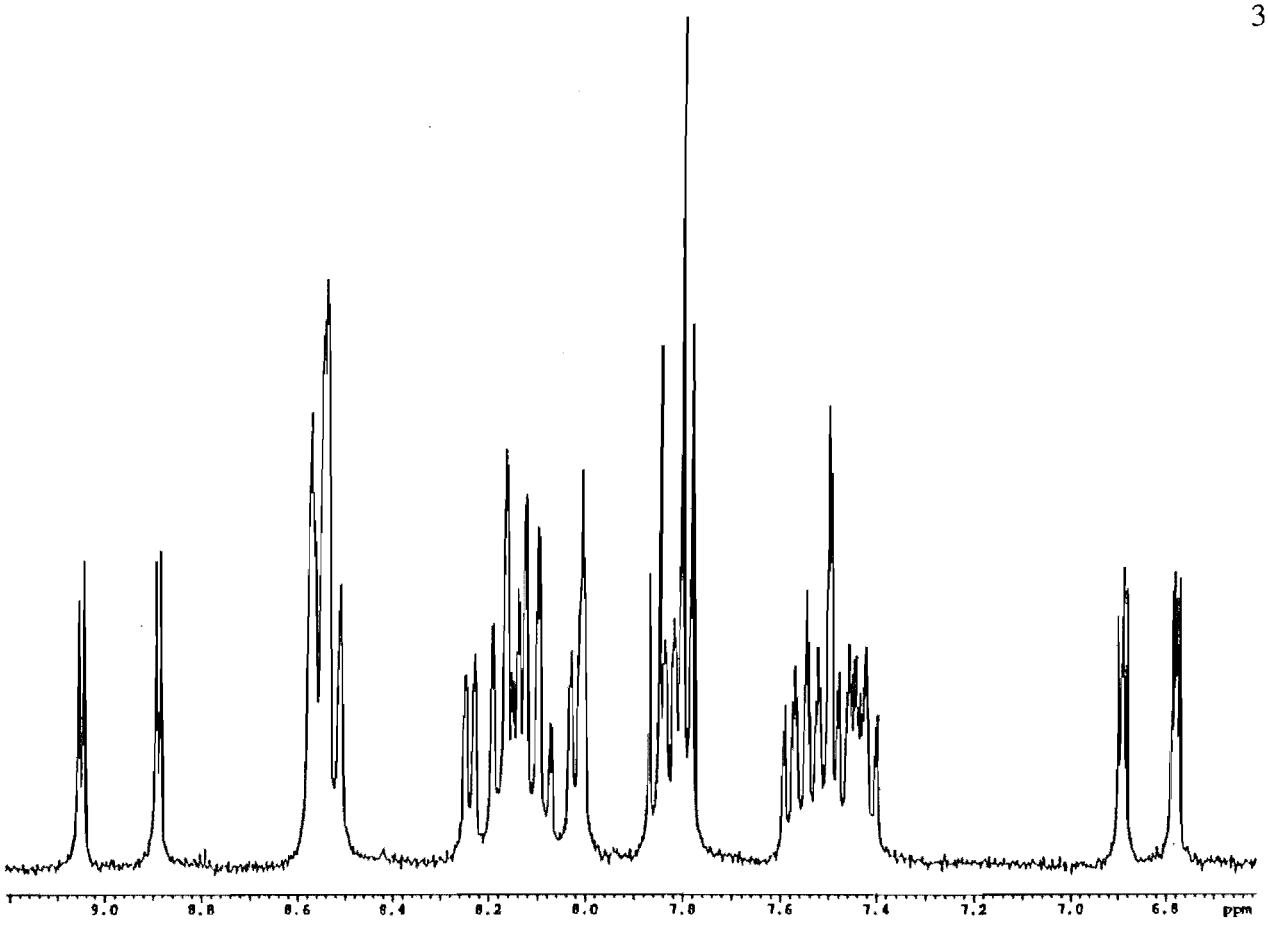

Figure 2.14 ^{1}H NMR Spectrum of **87**.

enhancement of H5 would denote N3-N2" coordination of ruthenium(II), but the absence of an nOe implies that the 4-pyrazole ring is in the non-chelating orientation shown in the structure **87**. In the spectrum of **87**, the H4' and H5' protons would be expected to be downfield of the H4" and H5" protons, reflecting the σ-donation of electron density from the coordinated pyrazole ring to the metal, relative to the free pyrazole ring. The H3', which is above a pyridine ring, would be expected to be upfield of H3" as a result of interligand through-space ring current anisotropy. The 1D TOCSY experiment (Figure 2.15) confirms this. Irradiation of the H5' doublet (9.06ppm) (trace I) shows up the H4' doublet of doublets (6.89ppm) and the H3' doublet (7.50ppm), thus locating the coordinated pyrazole ring and demonstrating the substantial coordination induced shifts of H3' (-0.38ppm), H4' (+0.27ppm) and H5' (+0.29ppm). Similarly the spin system of the non-coordinated ring can be located as H5" at 8.90ppm (+0.12ppm), H4" at 6.78ppm (+0.11ppm) and H3" at 8.01ppm (+0.09ppm) by irradiating H5" (trace II). The AB quartet at 7.79ppm (-0.05ppm) and 7.86ppm (-0.97ppm) was assigned to the H5 and H6 protons respectively. Molecular models show that the H6 proton is much closer to a pyridine ring than H5 and therefore exhibits a greater CIS. The small positive CIS of H5 reflects the combined effects of σ-donation and ring-current anisotropy. The spectrum of **87** is summarised in Table 2.6. The 1D

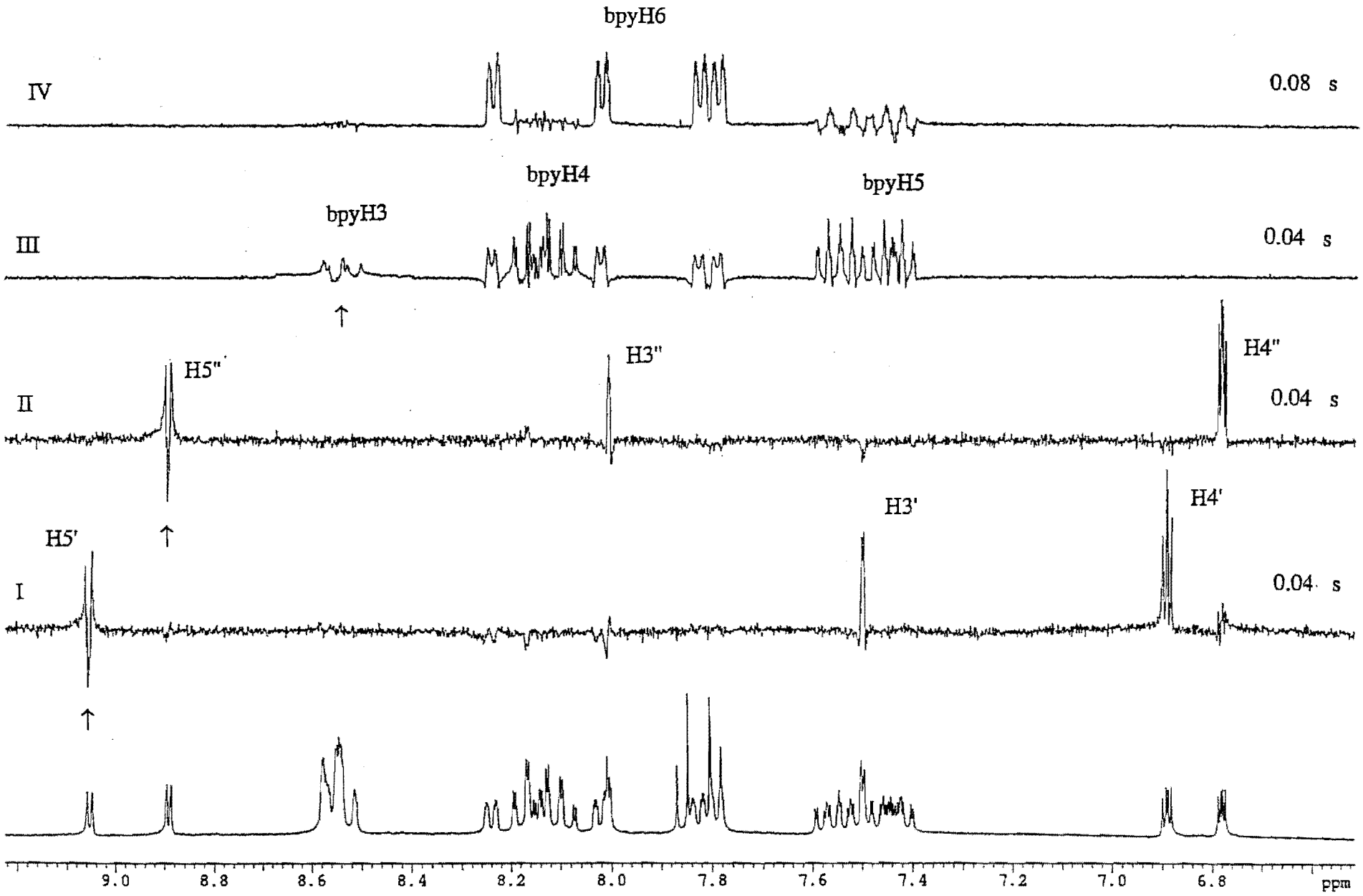

Figure 2.15 1D TOCSY Spectra of 87

TOCSY spectra also demonstrate the effect of the ligand **53** on the chemical shift of the bpy ligands and resolves these protons from overlapping multiplets (trace III and IV). For example, the bpyH6 protons (trace IV) are spread out in the spectrum due to the varied ring current effects of pyridine, pyrimidine and pyrazole rings. Once located by 1D TOCSY spectra the pyridine ring systems, but not the individual rings, were assigned using a COSY spectrum.

The ^{1}H NMR spectrum of the complex **88** was similarly assigned by 1D TOCSY and COSY spectra and is summarised in Table 2.6. A homoleptic complex $Ru(\mathbf{53})_3^{2+}$ (**89**) was synthesised by reacting three equivalents of **53** with $Ru(DMSO)_4Cl_2$ and was isolated as a yellow hexafluorophosphate salt. The complex **89** was characterised by mass spectrometry and ^{1}H NMR spectroscopy.

Table 2.6. ^{1}H NMR Chemical shifts[a] and Coordination Induced Shifts[b] of **53**, **87** and **88**

	H5	H6	H3'	H4'	H5'	H3''	H4''	H5''
53	7.84	8.83	7.88	6.62	8.77	7.92	6.67	8.78
87	7.79	7.86	7.50	6.89	9.06	8.01	6.78	8.90
CIS[b]	-0.05	-0.97	-0.38	+0.27	+0.29	+0.09	+0.11	+0.12
Bpy ligands								
H3		H4		H5		H6		
8.53		8.10		7.42		7.79		
8.56		8.13		7.46		7.83		
8.56		8.17		7.55		8.24		
8.56		8.17		7.57		8.02		
88	7.79	7.87	7.47	6.88	9.04	8.00	6.78	8.89
CIS[b]	-0.05	-0.96	-0.41	+0.26	+0.27	+0.08	+0.11	+0.11
Dmb ligands								
H3		4-CH_3[c]		H5		H6		
8.37		2.62[c]		7.25		7.59		
8.40		2.61[c]		7.29		7.62		
8.40		2.59[c]		7.34		8.03		
8.40		2.58[c]		7.38		7.82		

[a] For deuterated acetonitrile solutions. [b] $CIS=\delta_{complex}-\delta_{ligand}$. [c] Methyl group not assigned

The ^{1}H NMR spectrum of **89** was complicated by the presence of two isomers. In such complexes the coordination of three unsymmetrical ligands produces the meridonal (mer) and facial (fac) isomers in a statistical ratio (mer:fac) of 3:1. This ratio is observed for **89** in the ^{1}H NMR spectrum, which was tentatively assigned by comparison with the spectra of **53** and **87**.

Table 2.7 summarises the UV/VIS spectra and cyclic voltammetry of **87**, **88** and **89**. Included in the table are data for the related complexes $Ru(bpy)_3^{2+}$ and $Ru(\mathbf{86})(bpy)_2^{2+}$.[6,207,11]

All complexes show strong ligand centred absorptions at less than 300nm. The heteroleptic complexes have low energy absorptions with maxima at 412 nm and 418nm respectively with shoulders either side of the maxima. These absorptions were assigned as MLCT bands and are at higher energy than the MLCT of $Ru(bpy)_3^{2+}$ (451nm). Also the spectra of **87** and **88** were found to resemble the spectra of the ruthenium(II) complexes of structurally related ligands that contain a pyrazole ring.[11] The homoleptic complex has a symmetrical absorption (384nm) analogous to that of $Ru(bpy)_3^{2+}$ (451nm) but, as for **87** and **88**, at much higher energy. These results show that electron transfer from metal to ligand is more difficult for **87-89** than for $Ru(bpy)_3^{2+}$, which reflects the higher energy of the π^* orbitals of **53** relative to bpy.

Table 2.7. Absorption Maxima[a] and Redox Potentials[b] for **87**, **88** and **89**.

Complex	λ	E_{ox1}	E_{red1}	E_{red2}	E_{red3}	E_{red4}	$\Delta E_{ox\text{-}red}$
$Ru(bpy)_3^{2+}$	451	+1.27	-1.31	-1.50	-1.77	c	2.58
$Ru(\mathbf{86})(bpy)_2^{2+}$	370, 410, 430	+1.30	-1.36[e]	c	c	c	2.66
87	386, 412, 430	+1.26	-1.39[d]	-1.58[e]	-1.88[e]	c	2.65
88	386, 418, 428	+1.17	-1.44[d]	-1.65[e]	-1.91[e]	c	2.61
89	386	+1.35	-1.46[d]	-1.61[e]	-1.80[e]	-2.12[e]	2.81

[a] In nanometres. [b] In volts vs SCE in acetonitrile. [c] Not observed. [d] Irreversible. [e] Quasi-irreversible

The complex **87** exhibits a reversible one electron oxidation (+1.26V) and three one electron reductions (-1.39, -1.58, and -1.88V) and is therefore as easy to oxidise as $Ru(bpy)_3^{2+}$ but slightly harder to reduce. The first reduction is irreversible and occurs at slightly more negative potential than the first reduction of $Ru(\mathbf{86})(bpy)_2^{2+}$ which is also irreversible.[11] Reduction of pyrazole-containing ligands is known to lead to ligand dissociation.[12] The oxidation of **88** is 0.09V lower than the oxidation of **87** and its reductions are more negative, an effect which has been previously been described for other $RuL(dmb)_2^{2+}$ complexes in this work. The homoleptic complex **89** exhibits a reversible one electron oxidation at +1.35V and a first reduction at -1.46V. Relative to $Ru(bpy)_3^{2+}$ the increase in oxidation potential implies a lowering of the metal $d\pi$ orbitals of **89**, whilst the increase in the reduction potential implies raising of the π^* LUMO. Thus the complex is both harder to oxidise and harder to reduce than $Ru(bpy)_3^{2+}$ and the $E_{ox\text{-}red}$ value of 2.81 is consistent with the observed higher energy of the MLCT of **89** (386nm), since the same orbitals are known[6] to be involved.

Chapter 3

2-Substituted Perimidine Ligands and Complexes.

2-Substituted Perimidine Ligands and Complexes.

3.1. Introduction.

Binuclear complexes incorporating a bipyrimidine bridge exhibit strong metal-metal interactions, due to the short (5.5Å) inter-metal separation. For example, a strong interaction ($\Delta E_{1/2}$=160mV) is observed between the ruthenium(II) atoms of the complex $[Ru(bpy)_2]_2bpm^{4+}$.[25] Direct overlap of the d_{yz} orbitals, which point toward each other in binuclear bipyrimidine complexes, has been described, by others,[33] as contributing to this interaction. The larger interaction ($\Delta E_{1/2}$=200mV) in the complex **64** has already been described in chapter 2.

By decreasing the charge repulsion in bridged binuclear complexes, the degree of metal-metal interaction may be increased. This has been demonstrated in the complexes of 2,2-bibenzimidazolate (bibzm-**6**).[72] The charge repulsion of the ruthenium(II) atoms of the complex $[Ru(bpy)_2]_2bibzm^{2+}$,[65,72,76] is much less than in the complex $[Ru(bpy)_2]_2bpm^{4+}$, and in combination with the stronger σ donor property of bibzim, contributes to a stronger metal-metal interaction ($\Delta E_{1/2}$=290mV).

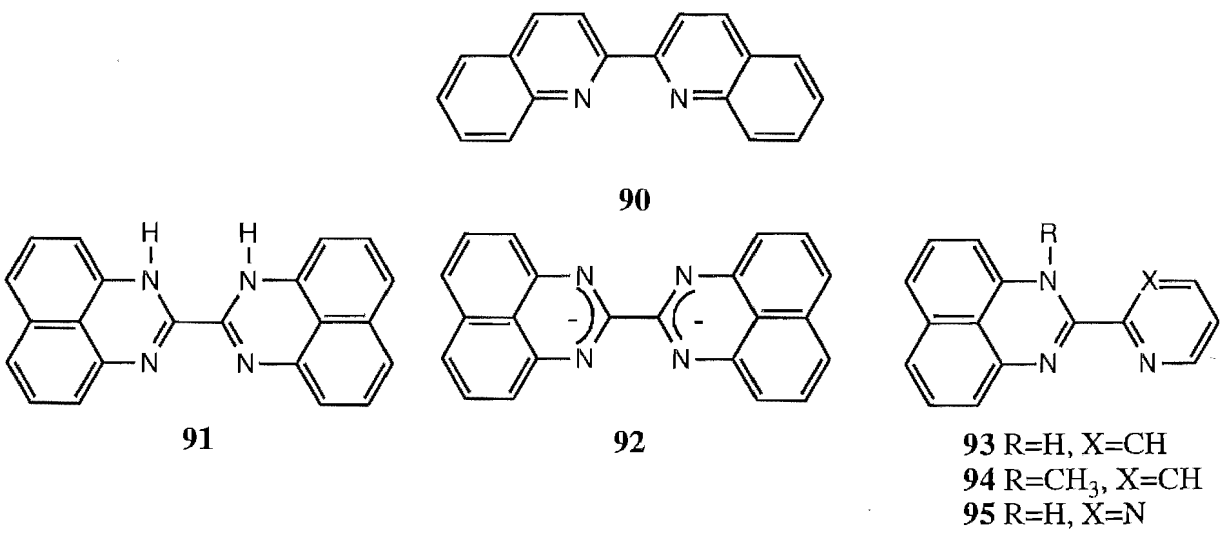

90

91

92

93 R=H, X=CH
94 R=CH_3, X=CH
95 R=H, X=N

Figure 3.1

Benzo-fusion in bidentate ligands has the effect of lowering the energy of the π^* orbitals. For example, the π^* orbitals of 2,2'-biquinoline (**90**) (Figure 3.1), are lower in energy than those of bpy. As a consequence, the ruthenium complexes of **90** have properties which are significantly different to those of $Ru(bpy)_3^{2+}$.[207] Furthermore, benzo-fused bridging ligands should be able to

form binuclear complexes with interesting properties. Since the electron density in the LUMO of the bridging ligand at the coordination centres has been shown to be a major contributor to the metal-metal interactions,[32] ring fusion to a bipyrimidine-like bridging ligand should have the desirable effect of increasing the interaction, by lowering the energy and increasing the electron density of the π^* LUMO.

The known compound 2,2'-biperimidine ($bipH_2$, **91**)[208,209,210] (Figure 3.1) is a potential bridging ligand which would incorporate the properties described above. To act as a bridge, $bipH_2$ requires double deprotonation to give the dianion (**92**), which would significantly decrease the inter-metal charge repulsion. In addition, the four fused rings of bip lower the energy of the π^* orbitals of the ligand relative to bpm, thus increasing the electron density of the bridge at the coordination centres.

2,2'-Biperimidine was first synthesised by Sachs[208] in 1909 and two further syntheses have since been described.[209,210] A number of substituted monoperimidines have also been reported,[211-214] including 2-(2-pyridinyl)perimidine[211] (**93**), which is a potential mononucleating bidentate ligand. Recent interest has been shown in the tautomerism[213,214] and potential DNA intercalating ability[213] of perimidine derivatives.

We begin this chapter with a detailed study of the mononuclear palladium(II) and ruthenium(II) complexes of **93** (Figure 3.1), as a preliminary to a study of 2-substituted perimidines as binucleating ligands. The syntheses of two new perimidine ligands, **94** and **95** (Figure 3.1), and a study of their palladium(II) and ruthenium(II) complexes are included, whilst attempts to form ruthenium(II) complexes with **91** are also discussed.

3.2. Results and Discussion.

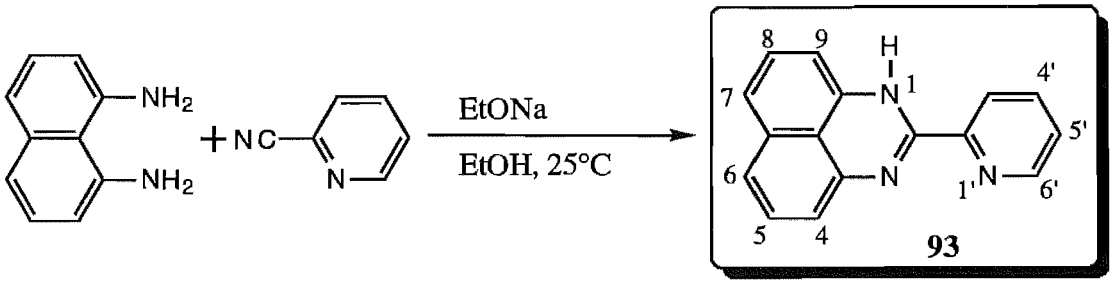

Scheme 3.1

2-(2-Pyridinyl)perimidine (**93**) was prepared by reacting 1,8-diaminonaphthalene with 2-cyanopyridine in a sodium ethoxide solution at room temperature (pH 5-7) (Scheme 3.1), as has

been described by Browne.[212] An intra-molecular hydrogen bond between N1H and N1' of **93** allows coplanarity of the pyridine and perimidine rings, hence the π-electron density is delocalised throughout the molecule. This conjugation lowers the energy of the π^* orbital of **93**, resulting in the deep red colour of the ligand.

The ^{13}C NMR spectrum of **93** in CD_3CN was assigned by comparison with the ^{13}C NMR spectra of structurally related compounds.[213,214] In general, C9 is upfield of C4 in the ^{13}C NMR of known unsymmetrical perimidines and in the spectrum of **93** these carbons were assigned as C9 (103.2ppm) and C4 (115.2ppm). These assignments could then be correlated, using an HMQC spectrum, to the doublets (6.61ppm) and (6.84ppm) in the ^1H NMR spectrum (Figure 3.1), thus locating H9 and H4.

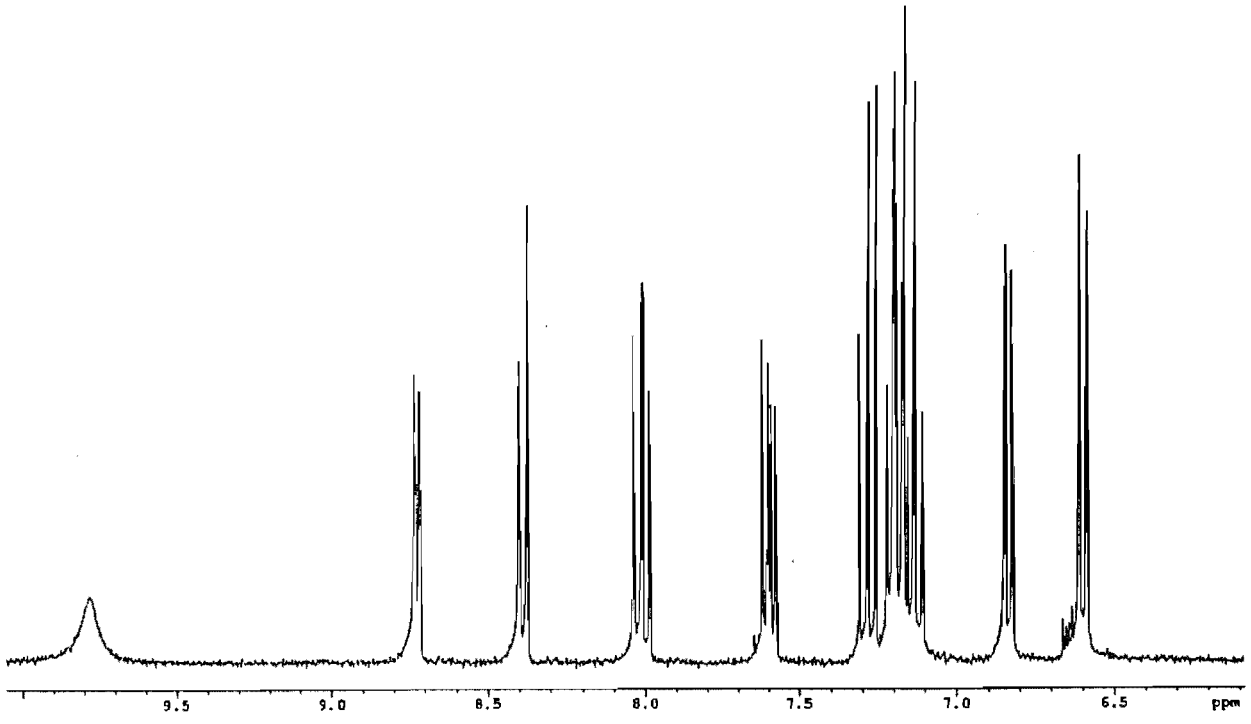

Figure 3.1 ^1H NMR Spectrum of **93**.

The four remaining naphthalene protons of **93** were assigned using 1D TOCSY spectra (Figure 3.2). By irradiating H4 (trace I), both H5 (7.28ppm), and H6 (7.17ppm) can be located and similarly irradiating H9 (trace II) locates H8 (7.19ppm) and H7 (7.17ppm). The H5-H6 coupling constant of a pyridine ring is generally smaller than the H3-H4 coupling constant. This allowed for straight-forward assignment of the pyridine ring protons in the ^1H NMR spectrum of **93** as H3' (8.39ppm), H4' (8.01ppm), H5' (7.60ppm) and H6' (8.73ppm).

Reaction of **93** with one equivalent of $PdCl_2$ in hot HCl gave a brown solid, which was characterised by elemental analysis and proposed to be the complex **96** (Scheme 3.2). The

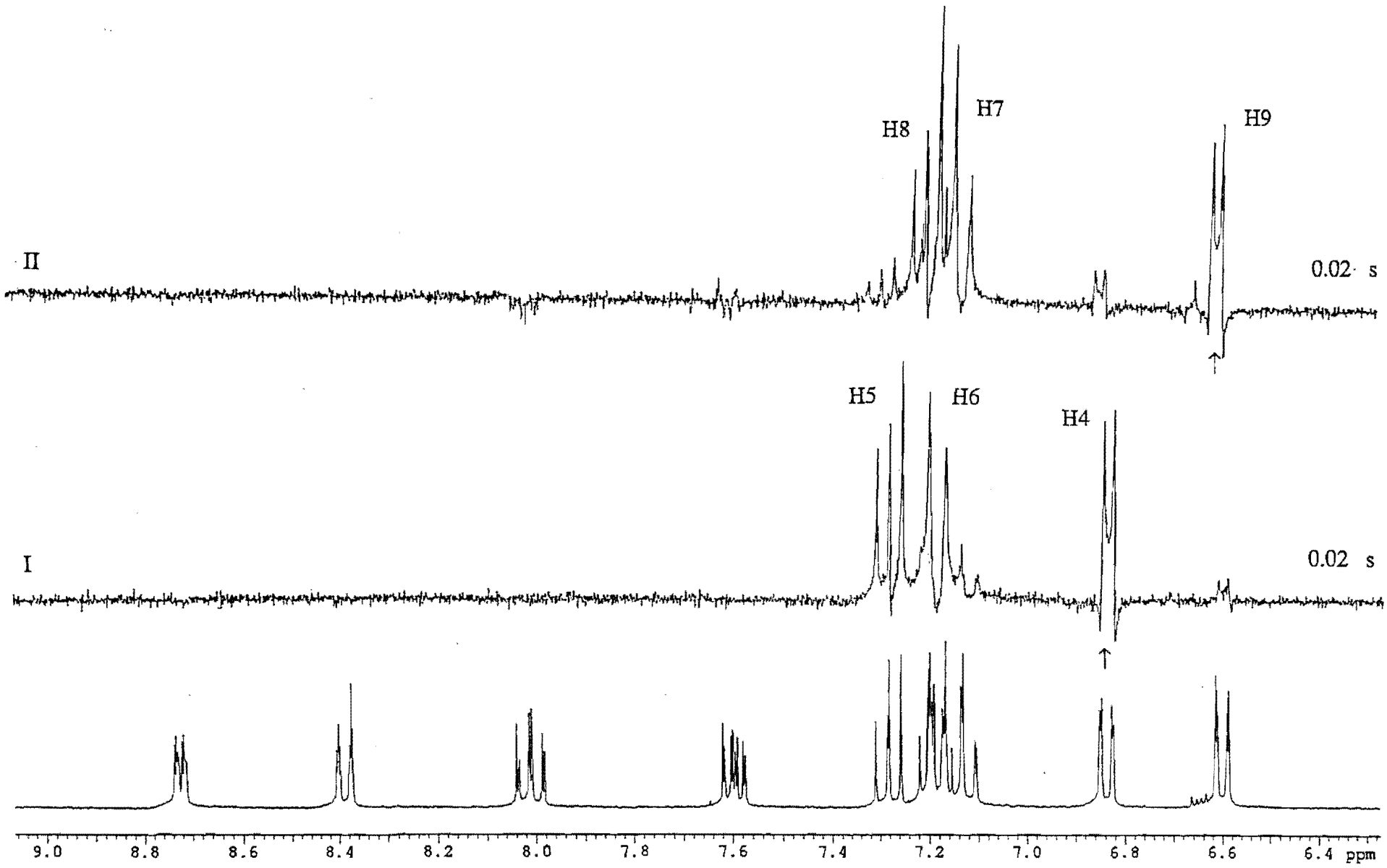

Figure 3.2 1D TOCSY Spectra of **93**

complex was sufficiently soluble in DMSO to be analysed by ^{1}H NMR, but rapidly dissociated in solution with release of the free ligand by cleavage of the Pd-N bonds. The dissociation of **96** is probably assisted by the lability of the N-H bond and caused significant broadening of the signals in the ^{1}H NMR, hence only tentative assignments of the individual protons were possible.

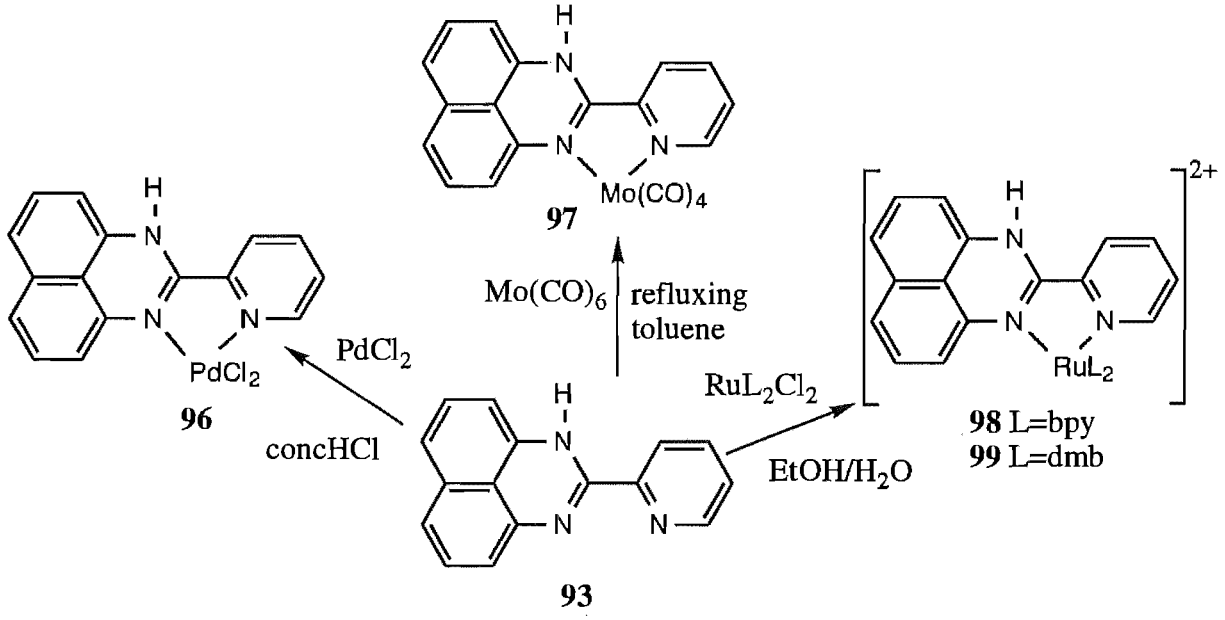

Scheme 3.2

The molybdenum(0) complex **97** was prepared from a 1:1 mixture of **93** and $Mo(CO)_6$ in degassed and refluxing toluene (Scheme 3.2). This method, which has recently been used by Ruminski *et al.*[19] to prepare structurally related complexes, differs from the previous syntheses of **58**, **71** and **78** using $Mo(CO)_4(\eta^4\text{-}C_7H_8)$, as described in the previous chapter. Ruminski *et al.* also described purification of the monomolybdenum(0) and dimolybdenum(0) complexes of dpop (**20**) by chromatography on alumina (eluent=acetone). We have found that **97** undergoes dissociation to the free ligand under these conditions, even with neutral or acidified alumina. In addition purification by recrystallisation in acetone/ether or THF/ether caused dissociation of the complex.

The ^{1}H NMR spectrum (DMSO-d_6) of the crude reaction mixture of **97** was assigned by comparison with the spectrum of the free ligand in the same solvent. Relative to the spectrum of the free ligand, all protons move downfield on coordination. Specifically, the CIS values of **97** are +0.43ppm (H1), +0.74ppm (H4), +0.17ppm (H5), +0.23ppm (H6), +0.25ppm (H7), +0.14 (H8), +0.09ppm (H9), +0.30ppm (H3'), +0.30ppm (H4'), +0.25ppm (H5'), 0.37ppm (H6'), all of which reflect the donation of σ-electron density from the ligand to the metal. The shifts of the naphthalene ring protons imply that delocalised electron density from the fused rings has a significant contribution to the ligand-metal bonding, whilst the CIS values of H6' and H4 are

particularily large due to their close proximity to the deshielding carbonyl groups. In addition, after only five minutes, signals for the free ligand were observed in the ^{1}H NMR spectrum of **97**, implying dissociation of the complex (approximately 50%).

The reaction of **93** with $Ru(bpy)_2Cl_2$ gave the complex **98** (Scheme 3.2). The ^{1}H NMR spectrum of **98** was complicated by the overlap of signals, and by the dissociation of the complex and thus could not be assigned. To assist in the assignment of **98**, the complex **99** was prepared, in which the bpy ligands are replaced with dmb (Scheme 3.2).

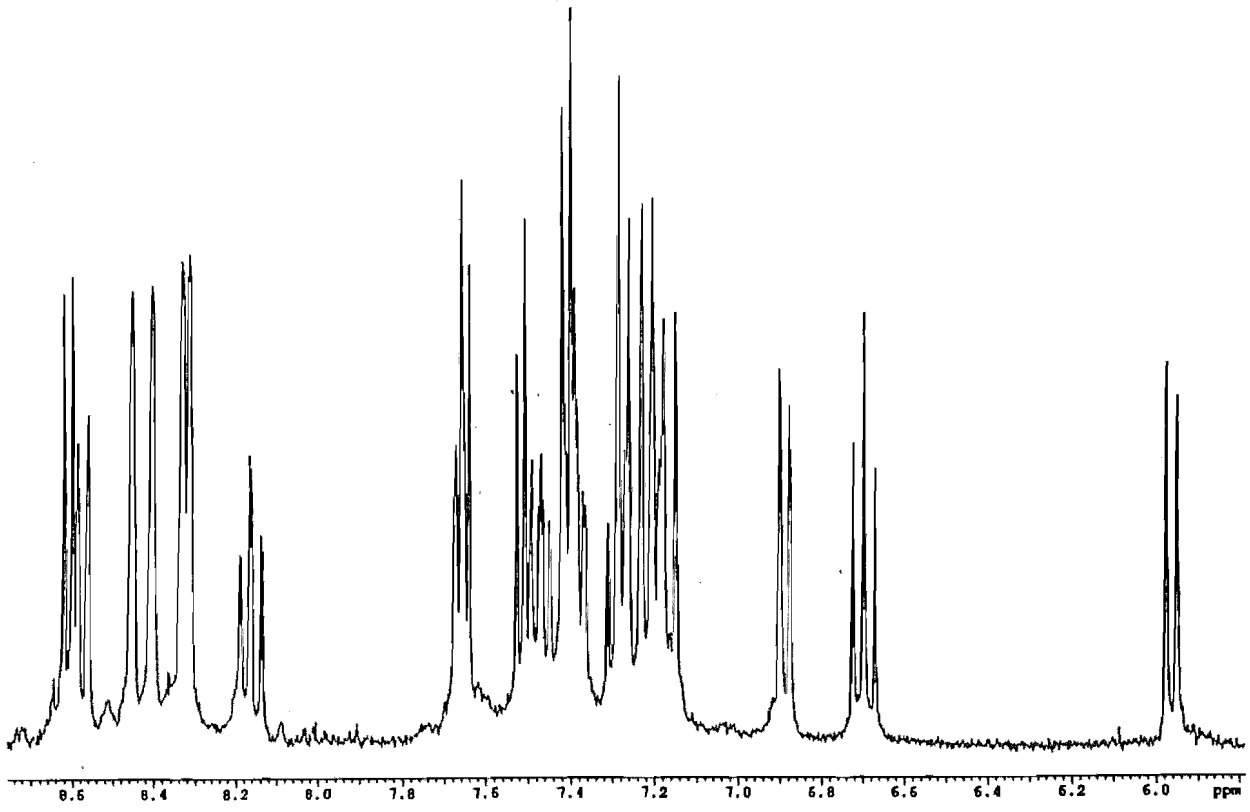

Figure 3.3 ^{1}H NMR Spectrum of **99**.

The ^{1}H NMR spectrum of **99** (Figure 3.3) consists of 22 non-equivalent aromatic protons. Spectra obtained after leaving the complex in solution for 5-10 minutes were too complicated to assign and showed evidence of complex dissociation. The N1H proton is absent in the spectrum implying a monocation, although this could not be confirmed, either by elemental analysis or by mass spectrometry.

The complex was stable long enough (5-10minutes) to acquire a series of 1D TOCSY spectra from which the protons of **93** were assigned (Figure 3.4). Briefly, the pyridine ring spin system of **93** were located by irradiation of H4' (8.16ppm) (trace III), whilst the two naphthalene spin systems were assigned by irradiation of H9 (6.89ppm) (trace II) and H4 (5.96ppm) (trace I). The chemical shifts and CIS values of these protons are summarised in Table 3.1. The increasing

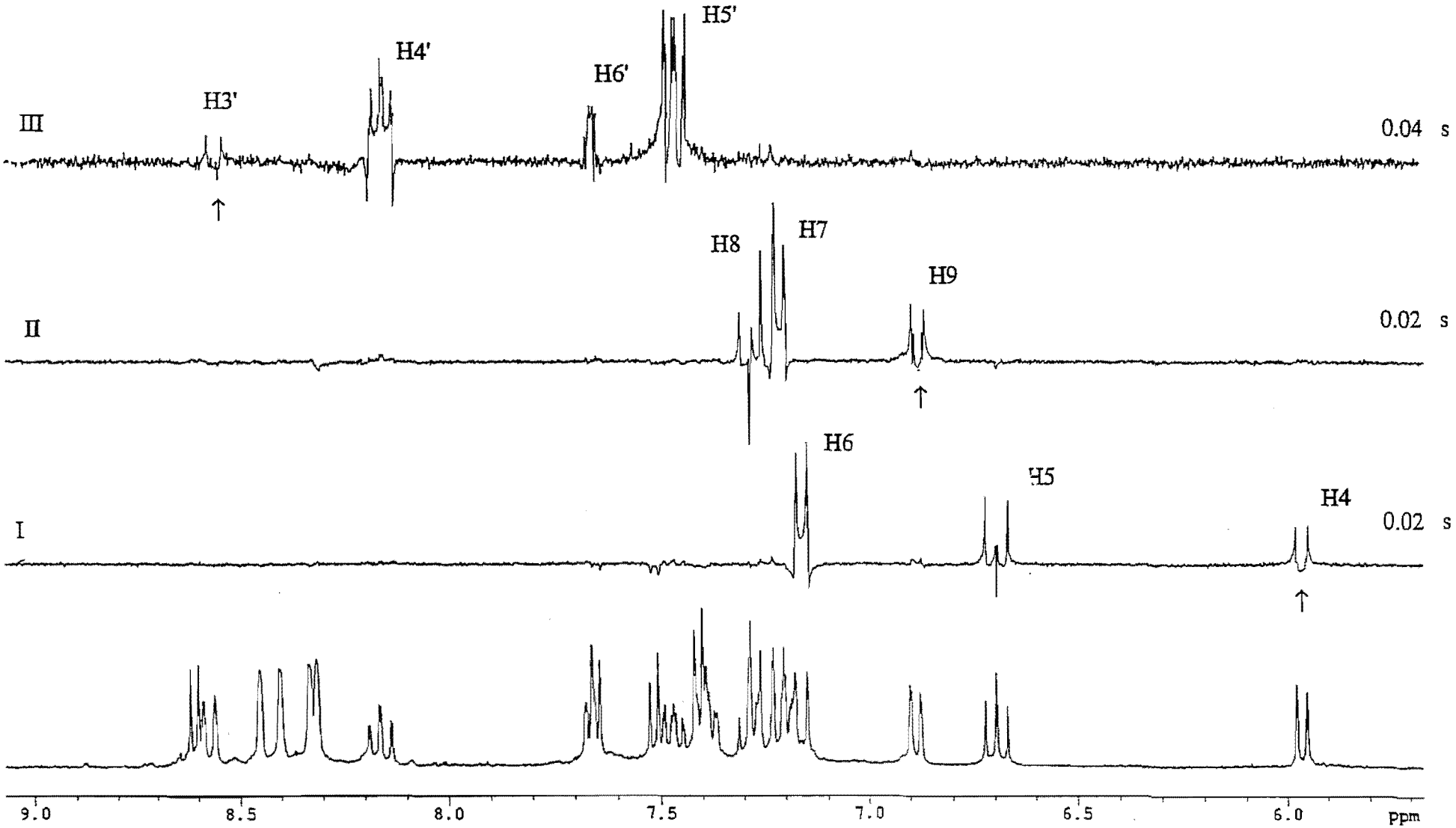

Figure 3.4 1D TOCSY Spectra of **99**

negative CIS values, in the order H5', H5, H4 and H6', reflect their proximity to a shielding dmb pyridine ring. The remaining protons show positive CIS values, reflecting the net donation of electron density from ligand to metal and also, in the case of H3', the change in conformation about the inter-ring bond required for metal chelation.

The dmb H3, H5 and H6 protons, but not the methyl groups, were tentatively located using 1D TOCSY spectra similar to those shown in Figure 3.4. These results are summarised in Table 3.1. The spectrum of **98** was then tentatively assigned by comparison with the spectrum of **99**. An interesting feature in the ^{1}H NMR spectrum of **99** is the downfield position (8.61ppm) of one of the dmbH6 protons. This proton lies above the aromatic (NH1-N3) ring of **93** and is therefore deshielded, relative to the three remaining dmbH6 protons, which lie above pyridine rings.

Table 3.1. ^{1}H NMR chemical shifts[a] of **99** and **93**. Coordination Induced Shifts[b] of **99**.

	H1	H4	H5	H6	H7	H8	H9	H3'	H4'	H5'	H6'
99	c	5.96	6.70	7.17	7.22	7.29	6.89	8.58	8.16	7.47	7.66
93	9.78	6.84	7.28	7.19	7.12	7.19	6.61	8.39	8.01	7.60	8.73
CIS	c	-0.88	-0.58	-0.02	+0.10	+0.10	+0.28	+0.19	+0.15	-0.13	-1.07

DMB Ligands			
H3	4-CH_3[d]	H5	H6
8.40	2.56	7.19	7.41
8.31	2.57	7.27	7.52
8.33	2.58	7.38	7.65
8.45	2.63	7.40	8.61

[a] For deuterated acetonitrile solutions. [b] CIS = $\delta_{complex}-\delta_{ligand}$. [c] Not observed. [d] Not assigned.

An attempt to prepare the homoleptic complex $Ru(\mathbf{93})_3^{2+}$ by reacting three equivalents of the ligand with $Ru(DMSO)_4Cl_2$ gave a black solid. The ^{1}H NMR spectrum of this solid was extremely complicated and the complex, which was found to be very unstable, was not further investigated.

The complexes of **93** were found to be consistently unstable in solution which can be explained by a coordination induced weakening of the N1-H bond. This proton is easily removed in solution resulting in dissociation of the ligand from the metal. A solution to this problem might be to stabilise the complexes by using the ligand **94**, in which N1 is methylated.

The synthesis of the new ligand is shown in Scheme 3.3 and is based on alkylation reactions with related perimidines, as described by Paragamanian *et al.*[211] The ligand **93** was deprotonated in a suspension of NaH in 1,2-dimethoxyethane and treated with MeI. This gave a yellow coloured compound **94** which was recrystallised from petroleum ether.

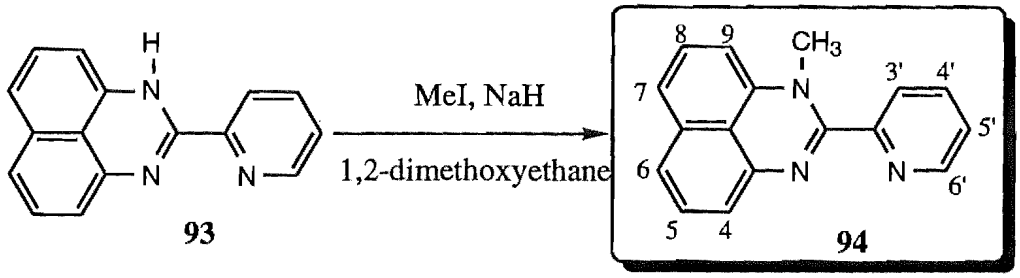

Scheme 3.3

In the ^{1}H NMR spectrum of **94**, H4 and H9 were distinguished by the observed nOe between the methyl group and H9. Thus the two naphthalene spin systems could then be assigned using 1D TOCSY spectra, analogous to those in Figure 3.1. The methyl group prevents the conjugation of the perimidine and pyridine rings and accounts for the absence of the deep red colour observed for **93**. The ^{13}C NMR spectrum of **94** was assigned by comparison with the spectra of **93** and structurally related complexes.[213,214]

The reaction of **94** with one equivalent of $PdCl_2$, in hot HCl, gave the complex **100** (Scheme 3.4) as a brown solid. Recrystallisation, by slow diffusion of a layer of methanol into a saturated solution of the solid in DMF, gave crystals of sufficient quality for the structure of **100** to be determined by X-ray crystallography.

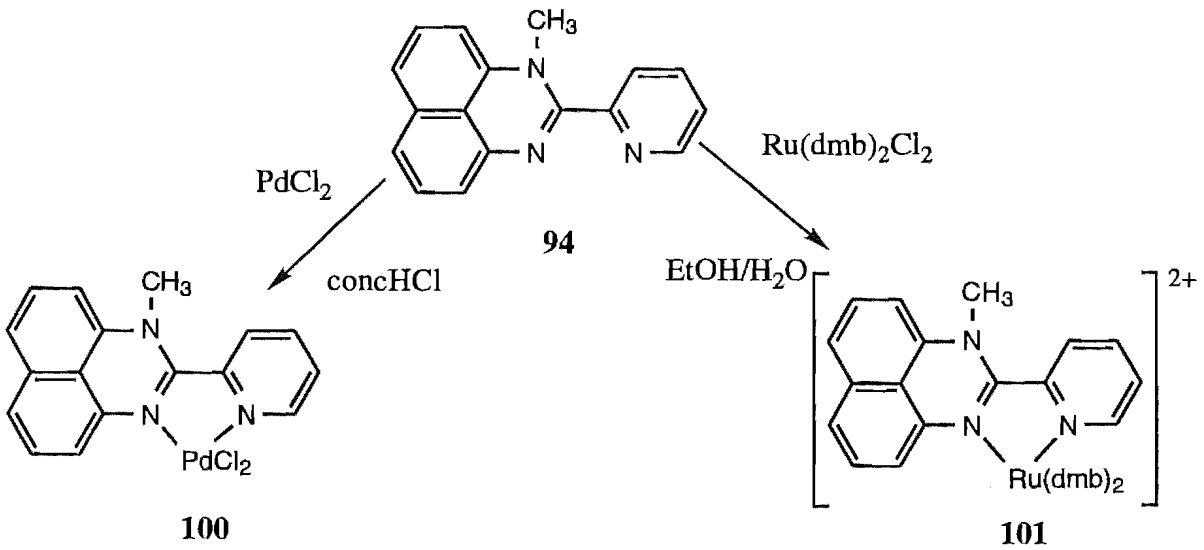

Scheme 3.4

Figure 3.5a shows a perspective view and atom labelling of the structure of **100**. Table 3.2 lists the bond lengths and bond angles with least-squares-estimated standard deviations in parentheses. This structure determination confirms not only the structures of the ligand and complex, but also the bidentate mode of coordination of the ligand. Figure 3.5b shows a perspective view of **100** perpendicular to the plane of the naphthalene unit of the perimidine system. This shows that the complex deviates significantly from planarity. Specifically, the

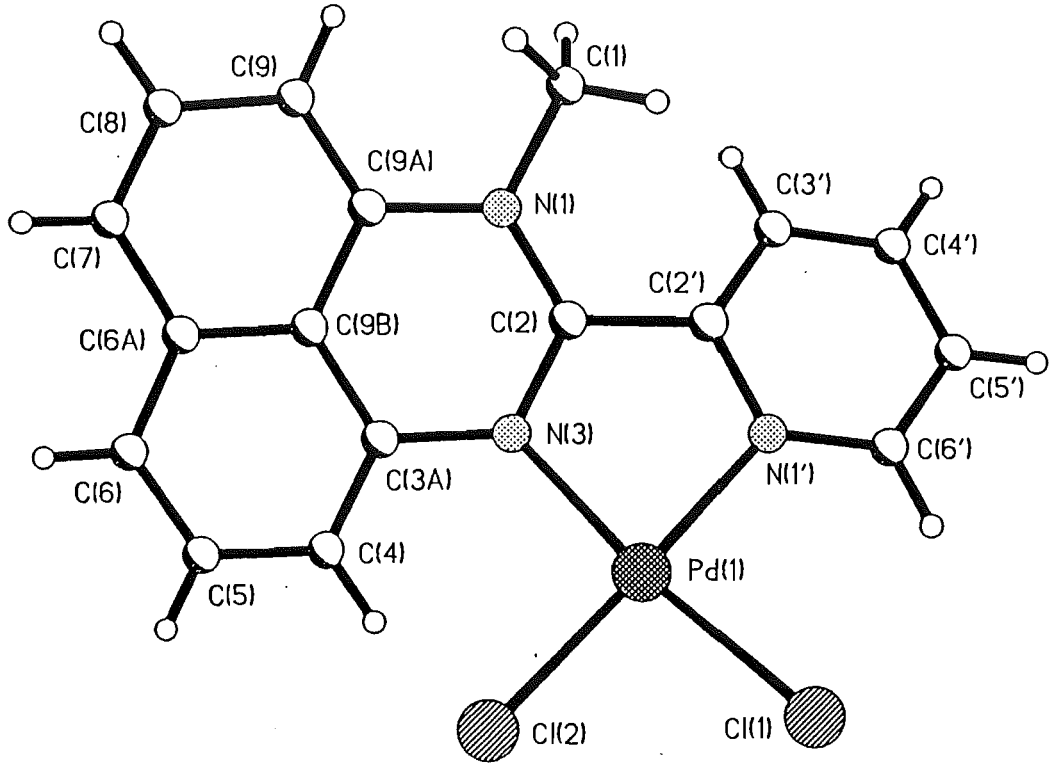

Figure 3.5a. Perspective view and atom labelling of the structure of **100**.

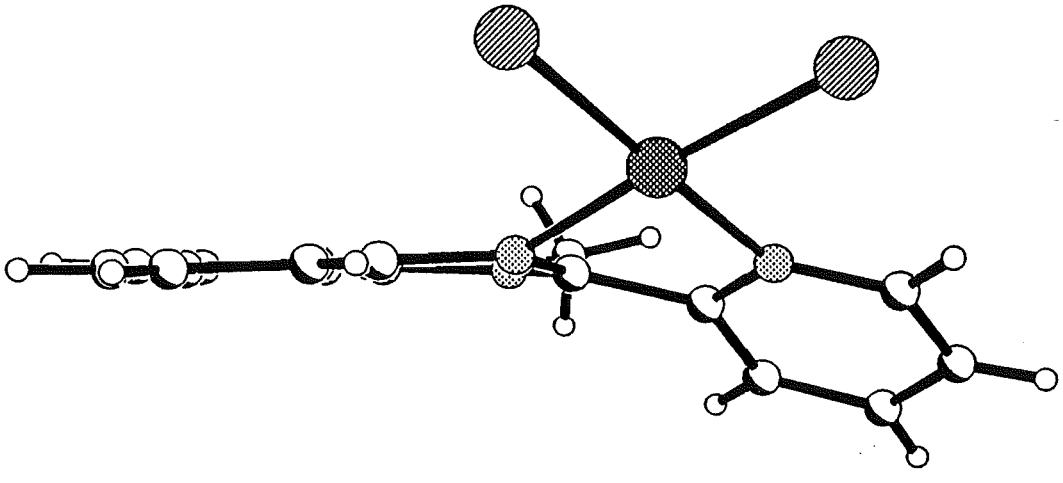

Figure 3.5b. View perpendicular to the plane of the naphthalene unit.

Table 3.2. Bond lengths (Å) and angles (°) for **100**.

Pd(1)-N(1')	2.023(7)	Pd(1)-N(3)	2.085(7)
Pd(1)-Cl(2)	2.296(2)	Pd(1)-Cl(1)	2.298(2)
C(1)-N(1)	1.466(11)	N(1)-C(2)	1.370(10)
N(1)-C(9A)	1.418(11)	C(2)-N(3)	1.343(11)
C(2)-C(2')	1.488(11)	N(3)-C(3A)	1.411(10)
C(3A)-C(4)	1.380(12)	C(3A)-C(9B)	1.427(12)
C(4)-C(5)	1.400(12)	C(5)-C(6)	1.372(14)
C(6)-C(6A)	1.428(14)	C(6A)-C(9B)	1.418(12)
C(6A)-C(7)	1.437(14)	C(7)-C(8)	1.33(2)
C(8)-C(9)	1.426(14)	C(9)-C(9A)	1.383(12)
C(9A)-C(9B)	1.424(13)	N(1')-C(6')	1.327(10)
N(1')-C(2')	1.360(10)	C(2')-C(3')	1.399(11)
C(3')-C(4')	1.365(12)	C(4')-C(5')	1.378(12)
C(5')-C(6')	1.398(11)		
N(1')-Pd(1)-N(3)	80.7(3)	N(1')-Pd(1)-Cl(2)	176.2(2
N(3)-Pd(1)-Cl(2)	97.8(2)	N(1')-Pd(1)-Cl(1)	93.1(2)
N(3)-Pd(1)-Cl(1)	173.6(2)	Cl(2)-Pd(1)-Cl(1)	88.3(1)
C(2)-N(1)-C(9A)	119.6(7)	C(2)-N(1)-C(1)	122.8(7)
C(9A)-N(1)-C(1)	117.2(7)	N(3)-C(2)-N(1)	124.0(7)
N(3)-C(2)-C(2')	114.6(7)	N(1)-C(2)-C(2')	121.3(7)
C(2)-N(3)-C(3A)	118.7(7)	C(2)-N(3)-Pd(1)	107.8(5)
C(3A)-N(3)-Pd(1)	131.0(6)	C(4)-C(3A)-N(3)	120.4(8)
C(4)-C(3A)-C(9B)	121.2(8)	N(3)-C(3A)-C(9B)	118.4(8)
C(3A)-C(4)-C(5)	120.1(9)	C(6)-C(5)-C(4)	120.3(10)
C(5)-C(6)-C(6A)	121.1(9)	C(9B)-C(6A)-C(6)	118.9(9)
C(9B)-C(6A)-C(7)	116.5(10)	C(6)-C(6A)-C(7)	124.5(9)
C(8)-C(7)-C(6A)	122.5(10)	C(7)-C(8)-C(9)	121.1(10)
C(9A)-C(9)-C(8)	119.3(10)	C(9)-C(9A)-N(1)	123.1(9)
C(9)-C(9A)-C(9B)	119.7(8)	N(1)-C(9A)-C(9B)	117.2(7)
C(6A)-C(9B)-C(9A)	120.7(8)	C(6A)-C(9B)-C(3A)	118.3(9)
C(9A)-C(9B)-C(3A)	120.9(8)	C(6')-N(1')-C(2')	120.0(7)
C(6')-N(1')-Pd(1)	127.0(6)	C(2')-N(1')-Pd(1)	112.8(6)
N(1')-C(2')-C(3')	120.3(8)	N(1')-C(2')-C(2)	114.3(7)
C(3')-C(2')-C(2)	124.9(7)	C(4')-C(3')-C(2')	119.6(8)
C(3')-C(4')-C(5')	119.4(8)	C(4')-C(5')-C(6')	119.2(8)
N(1')-C(6')-C(5')	121.2(8)		

pyridine ring is both twisted out of the plane of the perimidine unit (angle between the respective meanplanes = 35.8°) and, along with C2, displaced below the plane of the perimidine unit. These distortions presumably occur to relieve a steric interaction between the methyl group and the C3' hydrogen. As expected the coordination geometry at the palladium atom is square planar. The molecular packing of **100** (not shown) is controlled by π-π stacking interactions between the naphthalene units of adjacent molecules related by a crystallographic centre of inversion. These are separated by approximately 3.5Å.

In the ^{1}H NMR spectrum of **100** (DMSO-d_6) the pyridine ring was unambiguously assigned as H3' (8.12ppm), H4' (8.30ppm), H5' (7.89ppm), H6' (8.98ppm), with the CIS values of +0.25, +0.19, +0.23, +0.19ppm all reflecting the donation of σ electron density from the ligand to the metal. The naphthalene ring protons showed similar positive coordination induced shifts, but the two spin systems were overlapping in the ^{1}H NMR, and hence, could not be definitively assigned.

The reaction of **94** with one equivalent of $Ru(dmb)_2Cl_2$ gave the complex **101** (Scheme3.4), which was characterised by mass spectrometry and ^{1}H and ^{13}C NMR. Unlike **98** and **99**, which were unstable in solution, the complex showed no evidence of dissociation, even after being in solution for more than 24 hours.

Table 3.3. ^{1}H NMR chemical shifts[a] of **101** and **94**. Coordination Induced Shifts[b] of **101**.

	1-CH_3	H4	H5	H6	H7	H8	H9	H3'	H4'	H5'	H6'
101	3.74	6.13	6.77	7.25	7.31	7.39	6.71	8.33	8.08	7.40	7.69
94	3.15	6.84	7.34	7.29	7.25	7.32	6.47	7.76	8.00	7.54	8.73
CIS[b]	+0.59	-0.71	-0.57	-0.04	+0.06	+0.07	+0.24	+0.57	+0.08	-0.14	-1.04

DMB Ligands			
H3	4-CH_3[c]	H5	H6
8.46	2.54	7.19	7.48
8.25	2.58	7.28	7.62
8.30	2.58	7.46	7.92
8.51	2.64	7.36	8.41

[a] For deuterated acetonitrile solutions. [b] CIS = $\delta_{complex}$-δ_{ligand}. [c] Not assigned.

The ^{1}H NMR spectrum of **101** (Figure 3.6) is similar to that of **99** (Figure 3.3). 1D TOCSY spectra, analogous to those displayed in Figure 3.4, were used to assign all the pyridine and perimidine protons of the complex. In addition, the assignment of the individual dmb spin systems was achieved using the 2D COSY spectrum also shown in Figure 3.6. In this spectrum, a long range correlation can be observed from each of the dmbH3 protons to a dmbH5 in the region

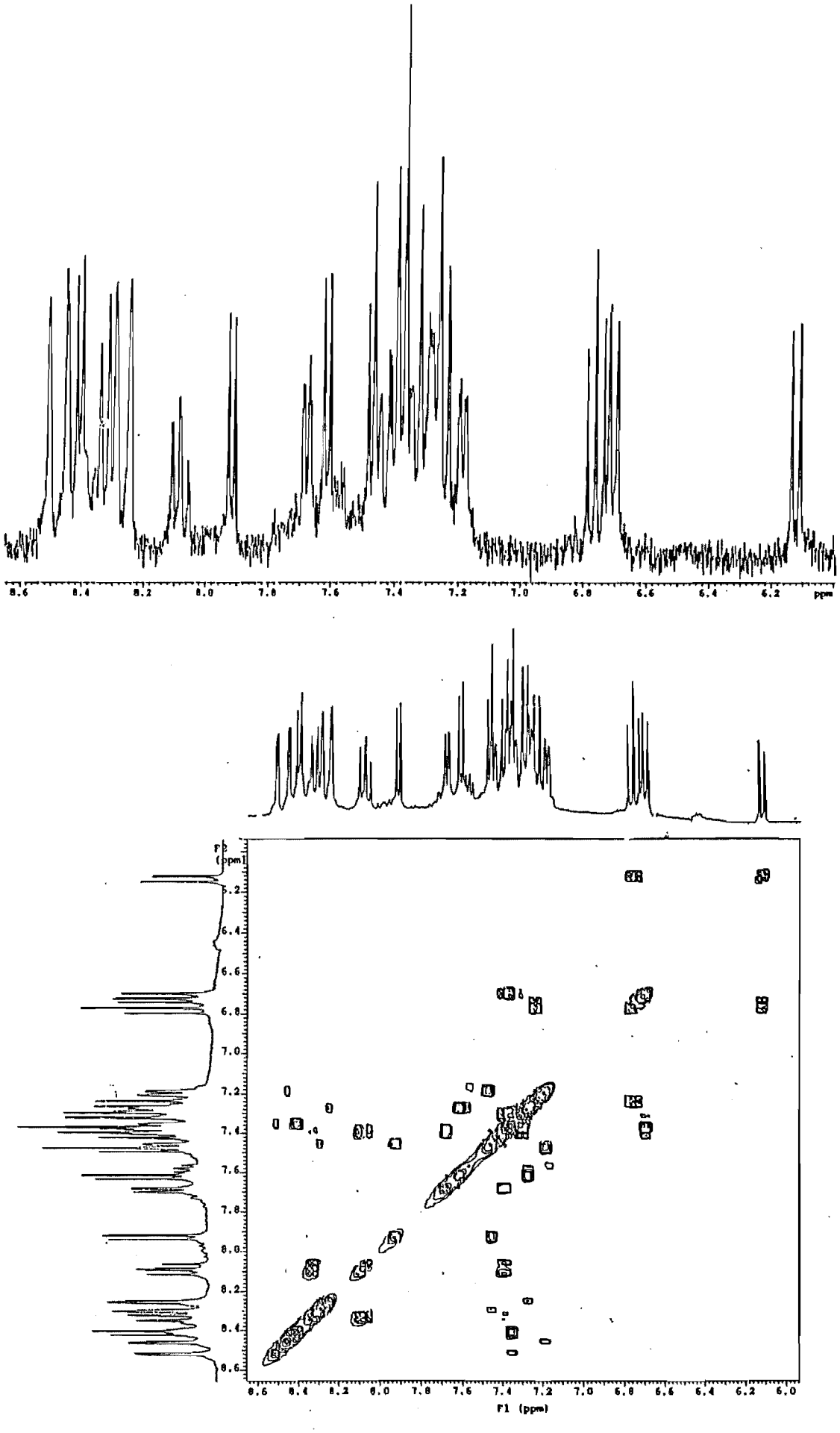

Figure 3.6 ^{1}H NMR and 2D COSY Spectra of **101**.

of extensive overlap from 7.18-7.5ppm. Thus located, the dmbH5 protons can then be correlated to the corresponding dmbH6. The ^{1}H NMR spectrum of **101** is summarised in Table 3.3.

Through-space interligand ring-current anisotropy, σ donation and π back-donation of electron density and coordinative disruption of inter-ring conjugation were all invoked to describe the CIS values of **99**. These factors can also account for the observed CIS values of **101** in Table 3.3, although chelation induced conformational change cause a greater deshielding of H3' (+0.57ppm) than in **99** (+0.19ppm) due to the greater steric demand of the N1 methyl group.

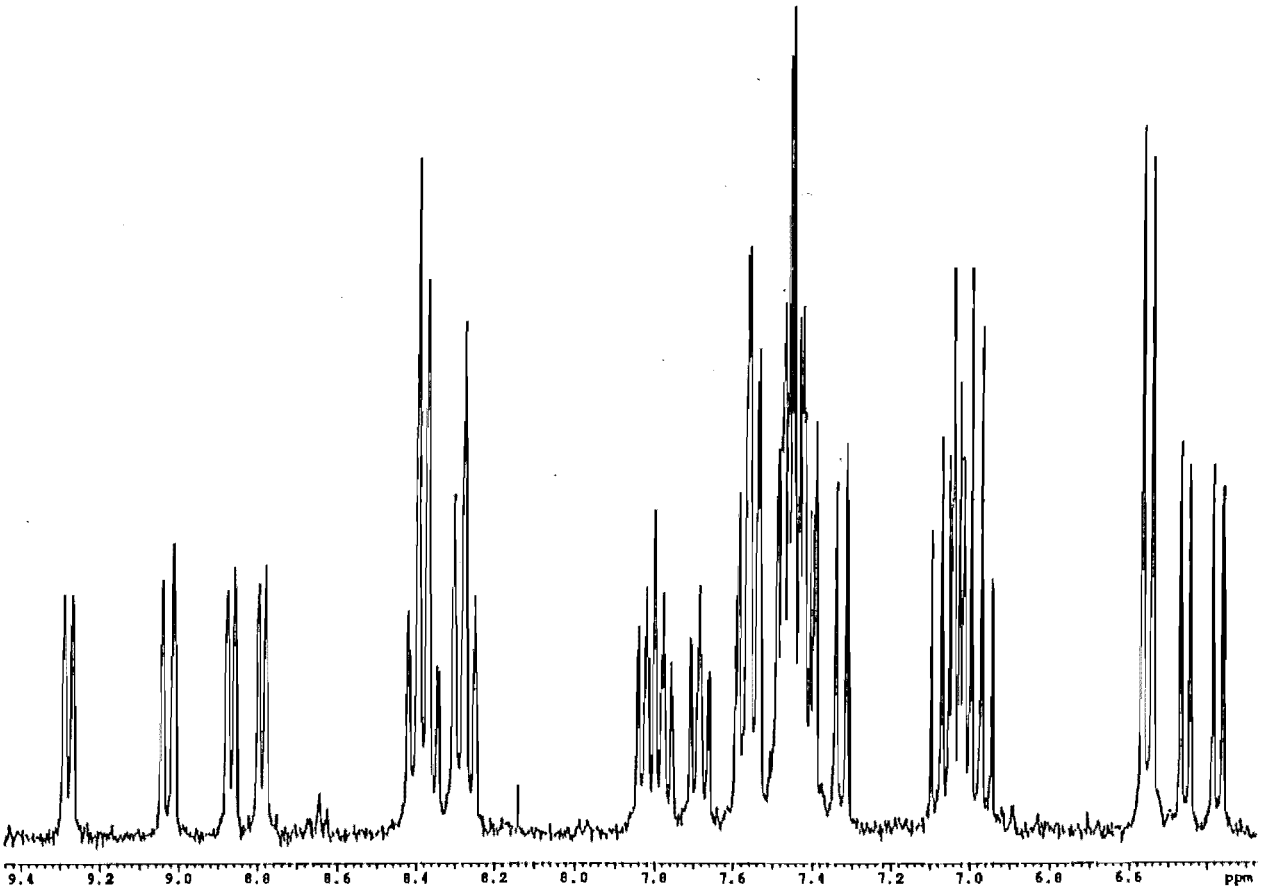

Figure 3.7 ^{1}H NMR Spectrum of **102**.

The complex $Ru(DMSO)_4Cl_2$ was reacted with three equivalents of the ligand **94** to give a dark purple solid. After purification by chromatography on alumina, the resultant complex (**102**) (Scheme 3.5) was characterised by ^{1}H NMR and mass spectrometry. The ^{1}H NMR spectrum of **102** has 30 non-equivalent aromatic protons (Figure 3.7), thus indicating that the complex has three non-equivalent ligands in a 1:1:1 ratio. Homoleptic complexes of the form $Ru(L\text{-}L')_3^{2+}$ generally exist as a mixture of the mer and fac isomers in a 3:1 ratio and, thus, have four non-equivalent ligands, three corresponding to the mer isomer and one corresponding to the fac isomer. Keene *et al.* have recently reported the separation of such isomers in structurally related homoleptic

complexes.[215] If the complex **102** has the homoleptic structure $Ru(\mathbf{94})_3^{2+}$, the spectrum implies that only the mer isomer has formed, and not a mixture of mer and fac.

All three pyridine rings were assigned from 1D TOCSY irradiations of the four most downfield doublets, whilst similar irradiation of the three most upfield doublets located almost all of the naphthalene spin systems, with the exception of H7 and H8 which show considerable overlap. The pyridine and perimidine rings of each ligand were correlated by an nOe from the appropriate N1-CH_3 (not shown in Figure 3.7), which showed enhancement of the relevant H3' and H9 protons. For example, the deshielded H3' (9.02ppm) was correlated to the deshielded H6' (8.88ppm) by a 1D TOCSY experiment, and by an nOe to the strongly deshielded methyl group (4.33ppm) which in turn is correlated by an nOe to an H9 of a naphthalene ring. In this manner nearly all of the protons of the three ligands could be assigned.

Given that the complex was shown, by mass spectrometry, to contain a chlorine atom, the novel structure for **102** (Scheme 3.5) was proposed. In this case, one ligand exhibits monodentate coordination through the pyridine ring, with the N1-CH_3 of the ligand deshielded by an adjacent chlorine atom which is coordinated to ruthenium(II), whilst the H6' is deshielded by a perimidine ring of another ligand. The two other ligands exhibit bidentate coordination to ruthenium(II), with the H6' of one deshielded by the coordinated chlorine atom, whilst the H6' of the other is adjacent to and in the deshielding region of the monodentate coordinated pyridine ring. On reflection, this complex is more likely to form than the homoleptic $Ru(L\text{-}L')_3^{2+}$ complex because of the steric demand of the bulky perimidine ring of **94**.

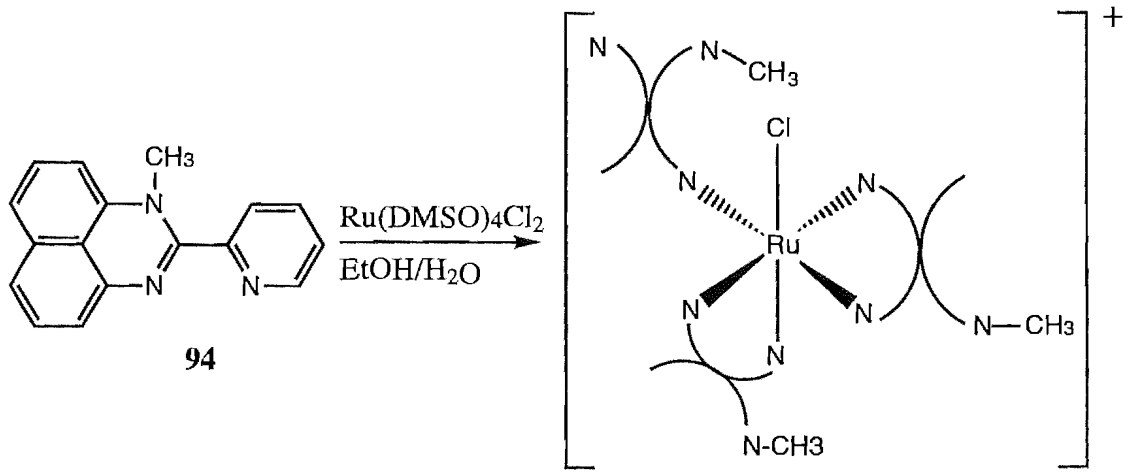

94

102

Scheme 3.5

Table 3.4 summarises the UV/VIS spectra and cyclic voltammetry of **101** and **102**. MLCT transitions occur at 454 and 504nm for **101** and at lower energy (496 and 530nm) for **102**. Thus electron transfer from metal to ligand is easier for these complexes than in the case of $Ru(bpy)_3^{2+}$ (451nm). Oxidation and reduction of the complexes is also easier than for $Ru(bpy)_3^{2+}$; hence the values for $\Delta E_{ox\text{-}red}$ are much smaller, which correlates with the low energy MLCT bands and reflects the smaller HOMO-LUMO gap in the complexes. The chlorine of **102** and dmb ligands of **101** also contribute to a lowering of the oxidation potential by destabilising the metal d orbitals. The cyclic voltammogram of **102** is shown in Figure 3.8.

Table 3.4. Absorption Maxima[a] and Redox Potentials[b] of **101** and **102**.

Complex	λ	E_{ox}	E_{red1}	E_{red2}	E_{red3}	E_{red4}	$\Delta E_{ox\text{-}red}$
$Ru(bpy)_3^{2+}$	451	+1.27	-1.31	-1.50	-1.77	-	2.58
101	454, 504sh	+1.22	-1.25	-1.68	-1.87	-2.20[c]	2.47
102	496, 530	+0.84	-1.14	-1.31	-1.57	-2.00	1.98

[a] In nanometres. [b] In volts vs SCE in acetonitrile. [c] Irreversible.

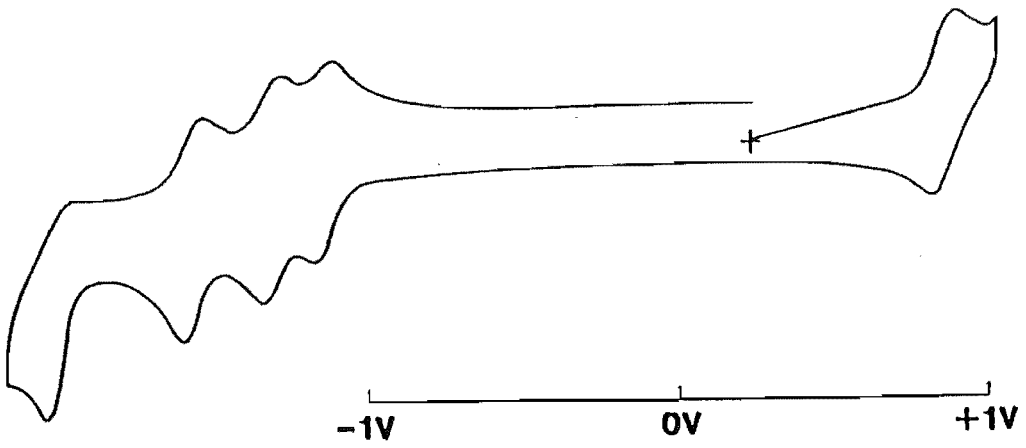

Figure 3.8 Cyclic Voltammogram for **102**.

Methylation of **93** has produced the new ligand **94**. With the exchangeable proton removed, this ligand has been shown to form much more stable complexes than **93**. However, neither ligand has the potential to form binuclear complexes, the study of which is the major objective of this research. To this end, the potentially binucleating ligand **91** was synthesised using the method of Patschorke *et al.*,[209] in which two equivalents of 1,8-diaminonaphthalene were condensed with one equivalent of ethyl oxalate at 220°C (Scheme 3.6). The compound **91** is insoluble in most common solvents, although a ^1H NMR spectrum was obtained in DMSO-d_6.

Haga[65] has described the synthesis of $[Ru(bpy)_2]_2bibzm^{2+}$ from $Ru(bpy)_2bibzmH_2^{2+}$, in which the formation of the dianion in solution, by double deprotonation of $Ru(bpy)_2bibzmH_2^{2+}$, is facile because the N-H bond is weakened by coordination of the first ruthenium(II). We

intended to use this approach in the synthesis of the biruthenium(II) complex **104** by initially preparing the monoruthenium(II) complex **103** (Scheme 3.7).

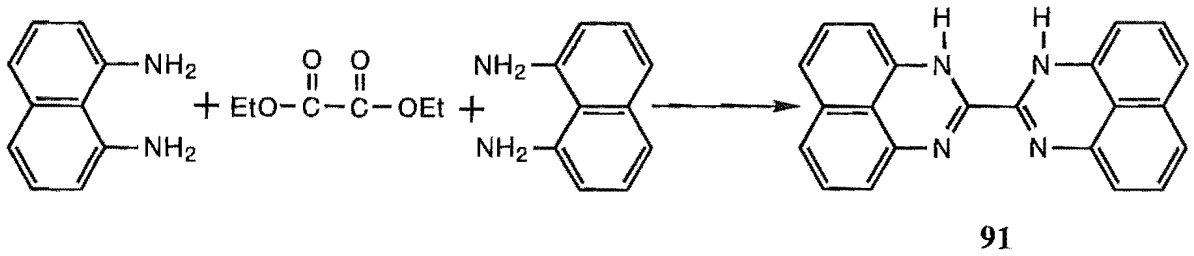

91

Scheme 3.6

The reaction of **91** with one equivalent of $Ru(dmb)_2Cl_2$ in refluxing ethanol/water failed to give a mononuclear complex due to the insolubility of the ligand. Instead, the reaction was performed in refluxing ethylene glycol. This was more successful in coordinating **91** to ruthenium(II), although the product of the reaction was a mixture of complexes, with the ligand adopting a monodentate coordination mode. Attempts to separate the resulting mixture of complexes by chromatography on alumina were unsuccessful. In mononuclear complexes **91** is therefore more likely to exhibit monodentate coordination rather than the more sterically demanding bidentate mode of **103**. Failure to synthesise **103** effectively prevented a synthesis of **104**, using this approach.

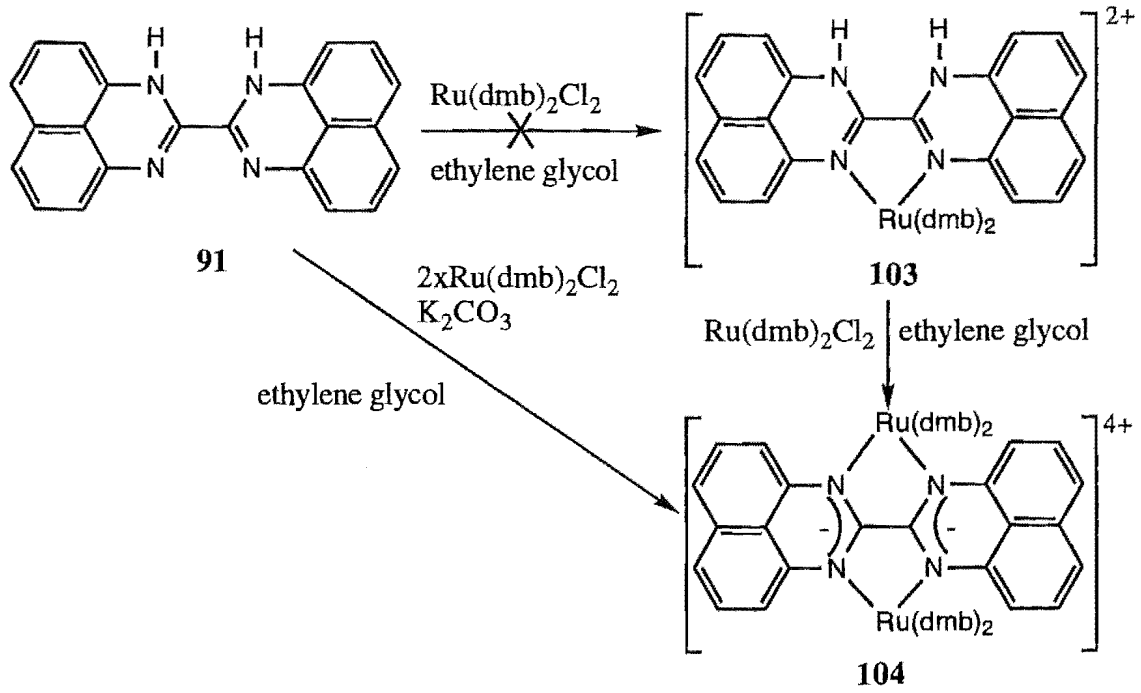

91 **103** **104**

Scheme 3.7

An attempt was made to synthesise a biruthenium(II) complex directly, by reacting **91** with K_2CO_3 and two equivalents of $Ru(dmb)_2Cl_2$ in refluxing ethylene glycol. This also gave a mixture of complexes which could be neither separated by chromatography on alumina, nor

identified by ^{1}H NMR. The complexes may also have decomposed in this reaction, since N-unsubstituted perimidines are known to decompose under basic conditions,[211] which also discouraged the use of a stronger base in any further reactions. In fact neutral alumina was used in the purification attempts to avoid decompositon of the complexes in the mixture.

The compound **91** has proved to be unsuitable as a bidentate bridging ligand for ruthenium(II) because of its insolubility, inability to form a bidentate monoruthenium(II) complex and tendency to decompose rapidly in base. Instead, **95** was proposed as an alternative to **91**, which should be more soluble and less sterically demanding, and hence, be able to form mono- and binuclear complexes, given that similar mononuclear complexes of **93** and **94** have been prepared.

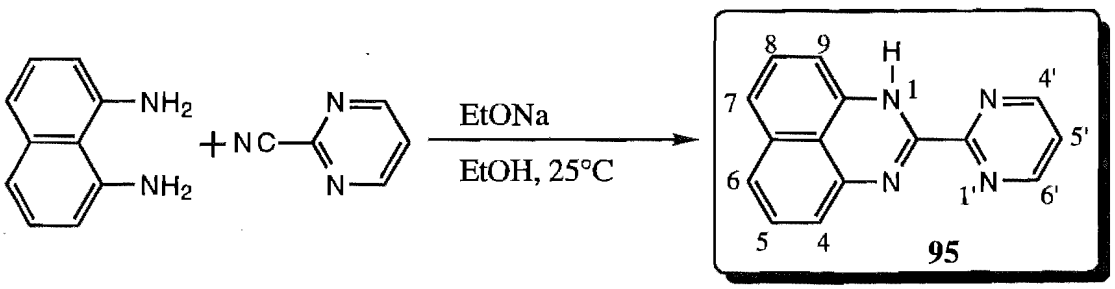

Scheme 3.8

The compound **95** was synthesised under the same reaction conditions as for the synthesis of **93**, but with the exception that 2-cyanopyridine was replaced by 2-cyanopyrimidine (Scheme 3.8). The new ligand was then characterised by mass spectrometry and its ^{1}H NMR spectrum was assigned by comparison with the spectra of **93** and **94**.

A palladium(II) complex (**105**) (Scheme 3.9) was prepared by reacting the ligand with $PdCl_2$ in hot HCl, but was found to be insoluble in common solvents. In addition the elemental analysis of this complex was found to be unsatisfactory. Given the structure of previous complexes **96** and **100**, the complex was tentatively assigned the structure shown.

The reaction of **95** with one equivalent of $Ru(dmb)_2Cl_2$, which gave the complex **106**, was more successful (Scheme 3.9). Mass spectrometry of the complex confirmed that the N1 nitrogen was protonated, although this proton was not observed in the ^{1}H NMR spectrum. The spectrum of **106**, which consists of 25 non-equivalent aromatic protons, was assigned in an analogous manner to the spectra of **99** and **101** using 1D TOCSY spectra. Most chemical shifts and CIS values were similar to those in the spectrum of **99**, including the deshielded dmbH6 proton, which lies above the non-aromatic perimidine ring of **95**. The major difference in the

spectrum of **106** is the absence of an H3' pyridine proton and, as a consequence of complex formation, the equivalent H4' and H6' of **95** become non-equivalent, with H4' exhibiting a positive CIS and H6' exhibiting a negative CIS for reasons already described for the pyridine rings of **99** and **101**.

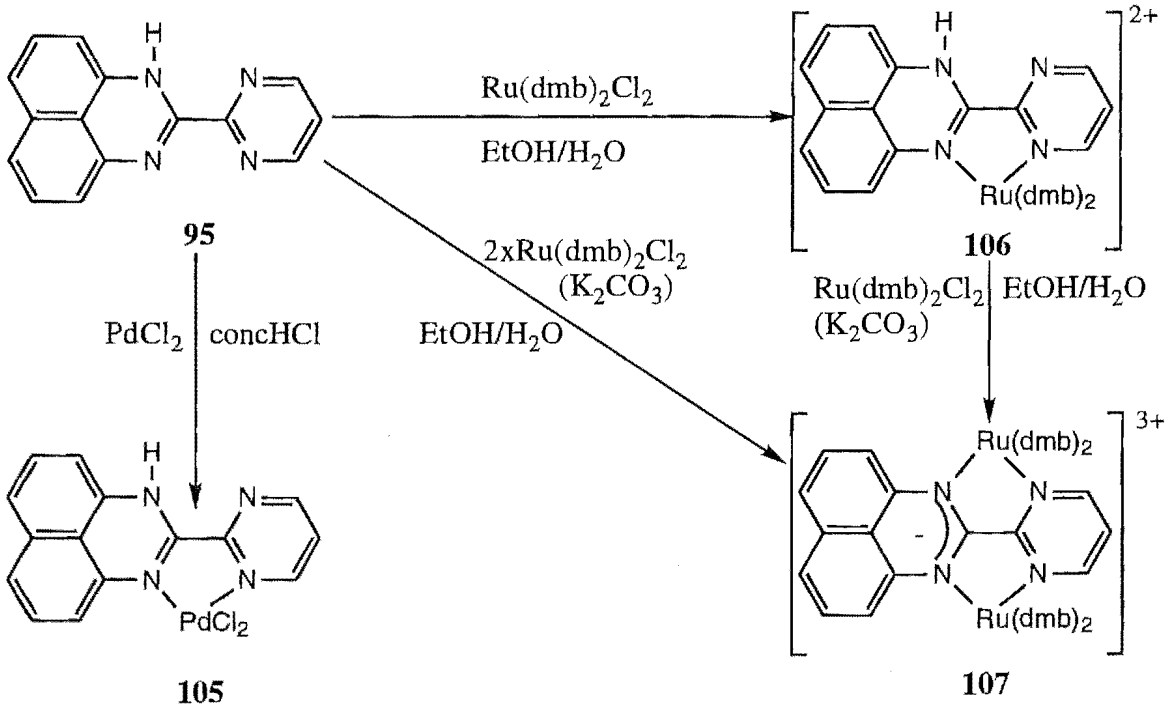

Scheme 3.9

Unfortunately, attempts to prepare the binuclear complex **107** were less successful. Firstly, a mixture of complexes was obtained from the reaction of **106** with one equivalents of $Ru(dmb)_2Cl_2$. No binuclear complex could be distinguished in the ^1H NMR spectrum of the mixture. The mononuclear complex **106**, but not the binuclear complex, was isolated from this mixture by either chromatography on alumina, or by ion-exchange chromatography on C-25 sephadex. The reaction was repeated in the presence of K_2CO_3 to effect deprotonation of the N1 nitrogen. Again a mixture of complexes, with an even more complicated ^1H NMR spectrum was obtained from which no binuclear complex could be isolated by chromatography. Similarly, reacting the ligand (**95**) with two equivalent of $Ru(dmb)_2Cl_2$, both with, and without, K_2CO_3 was successful in generating **106**, but not **107**. In retrospect it seems that NH perimidines are not suitable ligands for the preparation of binuclear complexes.

Chapter 4

Complexes of

4,6-Bis-(2-pyridinyl)pyrimidine.

Complexes of 4,6-Bis-(2-pyridinyl)pyrimidine.

4.1. Introduction.

In chapter 2 a strong metal-metal interaction ($\Delta E_{1/2}$=200mV) was reported for biruthenium complexes **64** and **65** containing a 4,4'-dimethyl-2,2'-bipyrimidine (**40**) bridge. Stronger inter-metal communication has been described by others in biruthenium complexes with biimidazolate (**7**)[77] or bibenzimadazolate (**6**)[65,72,76] bridges, in which the anionic ligand decreases the repulsion between the metals. Two perimidine compounds were proposed as anionic bridging ligands in this work, but were found to be unsuitable for reasons already described in chapter 3.

Alternatively, two metals may be bridged by a pyrazine ring which allows strong inter-metal communication, as in the well known Creutz-Taube complex.[17,18] The stability of such complexes can be increased by using a chelating bridging ligand which incorporates a pyrazine ring. For example, substitution of two pyridine rings at, either the 2,3 or the 2,5 positions of a pyrazine ring, produces the bridging ligands 2,3-bis-(2-pyridinyl)pyrazine (2,3-dpp, **15**)[114] and 2,5-bis-(2-pyridinyl)pyrazine (2,5-dpp, **16**)[115] respectively. Other bridging ligands structurally related to **15** and **16** have been described, particularly the ring fused analogues **18**,[25,26,117,129,130,134,135,141,142] **19**[129,130,134,135] and **20**.[19,143-145]

The ligands **15** and **16** have been particularly well studied and their diruthenium(II)[32,33,116,119,126-128] complexes have been shown to exhibit strong metal-metal interactions. For example, the separation of the first and second oxidation potentials ($\Delta E_{1/2}$) in the diruthenium complexes of **15** and **16** is typically 170mV. Also, a number of polynuclear ruthenium(II) complexes of **15** have been prepared containing up to 22 metal atoms.

Complexes of **16** are planar, since there are no steric interactions between the pyridine rings. However, this is not the case for binuclear complexes of **15**, in which considerable twisting is required, within the bridging ligand, to relieve the steric interaction between the pyridine rings. Although no X-ray structures of binuclear complexes of **15** have been determined, such twisting has been observed in the crystal structure of a doubly cyclopalladated complex of a ligand isoelectronic to **15**.[216] Similarly, variable-temperature NMR studies of the diplatinum(IV) complexes of **15** have detected twisting of the pyridine rings,[24] whilst, more recently, an X-ray crystal structure of the free ligand **15** has been determined.[217] The inter-metal separation in such complexes of **15** is typically 6.7Å.[216]

In contrast, there are very few examples of chelating binucleating ligands that bridge two metals with a pyrimidine ring. Although the two dipyridylpyrimidines **108** and **109** have been known for nearly 30 years,[218] there has been no study of their coordination chemistry, with the exception of a discussion of their iron(II) complexes in the original report of the preparations of the ligands. It was proposed that **108** would form mononuclear complexes with tridentate coordination analogous to that of 2,2',6',2''-terpyridine. Bidentate coordination of **108** should also be possible, as was observed for the related dipyrazolylpyrimidine **53** in Chapter 2. However, studies of **53**, in this work, imply that **108** would be unable to form binuclear complexes with octahedral metals, such as ruthenium(II), since the N3, N1'' coordination sites are less accessible, relative to the N1, N1' sites.

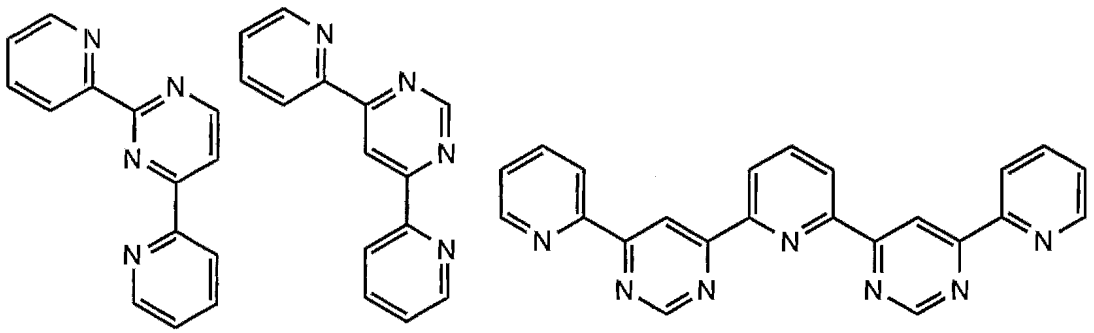

108 **109** **110**

Figure 4.1

The dipyrazolyl (**22**) and 3,5-dimethylpyrazolyl (**23**) analogues of **109** have been used as bridging ligands[96,151] and, given that the two bidentate sites of **109** are equally accessible, it is surprising that there have been no reports of binuclear complexes of this ligand. On the basis of an X-ray crystal structure of a cyclopalladated analogue,[219] two metals coordinated to **109** would be separated by about 5.9Å, much closer than in the binuclear complexes of the pyrazine containing ligands **15** and **16**; thus a larger interaction may be possible in binuclear complexes of **109**. In this chapter a study of the coordination chemistry of **109** is described, with particular emphasis on ruthenium(II) complexes. The synthesis and biruthenium(II) complex of the related new ligand **110** is also described.

4.2. Results and Discussion.

4,6-Bis-(2-pyridinyl)pyrimidine was prepared in two steps. Firstly, Claisen condensation of 2-methoxycarbonylpyridine (**111**) and 2-acetylpyridine (**112**) gave the compound 1,3-(2-pyridinyl)-1,3-propanedione (**113**), from which the pyrimidine ring of **109** was readily formed

by refluxing in formamide (Scheme 4.1). Literature procedures were used in both reactions.[218,220]

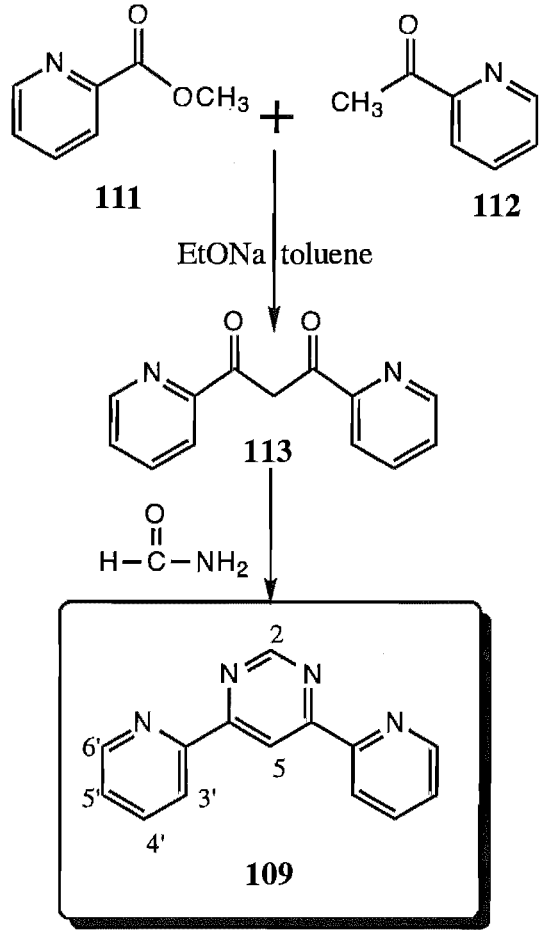

Scheme 4.1

The pyridine rings, in the ^{1}H NMR spectrum of **109** (Figure 4.2), were readily assigned, due to the smaller coupling constant of H5'-H6' relative to that of H3'-H4'. Differentiation of H2 and H5, which are close in chemical shift, was more difficult. No nOe was observable from H3' to H5, thus implying that the ligand has a conformation in which the inter-ring bonds are transoid with respect to the nitrogens. However, in the ^{13}C NMR spectrum (CD_3CN) of **109**, C2 (159.0ppm) is well downfield of the more electron rich C5 (113.2ppm). Correlation of C2 and C5 to proton signals at 9.38ppm and 9.43ppm respectively, by an HMQC spectrum, enabled H2 and H5 to be assigned.

The first complexes of **109** that were prepared were of palladium(II). As shown in Scheme 4.2, the binuclear complex **115** was prepared by reacting **109** with two equivalents of $PdCl_2$ in HCl. This complex was found to be insoluble in common solvents, but was characterised by elemental analysis and assigned the structure shown. Reaction of **109** with one equivalent of $PdCl_2$ gave an insoluble yellow solid, which was estimated, by elemental analysis, to

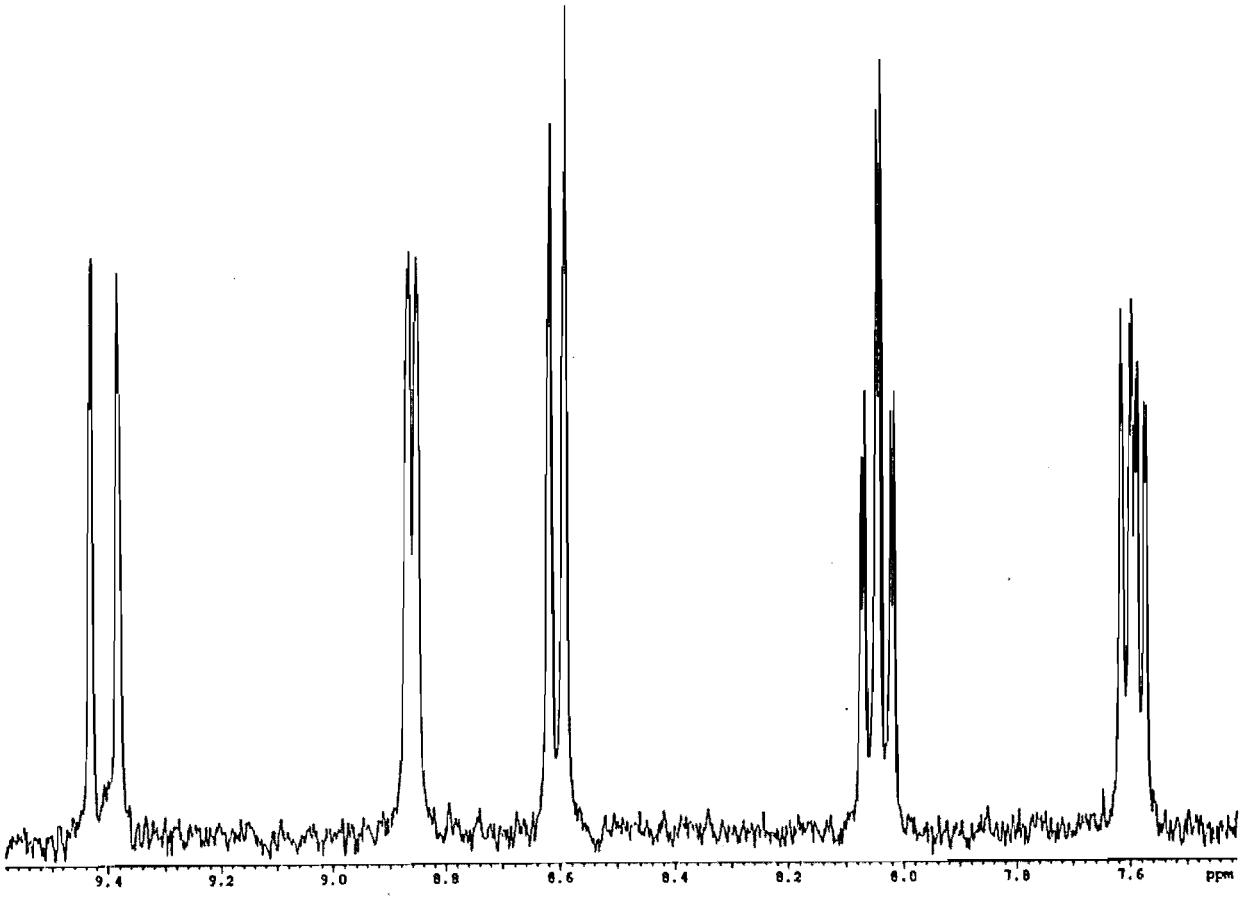

Figure 4.2 ^{1}H NMR Spectrum of **109**.

be a mixture of the mono- and binuclear complexes **114** and **115**. Thus formation of the binuclear complex is facile, even with one equivalent of $PdCl_2$.

The reaction of **109** with one equivalent of $Mo(CO)_6$, in refluxing toluene, gave the purple mononuclear complex **116** (Scheme 4.2). Similarly, reaction with two equivalents of $Mo(CO)_6$ gave the blue binuclear complex **117**. Both complexes were purified by chromatography on alumina and characterised by elemental analysis.

^{1}H NMR spectra of **116** and **117** in coordinating solvents, such as d_6-DMSO or CD_3CN, showed evidence of complex dissociation. The complexes were found to be more stable in d_6-acetone and their ^{1}H NMR spectra are summarised in Table 4.1. The protons H2 and H5 were assigned by an nOe from H3' to H5, since, unlike the free ligand, the inter-ring bond has a cisoid orientation of the nitrogens as a result of the chelate ring, in both **116** and **117**. The pyridine rings were assigned by their coupling constants, as in the spectrum of **109**, whilst the coordinated (H3'-H6') and non-coordinated (H3''-H6'') rings of **116**, were distinguished by their relative positions, with (H3'-H6') exhibiting the greater coordination induced shifts. Almost all the CIS values for **116** and **117** are positive which reflects the donation of σ-electron density from ligand to metal. In addition, H6' (**116**), H2 (**116**) and H6'(**117**) are held coplanar to, and hence deshielded by, an adjacent carbonyl group, whilst H2 (**117**) is deshielded by two carbonyls, and

thus exhibits a CIS twice as large as that of H2 (**116**). Finally, the CIS values of H5, and H3', in both complexes, reflect the change in conformation about the inter-ring bond that is required for metal chelation.

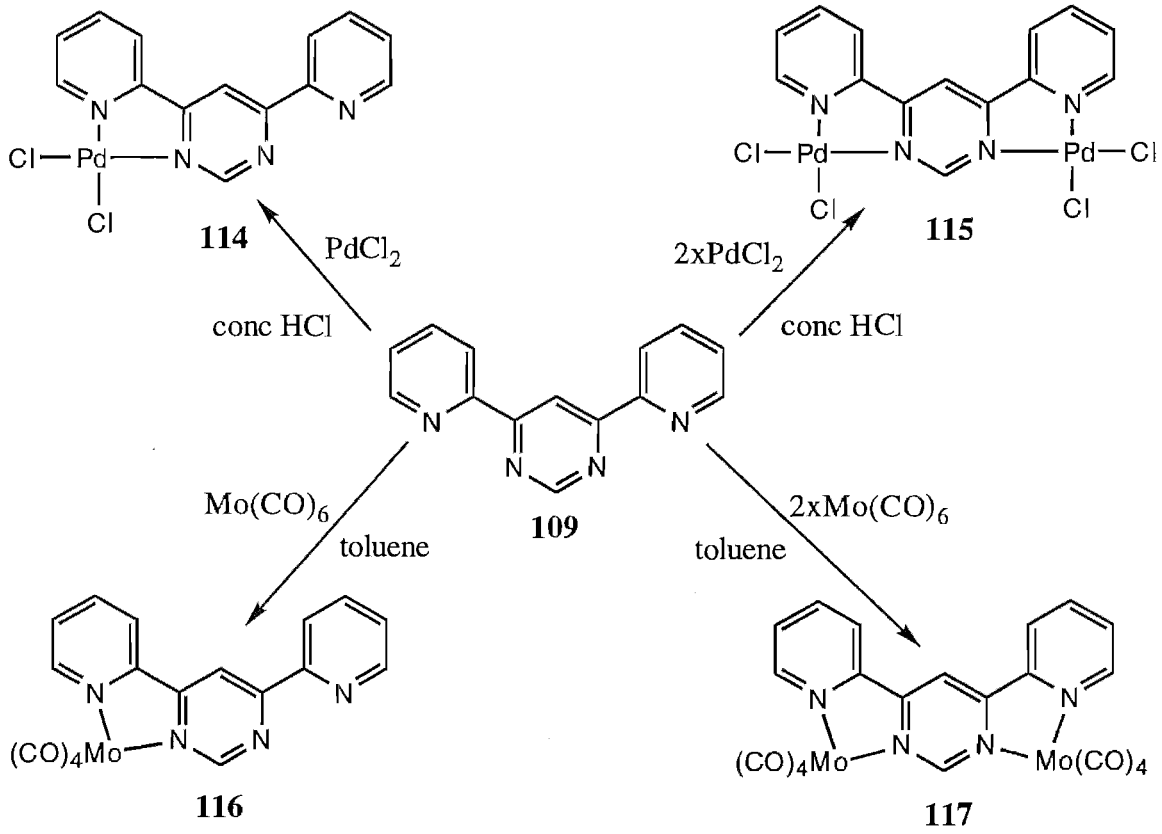

Scheme 4.2

Table 4.1. ^{1}H NMR Chemical Shifts[a] of **116**, **117** and **109**. Coordination Induced Shifts[b] of **116** and **117**.

	H2	H5	H3'	H4'	H5'	H6'	H3''	H4''	H5''	H6''
116	9.85	9.51	9.10	8.46	7.95	9.36	8.78	8.25	7.80	8.98
109	9.47	9.64	8.73	8.17	7.71	8.94				
CIS[b]	+0.47	-0.13	+0.37	+0.29	+0.24	+0.42	+0.05	+0.08	+0.09	+0.04
117	10.37	9.73	9.22	8.47	7.98	9.38				
CIS[b]	+0.90	+0.09	+0.49	+0.30	+0.27	+0.44				

[a] For deuterated acetone solutions. [b] CIS = $\delta_{complex}$-δ_{ligand}.

Both **116** and **117** exhibit strong ligand centred absorptions in their UV/VIS spectra (Figures 4.3a and 4.3b). Symmetrical absorption in the visible region of the spectra of **116** (λ_{max}=520nm) and 117 (λ_{max}=572nm) can be assigned to the MLCT transition dπ-π*(**109**). Thus the MLCT transition shifts to lower energy in the binuclear complex (Figure 4.3b) relative to the mononuclear complex (Figure 4.3a). This effect has also been observed in structurally related complexes of dpop (**20**) for which the lower binuclear MLCT energy has been explained as being due to both, a stabilisation of the dpop pπ*-LUMO when bonded to a second π withdrawing

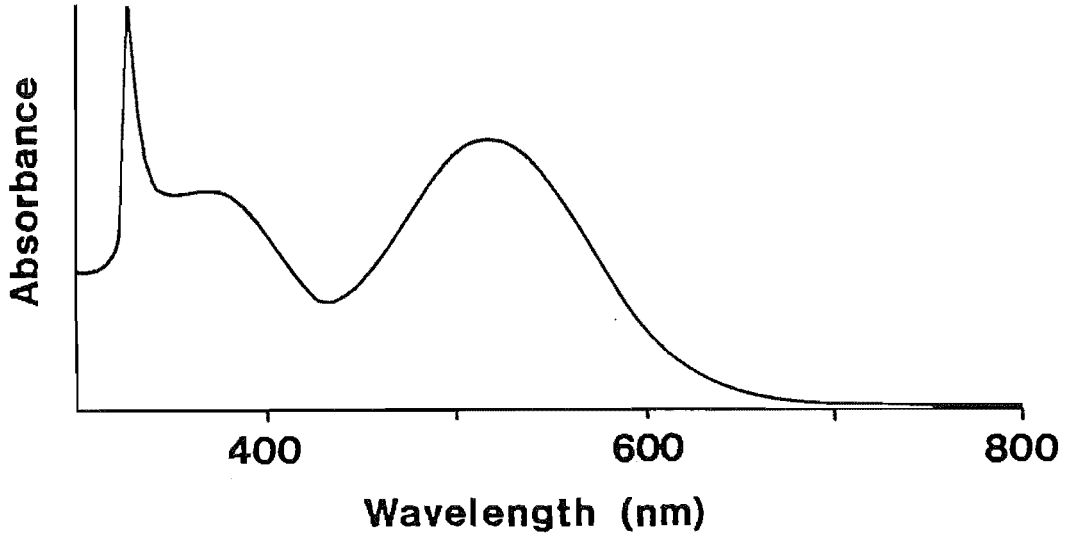

Figure 4.3a UV/VIS Absorption Spectrum of **116**.

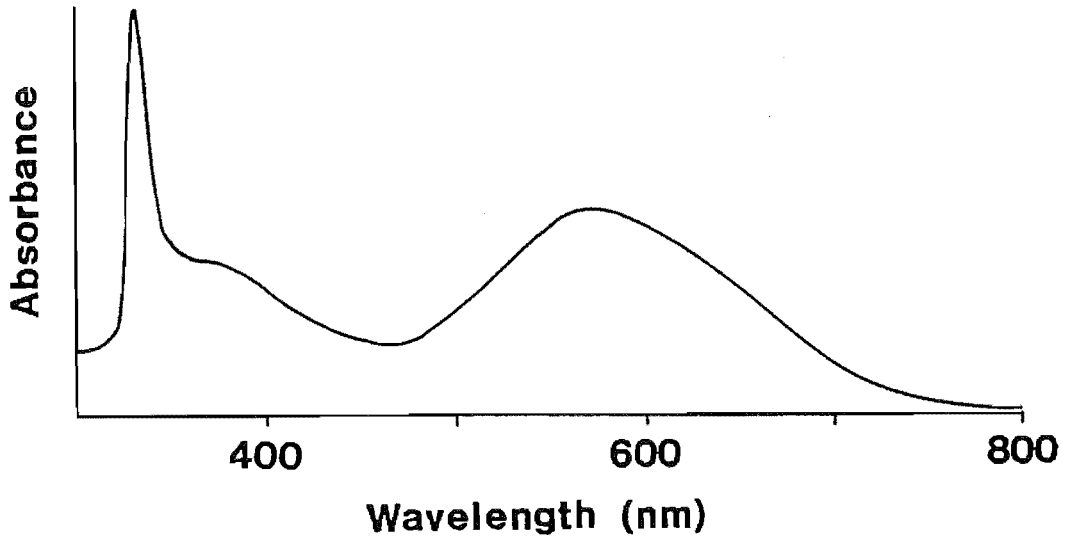

Figure 4.3b UV/VIS Absorption Spectrum of **117**.

$Mo(CO)_4$ fragment, and formation of a Mo dπ-dpop pπ-Mo dπ (non-bonding) HOMO, resulting in a lower energy HOMO-LUMO transition.[19]

The reaction of **109** with three equivalents of a cupric chloride solution in methanol gave a green solid, which was found by elemental analysis to have the stoichiometry Cu_2(**109**)$Cl_4.2H_2O$. This contrasts with a recent report, by Thompson *et al.*,[221] of the reaction of 4,6-bis-(2-pyridinythio)-pyrimidine (**118**) with cupric chloride, to give a binuclear complex of the stoichiometry Cu_2(**118**)$_2Cl_4$. X-ray crystallographic analysis showed that the complex Cu_2(**118**)$_2Cl_4$ has a structure in which each pentacoordinate Cu(II) is coordinated, in a monodentate manner, to the flexible thiopyridine group of one ligand, whilst forming a six-membered chelate ring with the pyridine and pyrimidine rings of the other ligand. Unfortunately,

the complex Cu_2(**109**)Cl_4 was found to be insoluble in common solvents and thus could not be analysed in this manner.

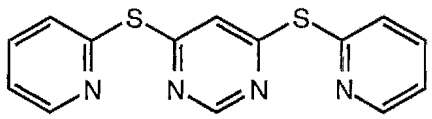

118

Figure 4.4

Thompson *et al.* also described the reaction of **118** with $Cu(ClO_4)_2$ in acetonitrile, which gave a complex with a metal to ligand stoichiometry of 1:1. The reaction of **109** with two equivalents of $Cu(ClO_4)_2.6H_2O$ gave a blue solid, which was shown, by elemental analysis, to have the stoichiometry Cu(**109**)$(ClO_4)_2(H_2O)_2$. The complex was found to be quite insoluble and crystals, suitable for X-ray analysis, could not be obtained. Similarly, reaction of **109** with two equivalents of $Ni(ClO_4)_2.6H_2O$ gave an insoluble yellow solid which was found to have the stoichiometry Ni(**109**)$(ClO_4)_2(H_2O)_2$. Studies with molecular models clearly show that the Ni(II) and Cu(II) complexes of **109** are unlikely to have a structure analogous to that of Cu_2(**118**)$_2Cl_4$, since five-membered chelation of **109** is less flexible than the six-membered chelation of **118**. Alternatively, a polymeric structure for the complexes may be possible.

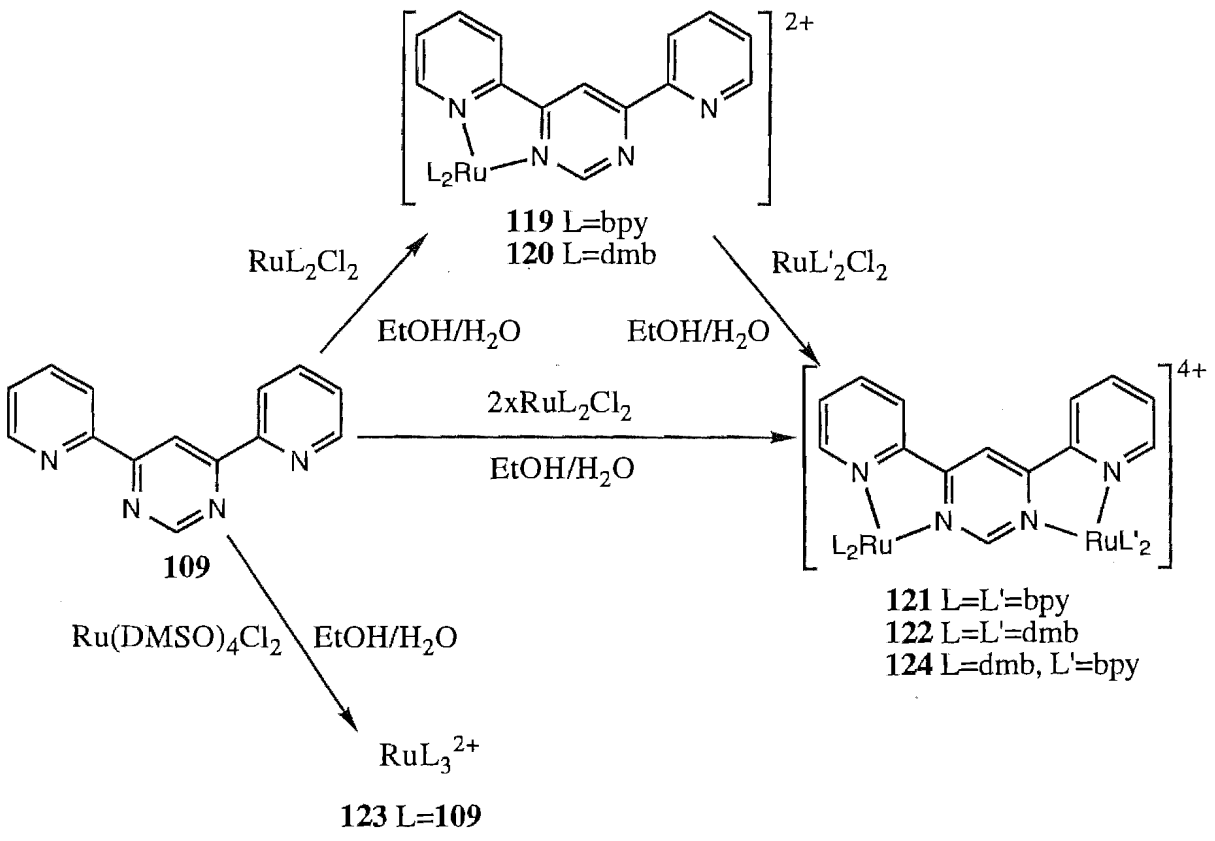

Scheme 4.3

The mono-ruthenium(II) complexes of **109** were prepared in a similar manner to ruthenium complexes already described in chapters 2 and 3. Both the bis-2,2'-bipyridinyl complex (**119**), and the bis-4,4'-dimethyl-2,2'-bipyridinyl complex (**120**), were purified by chromatography on alumina to remove traces of the corresponding binuclear complexes **121** and **122**, which also formed in the reactions (Scheme 4.3). The red monoruthenium complexes were then characterised by elemental analysis and mass spectrometry.

Table 4.2. ^{1}H NMR Chemical Shifts[a] of **119**, **120** and **109**. Coordination Induced Shifts[b] of **119** and **120**.

	H2	H5	H3'	H4'	H5'	H6'	H3''	H4''	H5''	H6''
119	8.54	9.42	8.89	8.20	7.59	7.90	8.51	8.06	7.65	8.88
109	9.38	9.43	8.61	8.05	7.60	8.86				
CIS[b]	-0.84	-0.01	+0.28	+0.15	-0.01	-0.96	-0.10	+0.01	+0.05	+0.02

Bpy ligands			
H3	H4	H5[c]	H6[c]
8.58	8.14	7.47	8.01
8.58	8.14	7.49	7.84
8.58	8.14	7.48	7.78
8.58	8.14	7.48	7.78

	H2	H5	H3'	H4'	H5'	H6'	H3''	H4''	H5''	H6''
120	8.52	9.39	8.86	8.17	7.57	7.90	8.51	8.06	7.65	8.89
109	9.39	9.43	8.61	8.05	7.60	8.86				
CIS[b]	-0.87	-0.04	+0.25	+0.12	-0.03	-0.96	-0.10	+0.01	+0.05	+0.03

Dmb ligands			
H3	4-CH_3[c]	H5[c]	H6[c]
8.42	2.60	7.32	7.79
8.42	2.60	7.32	7.64
8.42	2.58	7.28	7.59
8.42	2.58	7.28	7.57

[a] For deuterated acetonitrile solutions. [b] CIS = $\delta_{complex}$-δ_{ligand}. [c] Not assigned

The ^{1}H NMR spectra of the monoruthenium complexes **119** and **120** are shown in Figures 4.4, whilst the chemical and coordination induced shifts of the protons are summarised in Table 4.2. The pyridine rings in the complexes are non-equivalent, with one ring coordinating and the other non-coordinating. Thus the spectrum of **119** (Figure 4.4 top) consists of 26 non-equivalent protons. Although the replacement of bpy ligands with dmb ligands can assist in assignment of some protons, the change in chemical shift of the auxiliary ligand protons can generate additional overlap. For example (Figure 4.4 bottom), replacement of bpy with dmb allows isolation of H4' and H4'', but also results in overlap of H5' and H5'' with three of the

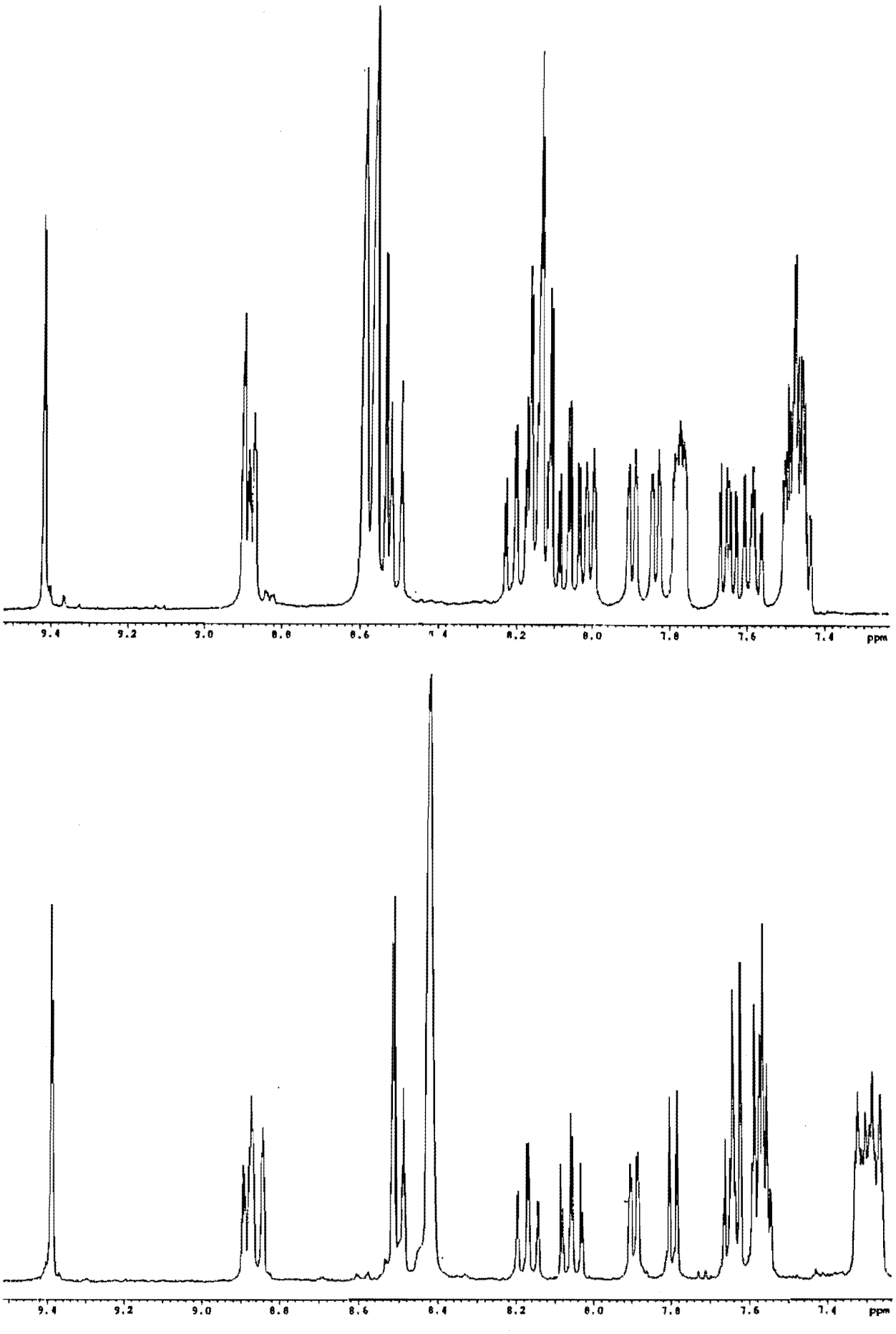

Figure 4.4 ^{1}H NMR Spectra of **119** (top) and **120** (bottom).

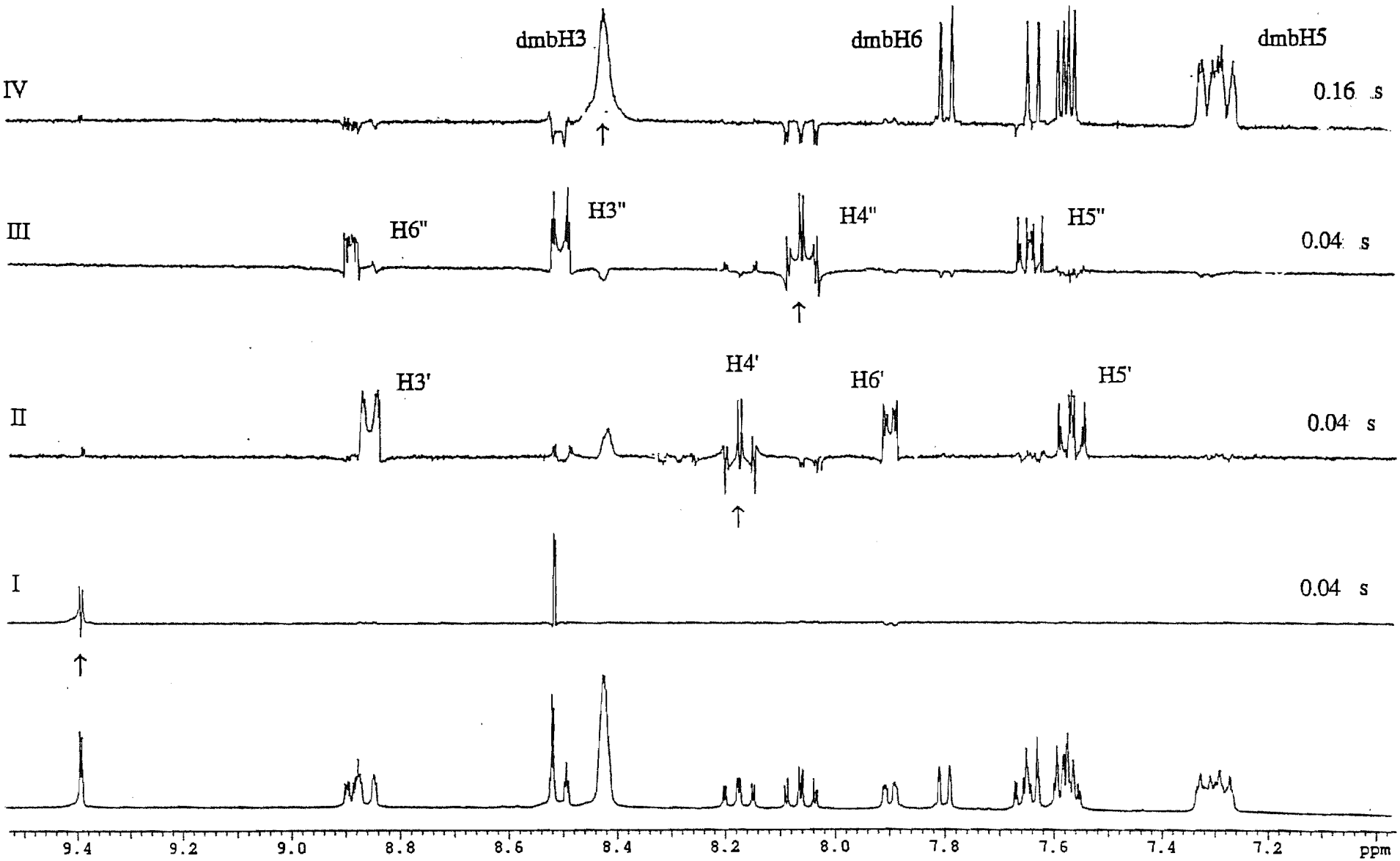

Figure 4.5 1D TOCSY Spectra of **120**

dmbH6 protons. Nevertheless, the ligand **109** in each of the complexes was assigned on the basis of coupling constants and chemical shifts and with the assistance of 1D TOCSY or 2D COSY spectra. For example (Figure 4.5), 1D TOCSY irradiation of the isolated triplets, H4' and H4", in the spectrum of **120**, produces individual sub-spectra corresponding to the two pyridine ring spin systems (trace II and III). Thus, by the characteristic position of the anisotropically shielded H6', which lies over a pyridine ring, the coordinated (H3'-H6') and non-coordinated (H3"-H6") rings may be distinguished. Similarly, the long-range coupling (1.5Hz) of the pyrimidine ring protons, H2 and H5, allows location of H2 by irradiation of H5 (trace I). In this case, H2 is the more upfield doublet, since this proton is also shielded by a pyridine ring. Also, by irradiating the dmbH3 protons, all the dmbH5 and dmbH6 protons may be located (trace IV). The ^{1}H NMR spectrum of **119** was readily assigned by comparision with the spectrum of **120**, and with the assistance of 1D TOCSY and 2D COSY spectra. 2D COSY spectra of either complex could not unambiguously assign the dmb or bpy spins systems.

In summary, the ClS values in the complexes **119** and **120** reflect ring current anisotropy effects (H2 and H6'), the net effect of metal to ligand σ-donation and π-back donation (H4' and H5'), and chelation induced conformational changes (H3' and H3").

A homoleptic ruthenium(II) complex, **123**, was prepared from the reaction of three equivalents of **109** with $Ru(DMSO)_4Cl_2$. The ^{1}H NMR spectrum (CD_3CN) of **123** was assigned by comparison with the spectra of **119**, and by 1D TOCSY spectra. As a consequence of the trisbidentate coordination of the unsymmetrical ligand, the complex exists as a 3:1 mixture of the geometrical isomers mer and fac. Hence there are four non-equivalent ligands (40 non-equivalent protons) in the spectrum, with all three ligands of the fac complex (10 non-equivalent protons) related by a C_3 axis of rotation. The pyridine and pyrimidine protons were readily assigned by comparison with the spectra of **119** and **120**, although the mer and fac isomers could not be distinguished in the spectrum. Attempts to separate these isomers on sephadex were unsuccessful. As mentioned previously, Keene *et al.* have recently separated the mer and fac isomers of structurally related complexes by sephadex ion-exchange chromatography.[215]

^{13}C NMR spectra were recorded for the three mononuclear complexes **119**, **120** and **123**. The spectra were assigned by comparison with the spectra of structurally related complexes and the chemical shifts are listed in Chapter 8.3.

The effect of the ligand **109** on the electronic properties of the complexes can be seen in the UV/VIS spectra of **119**, **120** and **123** which are summarised in Table 4.3. The complexes

exhibit strong ligand centred absorptions at λ<400nm and MLCT absorption bands at λ>400nm. The lowest energy absorptions (492nm (**119**), 506nm (**120**) and 488nm (**123**)) correspond to dπ-π*(**109**) transitions, since the pyrimidine containing ligand has lower lying π* orbitals than does bpy. Hence electron transfer, from metal to ligand, is easier in **119**, **120** and **123** than in $Ru(bpy)_3^{2+}$. The second highest energy MLCT transitions for **119** and **120**, 438nm and 436nm respectively, are likely to be due to electron transfer into the π*bpy orbitals. The lowest energy MLCT of **119** is also at lower energy than that of $Ru(\mathbf{15})(bpy)_2^{2+}$, an effect which is paralleled in the relative energies of the lowest MLCT of **123** and $Ru(\mathbf{15})_3^{2+}$. A similar trend can be seen in the $\Delta E_{ox\text{-}red}$ values, which show a smaller HOMO-LUMO gap in the complexes of **109**, particularly in the homoleptic complexes **123** (2.38V) and $Ru(\mathbf{15})_3^{2+}$ (2.63V). Pyrimidine is a poorer π-acceptor than pyrazine but is still better than pyridine, in line with the relative energies of the LUMO π* orbitals.[3,222,223] Hence the ligand **109** is less efficient than pyrazine at stabilising the metal d orbitals, by π back-bonding, than is **15** thus giving rise to a smaller HOMO-LUMO gap in the complexes of **109**. The lowest MLCT band of **123** (488nm) is not as symmetrical as that of $Ru(bpy)_3^{2+}$ and has a shoulder at 464nm. This absorption is likely to be a combination of dπ-π* transitions into the pyrimidine ring (488nm) and into one of the pyridine rings (464nm) of **109**.

Table 4.3. Absorption Maxima[a] and Redox Potentials[b] of **119**, **120** and **123**.

	λ	E_{ox}	E_{red1}	E_{red2}	E_{red3}	E_{red4}	$\Delta E_{ox\text{-}red}$
$Ru(bpy)_3^{2+}$	451	+1.27	-1.31	-1.50	-1.77	-	2.58
$Ru(\mathbf{15})(bpy)_2^{2+}$	475	+1.31	-1.06	-1.55	-1.74	-	2.37
$Ru(\mathbf{15})_3^{2+}$	455	+1.68	-0.95	-1.12	-1.39	-	2.63
119	408sh,438,492	+1.28	-1.03	-1.55	-1.76	-	2.31
120	406sh,436,506	+1.18	-1.07	-1.64	-1.85	-	2.25
123	464sh,488	+1.39	-0.99	-1.13	-1.33	-1.92	2.38

[a] In nanometres. [b] In volts vs SCE in acetonitrile.

Further insight into the properties of the complexes can be obtained from the redox potentials of **109**, **119**, **120** and **123**, as determined by cyclic voltammetry. The ligand exhibits two reversible one electron reductions; firstly, reduction of the pyrimidine ring at -1.76V and, secondly, reduction of a pyridine ring at -2.26V. These reductions are shown in Figure 6.4 (top). Figure 6.4 also shows the cyclic voltammograms of two of the mononuclear complexes **120** (middle of Figure) and **123** (bottom of Figure) whilst the redox potentials for all three mononuclear complexes are summarised in Table 4.3. The complexes each exhibit a reversible one electron oxidation and three (four in the case of **123**) reversible one electron reductions. The

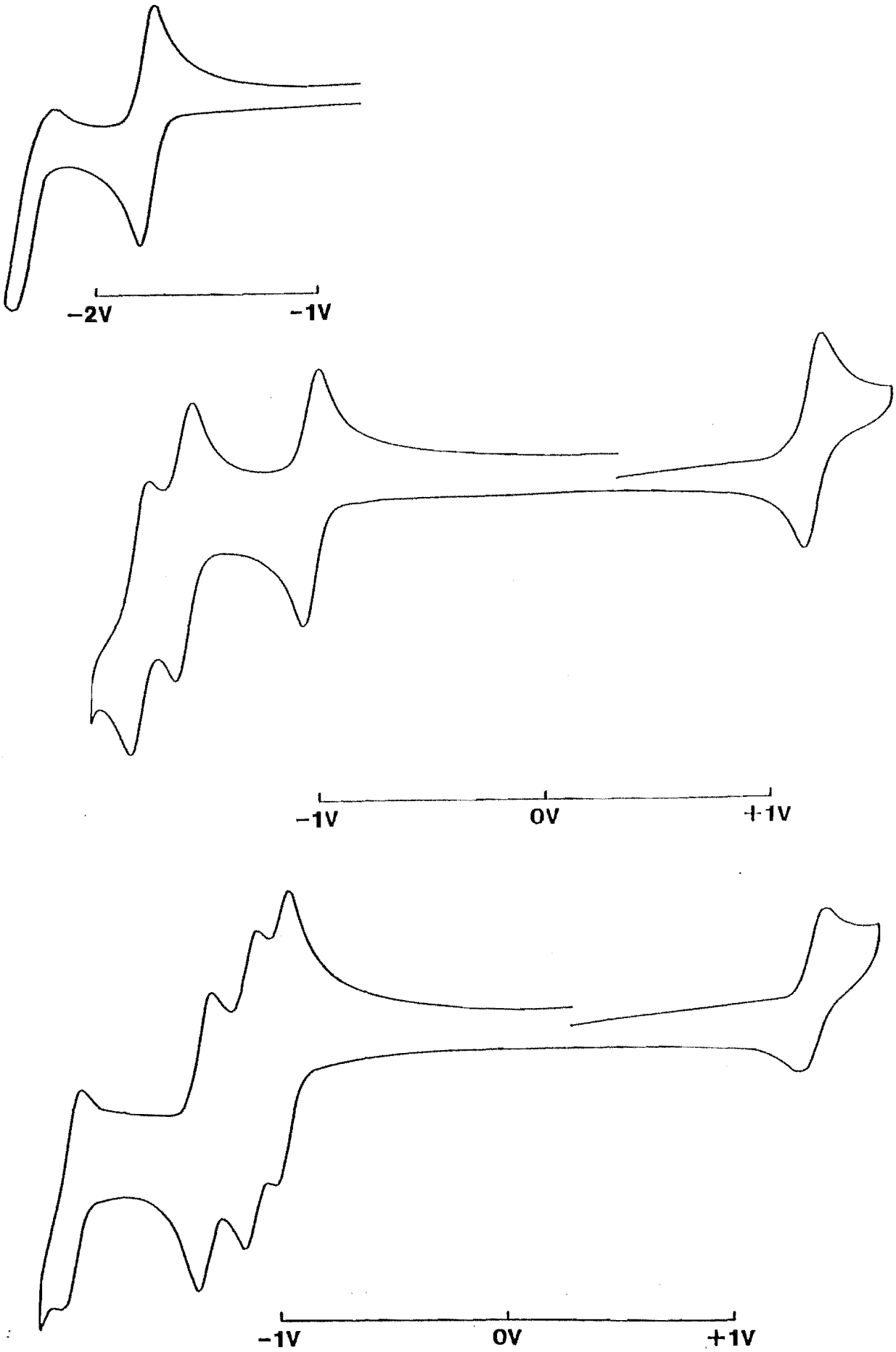

Figure 4.6 Cyclic Voltammograms of **109** (top), **120** (middle) and **123** (bottom).

first reduction of **119** and **120**, and the first, second and third reductions of **123**, were assigned to reduction of the pyrimidine ring of **109**. The second and third reductions of **119** and **120** are localised in the bipyridine ligands, whilst the fourth reduction of **123** may be attributed to a reduction of a pyridine ring of **109**. The different oxidations of the complexes **119**, **120** and **123** indicate the relative energies of the metal d orbitals of the complexes. Relative to **119**, the d orbitals of **120** are destabilised by the electron donating methyl groups of **120**. In the case of **123**, the d orbitals are stabilised by all three **109** ligands, which are better π-acceptors than bpy. The electrochemistry of **119** is comparable to that of Ru(**15**)(bpy)$_2^{2+}$. However, **123** is more easily oxidised than Ru(**15**)$_3^{2+}$, reflecting the weaker π-acceptor ability of **109** relative to **15**, although the complex has a similar first reduction potential. Thus the HOMO-LUMO gap of **123** is smaller than that of Ru(**15**)$_3^{2+}$, which is manifest in both the smaller value of $\Delta E_{ox\text{-}red}$ and the lower energy MLCT of **123**.

Having surveyed mono-ruthenium complexes of **109**, three homobinuclear complexes of the ligand were then prepared and analysed. The symmetrical biruthenium(II) complexes **121** and **122** were readily prepared by reacting the ligand with two equivalents of the corresponding ruthenium complex and, as discussed earlier, were also obtained, as by-products, in the reaction of the ligand with one equivalent of ruthenium(II) (Scheme 4.3). Complex **124** was prepared by reacting **120** with one equivalent of Ru(bpy)$_2$Cl$_2$ (Scheme 4.3). The binuclear complexes are dark purple in solution, compared to the mononuclear complexes which are red. This is indicative of a strong metal-metal interaction, with the absorption of the binuclear complex shifting to lower energy.

The complex **121** has the structure shown in Scheme 4.3 in which the ligand forms a bis-bidentate bridge between two ruthenium(II) centres. This was confirmed by mass spectrometry and ^{1}H NMR spectroscopy. As has been discussed previously, complexes containing two chiral octahedral ruthenium(II) centres should exist as both the racemic (ΔΔ/ΛΛ) and meso(ΔΛ) diastereoisomers, which are non-equivalent and therefore distinguishable by ^{1}H NMR. Such stereoisomerism exists in **121** and is demonstrated in the ^{1}H NMR spectrum of the complex (Figure 4.7).

The spectrum consists of 44 non-equivalent protons; 22 protons corresponding to the racemic isomer and 22 for the meso isomer. Unlike the mononuclear complexes, the pyridine rings of the bridging ligand are equivalent, since in the racemic isomer the rings are related by rotational symmetry, whilst in the meso isomer, they are related by a mirror plane. Many of the

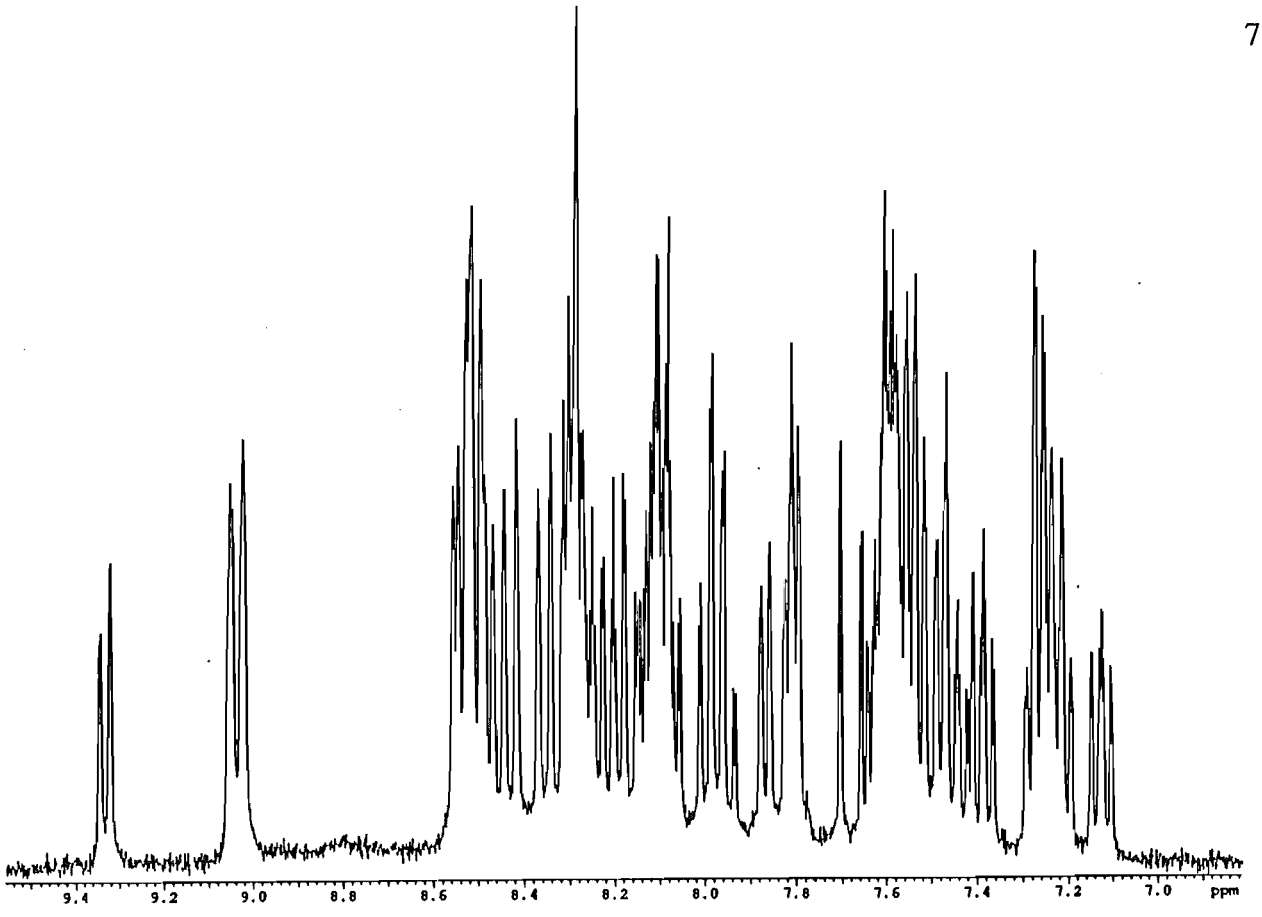

Figure 4.7 ^{1}H NMR Spectrum of **121**.

bridging ligand signals are overlapped by the mass of bpy signals, but were readily located using the 1D-TOCSY spectra shown in Figure 4.8. For example, irradiation of the closely spaced H5 doublets (9.33 and 9.35ppm) of the two non-equivalent pyrimidine rings locates the two H2 doublets (7.70 and 7.66ppm) (trace I). Similarly, irradiation of the exposed H3' doublet (9.04ppm) successively locates, with extended mixing time, H4' (8.26, 8.30ppm), H5' (7.59, 7.62ppm) and finally H6' (7.80, 7.87ppm) (trace II-IV).

The 1D TOCSY spectra did not, however, distinguish the diastereoisomers of **121**. Accordingly, attempts were made to separate these two isomers, by chromatography of the tetracation on C-25 sephadex, with NaCl (0.3-0.5M) as the eluent. Despite repeated attempts, the diastereoisomers could not be separated. Recently, Keene *et al.* have used ion-exchange to separate the diastereoisomers of related binuclear complexes of bpm and **15**, although these complexes have non-identical terminal ligands, which is crucial in effecting a good separation of the diastereoisomers.[167] In the present case, fractions of **121** were obtained which were slightly enriched in either of the diastereoisomers. Fractional recrystallisation of these fractions failed to increase this enrichment. However, by examining the ^{1}H NMR spectra of the enriched samples, it was possible to assign the bridging ligand protons of the two diastereoisomers and to assign the bpy protons (in some cases tentatively).

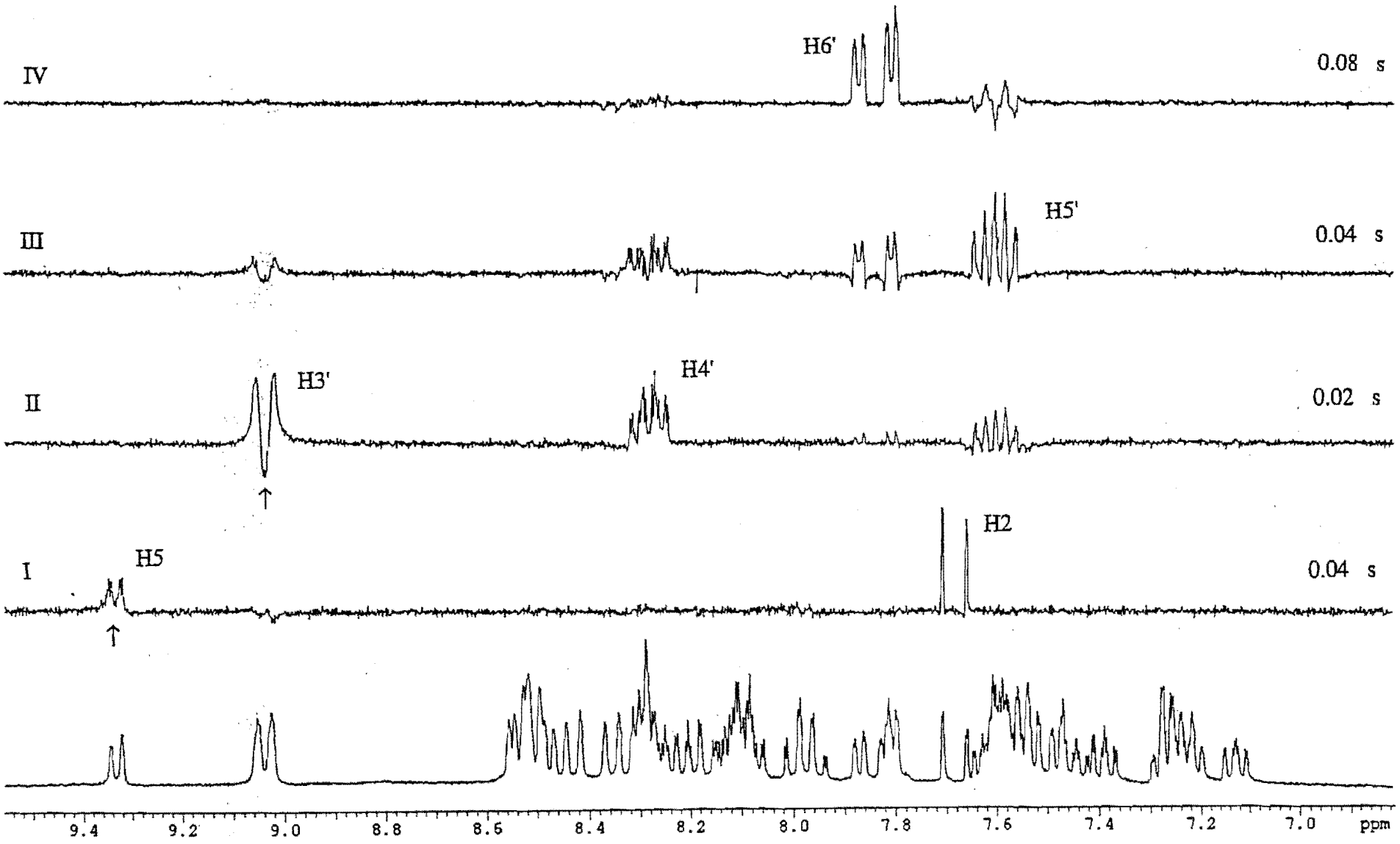

Figure 4.8 1D TOCSY Spectra of 121

Table 4.4. ^{1}H NMR Chemical Shifts[a] of **121a**, **121b** and **109**. Coordination Induced Shifts[b] of **121a** and **121b**.

	Ligand **109**						Bpy ligands			
	H2	H5	H3'	H4'	H5'	H6'	H3[c]	H4[c]	H5[c]	H6[c]
121a	7.70	9.33	9.04	8.26	7.59	7.80	8.36	7.99	7.13	7.48
109	9.38	9.43	8.61	8.05	7.60	8.86	8.44	8.08	7.23	7.52
CIS[b]	-1.68	-0.10	+0.43	+0.21	-0.01	-1.06	8.53	8.11	7.25	7.55[d]
							8.55	8.18	7.39	7.55[d]
121b	7.66	9.35	9.04	8.30	7.62	7.87	8.48	7.97	7.22	7.60
109	9.38	9.43	8.61	8.05	7.60	8.86	8.49	8.10	7.23	7.60
CIS[b]	-1.72	-0.08	+0.43	+0.25	+0.02	-0.99	8.51	8.12	7.27	7.60[d]
							8.52	8.20	7.44	7.82

a For deuterated acetonitrile solutions. b CIS = $\delta_{complex}$-δ_{ligand}. c Not assigned. d Tentative assignments.

The diastereoisomers are referred to as **121a** and **121b** and their individual spectra are summarised in Table 4.4. The H2 proton exhibits a larger negative coordination induced shift than was the case in the mononuclear complex, since this proton is now shielded, anisotropically, by two pyridine rings. In contrast, H6', and to a lesser extent H5', are shielded by one pyridine ring and thus exhibit a smaller CIS. Of the remaining protons, the CIS values of H3' and H5 show the effects of chelation induced conformational changes, whereas H4' and H5' show the effect of the net donation of electron density from ligand to metal. Molecular modelling studies of the complex show that a bpyH6 proton is deshielded in the meso isomer, whereas in the racemic isomer the same proton is shielded. A similar effect is known for diruthenium complexes of bpm.[167] In the spectrum of **121**, the most deshielded bpyH6 (7.82ppm) belongs to the diastereoisomer **121b** which can therefore be assigned the meso stereochemistry $\Delta\Lambda$; thus **121a** can be assigned the racemic stereochemistry $\Delta\Delta/\Lambda\Lambda$. The diastereoisomers exist in 7:6 ratio, in contrast with the complex **64**, in chapter 2, for which the meso form was the major isomer.

Two further binuclear ruthenium(II) complexes were also synthesised (Scheme 4.3), **122**, as mentioned above, and **124**, in which **109** is bridging between a $Ru(dmb)_2^{2+}$ unit and a $Ru(bpy)_2^{2+}$ unit. Both complexes were characterised by mass spectrometry and ^{1}H NMR spectroscopy. In a similar manner to the ^{1}H NMR spectrum of **121**, the bridging ligand protons of **122** and **124** were assigned by 1D TOCSY irradiations of H5 and H3', whilst the dmb and/or bpy protons were assigned only tentatively. No attempt was made to separate the diastereoisomers, which were found to be in a 5:3 ratio in **122**, and in a 7:6 ratio in **124**.

The electronic properties of the complexes were examined by UV/VIS absorption spectroscopy and cyclic voltammetry. All complexes show strong ligand centred absorptions at

λ<400nm and exhibit a series of MLCT bands at λ> 400nm, the latter of which are listed in Table 5.4. The bands at (432-434nm) for the complexes can be assigned as an MLCT transitions ($d\pi$-π^*) into the bipyridine ligands. The slight increase in the energy of this transition, relative to the mononuclear complexes, has already been observed for **64** and **65** and is due to the increase in electrostatic attraction toward the optical electron as a result of coordinating a second ruthenium(II). The large red shift of the lowest energy MLCT of the binuclear complexes (570-580nm), relative to the mononuclear complex, indicates a strong metal-metal interaction and corresponds to further lowering of the π^*-LUMO of the bridge, by back-bonding between the π^* orbitals of **109** and the d orbitals of the second RuL_2^{2+} unit. This red shift can be seen in Figure 4.9 which shows the UV/VIS absorption spectra of **121** (bottom) and **119** (top). The lowest MLCT transition exists as a shoulder to a further MLCT band at 532-540nm. Such unsymmetrical absorptions, have been described for structurally related complexes, for which numerous explanations have been provided.[30,33]

Table 4.5 also includes the redox potentials of **121**, **122** and **124**. Complex **121** has two reversible one electron oxidations (+1.36 and +1.52V) separated by 160mV and five reversible reductions (Figure 4.10). Cooper *et al.* have shown, for a series of binuclear ruthenium complexes, that a linear correlation exists between the splitting of the first and second reductions ($\Delta E_{red1\text{-}red2}$) and the number of bonds in the bridging ligand.[224] In the case of **121**, the value for $\Delta E_{red1\text{-}red2}$ of 0.64V is consistent with this relationship. Hence the first and second reductions were assigned to successive one electron reductions of **109**. The first reduction is centred on the pyrimidine ring and is typically lower than the reduction of **109** in the complex **119**. This reflects the synergistic lowering of the π^* orbitals of the bridge by both metals and parallels the red shift in the lowest energy MLCT. The second reduction corresponds to reduction of a pyridine ring of the bridge. Two successive one-electron reductions ($\Delta E_{red1\text{-}red2}$=0.50V) of a bridging ligand have previously been described for the structurally related complex $[Ru(bpy)_2]_2(\mathbf{15})^{4+}$.[126] The known twisting of the rings in this complex lessens the conjugation of the bridging ligand, which may

Table 4.5. Absorption Maxima[a] and Redox Potentials[b] of **121**, **122** and **124**

Complex	λ	E_{ox1}	E_{ox2}	E_{red1}	E_{red2}	E_{red3}	E_{red4}	E_{red5}
$[Ru(bpy)_2]_2(\mathbf{15})^{4+}$	527	+1.38	+1.55	-0.67	-1.17	-1.57[c]	-1.89[c]	-
121	432, 532, 570	+1.36	+1.52	-0.59	-1.23	-1.62[c]	-1.89	-2.03
122	434, 540, 580	+1.27	+1.43	-0.63	-1.27	-1.81[c]	-1.98[c]	-
124	432, 534, 572	+1.29	+1.50	-0.63	-1.25	-1.63	-1.77	-1.92

[a] In nanometres. [b] In volts vs SCE in acetonitrile. [c] Two electron.

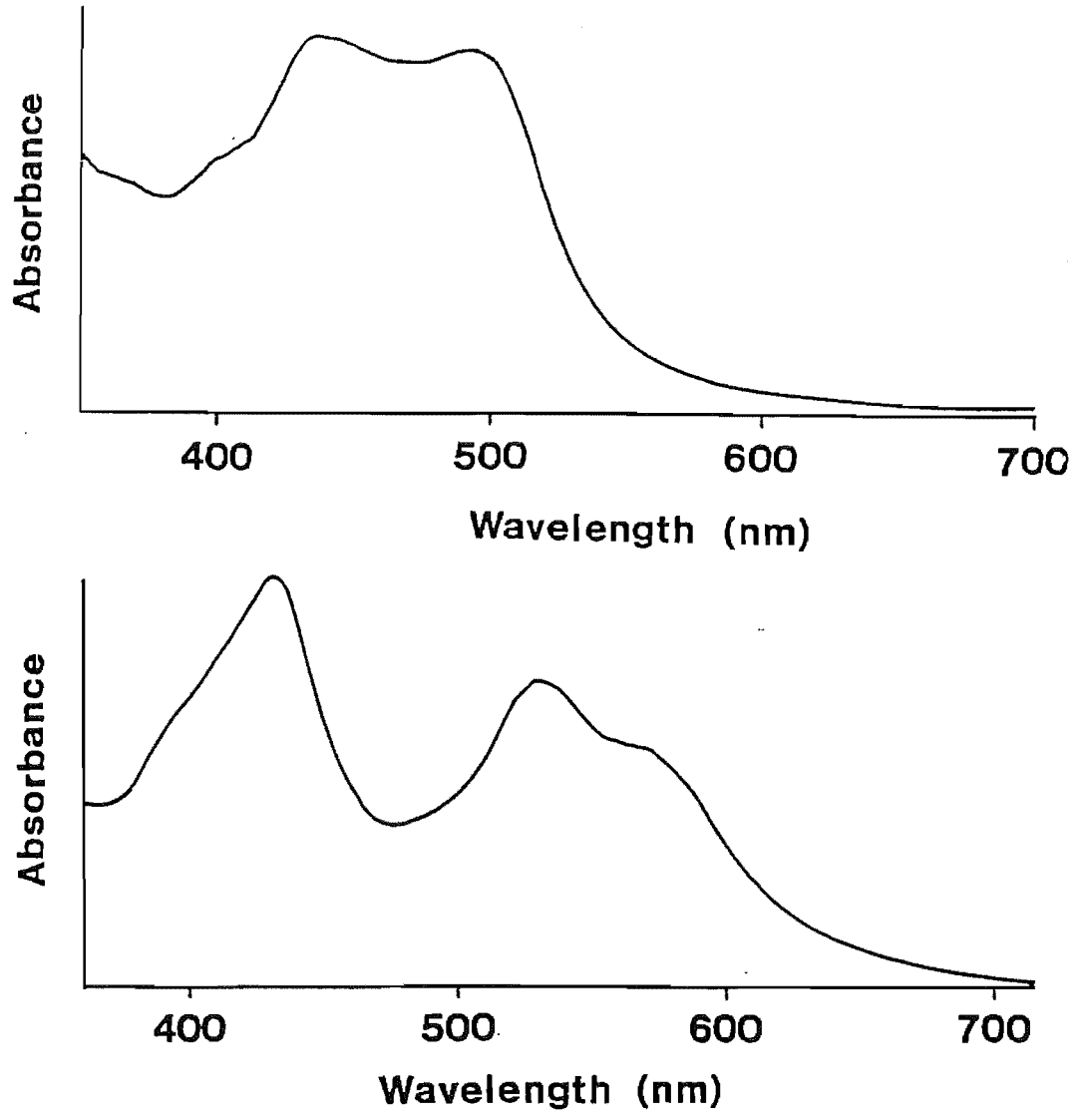

Figure 4.9 UV/VIS Absorption Spectra of **119** (top) and **121** (bottom)

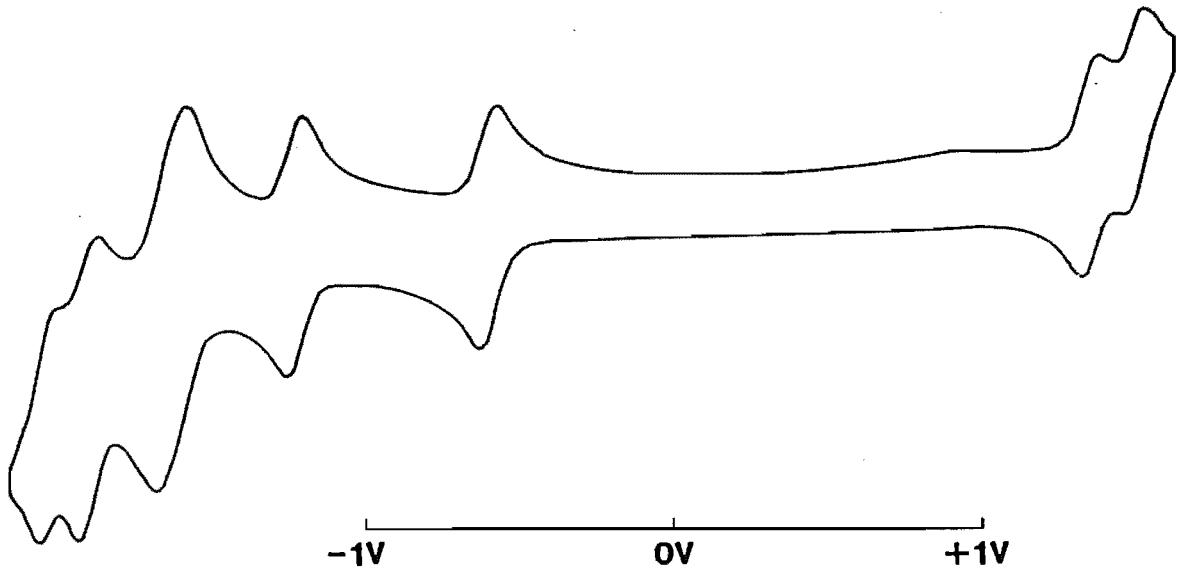

Figure 4.10 Cyclic Voltammogram of **121**

account for the smaller value of $\Delta E_{red1\text{-}red2}$ relative to the present case. In addition, two reversible two electron reductions, at more negative potentials, were reported for $[Ru(bpy)_2]_2(\mathbf{15})^{4+}$ and assigned to the successive reduction of couples of bpy coordinated to different metals. In the present case, the third reduction of **121** is a two electron process and can thus be assigned to reduction of the bpy ligands. The fourth and fifth reductions (fifth and sixth electrons respectively) are one electron processes and these are probably centred on the other two bpy ligands. One of these last two reductions may be centred on the bridging ligand, although the large coulombic repulsion would most likely impede a third reduction of **109** at this potential.

The oxidation potentials in **121** are split by 160mV, indicating that the metals are coupled via the π system of the ligand. Oxidation of the first metal (+1.36V) stabilises the d orbital of the metal and thus prevents back-bonding to the π^* orbital of **109**. This allows additional stabilisation of the d orbitals of the second metal, which can now back-bond more efficiently with the bridging ligand, thus raising the second oxidation potential (+1.52V). Molecular modelling studies, using CHEM 3D Plus, suggested values of the inter-metal separation in **121** and $[Ru(bpy)_2]_2(\mathbf{15})^{4+}$ of 6.2Å and 6.7Å respectively. Thus, despite the ability of **109** to decrease the distance between the metals, there is no increase in the metal-metal interaction, relative to $[Ru(bpy)_2]_2(\mathbf{15})^{4+}$ ($\Delta E_{1/2}$=170mV). This can be rationalised by the fact that pyrimidine is a poorer π-acceptor than pyrazine, which counteracts the relative decrease in the inter-metal separation of **121**. Hence, **121** exhibits a comparable interaction to $[Ru(bpy)_2]_2bpm^{4+}$, in which the metals are held at a distance of 5.6Å.[25,35]

In contrast, **122** exhibits less positive oxidations and more negative reductions, which is attributed to the electron donating methyl groups of the dmb ligands. Oxidations are raised by approximately 100mV, which is consistent with the oxidation of complexes described earlier in this work and with structurally related complexes.[176] The third and fourth reductions are more negative than those of **121**, which equates with the higher energy of the dmb π^* orbitals relative to bpy. Furthermore, the first and second reductions of **122** occur at similar potentials to those of **121**, thus confirming their assignments as bridging ligands reductions, although the potentials are slightly more negative due to the electron donating effect of the dmb ligands. The complex **124**, has different peripheral ligands on each of the two metals. Hence, the d orbitals of the ruthenium(II) bound to the dmb ligands are destabilised, relative to the ruthenium(II) bound to the bpy ligands. This is manifest in the oxidation potentials of the $Ru(dmb)_2^{2+}$ unit (+1.29V) and the $Ru(bpy)_2^{2+}$ unit (+1.50V) resulting in an increase in the splitting of the oxidation potentials

($\Delta E_{1/2}$=210mV) relative to **121**. Thus the peripheral ligands may cause an apparent increase in the degree of metal-metal interaction in the complex. The role of the peripheral ligands in such binuclear complexes has been the subject of a recent comprehensive study.[225]

A fourth binuclear complex of **109** was prepared in which the ligand bridges two different metals, namely ruthenium(II) and palladium(II) (Scheme 4.4). The heterobinuclear complex **125**, was prepared by reacting **119** with one equivalent of $Pd(PhCN)_2Cl_2$ in dichloromethane and was found to be a deep blue colour in acetonitrile solution. The complex was characterised by elemental analysis, mass spectrometry and ^1H NMR spectroscopy.

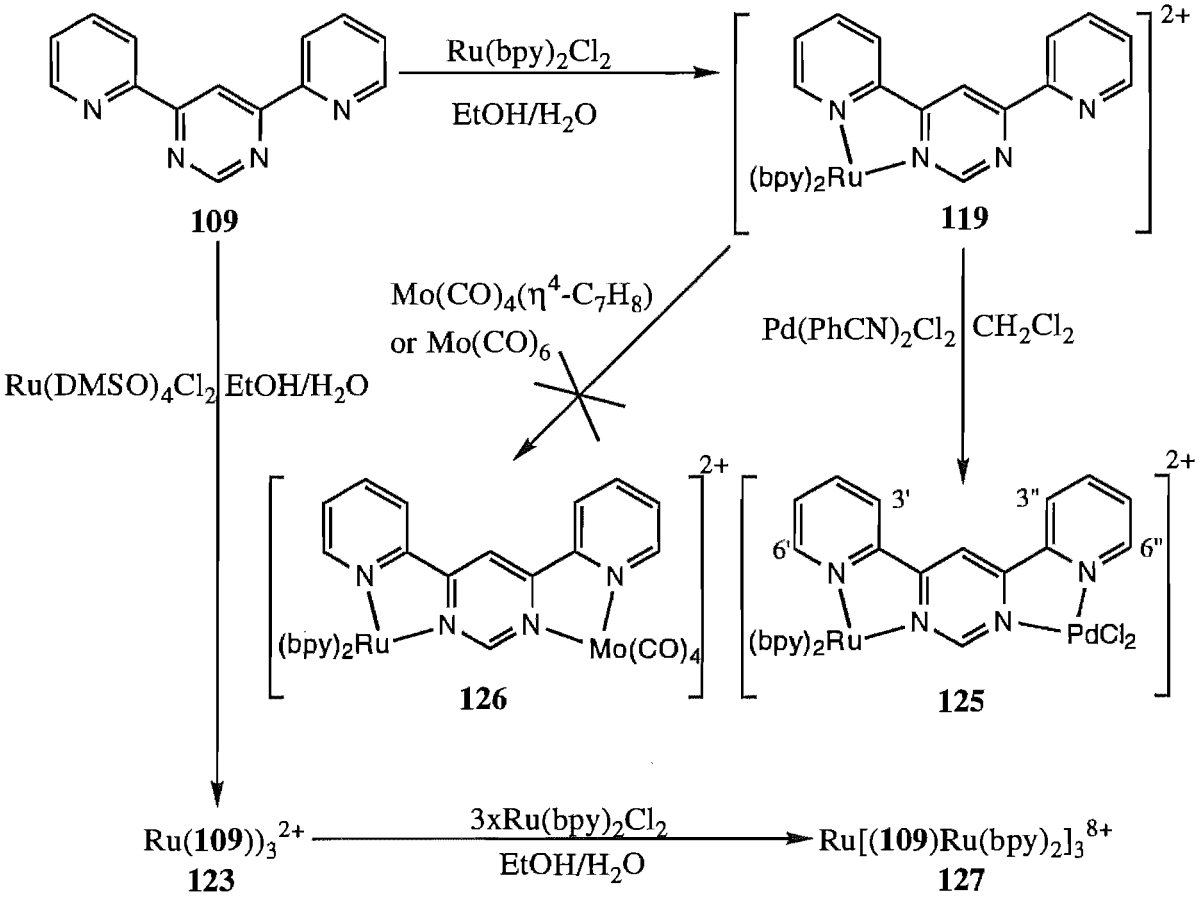

Scheme 4.4

The ^1H NMR spectrum of **125** is shown in Figure 4.11 and consists of 26 non-equivalent protons (Table 4.6). The pyridine rings of **109** were assigned by their coupling constants and chemical shifts and the assignments were confirmed by a 2D COSY spectrum (Figure 4.12). An nOe from both H3' (8.96ppm) and H3" (8.70ppm) to the signal at 9.42ppm enabled H5 and hence H2 (9.10ppm) to be assigned (Figure 4.12). This contrasts with the spectrum of **119**, in which H2 (8.54ppm, CIS = -0.84ppm) is shielded anisotropically by a pyridine ring and is well upfield of H5 (9.42ppm). In this case, H2 is shielded by a pyridine ring but deshielded by an adjacent chlorine, and hence, exhibits a smaller CIS (-0.28ppm). The CIS values for the H3'-H6'

and H3"-H6" rings are also contrasting. The factors which give rise to the CIS values of the coordinated pyridine ring in the complex **119** can also account for the CIS values of the H3'-H6' ring of **125**, although the positive shifts, in **125**, are slightly larger due to coordination of the electron withdrawing palladium. In contrast, the palladium coordinated ring exhibits larger CIS values; due to the σ-donation of electron density from ligand to metal (H4" and H5"), the deshielding effect of an adjacent chlorine (H6") and chelation induced conformational changes (H3"). This last effect also accounts for the upfield shift of H5.

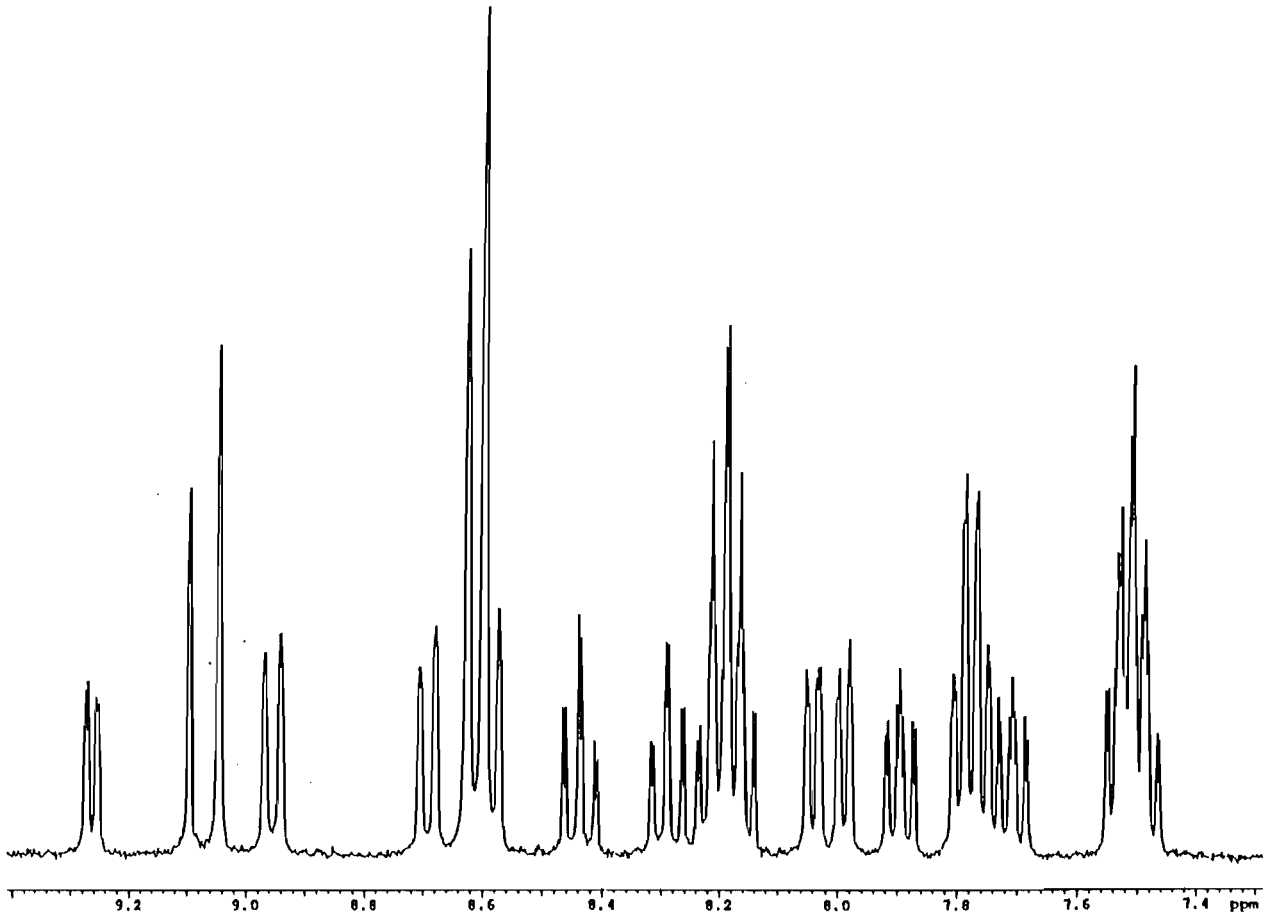

Figure 4.11 ^{1}H NMR Spectrum of **125**

Table 4.6 ^{1}H NMR Chemical Shifts[a] and Coordination Induced Shifts[b] for **125**.

	H2	H5	H3'	H4'	H5'	H6'	H3"	H4"	H5"	H6"
125	9.10	9.05	8.96	8.29	7.71	7.99	8.70	8.44	7.90	9.26
109	9.38	9.43	8.61	8.05	7.60	8.86				
CIS[b]	-0.28	-0.38	+0.35	+0.24	+0.11	-0.87	+0.09	+0.39	+0.30	+0.40

Bpy ligands			
H3[c]	H4[c]	H5[c]	H6[c]
8.59	8.16	7.49	7.76
8.61	8.19	7.51	7.78
8.61	8.19	7.51	7.80
8.61	8.22	7.53	8.04

[a] For deuterated acetonitrile solutions. [b] CIS = $\delta_{complex}$-δ_{ligand}. [c] Not assigned.

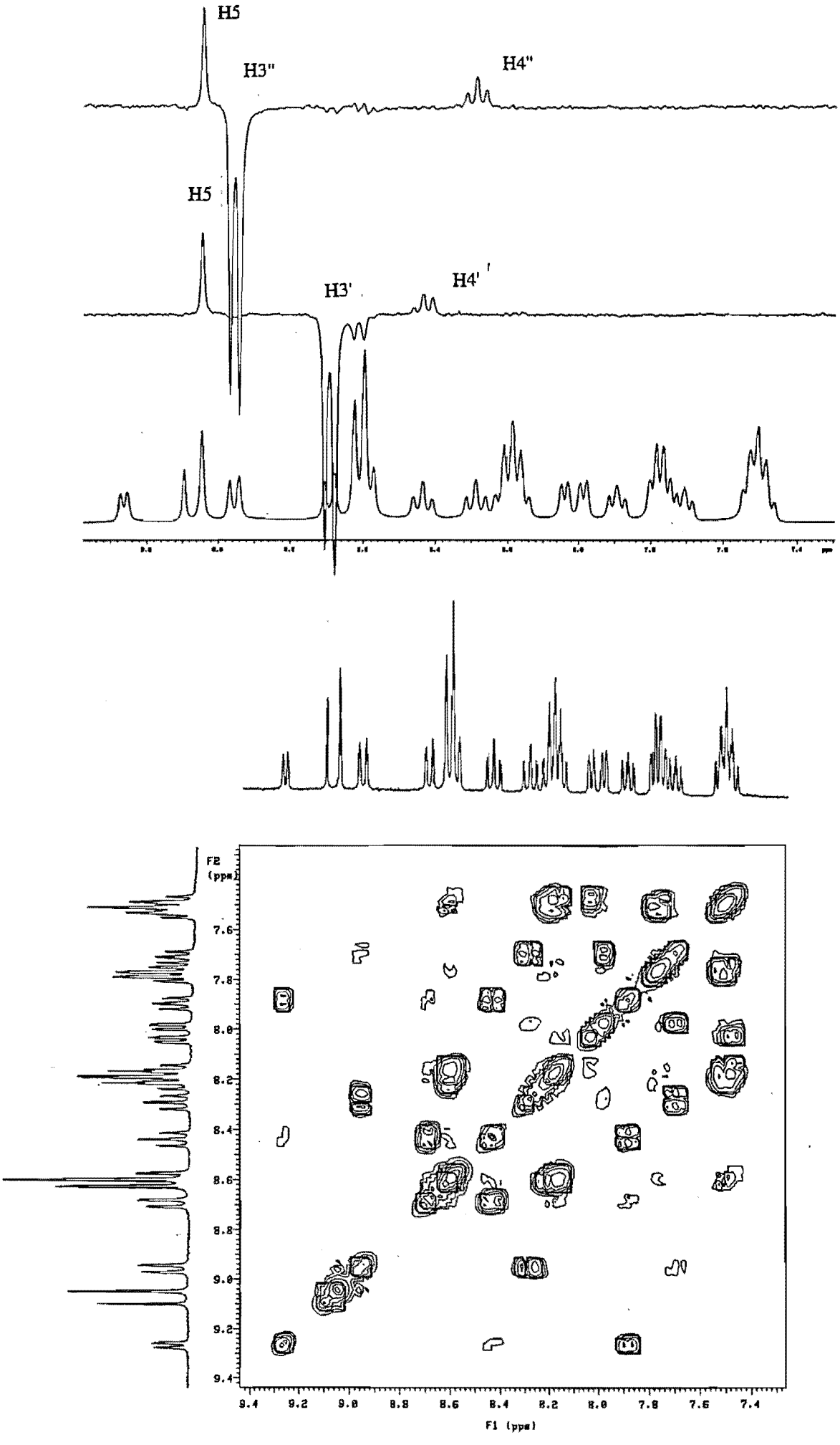

Figure 4.12 nOe Difference and 2D COSY Spectra of **125**

In the spectrum, the signal for H2 has a smaller integral than the signal for H5, indicating that the H2 proton has a longer relaxation time. The integral of H2 becomes equal to that of H5 if a delay of 2 seconds is implemented between the excitation pulse and the aquisition step.

A ^{13}C NMR spectrum of **125** was obtained and was assigned by comparison with the spectrum of **119** (see Chapter 8.3). As was found in the ^{1}H NMR spectrum (Figure 4.11), the carbon signals were found to be more widely spread than in the spectrum of **119**.

The electronic properties of **125** were examined by UV/VIS absorption spectroscopy and cyclic voltammetry. Coordination of the palladium(II) results in a lowering of the π^* orbital of the bridge. This is shown in the lowest energy $d\pi$-π^*(**109**) transition which occurs at 574nm, much lower in energy than the equivalent MLCT (492nm) of the mononuclear complex **119**. In addition, the complex exhibits a second MLCT transition (426nm) which is most likely $d\pi$-π^*(bpy).

Electrochemically, the complex exhibits a reversible one electron oxidation (+1.38V), a reversible one electron reduction (-0.47V) and a second irreversible one electron reduction (-1.02V). Oxidation of this complex is more difficult than for the complex **119** (+1.28V), since the electron, in being removed from the metal d orbital, must contend with the additional electrostatic attraction of the palladium(II). As mentioned above, coordination of palladium with **109** lowers the energy of the MLCT and also accounts for the greater ease of the first reduction, which has been assigned to reduction of the bridging ligand. The remaining reduction is most probably of the bridging ligand. The value for $\Delta E_{ox\text{-}red}$ of 1.85V parallels the lowest energy MLCT and indicates that the HOMO-LUMO gap in this complex is slightly smaller than in the biruthenium complexes of **109**.

Attempts were also made to prepare a second heterobinuclear complex, **126**, by reacting the mono-ruthenium complex **119** with one equivalent of $Mo(CO)_4(\eta^4\text{-}C_7H_8)$ in dichloromethane or with one equivalent of $Mo(CO)_6$ in refluxing toluene. However, in the former reaction very little product had formed after three days stirring, whilst in the latter reaction no product was formed at all.

An interesting tetranuclear species (**127**) (Scheme 4.4) was prepared by reacting the homoleptic complex **123** with three equivalents of $Ru(bpy)_2Cl_2$. Elemental analysis of **127** was unsatisfactory due to the presence of trace amounts of NH_4PF_6 and Ru(III) salts. The complex exists as a number of isomers, as a result of the mer/fac isomerism of the ruthenium core and the four chiral centres. Hence, the ^{1}H NMR spectrum of **127** was too complicated to assign. This

problem has previously been described, for structurally related polynuclear complexes of 2,3-dpp (**15**), by Balzani *et al.*[126]

Figure 4.13 shows the UV/VIS spectrum of **127** and also includes the spectrum of the homoleptic complexes **123** which has been previously described. Like the binuclear complexes **121**, **122** and **124**, the tetranuclear complex exhibits a large red shift in its lowest energy MLCT, relative to the mononuclear case, which indicates a strong metal-metal interaction. An absorption at λ=430nm corresponds to the transitions from outer metals into the bpy ligands, i.e. MLCT $d\pi$-π^*(bpy). At lower energy, two maxima can be distinguished at λ=512nm and λ=576nm. Different MLCT transitions are possible in the complex. For example, MLCT transitions into the bridging ligands **109** can occur from either the central metal or the outer metals. This may account for the maxima at 512nm and 576nm, with the lowest energy maxima corresponding to $d\pi$(outerRu(II))-π^*(**109**). Similar complexities, in the absorption of structurally related polynuclear complexes, have been described by others.[126]

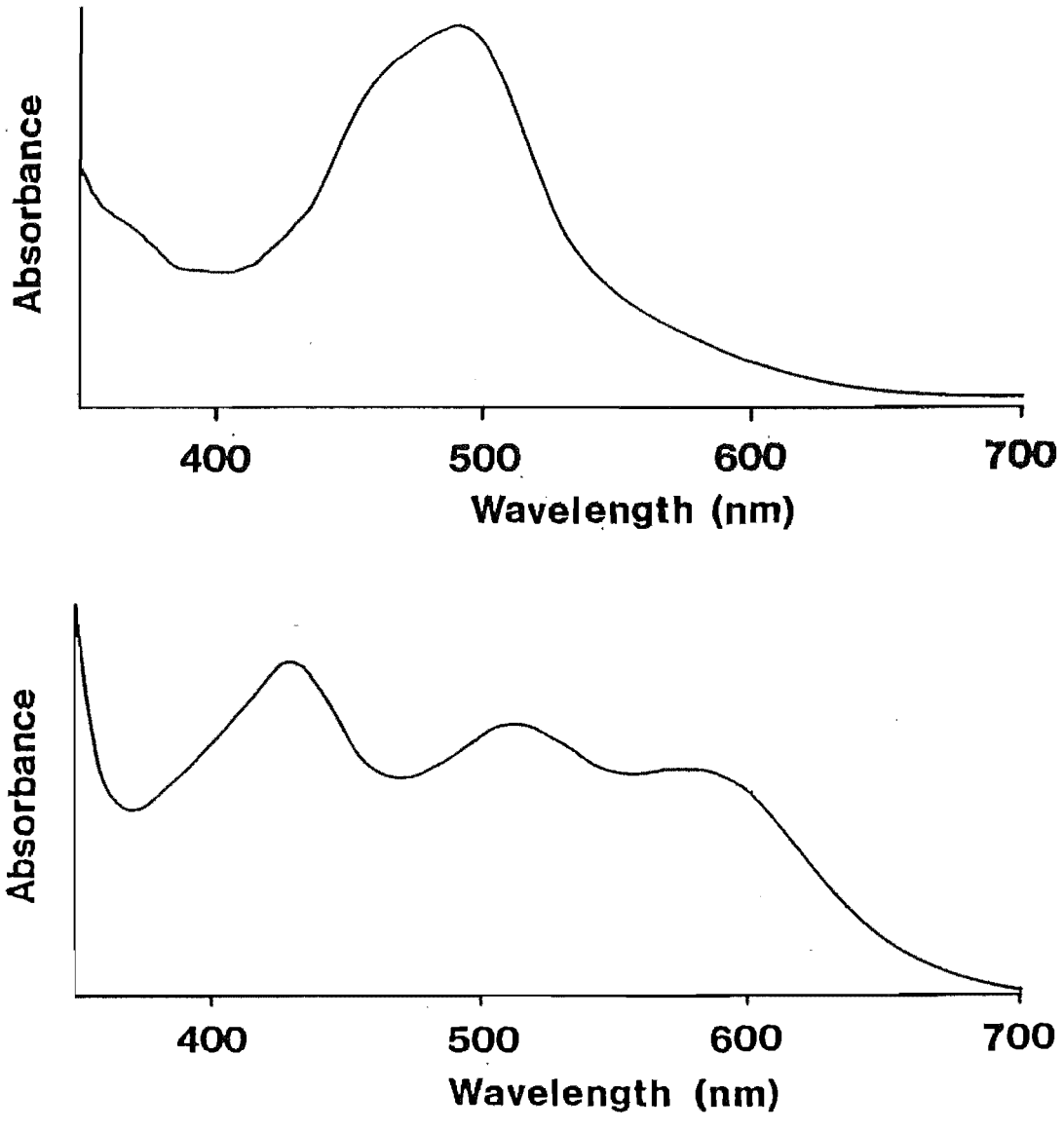

Figure 4.13 UV/VIS Spectrum of **123** (top) and **127** (bottom).

The cyclic voltammogram of **127** consists of reversible trielectronic (+1.26V) and monoelectronic (+1.48V) oxidations. The first of these can be attributed to oxidation of the three outer metals, whilst the second corresponds to oxidation of the central ruthenium(II) core, which is more difficult. In the corresponding tetranuclear complex of **15**, oxidation of the central ruthenium(II) could not be observed.[126] Seven reductions of the complex were also observed. One electron reductions of the pyrimidine of each of the three bridging ligands occurs as a triplet of reversible one electron reductions (-0.27V, -0.48V, -0.67V), whilst a similar triplet, at more negative potentials (-1.23V, -1.37V, -1.50V), corresponds to the reduction of the pyridine rings of each of the bridging ligands. The final reduction (-1.60V) is irreversible and corresponds to reduction of the peripheral bpy ligands. These results confirm the above assignments of the MLCT bands in the UV/VIS spectrum.

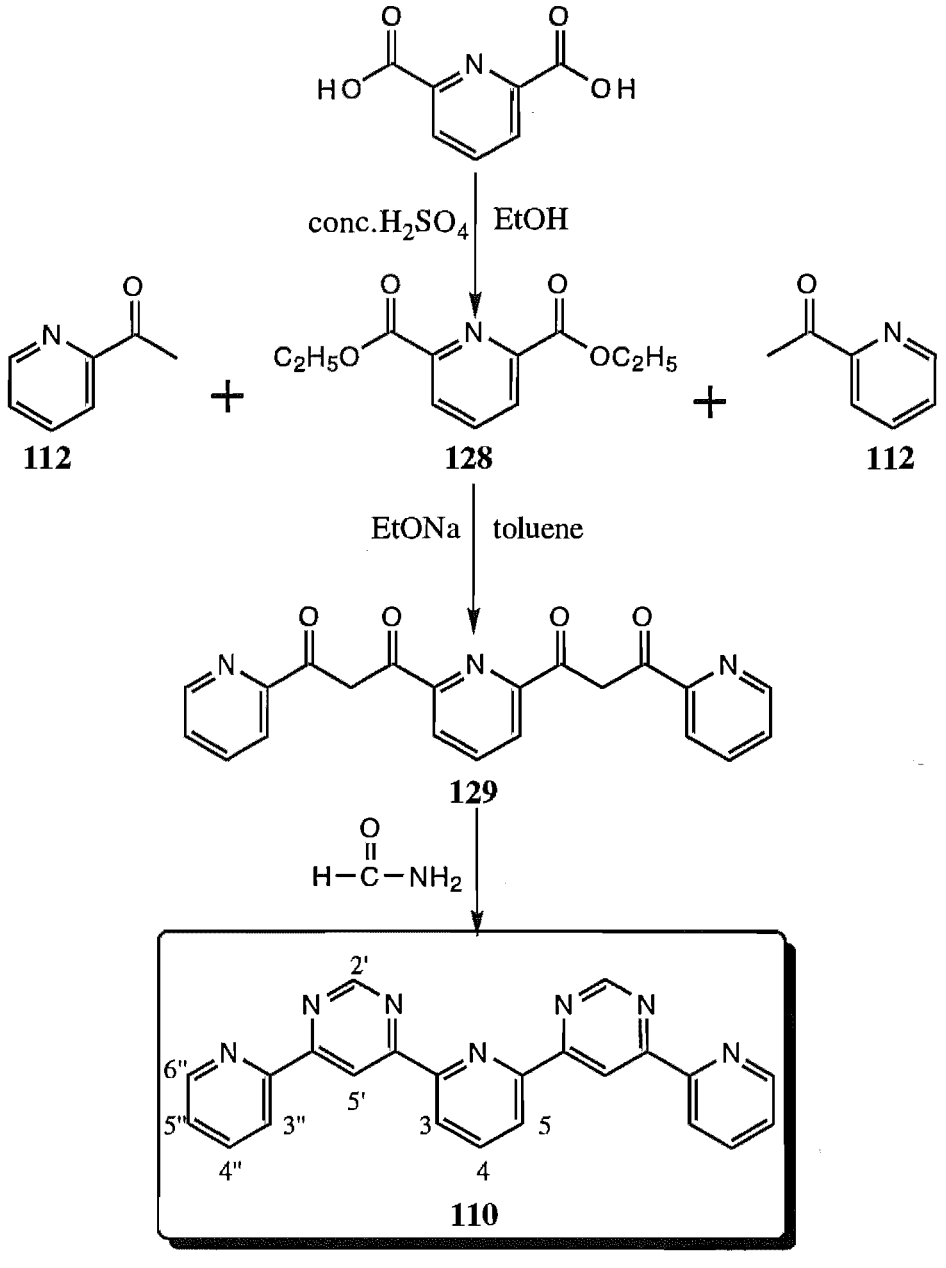

Scheme 4.5

The metal-metal interactions of binuclear complexes of **109** are strong and comparable, although slightly weaker, than similar complexes of **15**. With a view to extending the separation of the metals, the related new ligand **110** was prepared. This ligand appears to incorporate two bidentate coordinating sites, analogous to **109**, separated by a tridentate coordinating site. The synthesis and biruthenium complex of this ligand are described below.

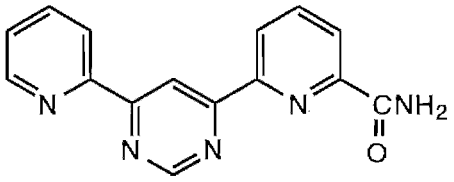

130

Figure 4.14

The ligand **110** was prepared in three steps, with the last two steps similar to the synthesis of **109** (Scheme 4.5). The diester **128** was prepared by refluxing the diacid in a solution of ethanol and conc.sulphuric acid. Claisen condensation of **128**, with two equivalents of 2-acetylpyridine (**112**) gave the tetraketone **129**, which was recrystallised from ethanol. By refluxing **129** in formamide, the two pyrimidine rings were formed to give the ligand 2,6-bis-[6-(2-pyridinyl)-4-pyrimidinyl]pyridine (**110**). Trace amounts of the amide (**130**) were obtained in the preparation of **110** (Figure 4.14). The amide may have formed from the corresponding acid or ester, which are potential side-products in the second step, as a result of the incomplete claisen condensation of **112** and **128**.

Both **129** and **130** were characterised by mass spectrometry and their ^{1}H NMR spectra were assigned from coupling constants, chemical shifts and by comparison with the spectra of **109**. In addition, 1D TOCSY spectra assisted in the assignment of the non-equivalent pyridine rings of **130**. Similarly, the ligand **110** was characterised by mass spectrometry and, in the ^{1}H NMR spectrum, the pyridine rings were readily distinguished on the basis of their coupling constants. As was the case with **109**, no nOe could be detected from H3" and H3/H5 to the pyrimidine H5', implying that the ligand predominantly adopts a conformation, in solution, in which the inter-ring bonds are transoid with respect to the nitrogens. Instead, H2' (9.45ppm) and H5' (9.64ppm) were assigned by comparison with the positions of H2 and H5 in the spectrum of the related ligand **109** (Table 4.7).

The binuclear complex **131** was prepared by reacting **110** with two equivalents of $Ru(bpy)_2Cl_2$, purified by sephadex ion-exchange chromatography (eluent 0.5M NaCl) and isolated as a red hexafluorophosphate salt (Scheme 4.6). The complex was characterised by mass

spectrometry and its ^{1}H NMR spectrum is shown in Figure 4.15. Compared with the spectrum of **121**, the spectrum of **131** appears to show no evidence of diastereoisomerism, on first inspection. The spectrum consists of 24 non-equivalent protons (Table 4.7) The 1D TOCSY spectra (Figure 4.16) conveniently isolates all the spin systems as individual subspectra, and is particularly useful in distinguishing the pyridine H6" (7.94ppm) of the bridging ligand from the bpyH6 protons, and in isolating the overlapping H4 (8.29ppm) and H4" (8.30ppm) signals, which belong to different spin systems (trace II and III). Irradiation of H5' (9.70ppm) (trace I)

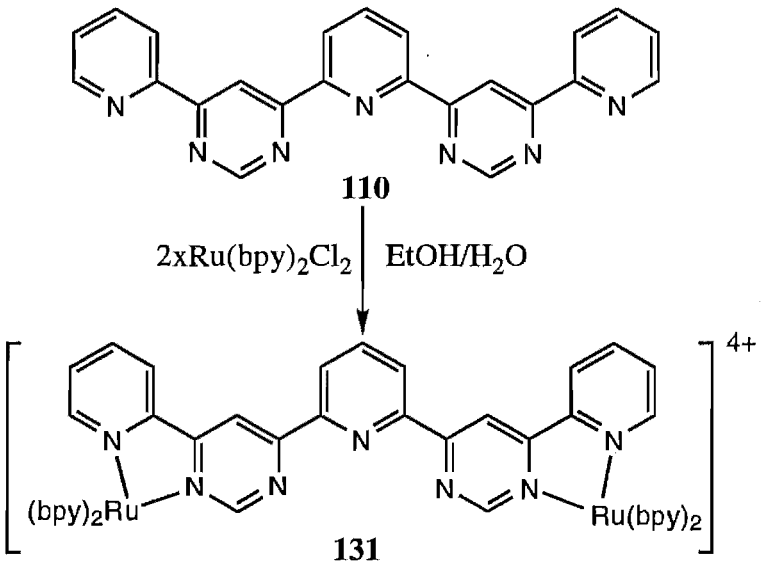

Scheme 4.6

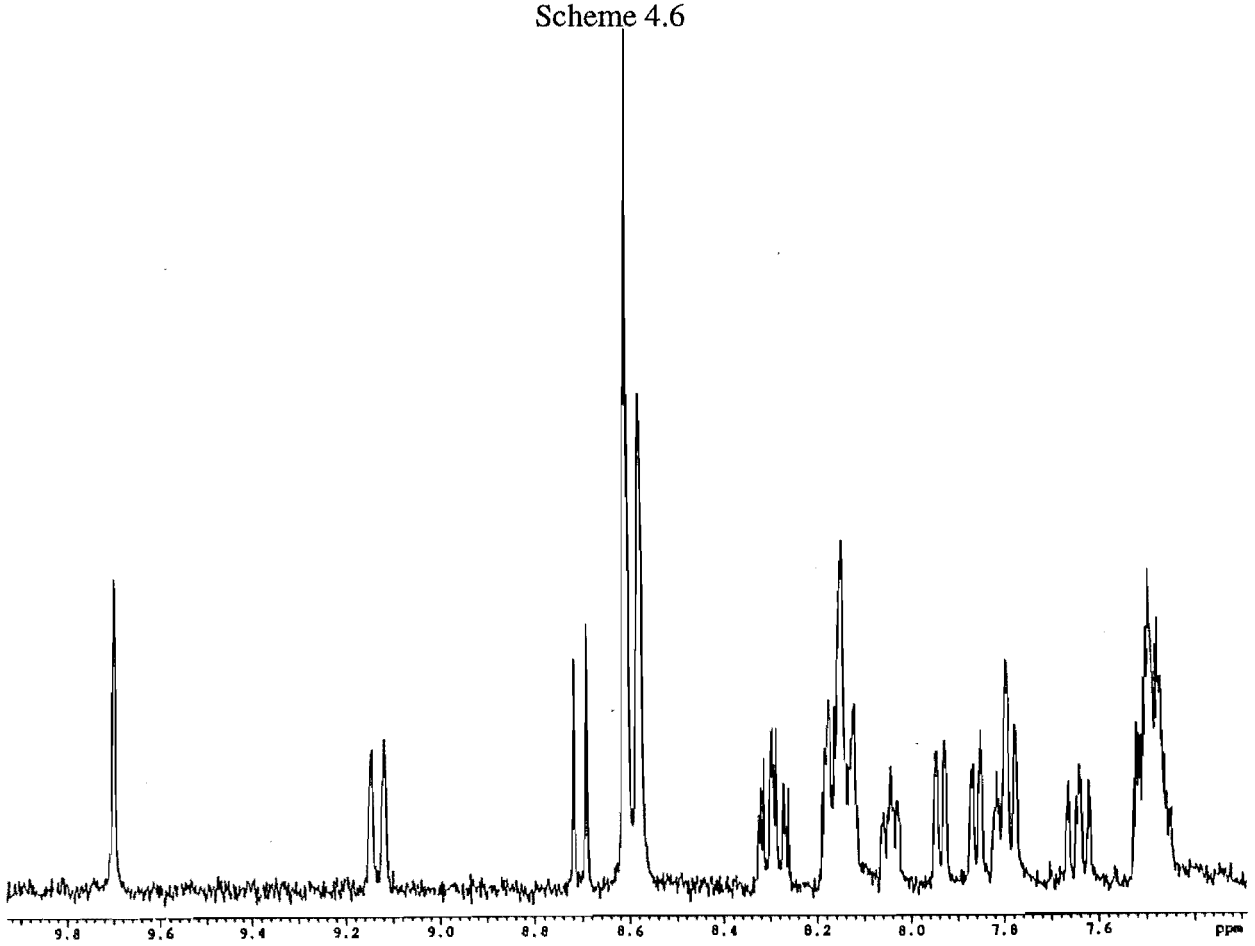

Figure 4.15 ^{1}H NMR Spectrum of **131**.

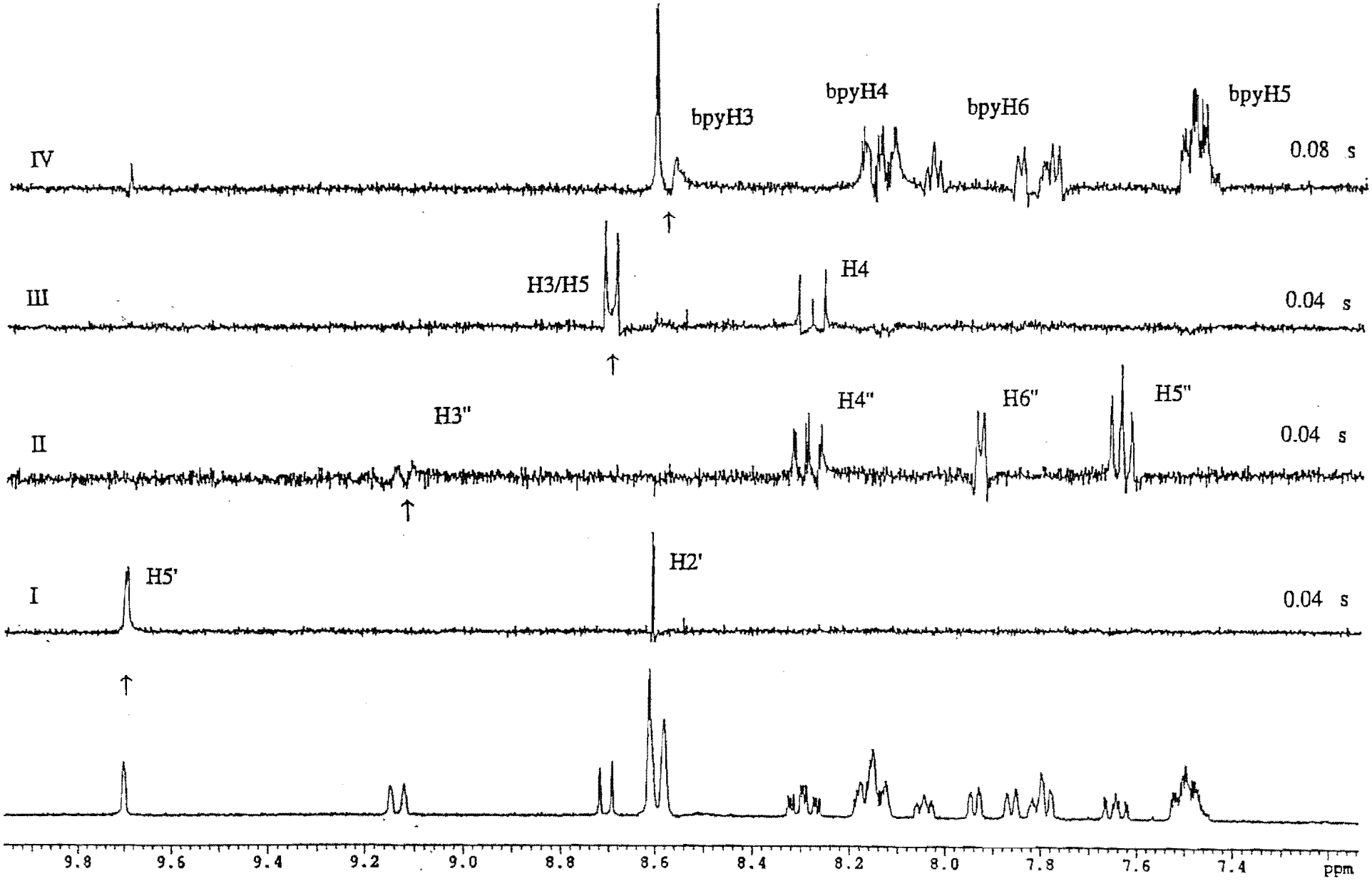

Figure 4.16 1D TOCSY Spectra of 131

Table 4.7. ^{1}H NMR Chemical Shifts[a] of **131** and **110**. Coordination Induced Shifts[b] of **131**.

	H3/H5	H4	H2'	H5'	H3''	H4''	H5''	H6''
131	8.71	8.29	8.61	9.70	9.14	8.30	7.64	7.94
110	8.76	8.27	9.45	9.64	8.66	8.09	7.65	8.95
CIS[b]	-0.05	+0.02	-0.84	+0.06	+0.48	+0.21	-0.01	-1.01

Bpy ligands[c]			
H3	H4	H5	H6
8.60	8.16	7.48	7.79
8.60	8.16	7.49	7.81
8.60	8.16	7.49	7.86
8.60	8.16	7.50	8.05 (8.03)

[a] For deuterated acetonitrile solutions. [b] CIS = $\delta_{complex}$-δ_{ligand}. [c] Not assigned to individual rings

also locates the anisotropically shielded H2' (8.61ppm) proton, whilst all the bpy protons can be located by irradiating bpyH3 (8.60ppm), although this does not assign the individual bpy rings. The most downfield bpyH6 has the same integral as the other three bpyH6, but appears as two overlapping doublets. This may be an indication of the presence of the diastereoisomerism of **131**, which is less pronounced than in **121** due to the greater separation of the chiral trisbidentate ruthenium groups.

The ^{1}H NMR spectrum of **131** is summarised in Table 4.7. Coordination induced conformational changes account for the CIS values of H5' and H3'' and H3/H5, although the disubstituted pyridine ring is little effected by the formation of a binuclear complex, since this ring is non-coordinated and the complex is still flexible (Figure 4.17) about the 2-4' and 6-4' bonds. The CIS values for the remaining protons and the effects which cause them are analogous to those of **109** already described.

Molecular modelling studies with CHEM 3D Plus have shown that the distance between the metals varies substantially with the conformation of the ligand. Three conformations, in which all rings are coplanar, are shown in Figure 4.17. In the staggered conformation (A), all the inter-ring bonds are cisoid, with respect to the nitrogens, and the inter-metal separation is 13.6Å. Rotations of 180°, about one or both of the inter-ring bonds to the central pyridine ring, give rise to the two other conformations B and C, in which the inter-metal separations are 13.2Å and 12.8Å respectively. With a large separation such as this, the two halves of the complex would be expected to behave as independent monomeric units, with little, if any, coupling of the metals.

The electronic properties of the complex were examined by absorption spectroscopy and cyclic voltammetry. In the UV/VIS spectrum the complex shows strong ligand centred

absorptions at λ<400nm and MLCT absorption bands at λ>400nm. Two maxima are observed in the MLCT region at λ=434nm and at λ=504nm. These were assigned, respectively, to the transitions dπ-π*(bpy) and dπ-π*(**110**).

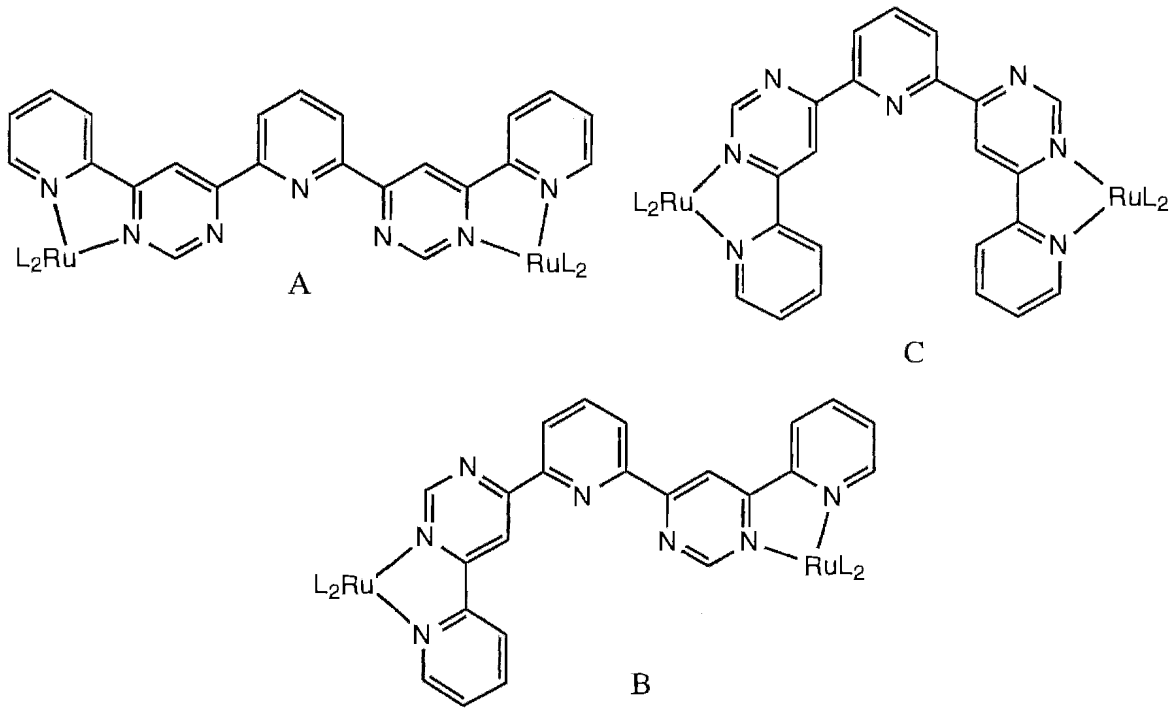

Figure 4.17.

The cyclic voltammogram of **131** consists of a reversible oxidation (+1.28V), which has a cathodic-anodic peak separation (ΔE_p) of 60mV. If the redox active sites in a molecule are non-interacting, it is reasonable to expect that the current-potential response for a given electrochemical method will have the same form as a single-step charge transfer for a monomeric centre.[226,227] For two non-interacting centres the difference in standard potentials is given by (RT/nF)ln4, or (35.61/n)mV at 298K.[227] Theoretical simulations of cyclic voltamograms have been described by Myers *et al.* [228] and expanded on by Taube *et al.*[227] These simulations have estabilished that a two-step process of $\Delta E_{1/2}$=35.61mV has the same shape and current of a single-step charge transfer of 2n electrons and correlates with the peak separation ΔE_p=58.5mV.[227] In the present case, this implies that the oxidations of the two Ru(II) centres of **131** occur at almost the same potential and, hence, is virtually indistinguishable from a one step two electron process. Thus there is effectively no coupling of the metals, via the π-system of the ligand, as compared with the strong coupling of **64, 121**. This contrasts with the biruthenium complex of **26**, for which a very weak metal-metal interaction ($\Delta E_{1/2}$=50mV) was reported.[154] Molecular modelling studies (CHEM 3D Plus) have suggested an inter-metal separation of 13.3Å for this complex. Overlap of the π sytems of **26** is disrupted by rotation about the 6,6' bond, thus weakening the interaction.

In the present case, the inter-metal separation is similar (12.8-13.6Å), although π system overlap is now hindered by rotation about, not one, but two inter-ring bonds (H2-H4' and H6-H4'), which accounts for the negligible metal-metal interaction.

The first reduction (-0.98V) of **131** is a reversible two electron process implying simultaneous reductions of the two pyrimidine rings of the bridge. A third (-1.54V) reduction of **131** may correspond to reduction of the bpy ligands, although the resultant reduction species undergoes absorption to the electrode surface.

A large segmental ligand, which has analogous bisbidentate-tridentate coordination ability to **110**, has recently been shown to effect the self-assembly of a supramolecular helical complex, with Fe(II) coordinated centrally between two bidentate coordinated Ag(I) ions.[165] Formation of a trinuclear complex from **131**, in which a terpyridyl-ruthenium unit is coordinated in the tridentate site of the bridging ligand, would be interesting. However, molecular models of the binuclear complex **131** indicated that the central coordination site is too sterically demanding to allow coordination of a $Ru(terpy)^{2+}$ unit. Hence, preparation of a trinuclear complex was not attempted.

Chapter 5

Complexes of

2,6-Bis-(1-pyrazolyl)-1,5-naphthyridine.

Complexes of 2,6-Bis-(1-pyrazolyl)-1,5-naphthyridine.

5.1. Introduction..

In chapter 4, the biruthenium(II) complex **121** was shown to exhibit a similar metal-metal interaction ($\Delta E_{1/2}$=160mV) to $[Ru(bpy)_2]_2(bpm)^{4+}$ ($\Delta E_{1/2}$=160mV), despite a larger distance between the metals of 6.2Å. Also, since the ligand is a weaker π-acceptor than dpp, the metal-metal interaction is less than in the complex $[Ru(bpy)_2]_2(dpp)^{4+}$, where the metals are at a distance of 6.7Å. In contrast, the related pentaheterocycle **110** has been shown to exhibit a two electron oxidation which is indistinguishable from a one step two electron process. Hence, at a greater inter-metal separation, in this case 12.8-13.6Å, the metals are non-interacting.

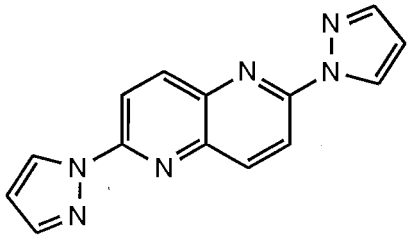

132

Figure 5.1.

The new compound **132** is a potential bridging ligand which should allow for an inter-metal separation smaller than that of **131**, but larger than that of **121**. The naphthyridine ring system has relatively low-lying π* orbitals and, despite the increase in inter-metal separation, should enable efficient metal-metal coupling in binuclear complexes of **132**. In addition, **132** has the advantage of being a bis bidentate chelating ligand and should thus give rise to stable complexes, whilst the two π-excessive pyrazole rings of the ligand should have interesting effects on the physicochemical properties of its complexes. Some ligands incorporating azole rings have already been discussed in chapter 2. This chapter describes the synthesis of **132** and includes a study of the mono- and biruthenium complexes of the ligand.

5.2. Results and Discussion.

The four step synthesis of **132** is shown in Scheme 5.1. In the first step, condensation of the commercially available reagents 3-aminopyridine and glycerol, by the method of Albert,[229] gave 1,5-naphthyridine (**133**).

The di-N-oxide **134** was readily obtained by heating a mixture of **133**, hydrogen peroxide and acetic acid. This method was derived from the synthesis of the mono-N-oxide of

4,4'-bipyridine, as described by Moran *et al.*[230] Forty years ago, Hart reported the chlorination of both the mono- and di-N-oxides (**134**) of **133**, in refluxing $POCl_3$. In both cases a single isomer was produced, with substitution of chlorine occurring adjacent to the nitrogen.[231] However, Ellis *et al.* later reported that 2-chloro-1,5-naphthyridine and 4-chloro-1,5-naphthyridine were obtained in equal amounts from the corresponding mono-N-oxide, under the same conditions. In Hart's synthesis of 2,6-dichloro-1,5-naphthyridine (**135**), **134** was reluxed in $POCl_3$ for 20 minutes, whereupon the solution was cooled and poured onto ice and aqueous ammonia to give a precipitate of **135**. In the present case, a mixture of **134** in $POCl_3$ was refluxed for 6 hours, whereupon the solvent was evaporated at reduced pressure and the residue treated with ice and aqueous ammonia and extracted with chloroform. The ^1H NMR spectrum of the chloroform extract indicated a mixture of compounds, of which **135** was identified as the major component, with a number of other mono- and dichlorinated compounds present, in particular 2,8-dichloro-1,5-naphthyridine (**136**).

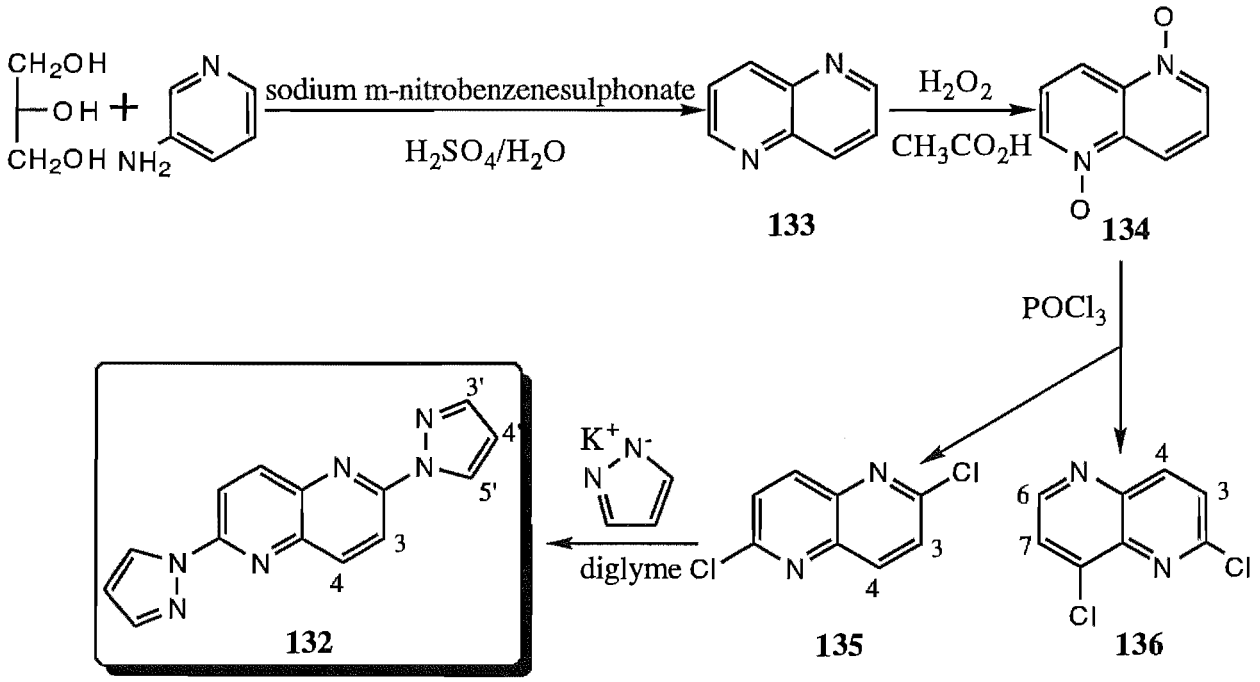

Scheme 5.1.

The symmetrical isomer **135** and unsymmetrical isomer **136** were isolated by chromatography on silica and readily distinguished on the basis of their ^1H NMR spectra. The spectrum of **135** consists of two doublets (H3 and H4), whilst that of **136** consists of four doublets (H3, H4, H6 and H7).

The final step in Scheme 5.1 is analogous to the preparation of **53** in chapter 2. Reaction of two equivalents of potassium pyrazolate with **135**, allows substitution of pyrazole for chlorine to give the doubly bidentate ligand 2,5-bis-(1-pyrazolyl)-1,5-naphthyridine (**132**). This new

compound was characterised by mass spectrometry and by ^{1}H NMR spectroscopy, in both $CDCl_3$, and in CD_3CN. For both spectra, the pyrazole rings were assigned on the basis of the smaller H3'/H4' coupling constant, relative to that of H4'/H5'. The H3 and H4 protons of the naphthyridine rings form an AB-quartet in $CDCl_3$ (8.40, 8.46ppm). In CD_3CN, the difference in the chemical shift of H3 and H4 is less than the coupling constant. Hence, H3 and H4 appear as a singlet at 8.84ppm.

Mono- and di-ruthenium complexes can be readily prepared by reaction of **132** with one or two equivalents of ruthenium(II) (Scheme 5.2), in an analogous manner to the syntheses of structurally related complexes described earlier in this work.

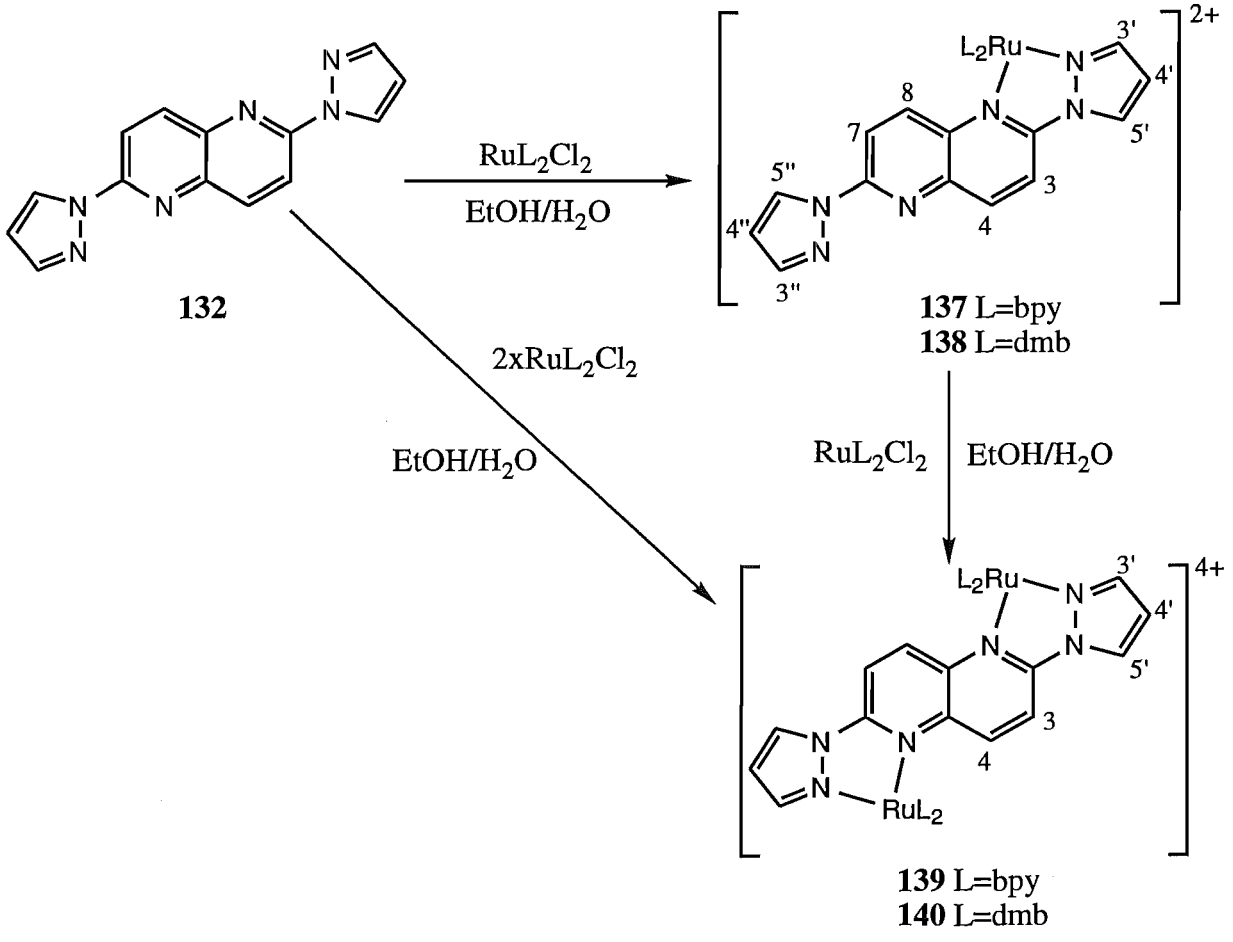

Scheme 5.2.

The monoruthenium complex, **137**, and its dmb equivalent, **138**, were obtained as yellow and orange solids, respectively. In addition, column chromatography, on alumina, was required to separate **138** from traces of the corresponding dinuclear complex **140**, which formed during the synthesis of the mononuclear complex. Mass spectrometry and ^{1}H NMR spectroscopy were used to characterise **137** and **138**.

The ^{1}H NMR spectrum of **137** is shown in Figure 5.2 (top) and comprises 26 non-equivalent protons, with some overlap of the bpy signals at 8.1-8.2ppm. The pyrazole ring

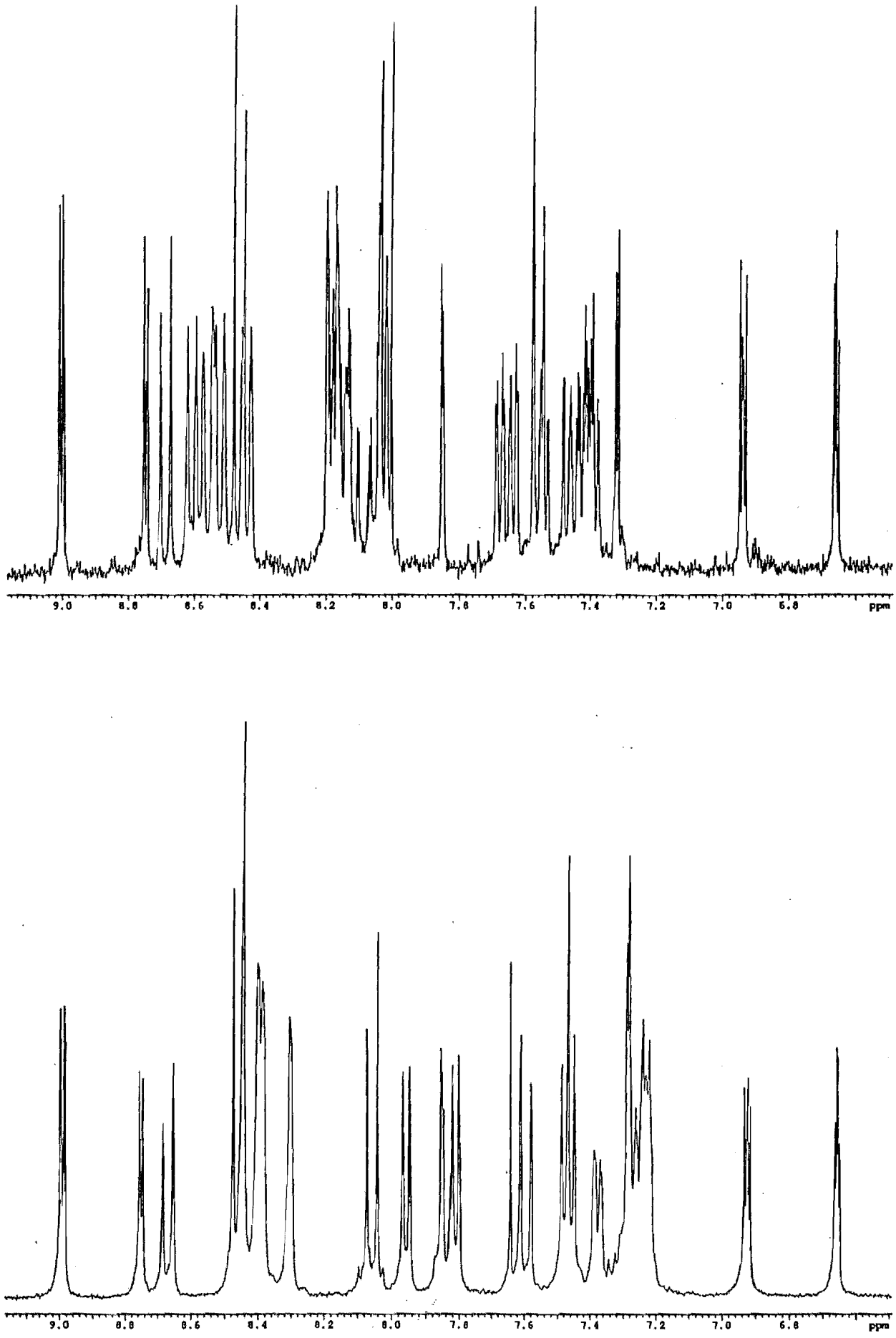

Figure 5.2 ^{1}H NMR Spectra of **137** (top) and **138** (bottom).

protons, of **132,** can be clearly observed in the spectrum and were assigned on the basis of coupling constants and chemical shifts. The assignments of the coordinated ring, H3' (7.32ppm), H4' (6.04ppm) and H5' (9.01ppm) and the non-coordinated ring H3" (7.85ppm), H4" (6.66ppm) and H5" (8.75ppm) were confirmed by 1D TOCSY irradiations of H4' and H4". The CIS values (Table 5.1) of the coordinated ring can be attributed to σ-donation of electron density from ligand to metal (H4' and H5'), chelation induced conformational changes (H5') and to ring current anisotropy effects (H3').

Table 5.1. ^{1}H NMR Chemical Shifts[a] of **137**, **138** and **132**. Coordination Induced Shifts[b] of **137** and **138**.

	H3	H4	H7	H8	H3'	H4'	H5'	H3"	H4"	H5"
137	8.47	8.69	8.02	7.57	7.32	6.94	9.01	7.85	6.66	8.75
132	8.49	8.49	8.49	8.49	7.90	6.67	8.84			
CIS[b]	-0.02	+0.20	-0.47	-0.92	-0.58	+0.27	+0.17	-0.05	-0.01	-0.09

Bpy ligands			
H3	H4	H5	H6
8.61	8.17	7.42	8.19
8.53	8.16	7.54	8.03
8.44	8.03	7.47	7.64
8.56	8.13	7.40	7.68

	H3	H4	H7	H8	H3'	H4'	H5'	H3'	H4"	H5"
138	8.46	8.67	8.06	7.61	7.29	6.93	9.00	7.86	6.66	8.76
132	8.49	8.49	8.49	8.49	7.90	6.67	8.84			
CIS[b]	-0.03	+0.18	-0.43	-0.88	-0.61	+0.26	+0.16	-0.04	-0.01	-0.08

Dmb ligands			
H3	4-CH_3[c]	H5	H6
8.44	2.52	7.22	7.96
8.40	2.59	7.24	7.48
8.39	2.61	7.38	7.81
8.31	2.63	7.27	7.46

[a] For deuterated acetonitrile solutions. [b] CIS = $\delta_{complex}$-δ_{ligand}. [c] Not assigned

The protons of the naphthyridine rings were assigned as H3 (8.47ppm), H4 (8.69ppm), H7 (8.02ppm) and H8 (7.57ppm). A long range ^{5}J coupling (1Hz) across the naphthyridine ring system allows the coupled protons H4 and H8 to be distinguished from H3 and H7, which exhibit only ^{3}J coupling. In addition, H4 and H8 can be differentiated since H8 lies over a pyridine ring and is therefore shielded anisotropically (-0.92ppm), whilst H4 exhibits a positive CIS values (+0.20ppm) as a result of the net donation of electron density from ligand to metal.

Similarly, H7 (-0.47ppm) is shielded anisotropically and is upfield of H3 (-0.02ppm), which exhibits the effects of chelation induced conformational changes. An nOe can also be observed from H5' to H3, since the coordinated pyrazole and the naphthyridine rings are held rigidly coplanar by the chelate ring, thus confirming the assignment of H3. The assignments for the naphthyridine ring system were also confirmed by 1D TOCSY spectra.

The proton chemical shifts and CIS values for **137** are summarised in Table 5.1. Included in the table are the chemical shifts of the bpy protons, for which the four spin systems were assigned by 1D TOCSY irradiations of the bpyH3 (8.4-8.6ppm) and bpyH6 (7.64 and 7.68ppm) protons. In this case, irradiation of the desired protons with a 180° pulse also results in the irradiation of nearby protons, thus complicating the individual sub-spectra. By comparing two or more traces, it was possible to deduce the erroneous peaks in each of the sub-spectra, thus assigning each of the bpy ring spin systems.

The problem of irradiating nearby protons in the 1D TOCSY spectra of **137** can be alleviated with the dmb analogue **138**. The ^{1}H NMR spectrum of **138** (Figure 5.2 bottom) is considerably simplified, relative to that of **137**, as a result of the absence of overlap due to the bpyH4 protons. Nearly all of the signals in the spectrum are well isolated and Figure 5.3 shows the complete assignment of the ^{1}H NMR spectrum of **138** by 1D TOCSY spectra. The naphthyridine and pyrazole spin systems can be located by irradiations of H7 (trace I), H4 (trace II), H5'' (trace III) and H5' (trace IV), whilst the remaining four subspectra (trace V-VIII) clearly show that all the dmb rings can be readily assigned. For example, by irradiation of the two isolated dmbH6 protons (trace V and VI) two dmb rings may be located. Similarly, irradiating dmbH3 (8.31ppm) locates the third ring (trace VII), whilst the fourth ring can be located by the difference of traces VII and VIII, with trace VIII obtained by irradiating the two closely spaced dmbH6 protons at 7.46 and 7.48ppm. As has been mentioned previously, this technique does not assign the individual dmb or bpy rings to their stereochemical environment in the complexes. In the spectrum of **138**, the ligand **132** was assigned in a similar manner to that described for **137**.

UV/VIS absorption spectroscopy and cyclic voltammetry were used to probe the electronic properties of the complexes **137** and **138**. The results of these studies are summarised in Table 5.2. The lowest energy absorption in the UV/VIS spectrum of **137** (438nm) and **138** (442nm) can be assigned as MLCT bands with the slightly lower energy of **138** being due to d-orbital destabilisation by the electron donating dmb ligands. These absorptions are

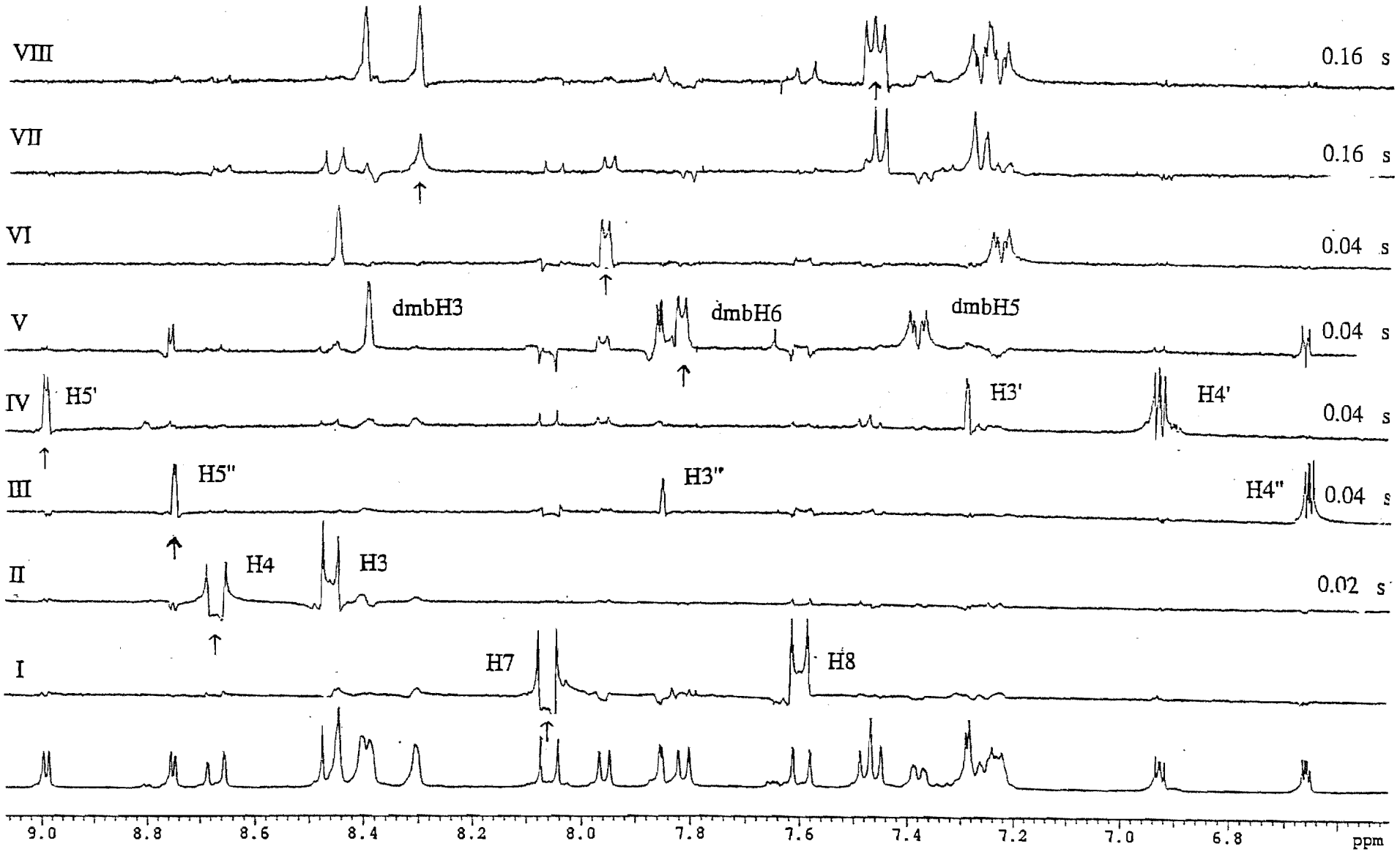

Figure 5.3 1D TOCSY Spectra of **138**

unsymmetrical and are probably due to a combination of the MLCT transitions π-π*(**132**) and π-π*(bpy), for **137**, or π-π*(**132**) and π-π*(dmb), for **138**. Relative to $Ru(bpy)_3^{2+}$, electron transfer from metal to ligand appears more difficult for the complexes of **132**.

The ligand **132** exhibits a reversible one electron reduction of the naphthyridine system at -1.78V. Hence, the π* orbitals of **132** are lower in energy than those of bpy (-2.18V).[10] The electrochemistry of **137** and **138** consists of a reversible one electron oxidation at +1.27 and +1.17V, respectively. The greater ease of oxidation of the dmb complex, **138**, relative to the bpy complex, **137**, has already been seen in related complexes in this work and is attributed to the electron donating ability of the dmb methyl groups.

Table 5.2. Absorption Maxima[a] and Redox Potentials[b] of **137** and **138**.

	λ	E_{ox}	E_{red1}	E_{red2}	E_{red3}	E_{red4}	$\Delta E_{ox\text{-}red}$
$Ru(bpy)_3^{2+}$	451	+1.27	-1.31	-1.50	-1.77	-	2.58
137	438	+1.27	-1.13[c]	-1.44	-1.62	-1.89	2.40
138	442	+1.17	-1.24[c]	-1.69[d]	-1.90		2.41

[a] In nanometres. [b] In volts vs SCE in acetonitrile. [c] Irreversible. [d] Two electron

The first one electron reduction of each of the complexes (-1.13 and -1.24V) is irreversible, which may be a result of reduction of **132**, followed by dissociation of a pyrazole group from the reduced ligand. This behaviour has been observed both in this work, in the complexes of **53**, and in structurally related complexes, by others.[12] The remaining reductions are reversible and may be attributed to reduction of the dmb or bpy ligands.

The binuclear complexes **139** and **140** were prepared as shown in Scheme 5.2 and obtained as red solids, which were characterised by mass spectrometry and ^1H NMR spectroscopy. Figure 5.4a shows the ^1H NMR spectrum of **139** which consists of 21 non-equivalent protons. Compared with the spectrum of **137**, the number of signals for the bridging ligand is now halved due to the higher symmetry of the binuclear complex. Thus both pyrazole rings are equivalent and the long-range coupling constant of H4 and H8 is absent, since these two protons are equivalent, as are H3 and H7. The pyrazole ring protons, H3' (7.30ppm), H4' (6.90ppm) and H5' (8.79ppm), were readily assigned by the smaller H3'/H4' coupling constant, relative to that of H4'/H5', whilst the naphthyridine protons H3 (8.01ppm) and H4 (7.76ppm) were distinguished by the observed nOe from H5' to H3 (Figure 5.4b). Both H3 and H4 have negative CIS values, with that of H4 larger since this proton is closer to a shielding pyridine ring than is H3. In a similar manner to the assignment of the bpy rings of **137** and the dmb rings of

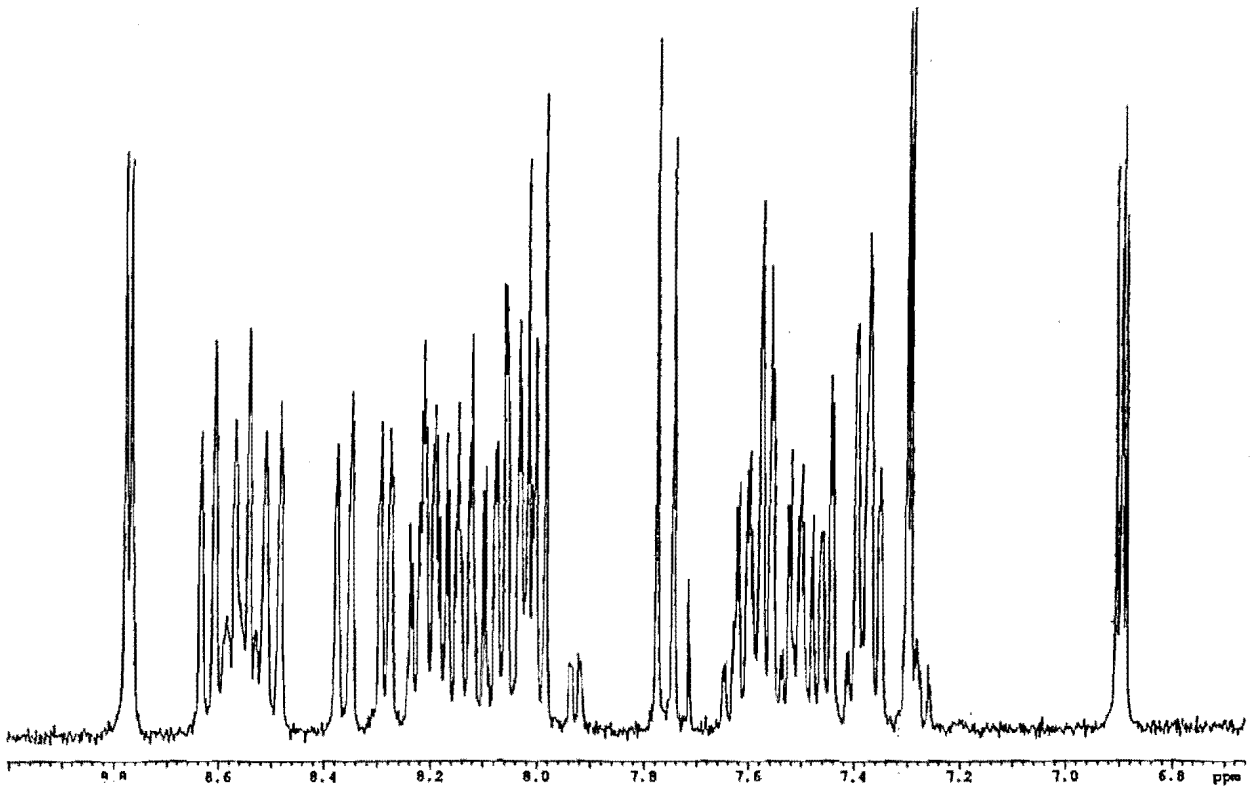

Figure 5.4a ^{1}H NMR Spectrum of **139**.

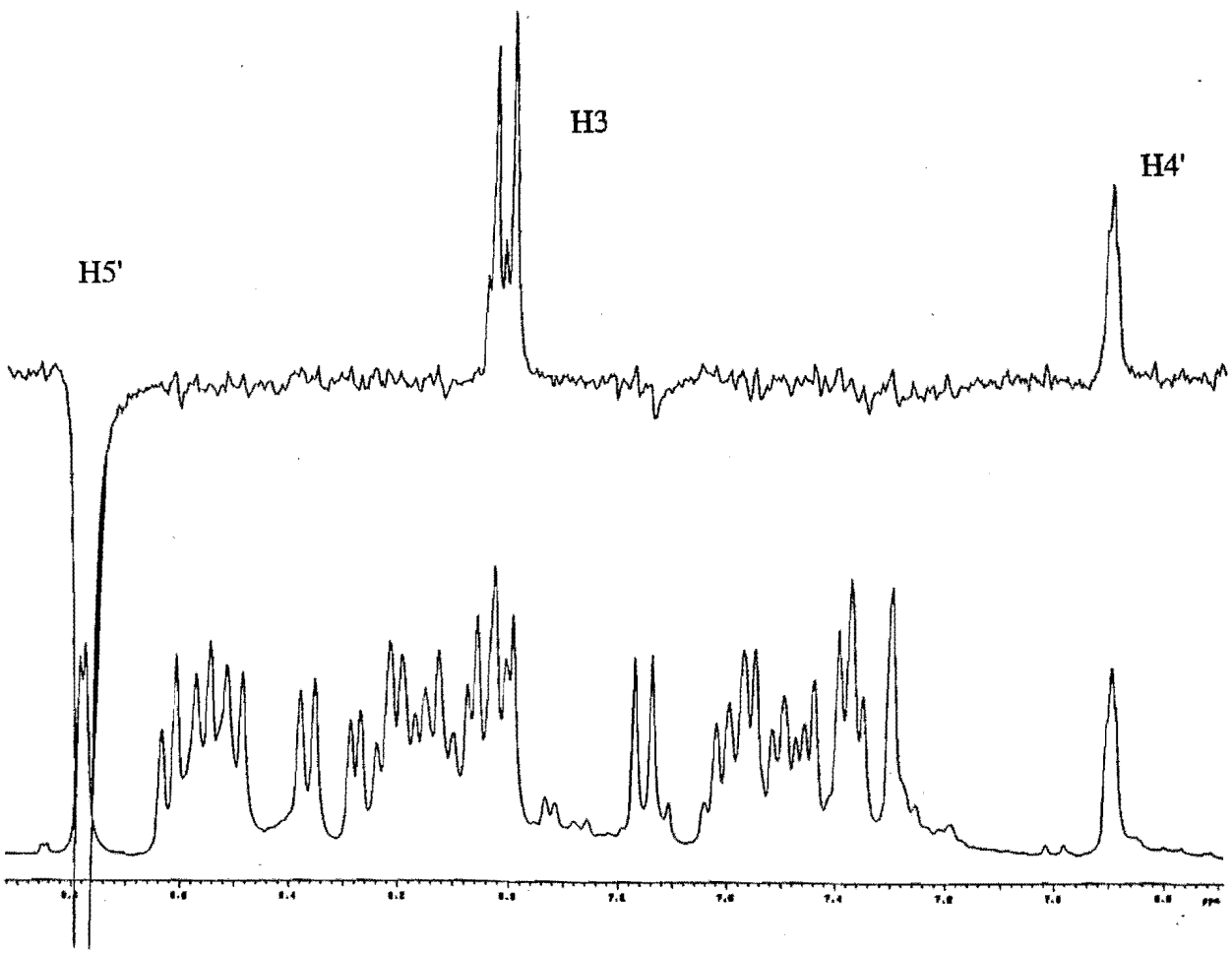

Figure 5.4b nOe Difference Spectrum of **139**

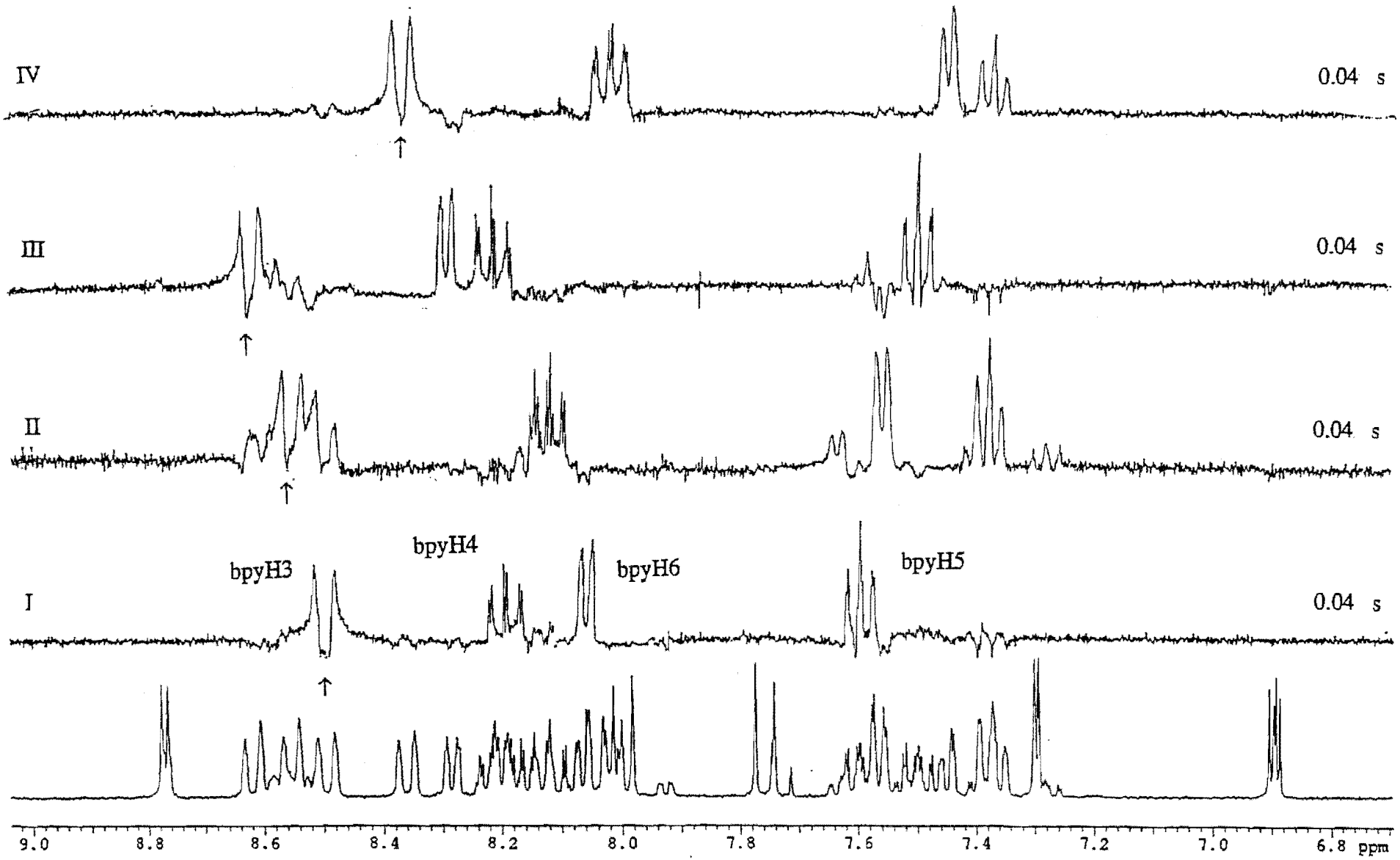

Figure 5.5 1D TOCSY Spectra of **139**

138, the bpy rings of **139** were assigned by 1D TOCSY irradiations of each bpyH3 in turn (Figure 5.5). The spectrum of **139** is summarised in Table 5.3.

Table 5.3. ^{1}H NMR Chemical Shifts[a] of **132** and **139**. Coordination Induced Shifts[b] of **139**.

	Ligand **132**					Bpy ligands			
	H3	H4	H3'	H4'	H5'	H3	H4	H5	H6
139	8.01	7.76	7.30	6.90	8.79	8.62	8.22	7.50	8.28
132	8.49	8.49	7.90	6.67	8.84	8.56	8.13	7.38	7.56
CIS[b]	-0.48	-0.73	-0.60	+0.23	-0.05	8.51	8.19	7.60	8.07
						8.37	8.03	7.37	7.45

[a] For deuterated acetonitrile solutions. [b] CIS = $\delta_{complex}$-δ_{ligand}.

In the spectra of Figures 5.4a and 5.5 there is evidence of a minor product and particularly with signals for H3 in the nOe (Figure 5.4b). The minor product could not be removed by recrystallisation or chromatography. As has been discussed earlier, binuclear complexes should exist as meso and racemic diastereoisomers, which, in this case, correspond to the major and minor isomers of **139**. This would imply that one diastereoisomer predominates, which has already been shown to occur in the complexes **64** and **65**.

In addition, the ^{1}H NMR spectrum of **140**, the dmb analogue of **139**, indicates a major and minor isomer (3:2 ratio). The nOe experiment in Figure 5.6a confirms this by showing an enhancement of two doublets for H3 (8.08, 8.10ppm), one for each isomer, when H5' (8.75-8.76ppm) is irradiated. Furthermore, the 1D TOCSY spectra of **140** (Figure 5.6b) shows that by irradiating these two H3 doublets, the corresponding H4 doublets (7.77, 7.82ppm) can be located amongst overlapping dmbH6 signals. The bridging ligand protons for the major and minor isomer were assigned by their relative integrals and with the assistance of a 2D COSY spectrum, which also confirmed the coupling of H3 and H4. These are summarised in Table 5.4.

Table 5.4. ^{1}H NMR Chemical Shifts[a] of **132** and **140**. Coordination Induced Shifts[b] of **140**.

	Major isomer					Minor isomer				
	H3	H4	H3'	H4'	H5'	H3	H4	H3'	H4'	H5'
140	8.10	7.82	7.27	6.90	8.76	8.08	7.77	7.27	6.90	8.75
132	8.49	8.49	7.90	6.67	8.84	8.49	8.49	7.90	6.67	8.84
CIS[b]	-0.39	-0.67	-0.63	+0.23	-0.08	-0.41	-0.72	-0.63	+0.23	-0.09

[a] For deuterated acetonitrile solutions. [b] CIS = $\delta_{complex}$-δ_{ligand}.

All attempts to separate the isomers by recrystallisation, or ion-exchange chromatograpy on sephadex, failed. The dmb protons could not be assigned to either isomer and no particular protons could be assigned to a unique stereochemical environment, unlike the case in the spectra of **64** and **121**, in which the shielding (meso) or deshielding (racemic) environment of a bpyH6

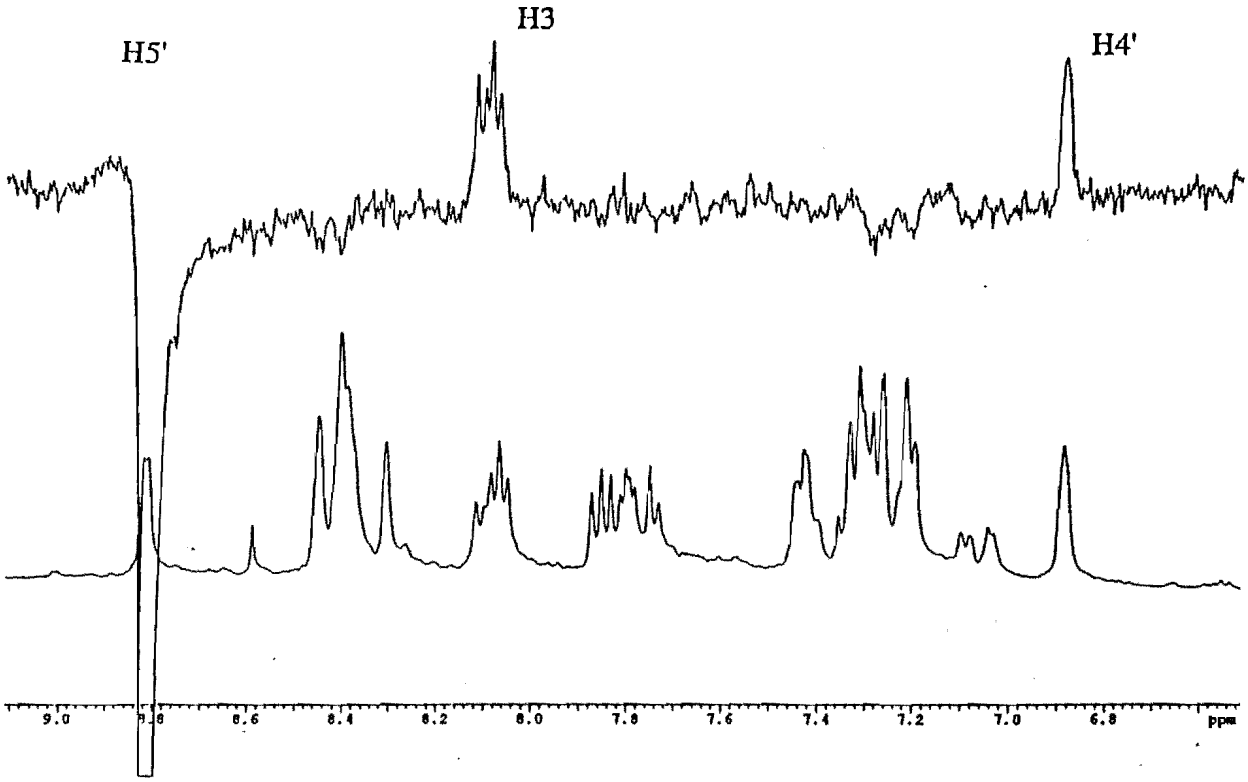

Figure 5.6a nOe Difference Spectrum for **140**

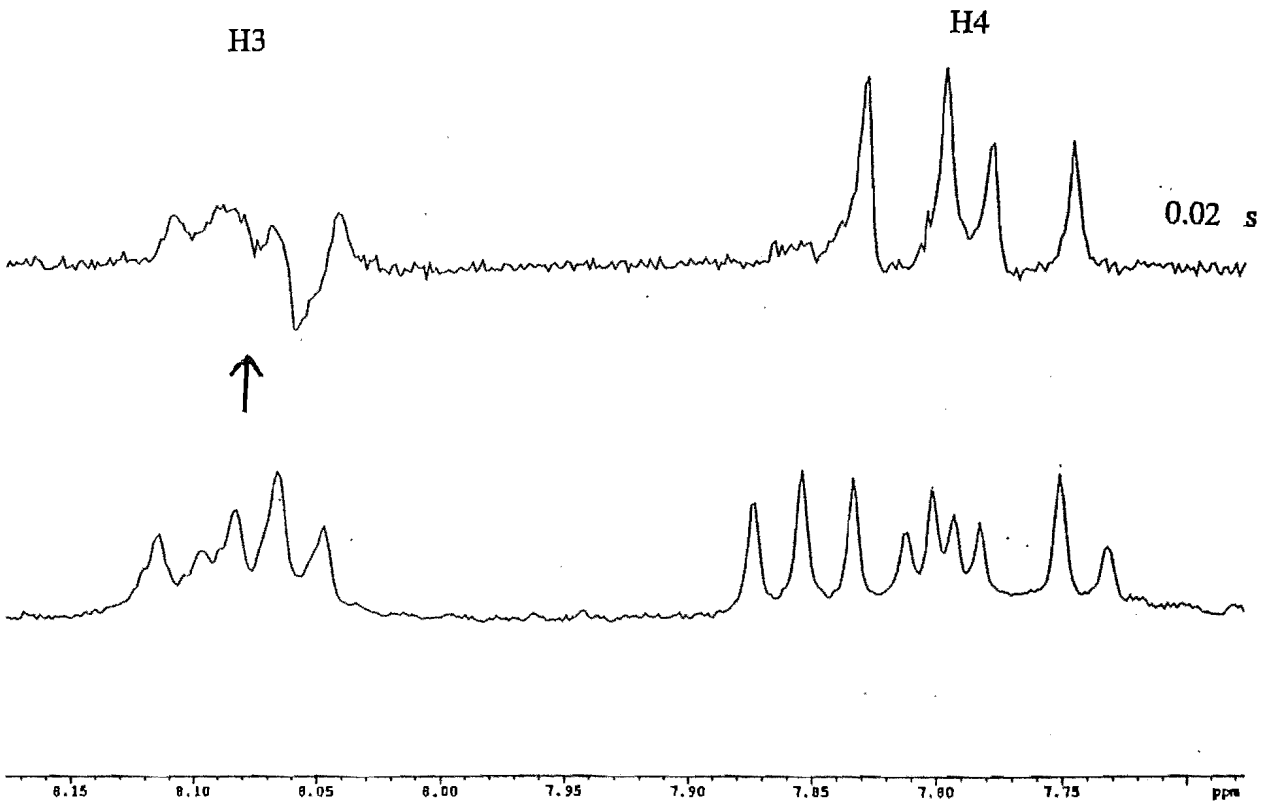

Figure 5.6a 1D TOCSY Spectrumof **140**.

proton allowed assignment of the meso and racemic diastereoisomers. However, this effect would be smaller in **140**, since the RuL_2^{2+} units are further apart than in **64** or **121**, as has been confirmed by studies with molecular models. Hence, the two isomers probably correspond to the diastereoisomers of **140**, although neither isomer could be unambiguously assigned to the meso or racemic forms. Similarly, the diastereoisomer shown in the spectrum of **139** (Figure 5.4a) can not be assigned.

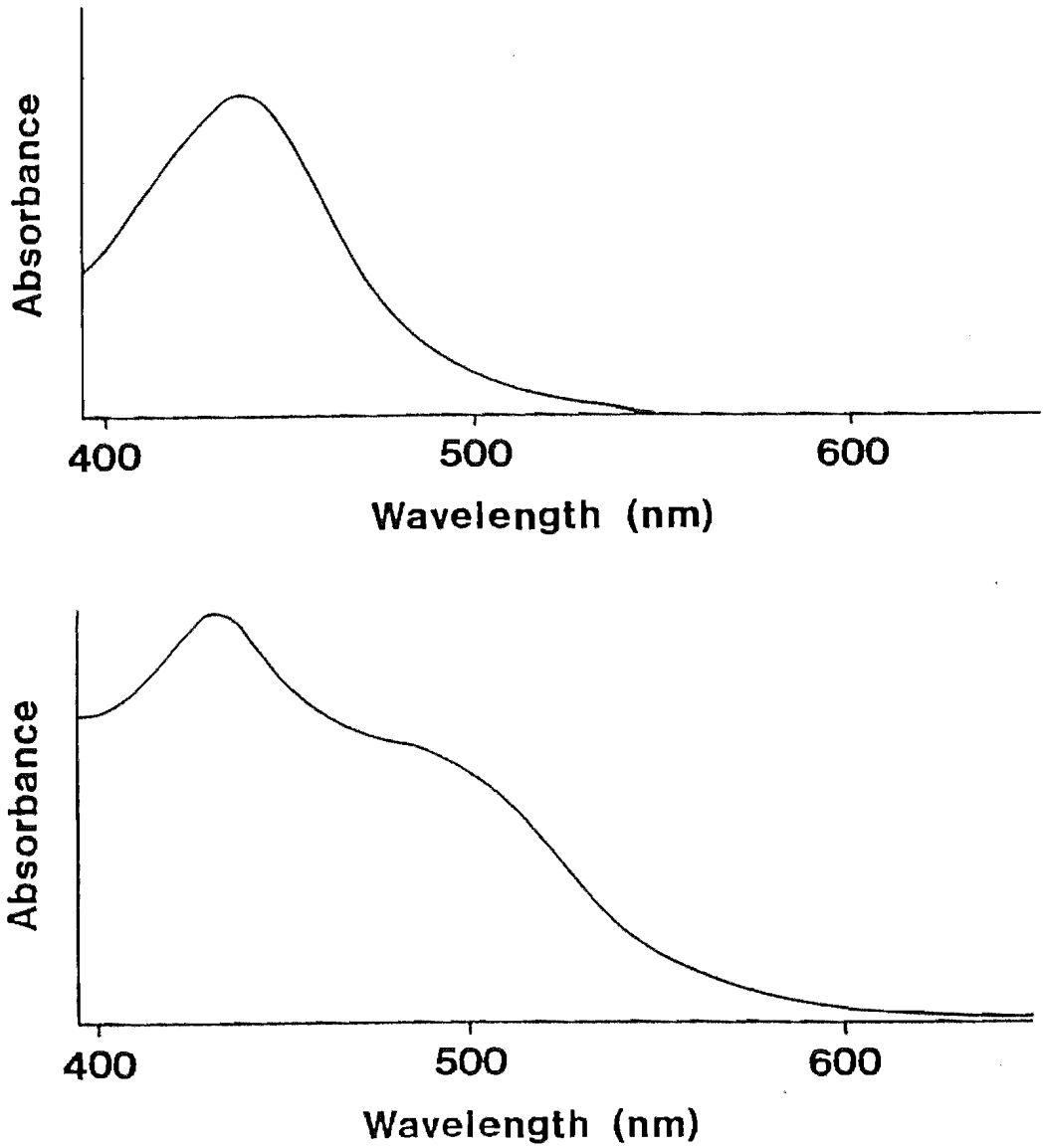

Figure 5.7 Visible Absorption spectra of **137** (above) and **139** (below).

The visible absorption spectra of **137** and **139** are shown in Figure 5.7. The spectrum of the mononuclear complex has already been described. In the spectrum of **139**, an MLCT band with a maximum at λ=436nm is accompanied by a less intense shoulder at 488nm. These were assigned as the transitions $d\pi$-π^*(bpy) and $d\pi$-π^*(**132**), respectively. The observed red shift of the lowest MLCT band in the binuclear complex (488nm), which can be observed in Figure 5.7, is typical of a complex in which a metal-metal interaction occurs and is attributed to a lowering

of the π* orbital of the bridge by back-bonding to the second ruthenium(II) centre. In this case, the red shift is smaller than that of the binuclear complexes $[Ru(bpy)_2]_2(bpm)^{4+}$,[35] $[Ru(bpy)_2]_2(dpp)^{4+}$,[126] **64** and **121**, but larger than the red shift of weakly interacting complexes such as $[Ru(bpy)_2]_2(\mathbf{25})^{4+}$ (**25**=2,2':4',4":2",2"'-quaterpyridine) (455nm, 471nm), thus implying an intermediate metal-metal interaction for the complex **139**.

The absorption maxima of **139** and also of **140** are summarised in Table 5.5. Analogous to **139**, the absorption bands of **140** can be attributed to the MLCT transitions dπ-π*(dmb) and dπ-π*(**132**). Also included in Table 5.5 are the redox potentials of both complexes, whilst the cyclic voltammogram of **139** is shown in Figures 5.8a and 5.8b.

Table 5.5. Absorption Maxima[a] and Redox Potentials[b] of **139** and **140**.

	λ	E_{ox1}	E_{ox2}	E_{red1}	E_{red2}	E_{red3}	E_{red4}	E_{red5}
$[Ru(bpy)_2]_2(\mathbf{5})^{4+}$	594	+1.53	+1.69	-0.41	-1.08	-	-	
139	434,482sh	+1.29	+1.38	-0.85	-1.46	-1.54	-1.67	-1.78
140	436,488sh	+1.20	+1.29	-0.89	-1.54	-1.64	-1.77	-1.89

[a] In nanometres. [b] In volts vs SCE in acetonitrile.

Unlike the mononuclear complexes, the first reduction of **139** (-0.85V), and of **140** (-0.89V), is a reversible one electron process. This reduction can be assigned to reduction of the bridging ligand and occurs at a less negative potential than in the mononuclear complex. This effect, which is a result of the synergistic lowering of the π* orbital of the ligand by the second coordinated ruthenium(II), parallels the red shift in the MLCT band, as shown in Figure 5.7. Dissociation of the ligand from the reduced complex, which may account for the irreversibility of the first reduction of **137** and **138**, does not occur for the binuclear complexes. As a consequence of the electron donating methyl groups, the π* orbitals of dmb are at higher energy, relative to those of bpy. Hence, the last four reductions of **140** are at more negative potentials (-1.54, -1.64, -1.77, -1.89V) than in **139** (-1.46, -1.54, -1.67, -1.78V).

The complexes **139** and **140** each exhibit a reversible two-electron oxidation. Table 5.5 shows that **140** is more easily oxidised than **139**, as has been previously described for structurally related dmb complexes in this work. The cathodic-anodic peak-separation (ΔE_p=135mV) is smaller than that of complexes with strongly interacting centres, such as **64** and **121**, but larger than the peak separation for a single-step charge transfer of two electrons (ΔE_p=58.5mV[227]), as seen in complexes with non-interacting centres, such as **131**. Hence, ΔE_p is sufficiently large to indicate coupling of the ruthenium(II) centres via the π system of the bridging ligand. Polcyn and Shain have shown that if $\Delta E_{1/2}$ is less than 120mV, for a two step

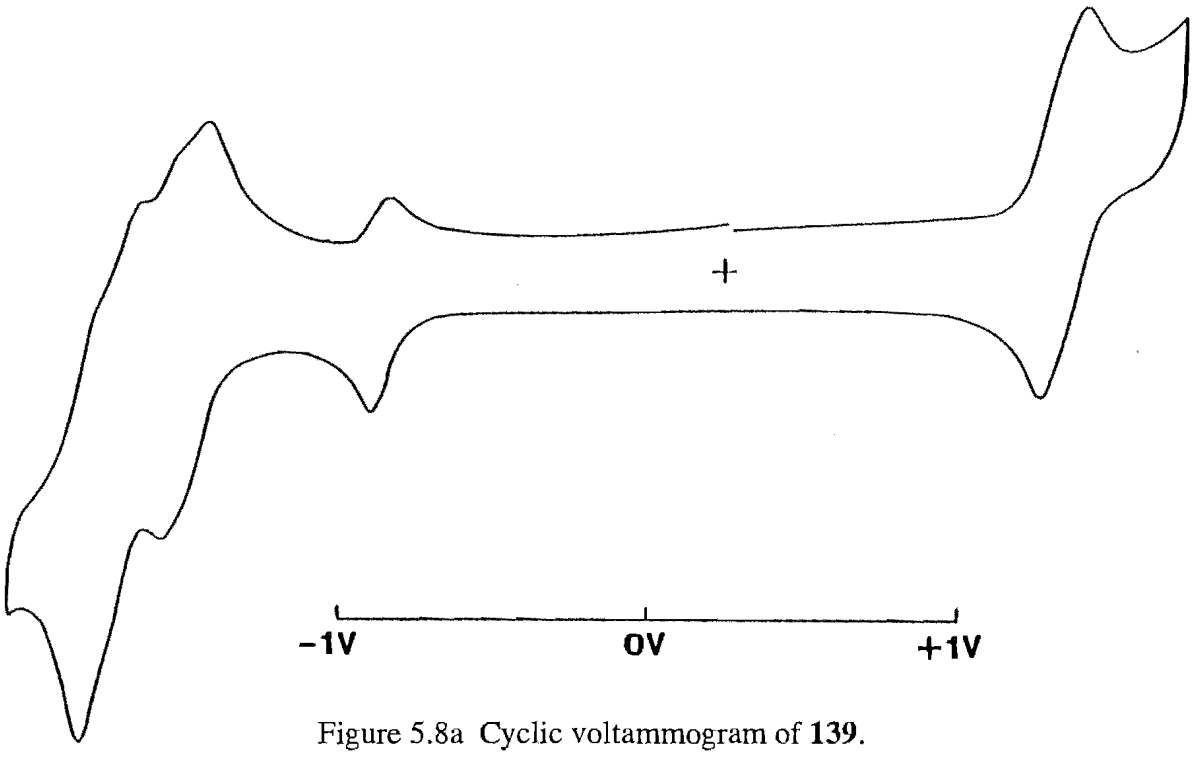

Figure 5.8a Cyclic voltammogram of **139**.

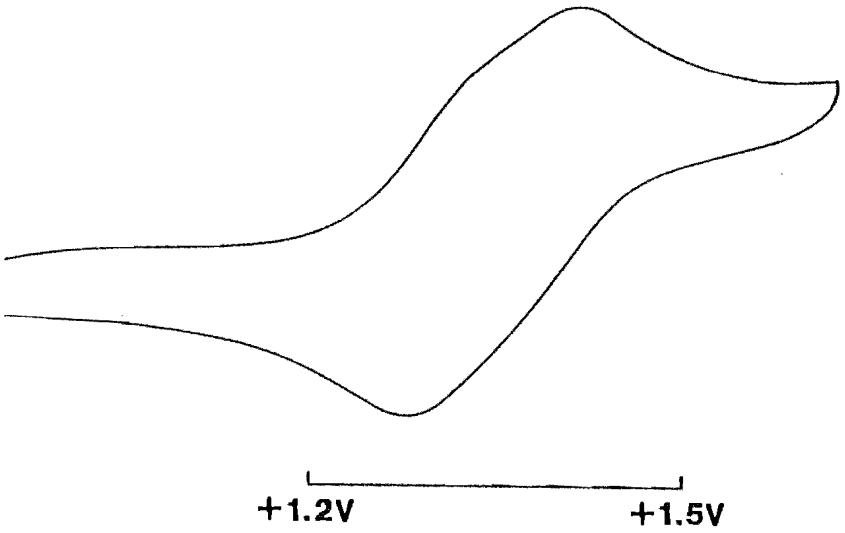

Figure 5.8b Expansion of the oxidation wave in Figure 5.8a.

process, the separate peaks are not resolved.[233] Hence, $\Delta E_{1/2}$ can not be measured directly from Figure 5.8a, although the splitting of the oxidations of **139** results in a visible shoulder on both the cathodic and anodic peaks of the oxidation wave (Figure 5.8b).

Richardson and Taube, have shown that an experimental value for ΔE_p can be used to obtain a value of $\Delta E_{1/2}$ from a working curve of $\Delta E_{1/2}$ versus ΔE_p, derived from theoretical simulations of voltammograms.[227] Furthermore, from a plot of ΔE_p versus E_p-$E_{1/2}{}^1$ (the difference between the most cathodic peak (for reduction) and the half wave potential of the first step) a value of E_p-$E_{1/2}{}^1$ can be obtained. For the oxidation of **139**, E_p is the most anodic peak and $E_{1/2}$ is the half-wave potential of the first oxidation (E_{ox1}). The values for $\Delta E_{1/2}$

(96±3mV) and E_p-$E_{1/2}{}^1$ (116mV) were derived from ΔE_p (135mV) using the expanded cyclic voltammogram (oxidations) of **139** (V=50mV/sec, x=50cm, y=200cm) (Figure 5.8b). From the observed value of E_p (1.403V), the potentials were calculated as $E_{1/2}{}^1$=1.403-0.116=1.287V (E_{ox1}) and $E_{1/2}{}^2$=1.287+0.096=1.383V (E_{ox2}). The potentials of the first and second oxidations of **140** were calculated in an analogous manner.

Molecular modelling studies (CHEM 3D Plus) of **139** and **140** predict a value of 7.5Å for the inter-metal separation. Hence, the metals are more separated than in the binuclear complexes of **109** (6.2Å, $\Delta E_{1/2}$=160mV) and **40** (5.59Å, $\Delta E_{1/2}$=200mV), which accounts for the decreased metal-metal interaction (96±3mV) of **139**. However, the π system of the naphthyridine bridge facilitates better inter-metal communication than in related biruthenium complexes, such as [Ru(bpy)$_2$]$_2$(**24**)$^{4+}$ ($\Delta E_{1/2}$=80mV) and [Ru(bpy)$_2$]$_2$(**25**)$^{4+}$ ($\Delta E_{1/2}$=56mV),[152,153] for which the metal-metal distances have been estimated to be 9.0 and 11.26Å using CHEM 3D Plus. Hence, **139** and **140**, show intermediate metal-metal interactions with the rigid conformation, low lying π* orbitals of the bridging ligand **132** and the relatively close inter-metal separation contributing to the stability of the mixed valence intermediate.

Chapter 6

Bis-bidentate 4,4'-Bipyridine Ligands and Complexes.

Bis-bidentate 4,4'-Bipyridine Ligands and Complexes.

6.1. Introduction..

In the binuclear complexes of **40**, **109** and **132**, the inter-ring bonds of the bridging ligand are coplanar. Thus, despite the trend of increasing inter-metal separation, which contributes to the decreasing metal-metal interaction, coupling of the metals can still occur via the undisrupted π system of the bridge. In contrast, the binuclear complex **131** has a flexible bridge of the ligand **110**, which, along with the large inter-metal separation (12.8-13.6Å), prevents coupling of the metals.

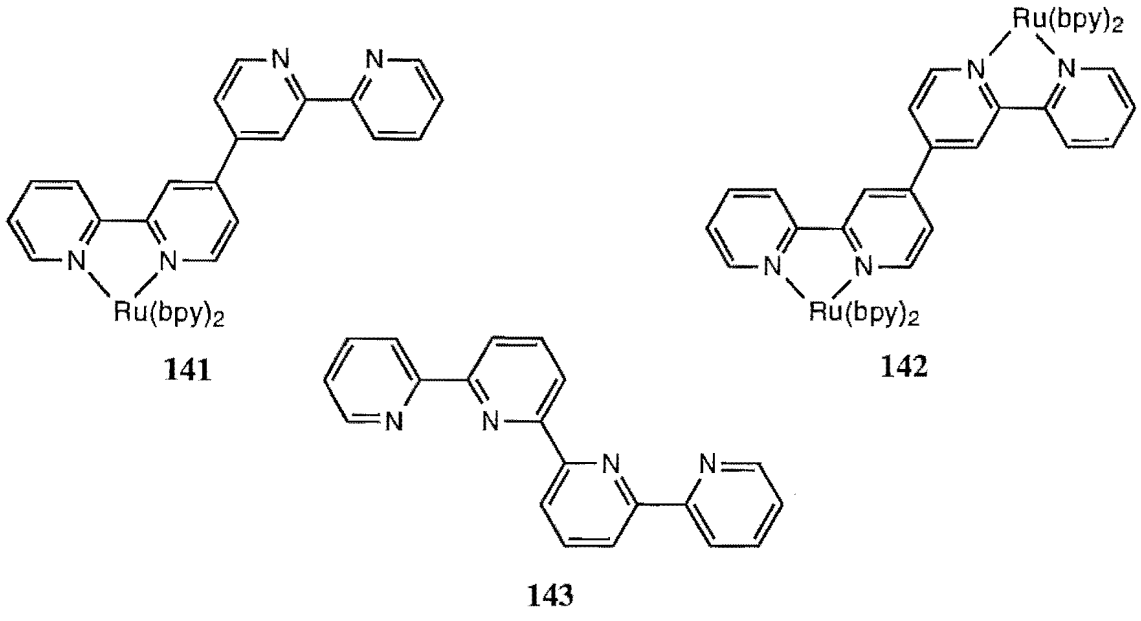

141 **142** **143**

Figure 6.1.

Steel *et al.* have described mononuclear (**141**) and binuclear (**142**) ruthenium(II) complexes of the ligand 2,2:4',4":2",2'"-quaterpyridine (**25**) (Figure 6.1).[153] In **142**, there exists the potential for overlap of the π system of each of the bpy subunits of the bridging ligand, although the conjugation of the rings is disrupted somewhat by rotation about the 4'-4" bond. Hence, the complex exhibits a weak but detectable metal-metal interaction **142** (ΔE_p=85mV, $\Delta E_{1/2}$=56±3mV). In contrast, a biruthenium complex of the related ligand 2,2':6',2":6",2'"-quaterpyridine (**143**) (Figure 6.1) showed no metal-metal interaction, due to the inability of the ligand to maintain conjugation of the bpy subunits, whilst bridging two octahedral metal centres.[234] Similarly, in known bridging ligands that contain isolated bpy subunits, inter-metal communication is prevented by the lack of conjugation between bpy subunits that are connected by saturated carbon chains.[3,153,235-237] The study of **142** has also shown that unlike other bridging ligands, such as **5** and **15**, which have low lying π* orbitals relative to bpy, **25** has

similar π orbital properties to bpy and thus does not not significantly modify the properties of **142** relative to $Ru(bpy)_3^{2+}$.

For the ^1H NMR spectrum of **141** and **142**, complete assignment of **25** was prevented by overlapping bpy protons.[238] In this chapter, we describe the unambiguous assignment of **25**, in the coordinating mode, by replacing the bpy ligands of **141** and **142** with dmb. An unsymmetrical binuclear complex of **25** with both bpy and dmb peripheral ligands, a homoleptic complex, a tetranuclear complex and a mixed metal palladium(II)/ruthenium(II) complex are also described. In most cases the NMR spectroscopy, absorption spectroscopy and cyclic voltammetry of the complexes are discussed.

The complex **142** and a recently reported diruthenium complex of a pyridinyl-benzimidazole analogue[239] are the only known examples of the use of bis-bidentate binucleating ligands containing a 4,4'-bipyridinyl bridge. This chapter also describes two new bis-bidentate 4,4'-bipyridine derivatives, **144** and **145**, which are pyrazole analogues (Figure 6.2) of **25**. The syntheses of the ligands and their mononuclear and binuclear ruthenium complexes are discussed.

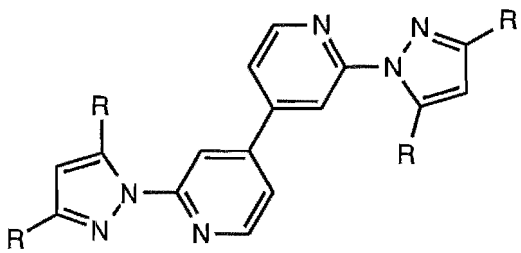

144 R=H
145 R=CH_3

Figure 6.2

6.2 Results and Discussion.

The dmb complexes, **146** and **147**, were prepared by reacting **25** with one and two equivalents of $Ru(dmb)_2Cl_2$, respectively (Scheme 6.1). In contrast, the unsymmetrical complex, **148**, was prepared by reacting **146** with $Ru(bpy)_2Cl_2$ (Scheme 6.1). Exact procedures are analogous to the preparation of complexes described earlier. All three complexes were characterised by mass spectrometry and ^1H NMR spectroscopy.

The ^1H NMR spectrum of **146** consists of 26 non-equivalent aromatic protons (Table 6.1). Many of the protons of **25** that were overlapped by bpy signals in the spectrum[238] of **141**, are isolated in the spectrum of **146**, in particular, H3''' (8.56ppm), H4 (8.13ppm), H5 (7.48ppm), H5' (7.79ppm), H5'' (7.87ppm), H5''' (7.52ppm), and H6 (7.83ppm). In the spectrum, the

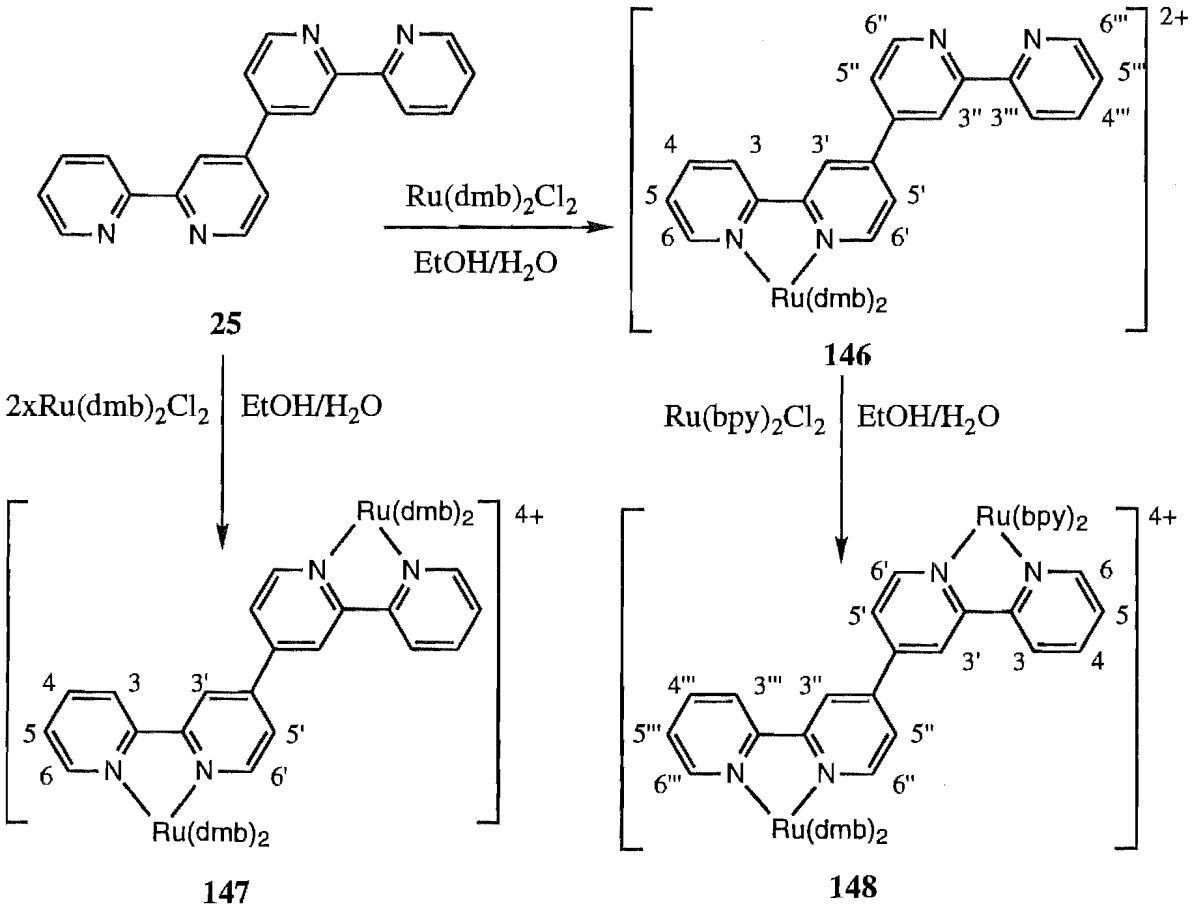

Scheme 6.1.

Table 6.1 ^{1}H NMR Chemical Shifts[a] of **25** and **146**. Coordination Induced Shifts[b] of **146**.

	Ligand **25**							Dmb ligands			
	H3	H4	H5	H6	H3'	H5'	H6'	H3[d]	H4[c,d]	H5[d]	H6[d]
25	8.56	8.00	7.51	8.80	8.91	7.87	8.88	-	-	-	-
146	8.75	8.13	7.48	7.83	8.88	7.79	7.92	8.42	2.58	7.29	7.59
CIS[b]	+0.19	+0.13	-0.03	-0.97	-0.03	-0.08	-0.96	8.42	2.58	7.29	7.61
	H3'''	H4'''	H5'''	H6'''	H3''	H5'	H6''	8.42	2.60	7.31	7.61
146	8.56	8.02	7.52	8.77	8.90	7.87	8.93	8.42	2.60	7.31	7.66
CIS[b]	+0.00	+0.02	+0.01	-0.03	-0.01	+0.00	+0.05	-	-	-	-

[a] For deuterated acetonitrile solutions. [b] CIS = $\delta_{complex}$-δ_{ligand}. [c] Methyl group [d] Not assigned.

protons of the inner-disubstituted rings (H3'-H6' and H3''-H6'') of **25** can be distinguished from the protons of the outer-monosubstituted rings (H3-H6 and H3'''-H6''') on the basis of their relative coupling patterns, since coupling due to H4 is absent from the signals for the inner rings. In addition, the H3-H6 and H3'-H6' rings exhibit coordination induced shifts (CIS), and can therefore be distinguished from H3''-H6'' and H3'''-H6''', which show near zero CIS values. For example, the triplets at 8.13 and 8.02ppm were assigned as H4 and H4''' respectively, since H4 exhibits the greater positive CIS value due to the net effect of σ-donation and π-backbonding of

electron density between ligand and metal. Similarly, both H6 and H6' exhibit large upfield shifts (-0.96 to -0.97ppm), relative to H6" and H6"' (+0.01 to +0.05ppm) due to ring-current anisotropy effects. A 2D COSY spectrum of **146** confirmed these assignments and allowed the remaining protons to be assigned unambiguously. For example, H4 (8.13ppm) correlates with signals at 7.48ppm and 8.75ppm thus assigning H5 and H3, respectively, whilst a further correlation from H5 locates H6. Similarly, H6' shows a strong correlation to a doublet of doublets at 7.79ppm (H5') which in turn shows a long-range coupling to a singlet at 8.88ppm (H3'). The non-coordinated rings were assigned in a similar manner. A combination of electron withdrawal, by the metal, and ring-current anisotropy accounts for the CIS of H5 (-0.03ppm) and H5' (-0.08ppm), whilst the chemical shifts of H3 and H3' are influenced by the change in ligand conformation on metal chelation.

The protons of **25** are more easily assigned when the ligand is in the bridging mode, since both halves of the molecule are coordinating to ruthenium and are, hence, equivalent by symmetry. Figure 6.3 shows the ^{1}H NMR spectra of **142** (top), **147** (middle) and **148** (bottom). The spectrum of **147** consists of 19 non-equivalent aromatic protons of which seven belong to the bridging ligand **25**, half of that in the spectrum of **146**. All bridging ligand protons are visible and can be assigned by their relative coupling constants and chemical shifts without the use of 1D TOCSY or 2D COSY spectra. In comparison, H4, H5' and H6 are overlapped by bpy signals in the spectrum of **142** (Figure 6.3 top).

Alternatively the symmetrical bridging ligand protons can be assigned in the spectrum of **142** using 1D TOCSY spectra (Figure 6.4). In this case, irradiation of H3' (trace I and II) and H3 (trace III and IV) locates the spin systems for the inner and outer rings of **25** respectively. Similar subspectra can also be obtained for the bpy protons by irradiating bpyH3.

In contrast, the bridging ligand of **148** is unsymmetrical, since one bipyridine subunit is coordinated to a $Ru(bpy)_2^{2+}$ unit, whilst the other is coordinated to a $Ru(dmb)_2^{2+}$. Thus, some of the signals for the bridging ligand protons occur as more complex multiplets in Figure 6.3 (bottom). For example, two overlapping doublets, corresponding to H3 and H3"' are now observed at 8.88ppm, whereas in the spectra of **142** and **147** these two protons are equivalent and appear as a doublet. The spectrum of **148** consists of 42 non-equivalent aromatic protons (14 for **25**), which were assigned from 1D TOCSY spectra, in a similar manner to the assignment of **142**, by irradiations of H3, H3', H6, bpyH3 and dmbH3. An analogous complex (**124**), of the ligand **109**, was described in chapter 4.

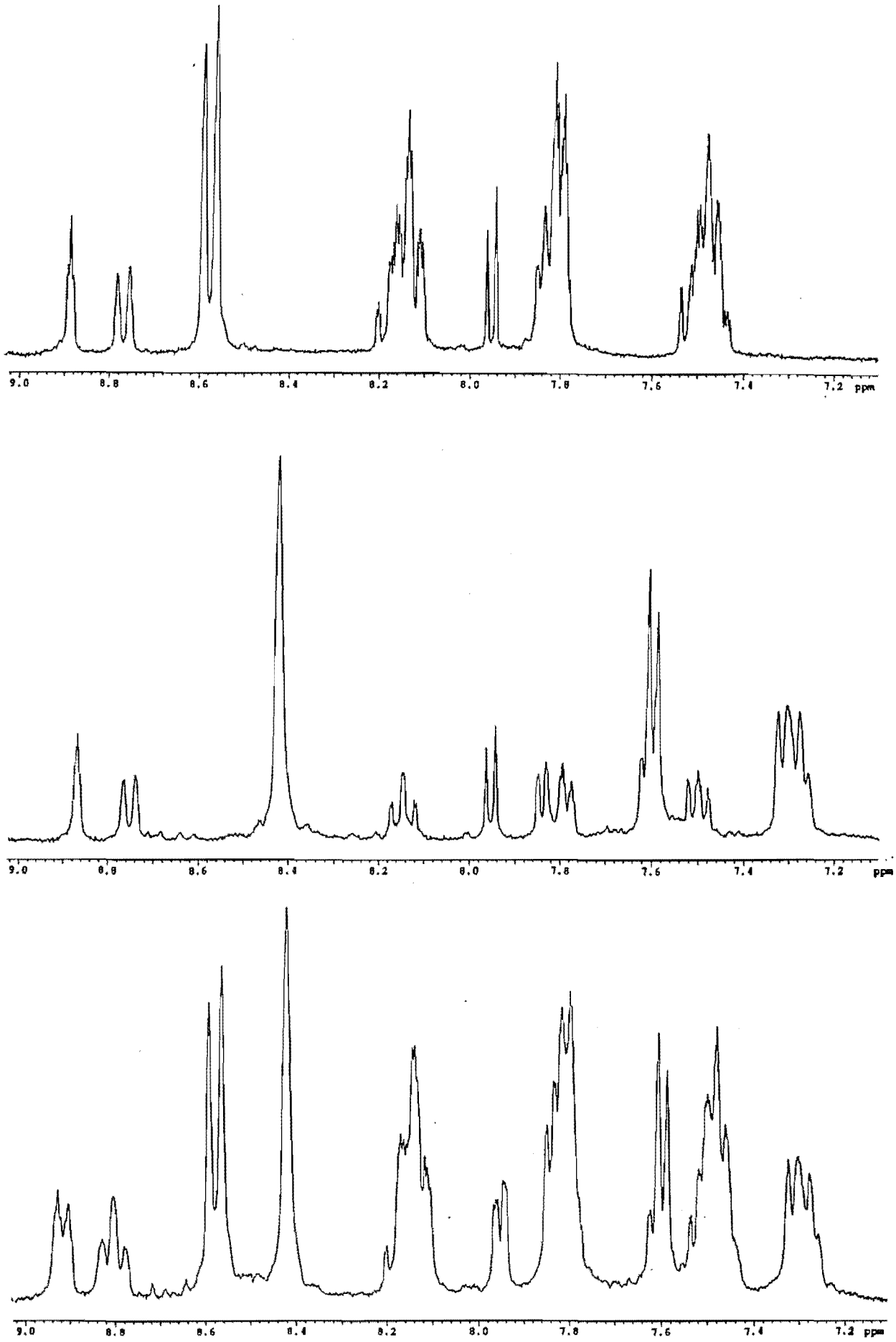

Figure 6.3 ^{1}H NMR Spectra of **142** (top), **147** (middle) and **148** (bottom).

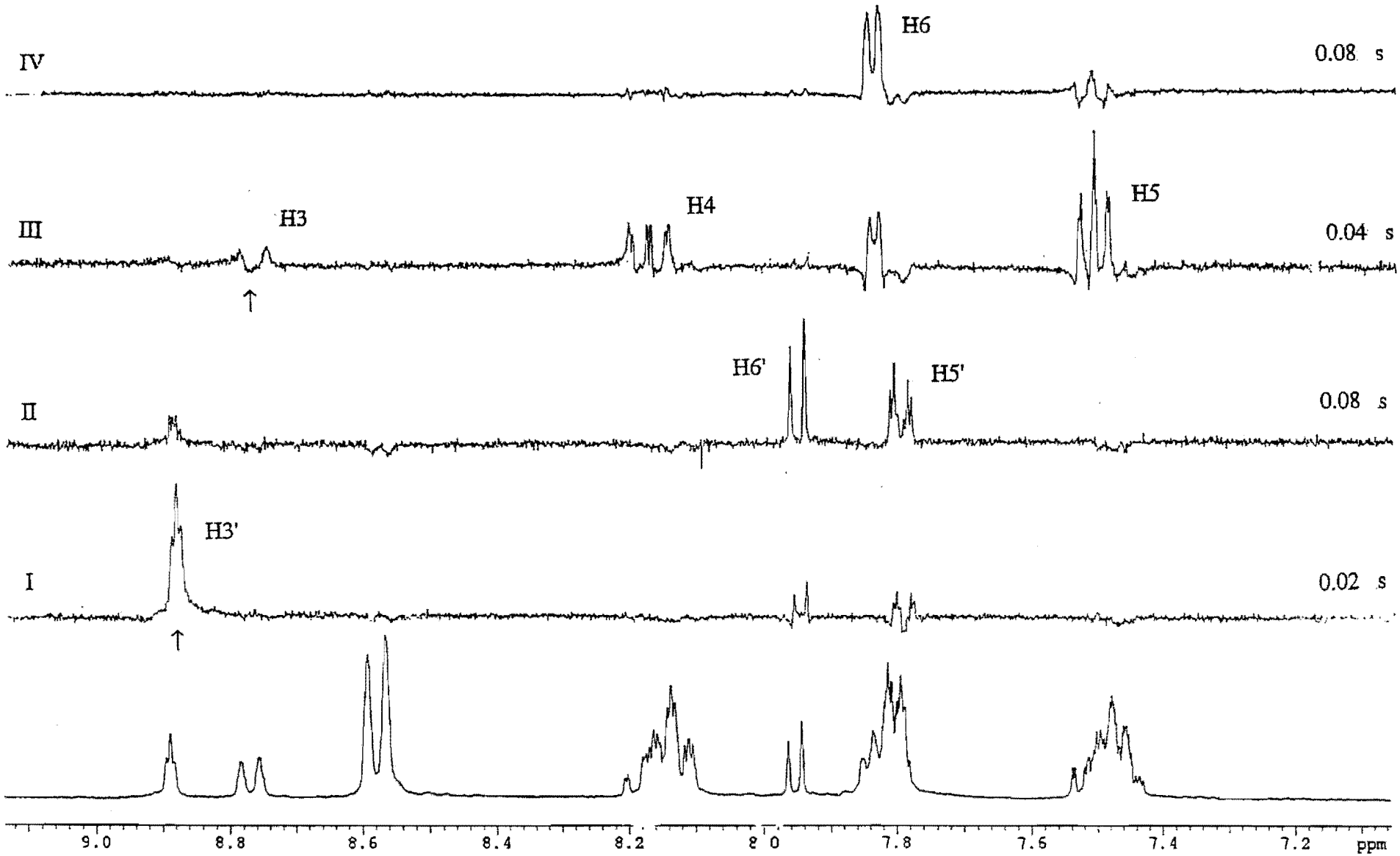

Figure 6.4 1D TOCSY Spectra of **142**

The chemical shifts of **142, 147** and **148** are summarised in Table 6.2 (peripheral ligand protons are omitted for simplicity). As a result of their electron donating methyl group, the dmb ligands push more electron density onto the metals, by σ-donation, than do the bpy ligands. This results in a slight increase in the electron density of **25,** by the synergic effect of metal-bridging ligand π-backbonding. Hence, the chemical shifts of **25**, in **147**, are shielded relative to the chemical shifts of **25** in **142**. Similarly, the protons in the H3"-H5" and H3'"-H5'" rings are shielded relative to those of the H3-H5 and H3'-H5' rings in the ^{1}H NMR spectrum of **148**, with the exception of H6/H6'" and H6'/H6". Here the effect of the different peripheral ligands is less pronounced, although the doublet is broadened, relative to that of H6 or H6' in the spectra of **142** and **147**.

Table 6.2 ^{1}H NMR chemical shift[a] and Coordination Induced Shifts[b] of μ-**25** in **142, 147** and **148**.

	H3	H4	H5	H6	H3'	H5'	H6'
25	8.56	8.00	7.51	8.80	8.91	7.87	8.88
142	8.77	8.17	7.51	7.84	8.89	7.80	7.95
CIS[b]	+0.21	+0.17	+0.00	-0.96	-0.02	-0.07	-0.93
147	8.75	8.15	7.50	7.84	8.87	7.78	7.95
CIS[b]	+0.19	+0.15	-0.01	-0.96	-0.04	-0.09	-0.93
148	8.80	8.15	7.50	7.84	8.91	7.78	7.95
CIS[b]	+0.24	+0.15	-0.01	-0.96	+0.00	-0.09	-0.93
	H3'"	H4'"	H5'"	H6'"	H3"	H5"	H6"
148	8.82	8.17	7.51	7.84	8.93	7.80	7.95
CIS[b]	+0.26	+0.17	+0.00	-0.96	+0.02	-0.07	-0.93

[a] For deuterated acetonitrile solutions. [b] CIS = $\delta_{complex}$-δ_{ligand}.

The factors which account for the CIS values of the mononuclear complex can also be invoked to explain the CIS values of the binuclear complexes, namely ring-current anisotropy (H6 and H6'), ligand-metal σ-donation and metal-ligand π-back-bonding (H4) and chelation induced conformational changes (H3 and H3'). A combination of the first two factors results in the slight shielding of H5 and H5'. The CIS value for H3 (+0.19 to +0.26ppm) is large relative to that of H3' (-0.02 to +0.01ppm), implying that these protons experience different effects due to chelation induced conformational changes. In the binuclear complexes, the 2,2' and 2"-2'" bonds of **25** are cisoid with respect to the nitrogens, whereas in the free ligand they are transoid. The latter conformation has been confirmed by the crystal structure of two crystalline modifications of **25**, which differ only in their molecular packing.[240] Each of these structures has a crystallographic centre of inversion which requires that the two central rings be

obligatorily coplanar, despite the biphenyl-like interactions between the *ortho* hydrogens. This biphenyl-like interaction is also likely to exist in the binuclear complex. Hence, the environment of H3'/H3" in the complex is similar to the environment in the free ligand, whereas H3/H3"' is deshielded in the cisoid conformation of **142**, **147** and **148**, relative to the shielding transoid conformation of **25**.

The meso and racemic diastereoisomers of **147** and **148** are not resolved in the spectra, as has been previously reported for **142**.[153] This contrasts with the spectroscopic resolution of the diastereoisomers in binuclear complexes of **40**, **109** and **132**, as described earlier, and suggests that, either the isomerism of binuclear complexes is less easily observed as the distance between the chiral metal centres increases, or, only one isomer is present.

The UV/VIS spectra and electrochemistry of the complexes **146**, **147**, **148** and, for comparison, **141**, **142** and $Ru(bpy)_3^{2+}$ are summarised in Table 6.3. All complexes exhibit strong ligand centred absorption bands (λ<400nm) and MLCT absorption bands (λ>400nm) in their UV/VIS spectra. In the mononuclear complex **146**, the lowest energy MLCT (464nm) was assigned to the transition dπ-π*(**25**), whilst the accompanying shoulder at higher energy (450nm) was assigned as dπ-π*(dmb). Hence, the lowest energy MLCT is shifted to lower energy relative to that of **141**, due to the metal d orbital destabilisation by the electon donating methyl groups of the dmb ligands.

Table 6.3 Absorption maxima[a] and Redox Potentials[b]

Complex	λ	E_{ox1}	E_{ox2}	E_{red1}	E_{red2}	E_{red3}	E_{red4}	E_{red5}
$Ru(bpy)_3^{2+}$	451	+1.27		-1.31	-1.50	-1.77	-	
141	455	+1.22		-1.32	-1.51	-1.84	-	
146	450sh,464	+1.13		-1.34	-1.67	-1.88		
142	471	+1.24[c] (85mV)		-1.10	-1.44	-1.57	-1.64	
147	448,490	+1.11	+1.17	-1.13	-1.51	-1.69[c]	-1.91[c]	
148	456,484	+1.12	+1.24	-1.12	-1.50	-1.67	-1.87[c]	-1.99

[a] In nanometres. [b] In volts vs SCE in acetonitrile. [c] Two electron.

Destabilisation of the d orbitals can also be seen in the greater ease of oxidation of **146** (+1.13V) relative to **141** (+1.22V). The oxidation and three reductions of **146** are all reversible one electron processes. The first reduction (-1.34V) is similar to that of **141** and is relatively unaffected by the dmb ligands. This implies that the first reduction of **141** and **146** corresponds to reduction of the ligand **25**. Successive reductions are assigned to the dmb ligands.

The binuclear complexes **147** (490nm) and **148** (484nm) show dπ-π*(**25**) transitions at lower energy than **146**. This small red shift has previously been observed for **141**[153] and implies

a relatively weak metal-metal interaction, since complexes with strong metal-metal interactions usually exhibit greater red shifts. Such red shifts are due to lowering of the energy of the π* orbital of the bridging ligand by the coordination of the second Ru(II). The next lowest MLCT can be attributed to transitions from the metal into the peripheral ligands.

The cyclic voltammogram of **147** consists of a reversible two electron oxidation (ΔE_p=85mV centred at 1.14V), two reversible one electron reductions and two reversible two electron reductions. Using the simulated working curves of Richardson and Taube (see chapter 5),[227] a value of 56±3mV for $\Delta E_{1/2}$ was calculated from ΔE_p. Since the value of $\Delta E_{1/2}$ is greater than that for a single step charge transfer of two electrons ($\Delta E_{1/2}$=35.61/n, n=1), the complex can be said to exhibit a weak metal-metal interaction, analogous to that shown previously for **142**. Furthermore, from plots of ΔE_p versus E_p-$\Delta E_{1/2}$ [1], the oxidation potentials of **146** were calculated as E_{ox1}=1.11V and E_{ox2}=1.17V.

The first reduction (-1.13V) of **147** can be assigned to reduction of the π* orbital of the bridging ligand, which is at lower energy than **146** for reasons already described. This result correlates with the red shift of the MLCT of the binuclear complex. As mentioned in chapters 4 and 5, Cooper *et al.* have proposed a relationship between ΔE (for the first and second reductions) and the number of bonds in the bridging ligand.[224] The second reduction of **142** has been found to correlate with this relationship[153] and this is also the case with **147**. Hence, the second reduction is centred on the bridging ligand. The remaining reductions were assigned to the dmb ligands.

The coordination of different peripheral ligands to each ruthenium was shown to have a significant effect on the ^{1}H NMR spectrum of **148** . Similarly, the effect of the peripheral ligands can also be seen in the cyclic voltammogram of the complex (Figure 6.5a, 6.5b). Figure 6.5a shows the cyclic voltammogram for **148**, whilst Figure 6.5b shows an expansion of the reversible two electron oxidation process (V=50mV/sec and X-axis=100mV/cm). A pronounced shoulder on the cathodic and anodic peaks implies a significant metal-metal interaction and clearly shows that the peripheral ligands can significantly modify the properties of the complex. The peak to peak separation ΔE_p=170mV is sufficiently large to allow the values $\Delta E_{1/2}$=120mV, E_{ox1}=+1.12V and E_{ox2}=+1.24V to be determined graphically. Similar values were obtained from the working curves of Richardson and Taube.[227] The oxidations occur at more or less the same potential as the oxidations of the parent mononuclear complex, with oxidation of the $Ru(dmb)_2^{2+}$ made easier, relative to $Ru(bpy)_2^{2+}$, by the destabilising effect that the electron

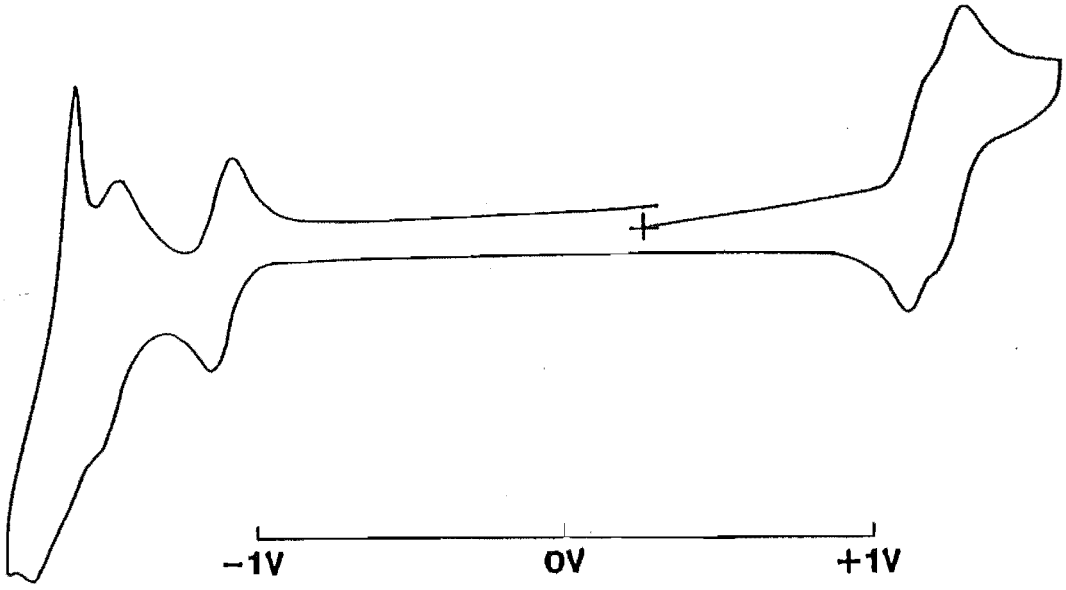

Figure 6.5a Cyclic Voltammogram of **148**.

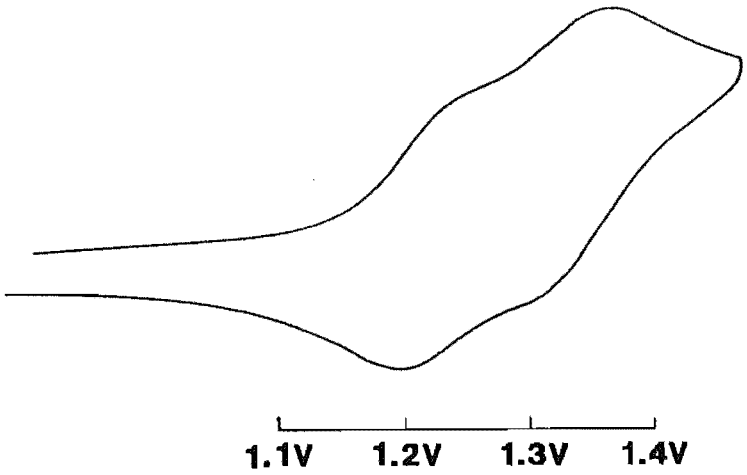

Figure 6.5b Expansion of oxidation wave in Figure 6.5a

donating methyl groups have on the d orbitals of the metal. Hence, each metal is independently affected by the peripheral ligands, resulting in a divergence of their d orbitals energies and an apparent increase in the metal-metal interaction. This effect was also observed for the complex **124**. The reductions of **148** are comparable to those of **142** and **147** and were assigned to the bridging ligand (first and second reductions), and the peripheral ligands (successive reductions).

Scheme 6.2 details the syntheses for three further complexes of **25**. The homoleptic complex **149** was prepared by reacting three equivalents of the ligand with $Ru(DMSO)_4Cl_2$ and characterised by mass spectrometry. As has been discussed in previous chapters, homoleptic complexes exist as a 3:1 mixture of the mer and fac isomers. The isomers were not sufficiently well resolved in the ^1H NMR spectrum of **149**, which contains many broad signals. For

example, 12 protons, corresponding to H3', H3'' and H6'', occur as a broad signal at 8.92-8.95ppm. Tentative assignments of the spectrum were made by comparison with the spectrum of **146**.

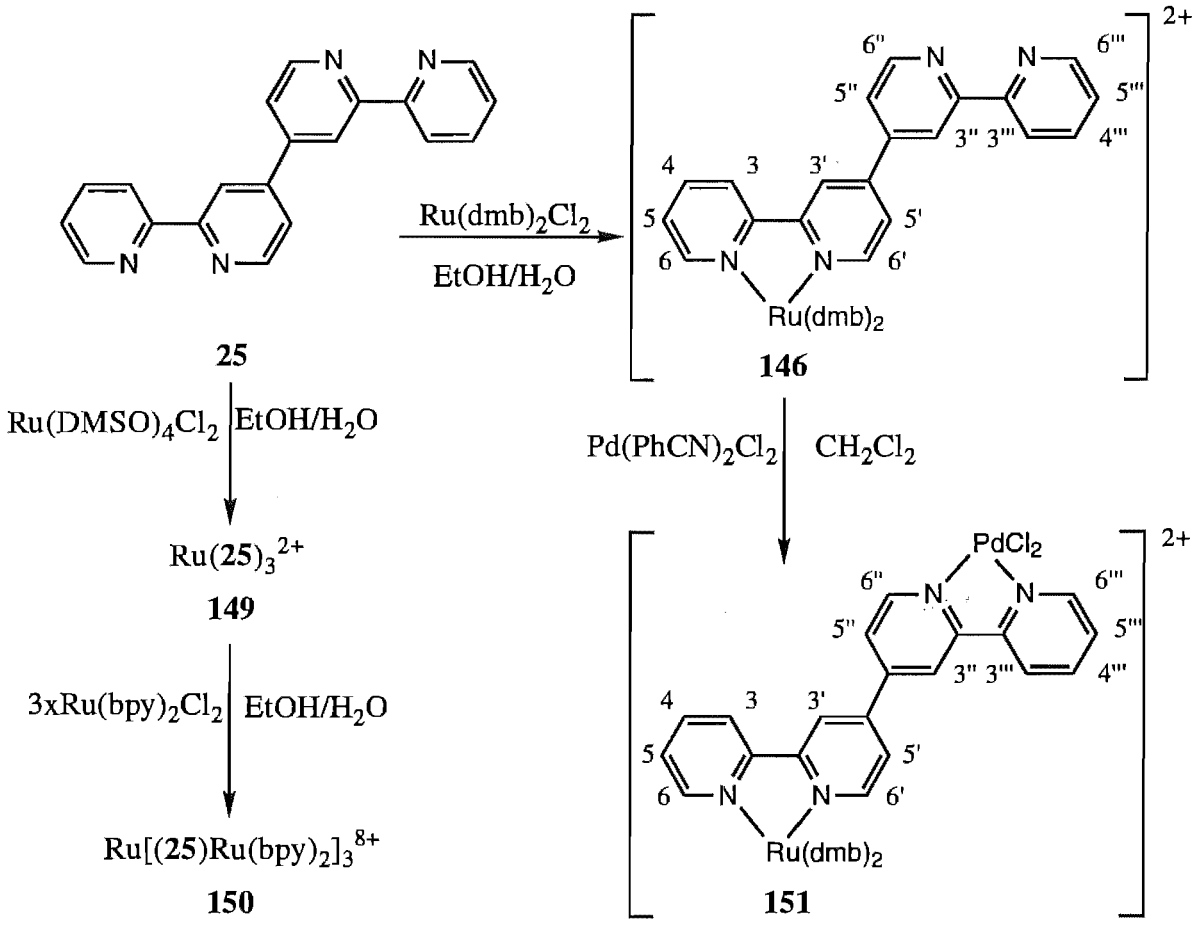

Scheme 6.2

Complex **149** exhibits an almost symmetrical MLCT absorption band (λ_{max}=468nm), at lower energy than the symmetrical MLCT absorption band of $Ru(bpy)_3^{2+}$ (λ_{max}=451nm) (Figure 6.6 top). Hence electron transfer from metal to ligand is easier for **149**. MLCT transitions into both the coordinated mono-substituted and coordinated di-substituted rings of **25**, account for the reduction in symmetry of the MLCT, relative to $Ru(bpy)_3^{2+}$.

The redox potentials of the complex consist of a reversible one electron oxidation (+1.25V) and two reversible reductions (-1.39 and -1.79V), the latter of which is a two electron processes. At more negative potentials absorption occurs, with an associated stripping curve in the cyclic voltammogram. Relative to $Ru(bpy)_3^{3+}$, the complex is easier to oxidise, but slightly harder to reduce.

The tetranuclear complex **150** was prepared by reacting **149** with three equivalents of $Ru(bpy)_2Cl_2$ and characterised, as an octahydrate, by elemental analysis. The ^1H NMR spectrum of **150** was complicated and unresolved, due to the presence of the numerous isomers

which exist for this complex, and could not be assigned. However, the electronic properties of the complex were examined by UV/VIS absorption spectroscopy and cyclic voltammetry. The UV/VIS spectrum (Figure 6.6 bottom) shows strong ligand centred absorptions below 400nm, whilst at lower energy an unsymmetrical MLCT absorption band exists (λ=482nm). The small red shift, relative to the homoleptic complex, indicates a weak metal-metal interaction analogous to that of **142** and **147**. As many as three MLCT transitions are possible for the complex (terminal Ru(II) to bpy, terminal Ru(II) to **25** and central Ru(II) to **25**) and these result in the unsymmetrical MLCT band. The transitions are less well resolved than in the UV/VIS spectrum of **127** (chapter 4), as a consequence of the weaker metal-metal interactions of **150**.

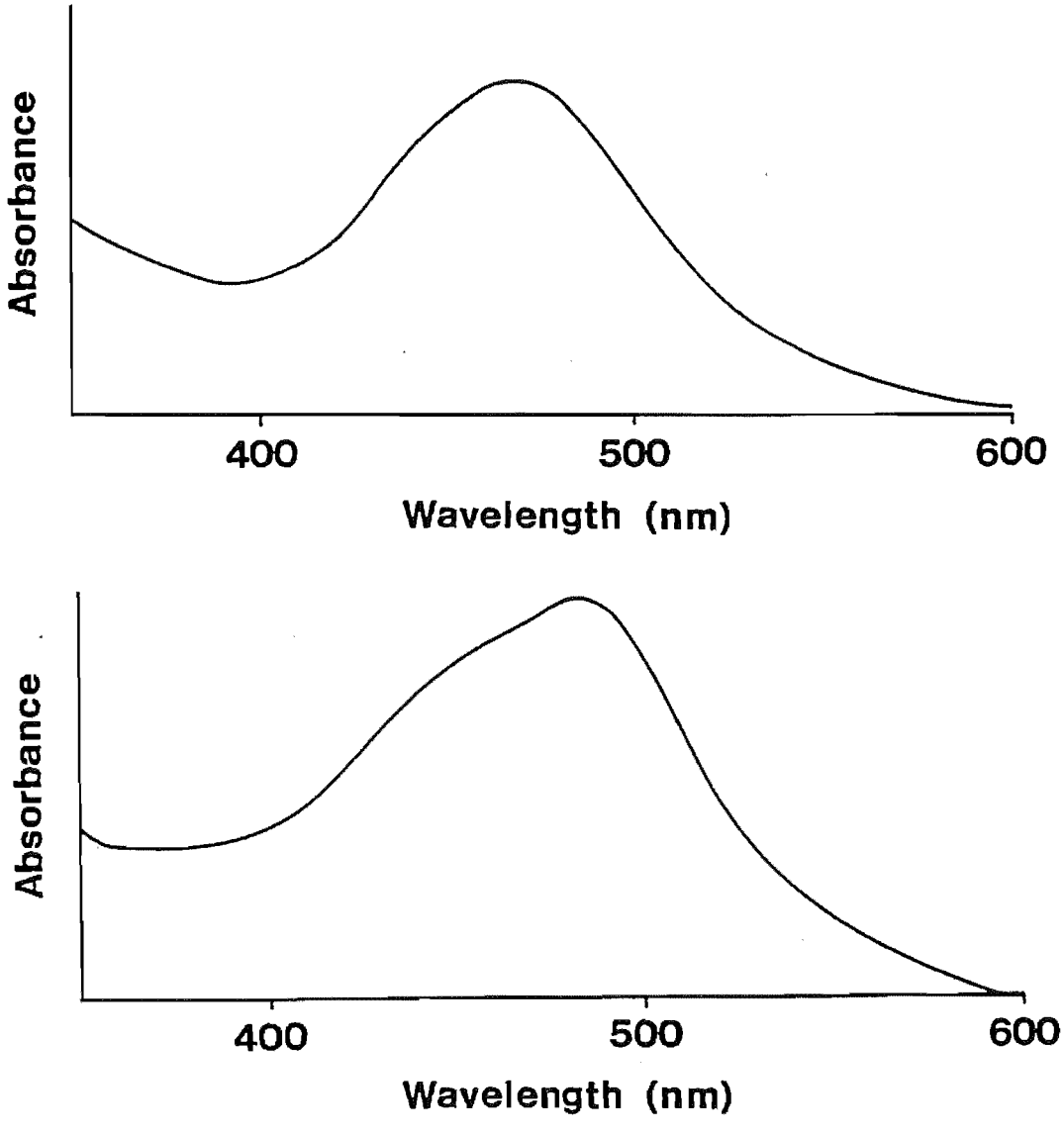

Figure 6.6 UV/VIS Absorption Spectra of **149** (top) and **150** (bottom).

The redox potentials of **150** consist of a reversible three electron oxidation (+1.31V) followed by a one electron oxidation (+1.96V). Hence, oxidation of the three terminal rutheniums occurs more readily than oxidation of the central ruthenium, which has also been

observed for **127**. The greater ease of oxidation of the terminal rutheniums implies that the lowest energy MLCT transition is dπ(terminal Ru(II))-π*(**25**) rather than dπ(central Ru(II))-π*(**25**). Furthermore, a reversible three electron reduction occurs at -0.92V, followed by an irreversible multi-electron reduction (-1.44V). The first reduction correlates with reduction of the three bridging ligands, whilst the multi-electron reduction is centred on the bpy ligands.

The third complex shown in Scheme 6.2 is the heterobinuclear complex **151**, which was prepared by reacting **146** with $Pd(PhCN)_2Cl_2$ in dichloromethane. The complex was characterised by mass spectrometry and was sufficiently soluble in CD_3CN to obtain a ^1H NMR spectrum which is summarised in Table 6.4.

The ^1H NMR spectrum of **151** consists of 28 non-equivalent protons, which were assigned by a 2D COSY spectrum, in an analogous manner to the assignment of the spectrum of **146**. Table 6.4 shows that the CIS values for the rings coordinated to palladium differ from those for the ruthenium coordinated rings. All CIS values for H3"-H6" and H3'"-H6'" are positive, with the exception of those for H3" (-0.23ppm) and H3'" (-0.07ppm), and can be attributed to the donation of σ electron density from ligand to metal, whilst H6" (+0.45ppm) and H6'" (+0.47ppm) are additionally deshielded by an adjacent chlorine atom. In contrast, H6 (-0.95ppm) and H6' (-0.87ppm) lie over pyridine rings and are anisotropically shielded. π-Back-bonding, from ruthenium to **25**, counters the effect of σ-donation from **25** to ruthenium, thus lowering the CIS values of the remaining protons, relative to the palladium coordinated ring protons (eg H4=+0.18ppm and H4'"=+0.31ppm). The exceptions are the CIS values for H3, H3', H3" and H3'", which are due to chelation induced conformational changes.

Table 6.4 ^1H NMR Chemical Shifts[a] of **25** and **151**. Coordination Induced Shifts[b] of **151**.

	Ligand **25**							Dmb ligands			
	H3	H4	H5	H6	H3'	H5'	H6'	H3[c]	H4[c,d]	H5[c]	H6[c]
25	8.56	8.00	7.51	8.80	8.91	7.87	8.88	-	-	-	-
151	8.82	8.18	7.52	7.85	8.99	7.85	8.01	8.43	2.59	7.30	7.61
CIS[b]	+0.26	+0.18	+0.01	-0.95	+0.08	-0.02	-0.87	8.43	2.59	7.30	7.61
	H3'"	H4'"	H5'"	H6'"	H3"	H5"	H6"	8.43	2.61	7.32	7.61
151	8.49	8.31	7.74	9.25	8.68	8.09	9.35	8.43	2.61	7.32	7.63
CIS[b]	-0.07	+0.31	+0.23	+0.45	-0.23	+0.22	+0.47	-	-	-	-

[a] For deuterated acetonitrile solutions. [b] CIS = $\delta_{complex}$-δ_{ligand}. [c] Not assigned. [d] Methyl group

The complex was insufficiently soluble in acetonitrile to be analysed by cyclic voltammetry. However, a UV/VIS spectrum of **151** was obtained and exhibits strong ligand centred absorptions (λ<400nm) and an unsymmetrical MLCT absorption band (λ_{max}=484nm,

sh=448nm). The lowest MLCT was assigned as dπ-π*(**25**) and exhibits a small red shift, relative to that of **146**, suggesting a weak metal-metal interaction. The shoulder at higher energy can be assigned to the transition dπ-π*(bpy).

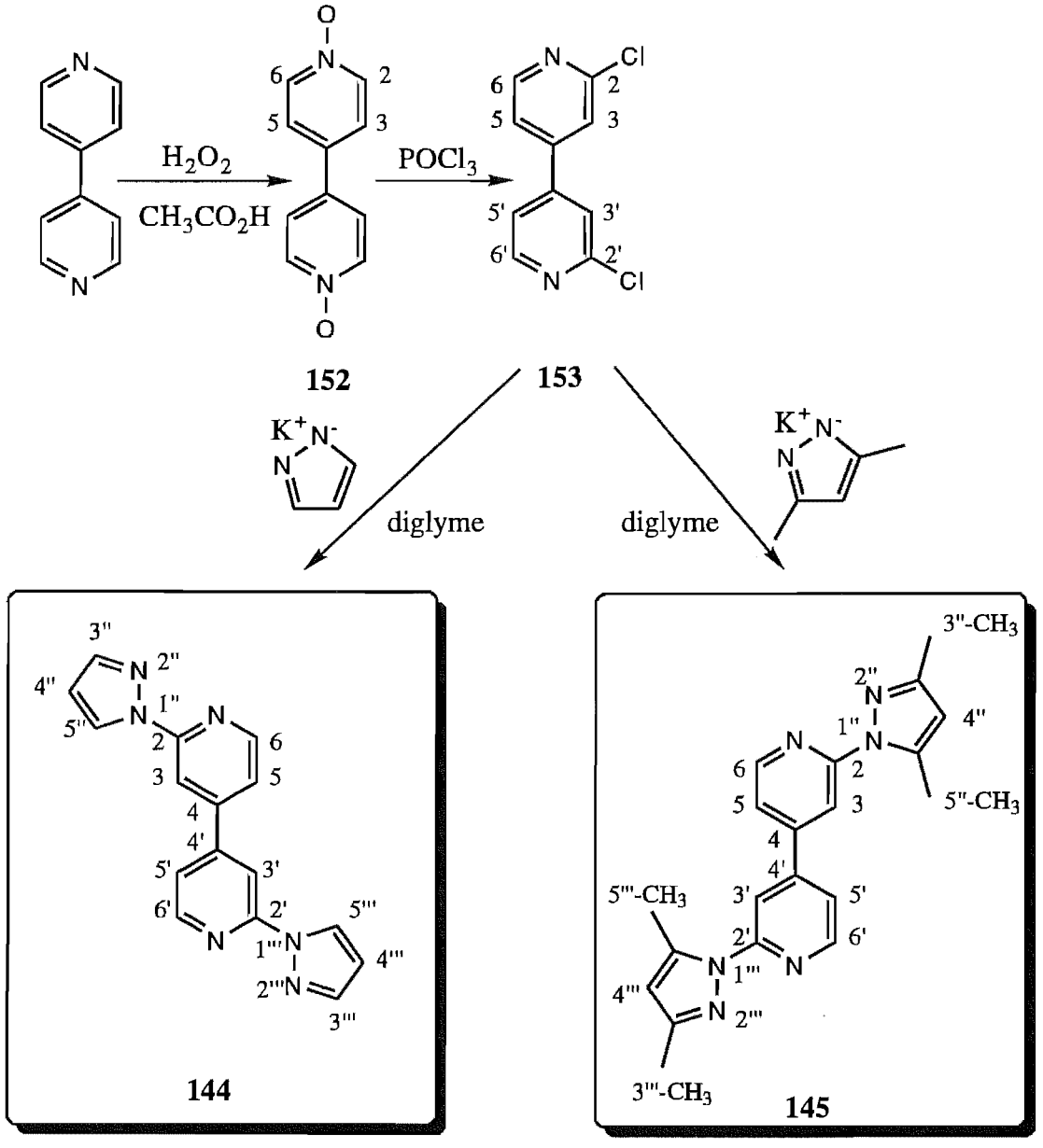

Scheme 6.3.

The syntheses of the new pyrazole analogues of **25**, 2,2'-bis-(1-pyrazolyl)-4,4'-bipyridine (**144**) and 2,2'-bis-(3,5-dimethyl-1-pyrazolyl)-4,4'-bipyridine (**145**), are shown in Scheme 6.3. The first two steps are derived from procedures for the synthesis of related bipyridines.[230] Firstly, 4,4'-bipyridine-di-N-oxide (**152**) was prepared by heating a solution of 4,4'-bipyridine and hydrogen peroxide in acetic acid. The compound was characterised by its ^{1}H NMR spectrum which consists of two doublets at 7.99ppm and 8.40ppm, with the upfield signal assigned to the more electron-rich H3/H5. In the second step, refluxing **152** in $POCl_3$ afforded 2,2'-dichloro-4,4'-bipyridine (**153**) which was characterised by its ^{1}H NMR spectrum. This was assigned on the basis that H5 is coupled to both H3 (long-range) and H6, and appears as a

doublet of doublets (8.01ppm), whilst the H6 doublet (8.17ppm) has a larger coupling than the H3 doublet (8.67ppm) and can thus be distinguished.

For the final step, **153** was reacted either with two equivalents of potassium pyrazolate, to give **144**, or with two equivalents of potassium 3,5-dimethylpyrazolate, to give **145**. Both ligands were characterised by mass spectrometry, elemental analysis and ^{1}H and ^{13}C NMR spectroscopy. The numbering of the atoms shown in Scheme 6.3 differs from that of **25**, but is consistent with the systematic nomenclature of the compounds.

^{1}H NMR spectra of the ligands were recorded in $CDCl_3$ and CD_3CN whilst the ^{13}C NMR spectra were obtained in CD_3CN. In the ^{1}H NMR spectra of **144** and **145**, the pyridine protons can be readily distinguished by their relative couplings as described for the spectra of **153**. The larger coupling between H4" (triplet, 6.62ppm) and H5" (doublet, 8.70ppm), relative to that between H3" (doublet, 7.87ppm) and H4", enabled the assignment of the pyrazole ring protons of **144**. A similar coupling of H4" broadens the CH_3-5" singlet (2.71ppm), relative to the CH_3-3" singlet (2.32ppm), in the spectrum of **145**. The protonated carbons in the ^{13}C NMR spectra were assigned by comparison with the spectrum of **43**.[11]

The ligands **144** and **145** were recrystallised from $CH_3CN/CHCl_3$ and CH_3CN respectively. The resulting crystals were of sufficient quality for the structure of the ligands to be determined by X-ray crystallography.

Figures 6.7a and 6.7b show perspective views and atom labelling of the structures of **144** and **145** respectively. Table 6.5 lists the bond lengths and bond angles with least-squares-estimated standard deviations in parentheses. For both structures the asymmetric unit comprises a full molecule. Hence, the potential molecular symmetry is not recognised in the crystallographic symmetry. This contrasts with the two reported[240] crystal structures of **25** in which the two halves of the molecule are crystallographically related by a centre of inversion and are obligatorily coplanar. For **144** and **145**, the two non-crystallographically related halves of the molecule have remarkably similar bond lengths and angles. However, significant differences exist in the torsional angles of the two halves of each molecule and these are discussed in detail later. The only significant differences in bond lengths and bond angles between the two molecules are those associated with the N(1)-atoms of the pyrazole rings wherein the presence of the 5-methyl substituent in **145** increases the bond lengths and angles about this atom relative to those in **144**. Such effects are well documented in the literature for the crystal structures of pyrazoles.[241]

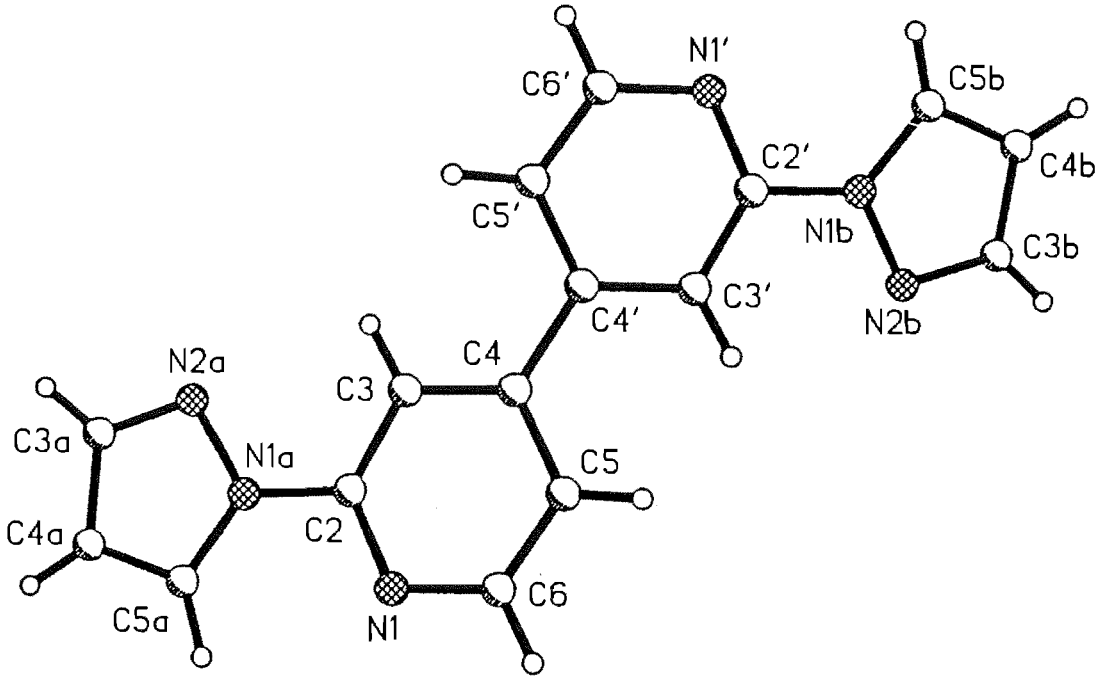

Figure 6.7a. Perspective view and atom labelling of the structure of **144**.

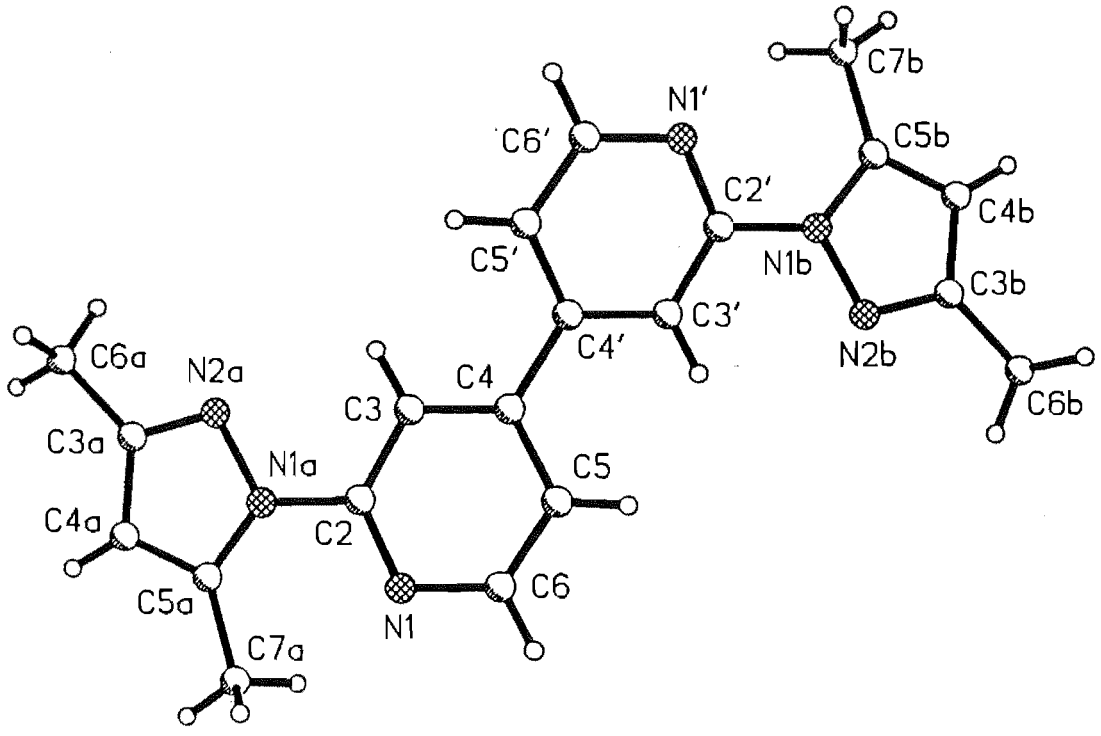

Figure 6.7b. Perspective view and atom labelling of the structure of **145**.

Table 6.5. Bond lengths (Å)and bond angles (°) for **144** and **145**.

	144	**145**		**144**	**145**
N(1)-C(2)	1.321(2)	1.324(5)	N(1)-C(6)	1.334(2)	1.343(4)
C(2)-C(3)	1.382(2)	1.376(5)	C(2)-N(1A)	1.404(2)	1.408(5)
C(3)-C(4)	1.380(2)	1.374(5)	C(4)-C(5)	1.388(2)	1.390(5)
C(4)-C(4')	1.475(2)	1.470(5)	C(5)-C(6)	1.372(2)	1.354(5)
N(1')-C(2')	1.322(5)	1.317(5)	N(1')-C(6')	1.335(2)	1.337(4)
C(2')-C(3')	1.375(2)	1.374(5)	C(2')-N(1B)	1.408(2)	1.391(5)
C(3')-C(4')	1.380(2)	1.378(5)	C(4')-C(5')	1.388(2)	1.384(5)
C(5')-C(6')	1.369(2)	1.372(5)	N(1A)-C(5A)	1.349(2)	1.357(5)
N(1A)-N(2A)	1.359(1)	1.383(5)	N(2A)-C(3A)	1.318(2)	1.320(5)
C(3A)-C(4A)	1.393(2)	1.399(6)	C(3A)-C(6A)		1.501(5)
C(4A)-C(5A)	1.353(2)	1.365(5)	C(5A)-C(7A)		1.483(6)
N(1B)-N(2B)	1.356(1)	1.368(4)	N(1B)-C(5B)	1.349(2)	1.388(5)
N(2B)-C(3B)	1.319(2)	1.312(5)	C(3B)-C(4B)	1.392(2)	1.411(6)
C(3B)-C(6B)		1.493(5)	C(4B)-C(5B)	1.356(2)	1.350(5)
C(5B)-C(7B)		1.488(5)			
C(2)-N(1)-C(6)	116.2(1)	115.2(4)	N(1)-C(2)-C(3)	124.8(1)	125.0(4)
N(1)-C(2)-N(1A)	115.0(1)	115.1(4)	C(3)-C(2)-N(1A)	120.2(1)	119.9(4)
C(4)-C(3)-C(2)	118.4(1)	118.3(4)	C(3)-C(4)-C(5)	117.6(1)	118.1(4)
C(3)-C(4)-C(4')	120.9(1)	121.3(4)	C(5)-C(4)-C(4')	121.5(1)	120.7(3)
C(6)-C(5)-C(4)	119.3(1)	118.7(4)	N(1)-C(6)-C(5)	123.8(1)	124.7(4)
C(2')-N(1')-C(6')	115.9(1)	116.2(4)	N(1')-C(2')-C(3')	124.7(1)	124.6(4)
N(1')-C(2')-N(1B)	115.1(1)	116.3(4)	C(3')-C(2')-N(1B)	120.1(1)	119.1(4)
C(2')-C(3')-C(4')	118.6(1)	119.3(4)	C(3')-C(4')-C(5')	117.5(1)	116.7(4)
C(3')-C(4')-C(4)	120.3(1)	120.8(4)	C(5')-C(4')-C(4)	122.1(1)	122.4(4)
C(6')-C(5')-C(4')	119.0(1)	119.8(4)	N(1')-C(6')-C(5')	124.1(1)	123.4(4)
C(5A)-N(1A)-N(2A)	112.1(1)	112.3(3)	C(5A)-N(1A)-C(2)	127.7(1)	130.8(4)
N(2A)-N(1A)-C(2)	120.3(1)	116.6(4)	C(3A)-N(2A)-N(1A)	103.7(1)	103.7(4)
N(2A)-C(3A)-C(4A)	112.4(1)	111.9(4)	N(2A)-C(3A)-C(6A)		119.9(4)
C(4A)-C(3A)-C(6A)		128.1(4)	C(5A)-C(4A)-C(3A)	104.9(1)	106.2(4)
N(1A)-C(5A)-C(4A)	106.9(1)	105.8(4)	N(1A)-C(5A)-C(7A)		126.4(4)
C(4A)-C(5A)-C(7A)		127.7(4)	N(2B)-N(1B)-C(5B)	112.2(3)	110.8(3)
N(2B)-N(1B)-C(2')	120.0(1)	118.2(4)	C(5B)-N(1B)-C(2')	127.8(1)	130.9(4)
C(3B)-N(2B)-N(1B)	103.7(1)	105.3(4)	N(2B)-C(3B)-C(4B)	112.4(1)	111.5(4)
N(2B)-C(3B)-C(6B)		120.7(4)	C(4B)-C(3B)-C(6B)		127.8(4)
C(5B)-C(4B)-C(3B)	104.9(1)	106.1(4)	C(4B)-C(5B)-N(1B)	106.7(3)	106.3(3)
C(4B)-C(5B)-C(7B)		128.8(4)	N(1B)-C(5B)-C(7B)		124.8(4)

Table 6.6. Selected torsional angles (°) for **144** and **145**.

	144	**145**
N(1)-C(2)-N(1A)-N(2A)	175.0(1)	171.6(5)
N(1)-C(2)-N(1A)-C(5A)	-2.4(2)	-16.2(8)
C(3)-C(2)-N(1A)-N(2A)	-4.6(2)	-8.2(6)
C(3)-C(2)-N(1A)-C(5A)	178.1(1)	164.1(5)
C(3)-C(4)-C(4')-C(3')	-147.3(1)	-147.4(5)
C(3)-C(4)-C(4')-C(5')	30.9(2)	34.9(7)
C(5)-C(4)-C(4')-C(3')	30.7(2)	32.2(7)
C(5)-C(4)-C(4')-C(5')	-151.1(1)	-145.6(5)
N(1')-C(2')-N(1B)-N(2B)	-171.9(1)	164.4(4)
N(1')-C(2')-N(1B)-C(5B)	7.1(2)	-20.5(8)
C(3')-C(2')-N(1B)-N(2B)	6.6(2)	-14.8(7)
C(3')-C(2')-N(1B)-C(5B)	-174.3(1)	160.3(5)

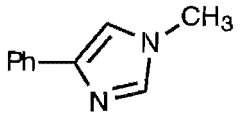

154

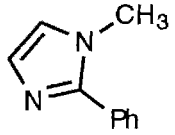

155

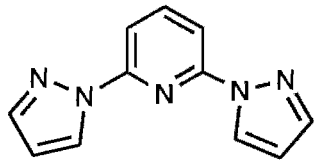

156

Figure 6.8.

The ligands crystallise with all inter-ring bonds in transoid conformations and with the pyrazole rings approximately coplanar with their attached pyridine rings. Table 6.6 lists the torsional angles for the inter-ring bonds. In the structure of **144**, the meanplanes of the pyrazole rings are inclined to those of the pyridine rings at angles of 4.4(1) and 8.1(1)°, whilst in **145**, the corresponding angles (11.9(4) and 17.3(4)°) are greater, as a consequence of the steric bulk of the attached methyl group. However, the effect of the methyl group is considerably less than in the recently reported[242] structures of 1-methyl-4-phenylimidazole (**154**) (Figure 6.8) and its 1-methyl-2-phenyl isomer (**155**), where in the first case the rings are nearly coplanar (7.3° twist) but in the second, the adjacent methyl group induces significant (32.3°) twisting about the inter-ring bond. The present results seem to lend support to the suggestion that such compounds are stabilised by intramolecular C(Ar)-H···N hydrogen bonds, as has recently been proposed for a family of 9-azaphenyl-9H-carbazoles.[243] The structurally related ligand 2,6-bis-(pyrazol-1-yl)pyridine (**156**) has been the subject of a recent X-ray crystal structure determination, which showed that this also has the pyrazole rings attached to the pyridine ring in approximately (3.5°) coplanar transoid conformations.[244] In addition, the molecular packing of **144** seems to be controlled by a system of intermolecular C(Ar)-H... N interactions, with the molecules packing in chains with the pyridine nitrogens interacting with pyrazole hydrogens of adjacent molecules.

The central (C(4)-C(4')) bond of both **144** and **145** exists in a transoid conformation with significant deviation from coplanarity of the two pyridine rings in both cases (Table 6.6). The meanplanes of the pyridine rings are inclined at an angle of 32.0(1)°, in the structure of **144**, while in the structure of **145** the corresponding angle is 32.9(4)°. This contrasts with the structures of **25** in which the central pyridine rings are coplanar.[240]

Conjugation between the π-excessive azole ring and the π-deficient azine ring has been previously proposed to exist in azolylazine ligands.[11,243] The structures of **144** and **145** provide experimental evidence for this proposal. In particular, the bonds linking the pyrazole rings to the pyridine rings (1.404(2) and 1.408(2)Å in **144** and 1.408(5) and 1.391(5)Å in **145**) are short relative to those in structurally related compounds, such as 1-phenylpyrazoles,[245] and the rings do not deviate significantly from coplanarity, even in the case of **145** which possesses adjacent methyl substituents. This is consistent with donation of electron density from the pyrazole to the pyridine rings. The resulting polarisation of the pyridine rings would discourage conjugation between the central pyridine rings in **144** and **145** and account for the significant twisting about the central bond. The magnitude of this latter interaction must be sufficient to counteract the stabilisation energy associated with the π-π stacking interactions observed in the planar structures of **25**.[240] It is relevant that in the structure of **156** the rings are coplanar with inter-ring bond lengths of 1.406Å; in this case the pyrazoles compete as electron donors.

The syntheses of seven ruthenium complexes (**157-163**) of **144** are shown in Scheme 6.4. All complexes were prepared using analogous procedures to those already described for structurally related complexes and were characterised by mass spectrometry and ^{1}H NMR spectroscopy. Additionally, ^{13}C NMR spectra were obtained for **159** and **160** and assigned by comparison with the spectra of the ligand and the complex Ru(**43**)(bpy)$_2^{2+}$.[11]

The ^{1}H NMR spectrum of the mononuclear complex **157** is shown in Figure 6.9, and consists of 28 non-equivalent protons. Pyrazole protons were readily distinguished on the basis of the smaller H3"-H4" (H3'"-H4'") coupling relative to that of H4"-H5" (H4'"-H5'") and assignments were confirmed with the aid of a 2D COSY spectrum (Figure 6.9). In particular, by correlations to H4" (6.88ppm) and H4'" (6.63ppm), the COSY spectrum allows the protons that are overlapped by other signals to be located unambiguously, namely H3" (7.43ppm), H3'" (7.87ppm) and H5'" (8.70ppm). A similar correlation from H4" locates H5" (9.01ppm). Turning to the pyridine protons of **144**, the doublet at 7.76ppm and the doublet of doublets at 7.67ppm are clearly coupled, as shown by raised intensity of the inner peaks in the ^{1}H NMR spectrum,

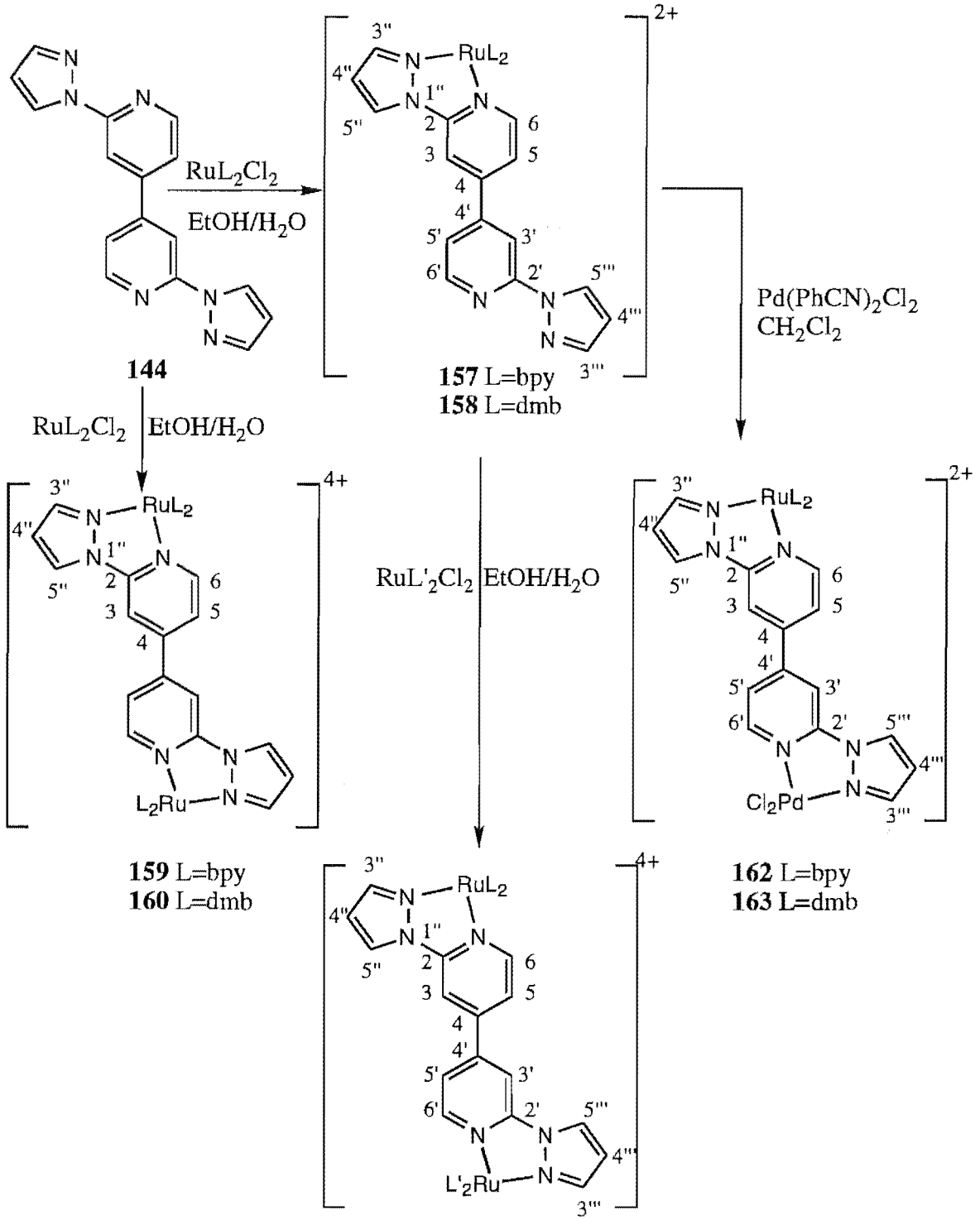

Scheme 6.4

and can be assigned as H6 and H5 respectively. Hence the remaining doublet of doublets can be assigned as H5' (7.71ppm) and correlated to the H6' doublet (8.69ppm) in the COSY spectrum. The protons H3 (8.50ppm) and H3' (8.44ppm) were distinguished by long-range correlation to H5 and H5' respectively, thus assigning all protons of **144**. The COSY spectrum was also used to make tentative assignments of the spin systems of the bpy rings.

The ^{1}H NMR spectrum of the dmb analogue, **158**, was also assigned with the assistance

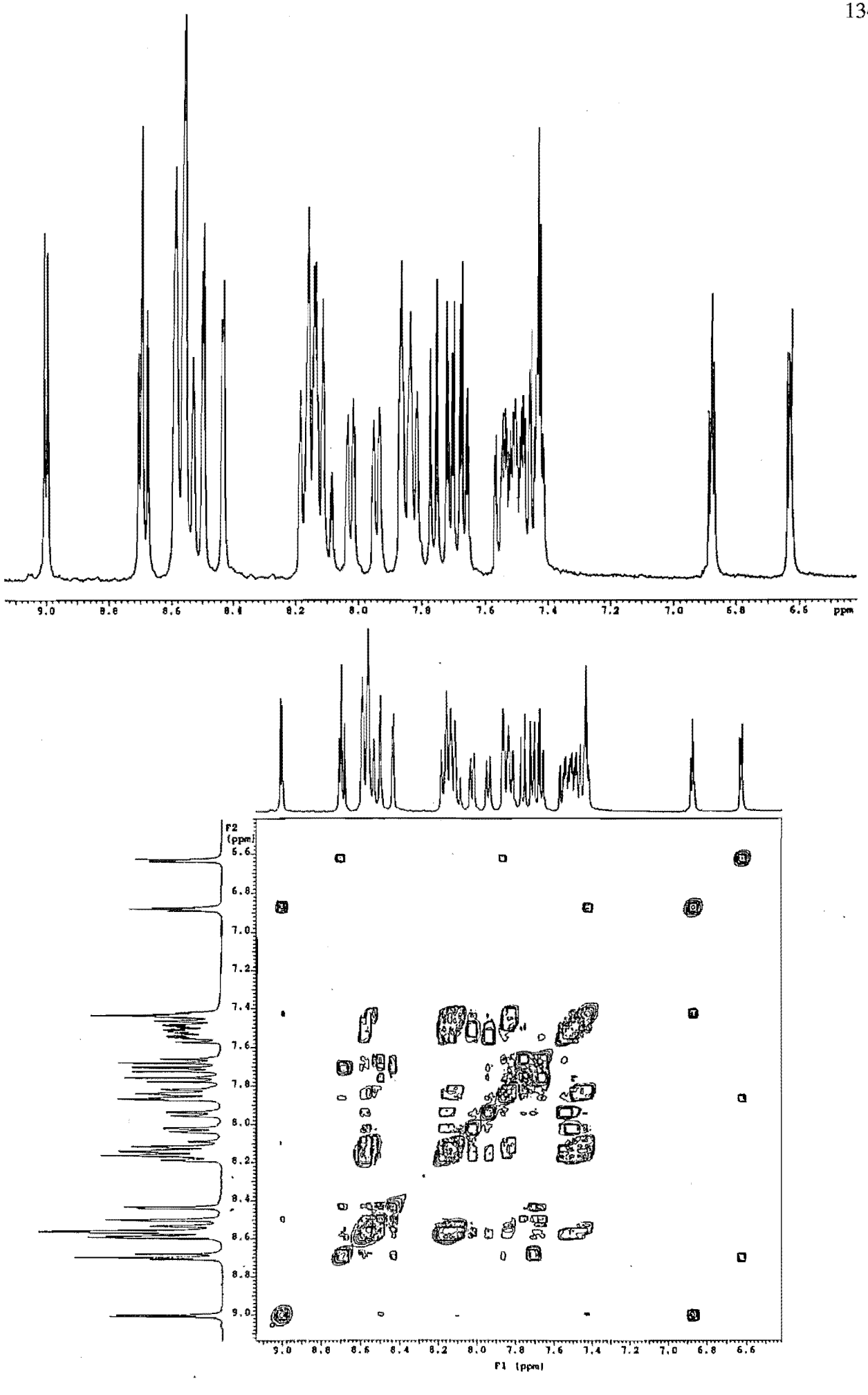

Figure 6.9 ^{1}H NMR and 2D COSY Spectra of **157**.

Table 6.7 ^{1}H NMR Chemical Shifts[a] of **144** and **157** and Coordination Induced Shifts[b] of **157**.

	Ligand **144**						Bpy Ligands			
	H3	H5	H6	H3"	H4"	H5"	H3	H4	H5	H6
144	8.38	7.73	8.63	7.87	6.62	8.70	-	-	-	-
157	8.50	7.67	7.76	7.43	6.88	9.01	8.55	8.11	7.44	7.82
CIS[b]	+0.12	-0.06	-0.87	-0.44	+0.26	+0.31	8.58	8.14	7.48	7.85
	H3'	H5'	H6'	H3'"	H4'"	H5'"	8.58	8.16	7.55	7.94
157	8.44	7.71	8.69	7.87	6.63	8.70	8.58	8.16	7.50	8.03
CIS[b]	+0.06	-0.02	+0.06	+0.00	+0.01	+0.00	-	-	-	
	Ligand **144**						Dmb Ligands			
	H3	H5	H6	H3"	H4"	H5"	H3	H4[c]	H5	H6
158	8.60	7.65	7.77	7.41	6.87	9.06	8.43	2.59	7.27	7.63
CIS[b]	+0.22	-0.08	-0.86	-0.46	+0.25	+0.36	8.41	2.60	7.32	7.65
	H3'	H5'	H6'	H3'"	H4'"	H5'"	8.41	2.61	7.36	7.75
158	8.42	7.76	8.65	7.86	6.61	8.67	8.41	2.62	7.34	7.83
CIS[b]	+0.04	+0.03	+0.02	-0.01	-0.01	+0.03	-	-	-	

[a] For deuterated acetonitrile solutions. [b] CIS = $\delta_{complex}$-δ_{ligand}. [c] Methyl group.

of a 2D COSY spectrum, although in this case the spectrum was more complicated due to the overlap of H6 (7.77ppm), H5' (7.76ppm) and H5 (7.65ppm), with the dmbH6 protons, the latter of which are shifted upfield relative to the bpyH6 protons of **157**.

The spectra of **157** and **158** are summarised in Table 6.6. The C2'-N1'" bond remains in the transoid conformation of the free ligand and the non-coordinating rings are well removed from the site of metal chelation. Hence the CIS values for H3'-H6' and H3'"-H5'" are close to zero. As a consequence of metal chelation, the conformation about the C2-N1" bond is now cisoid, which is reflected in the CIS values of H3 (+0.12 to +0.22ppm) and H5" (+0.31 to +0.35ppm) for both complexes. Ligand to metal σ-donation and metal to ligand π-back-bonding of electron density, which also contributes to the deshielding of H5", is reflected in the CIS values for H4" (+0.25 to +0.26ppm), whilst the shielding of H6 (-0.86 to -0.87ppm) and H3" (-0.44 to -0.46ppm) are consistent with the effects of ring-current anisotropy. Finally, the slight shielding of H5 (-0.06 to -0.08ppm) results from a combination of σ-donation and ring-current anisotropy. The larger CIS value for H4" (+0.26ppm), relative to that of H4 (+0.13ppm) in the spectrum of **146**, is consistent with pyrazole being a π-excessive π-donor and hence a weaker π-acceptor than pyridine.

In **159**, the bridging ligand is symmetrical about the 4,4' bond, as a consequence of coordination of a $Ru(bpy)_2^{2+}$ group to each of the two bidentate sites of **144**. This is reflected in

the ^{1}H NMR spectrum of the complex (Figure 6.10), which is simpler than the corresponding spectrum of **157** and consists of 22 non-equivalent protons (6 for μ-**144**). The spectrum was assigned by comparison with the spectrum of **157** and the assignments confirmed by the 1D TOCSY spectra in Figure 6.11. From the TOCSY spectra the bridging ligand protons were located unambiguously by irradiating H5" (trace I) and H5 (trace II), whilst the bpy protons were located by irradiating bpyH3 (trace III-V). As was the case for **157**, a 2D COSY spectrum was used to assign the bpy spin systems, although, of course, this does not assign the stereochemical environment of the rings. The diastereoisomers of **159** are not resolved in the spectrum, unlike in the spectra of **121**, where the metals are much closer together.

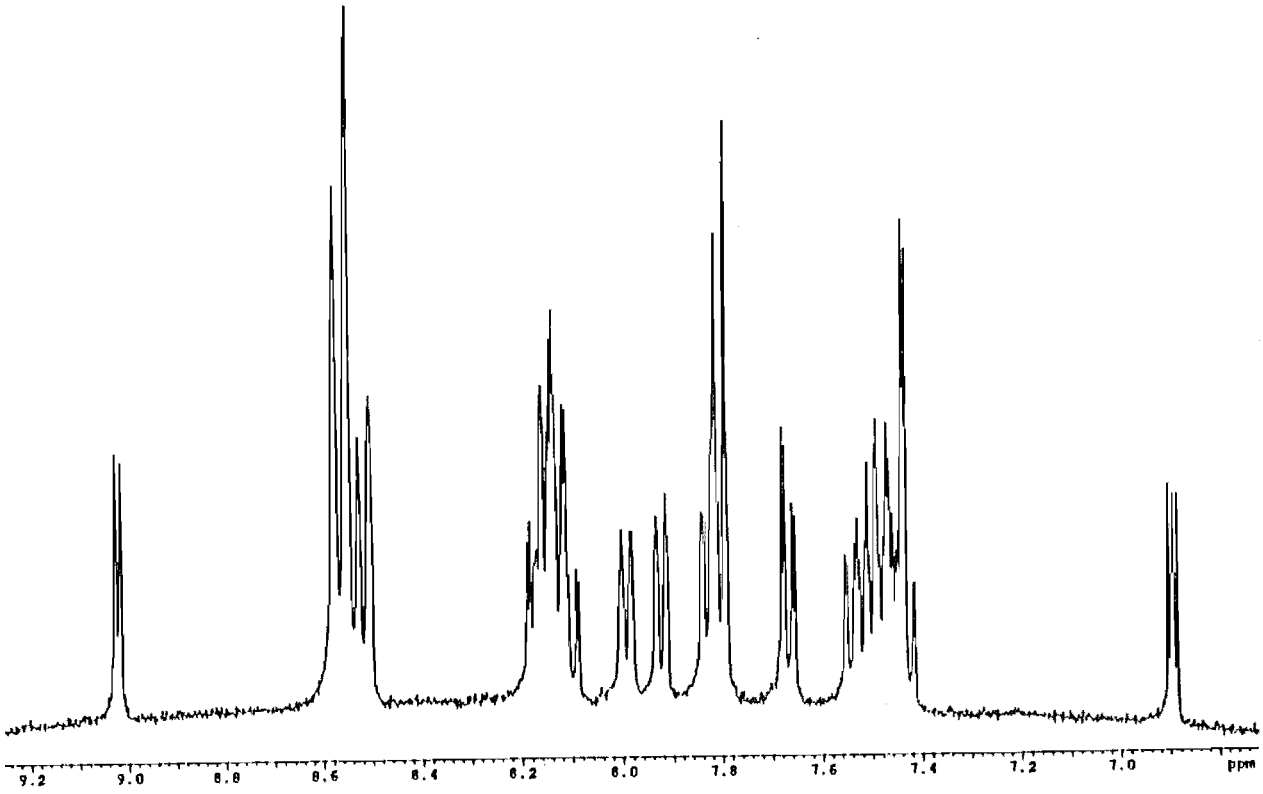

Figure 6.10 ^{1}H NMR spectrum of **159**.

^{1}H NMR spectra were recorded for the two remaining diruthenium complexes **160** and **161**. The spectrum of **160** was completely assigned, in a similar manner to the assignment of **157**, by a 2D COSY spectrum, whilst the spectrum of the unsymmetrical complex, **161**, was assigned by comparison with the spectra of **159** and **160**, and with the assistance of 1D TOCSY and 2D COSY spectra.

Table 6.8 summarises the spectra of the homobinuclear complexes. The bonds between the pyrazole and pyridine rings are now cisoid, for each of the two pyrazolylpyridine subunits of **144**, as a consequence of metal chelation. The change in conformation, and the electronic and through-space effects of metal chelation, are reflected in the CIS values for the bridging ligand

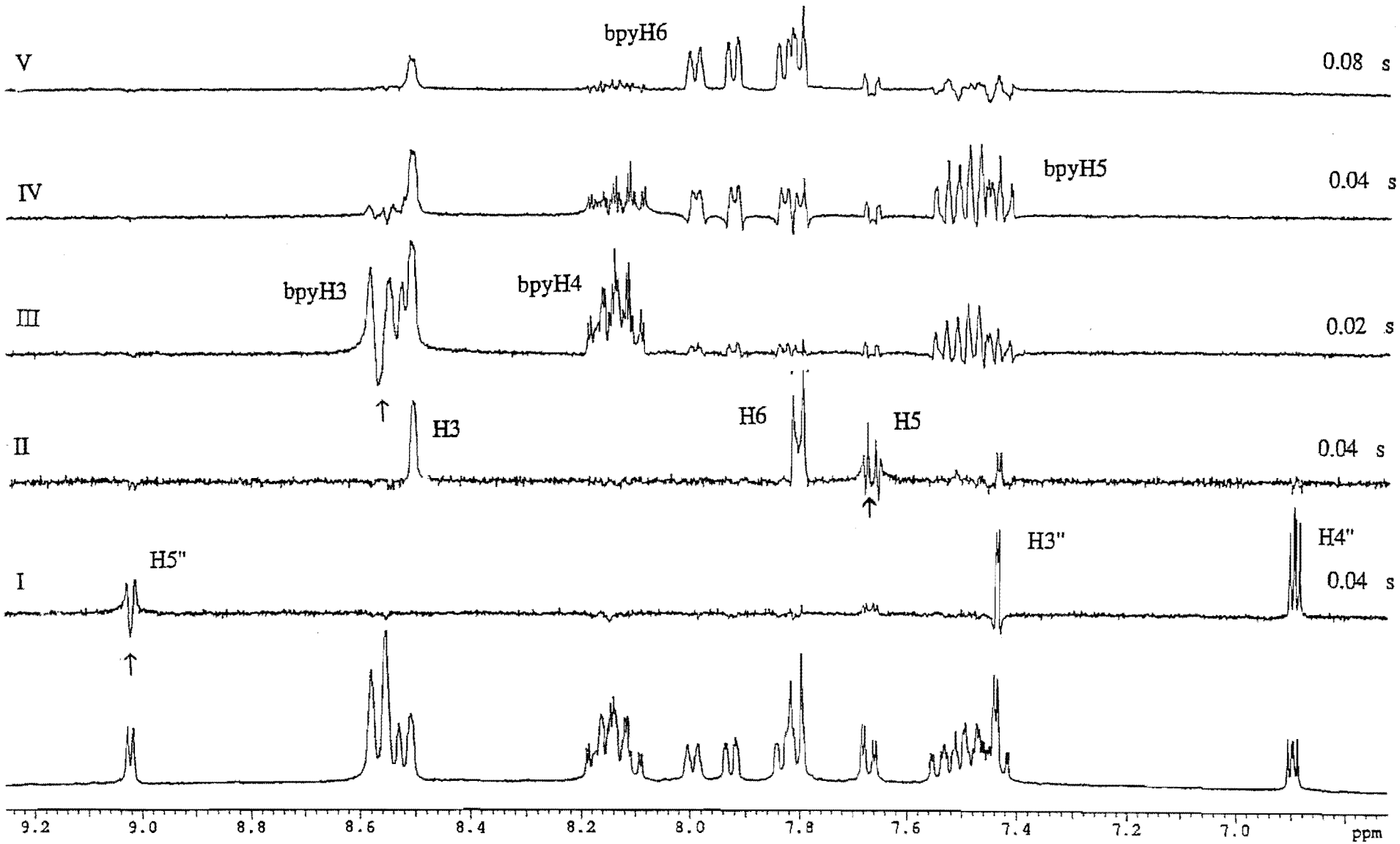

Figure 6.11 1D TOCSY Spectra of **159**

protons of **159-161**. These factors have already been described in more detail for the coordinated rings of **157** and **158**. The protons of **145** are generally slightly upfield in **160**, relative to their chemical shifts in **159**. This is consistent with the dmb ligands increasing the electron density on the ruthenium, which in turn increases the electron density of the bridging ligand by π-back-bonding.

Table 6.8 ^{1}H NMR Chemical Shifts[a] and Coordination Induced Shifts[b] of μ-**144** in **159**, **160** and **161**.

	H3	H5	H6	H3''	H4''	H5''
144	8.38	7.73	8.63	7.87	6.62	8.70
159	8.50	7.67	7.81	7.44	6.90	9.02
CIS[b]	+0.12	-0.06	-0.82	-0.43	+0.28	+0.32
160	8.39	7.66	7.81	7.42	6.89	8.91
CIS[b]	+0.01	-0.07	-0.82	-0.46	+0.27	+0.21
161	8.40	7.67	7.81	7.44	6.90	8.94
CIS[b]	+0.02	-0.06	-0.82	-0.43	+0.28	+0.24
	H3'	H5'	H6'	H3'''	H4'''	H5'''
161	8.39	7.66	7.81	7.41	6.89	8.93
CIS[b]	+0.01	-0.07	-0.82	-0.47	+0.27	+0.23

[a] For deuterated acetonitrile solutions. [b] CIS = $\delta_{complex}$-δ_{ligand}.

The UV/VIS absorption spectra of all the complexes show strong ligand centred absorptions at λ<400nm and MLCT absorption bands at λ>400nm. The MLCT bands for the mononuclear complexes are symmetrical and, with maxima at 434nm (**157**) and 438nm (**158**), are at higher energy than the MLCT of $Ru(bpy)_3^{2+}$ (451nm). The higher energy MLCT is consistent with ruthenium complexes of other pyrazole containing ligands such as $Ru(\mathbf{43})(bpy)_2^{2+}$ (442nm)[11] and the complex **87** described in chapter 2. A slight shift, of the MLCT, to lower energy is observed with the binuclear complexes (444-448nm), although this is not as pronounced as the shift of the MLCT (471nm) in **142**.[153] Coordination of the second $Ru(bpy)_2^{2+}$ unit lowers the π* orbitals of the bridging ligand and, hence, the red shift indicates that the lowest energy MLCT of **159-161** is dπ-π*(**144**). If the MLCT was dπ-π*(bpy) a blue shift would be expected, due to the additional electrostatic energy required to remove the optical electron from the first metal to the bpy ligand and thus further away from the second metal. The small size of the red shift may indicate the LUMO of the mononuclear and binuclear complexes are localised on different ligands.

Reduction of the free ligand **144** occurs at -1.80V, which confirms that the π* orbital of **144** is at lower energy relative to the π* orbital of bpy (-2.18V). Redox potentials for **157-161**

are summarised in Table 6.9, whilst the cyclic voltammograms of **157** and **159** are shown in Figure 6.12. The mononuclear complex **157** exhibits a reversible one electron oxidation (+1.24V) followed by four successive reversible one electron reductions (-1.40, -1.69, -1.84 and -2.17V). In line with the greater ease of reduction of **144**, relative to bpy, the first reduction can be deemed to be localised on the ligand **144**, with the second and third reductions localised on bpy. Hence, the complex is slightly easier to oxidise and slightly harder to reduce than $Ru(bpy)_3^{2+}$, with the $E_{ox\text{-}red}$ values (2.64 and 2.58V) consistent with the lowest energy MLCT's. The redox processes of **158** can be similarly assigned, with oxidation easier than in **157** due to metal d orbital stabilisation by the dmb ligands. The fourth reduction of **157** (-2.12) and **158** (-2.17V) may correspond to a second reduction of **144**, rather than a second bpy or dmb reduction. The ligand **144** is larger than bpy or dmb, in terms of the number of bonds. Hence, the coulombic repulsion, experienced by the second added electron, would be expected to be less for **144**, than for bpy or dmb.

Table 6.9 Absorption Maxima[a] and Redox Potentials[b] for **157-161**.

	λ_{max}	E_{ox1}	E_{ox2}	E_{red1}	E_{red2}	E_{red3}	E_{red4}	E_{red5}	$E_{ox\text{-}red}$
$Ru(bpy)_3^{2+}$	451	+1.27		-1.31	-1.50	-1.77			2.58
157	434	+1.24		-1.40	-1.55	-1.77	-2.12		2.64
158	438	+1.13		-1.45	-1.69	-1.84	-2.17		2.58
142	471	+1.24[c] (85mV)		-1.10	-1.44	-1.57	-1.64		2.34
159	444	+1.23	+1.29	-1.09	-1.51[c]	-1.63	-1.86[c,d]		2.32
160	448	+1.12	+1.18	-1.11	-1.56	-1.71	-1.91	-1.96	2.23
161	446	+1.14	+1.27	-1.10	-1.73[e]				2.24

[a] In nanometres. [b]In Volts versus SCE. [c]Two electron. [d]Irreversible. [e] ≈five electron

In the cyclic voltammogram of **159** and **160**, the oxidation process appears as a two electron wave (ΔE_p=85mV) centred at 1.26 and 1.15V respectively. For the observed response, the simulations of Richardson and Taube[227] reveal two individual one electron transfers ($\Delta E_{1/2}$=56±3mV), indicating a weak metal-metal interaction for the complex analogous to that of **142**.[153] Analogous to **142**, the weakness of the interaction can be attributed to rotation about the 4,4' bond which disrupts π system overlap of the 2-(1-pyrazolyl)pyridine subunits. The extent to which π system overlap is disrupted, is undoubtedly less than in **131**, where the metal-metal interaction is negligible, due to rotation about two of the inter-ring bonds of the bridging ligand. In the crystal structures of **144** and **145**, the 4,4' bond is transoid, as it is in the equivalent bond of both crystalline modifications of **25**.[240] Assuming this conformation in the metal complexes, the inter-metal separation has been estimated to be 11.2 Å (using

CHEM3D-PLUS and the above crystallographic data). Furthermore, such calculations indicate that the metal-metal distance is relatively independent (< 0.1 Å variation) of this torsional angle. In contrast, the metal-metal distance of **131** was shown to vary significantly (12.8-13.6Å) with the conformation of the bridge.

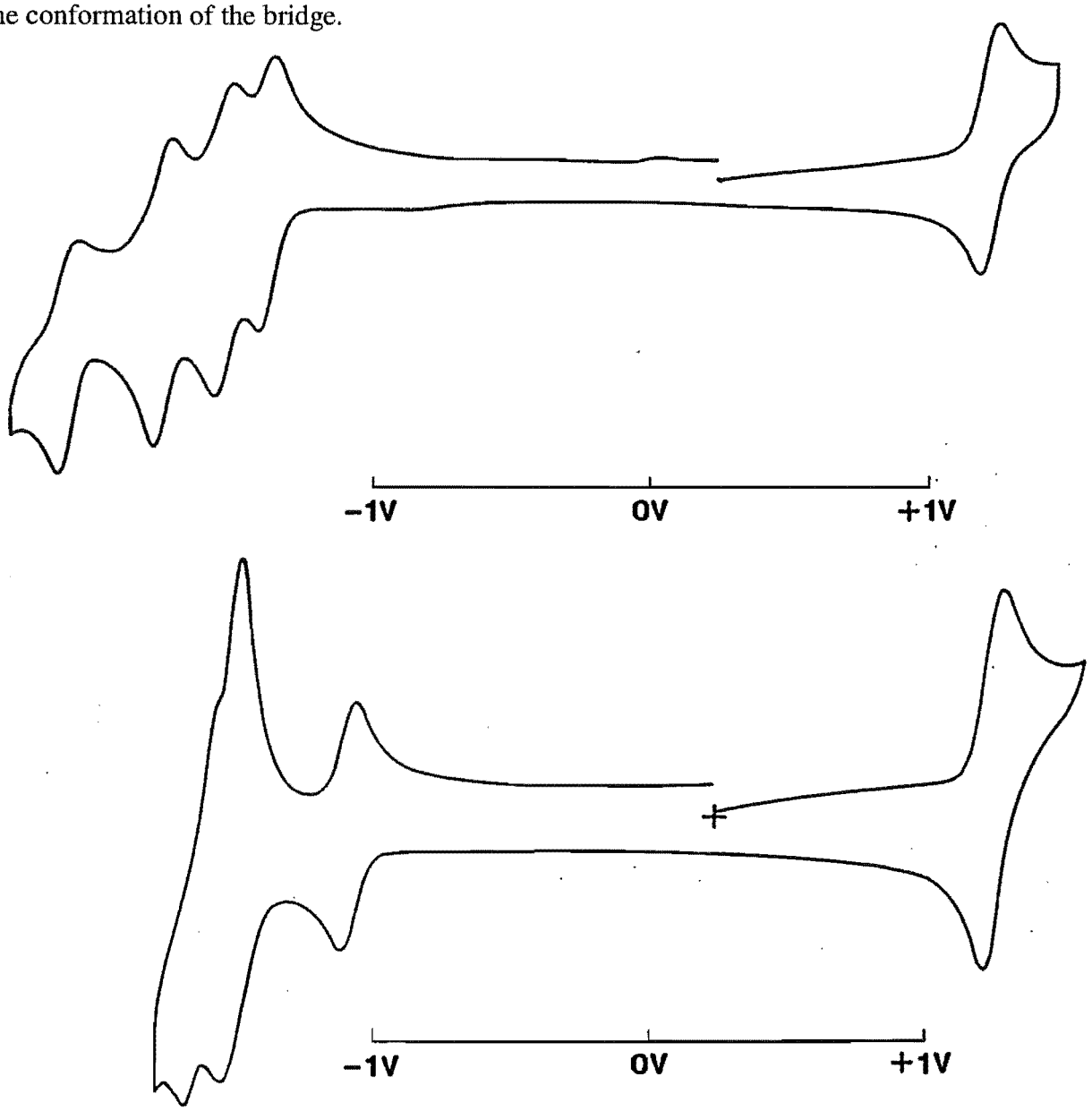

Figure 6.12 Cyclic Voltammograms of **157** (top) and **159** (bottom)

For the complex **161**, the splitting of the oxidation potentials is greater ($\Delta E_{1/2}$=130mV) than in **159** and **160**. The first oxidation correlates with the first oxidation of **160**, whilst the second oxidation correlates with the second oxidation of **159**. Hence, oxidation of the $Ru(dmb)_2^{2+}$ unit is easier than for the $Ru(bpy)_2^{2+}$ unit, resulting in an apparent increase in the metal-metal interaction relative to **159** and **160**. As was the case with **124** and **148**, the d orbitals of the $Ru(dmb)_2^{2+}$ unit are higher in energy than those of the $Ru(bpy)_2^{2+}$ unit, due to the electron donating methyl groups of the dmb ligands which push additional electron density onto the metal.

The first reduction of each of the binuclear complexes (-1.09 to -1.11V) occurs at a less negative potential than in the mononuclear complexes and may be attributed to reduction of the bridging ligand LUMO, which is stabilised, relative to the mononuclear complexes, by back-bonding to the second ruthenium. This also confirms the weak metal-metal interaction and correlates with the red shift in the MLCT. Further reductions of **159** occur as a reversible two electron reduction (-1.51V, ΔE_p=85mV), reversible one electron reduction (-1.63V) and an irreversible two electron reduction (-1.86V). The corresponding reductions of **160** occur as a succession of reversible one electron processes (-1.56, -1.71, -1.91,-1.96V). The difference between the first and second reductions for both these complexes is in agreement with the relationship of Cooper et. al.,[224] which correlates the difference in the first and second bridging ligand reductions with the number of bonds in the bridging ligand. Hence, the second reduction of **160** can be assigned to the bridging ligand, whilst successive reductions are dmb centred. Bpy is more easily reduced than dmb. Thus for **159**, the second reduction of the bridging ligand and the first bpy reduction occur as a two electron reduction (-1.51V, ΔE_p=85mV). The second reduction of **144** in **161** occurs as part of a multielectron wave centred on -1.73V (ΔE_p=260mV).

The syntheses of two heterobinuclear complexes were shown in Scheme 6.4. The complexes **162** and **163** were readily prepared by reacting the corresponding monoruthenium complex with one equivalent of $Pd(PhCN)_2Cl_2$. The ^1H NMR spectrum of **162** consists of 28 non-equivalent protons (Figure 6.13) and is summarised in Table 6.10. Compared to the spectrum of **157**, the proton signals for the bridging ligand are well spread, due to the different coordination environments of the two metals. Figure 6.14 demonstrates the unambiguous assignment of all four spin systems of the bridging ligand, in the ^1H NMR spectrum, by four separate 1D TOCSY irradiations of H6' (trace I), H5 (trace II), H5'' (trace III) and H5''' (trace IV), thus locating the spin systems for each of the four rings. A 2D COSY spectrum, similar to that shown in Figure 6.9, was used to assign the bpy ring spin systems. The ^1H NMR spectrum of **163**, the dmb analogue of **162**, was assigned in a similar manner to the spectrum of **162** using 1D TOCSY and 2D COSY spectra.

The effect of the coordination environment of the $Ru(bpy)_2^{2+}$ has already been described in detail for the coordinated ring protons of **157** and **158**. Similar coordination induced shifts for H3-H6 and H3"-H5" are observed for **162**. The rings coordinated to palladium exhibit different coordination induced shifts. The CIS values of H3'-H6' and H3'"-H5'" generally reflect the σ-donation of electron density from ligand to metal, although the protons H6' (+0.51ppm) and H3'"

(+0.32ppm) are further deshielded by adjacent chlorine atoms, whilst chelation induced conformational changes contribute to CIS values of H3' (-0.09ppm) and H5" (+0.05ppm).

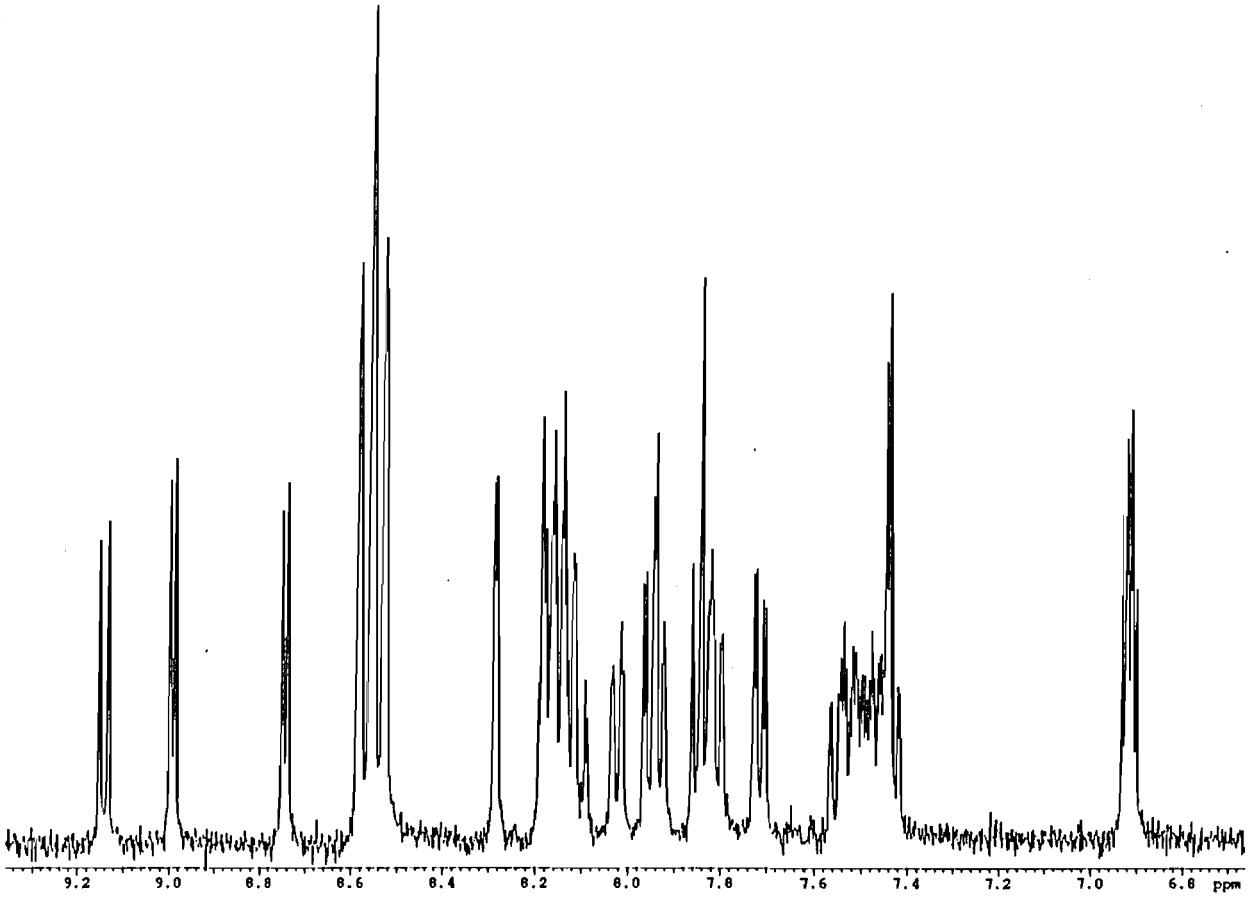

Figure 6.13 ^{1}H NMR Spectrum of **162**.

Table 6.10 ^{1}H NMR Chemical Shifts[a] of **144** and **162**. Coordination Induced Shifts[b].of **162**

	Ligand **144**					Bpy Ligands				
	H3	H5	H6	H3"	H4"	H5"	H3	H4	H5	H6
144	8.38	7.73	8.63	7.87	6.62	8.70	-	-	-	-
162	8.53	7.72	7.85	7.45	6.91	9.00	8.54	8.12	7.45	7.81
CIS[b]	+0.15	-0.01	-0.78	-0.42	+0.29	+0.30	8.57	8.14	7.48	7.83
	H3'	H5'	H6'	H3"'	H4"'	H5"'	8.57	8.14	7.54	7.93
162	8.29	7.96	9.14	8.19	6.92	8.75	8.57	8.16	7.52	8.02
CIS[b]	-0.09	+0.23	+0.51	+0.32	+0.30	+0.05	-	-	-	

[a] For deuterated acetonitrile solutions. [b] CIS = $\delta_{complex}$-δ_{ligand}.

UV/VIS absorption spectra for the two heterobinuclear complexes show strong ligand centred transitions (λ<400nm) and an MLCT transition (λ>400nm). The MLCT absorptions are symmetrical (**162**=442nm, **163**=448nm) and exhibit a very slight red shift, relative to the corresponding mononuclear complex, thus implying a weak metal-metal interaction.

Four complexes (**164-167**) were prepared from the ligand **145** using procedures analogous to those previously described for ruthenium complexes in this work (Scheme 6.5). All complexes were characterised by mass spectrometry and ^{1}H NMR spectroscopy.

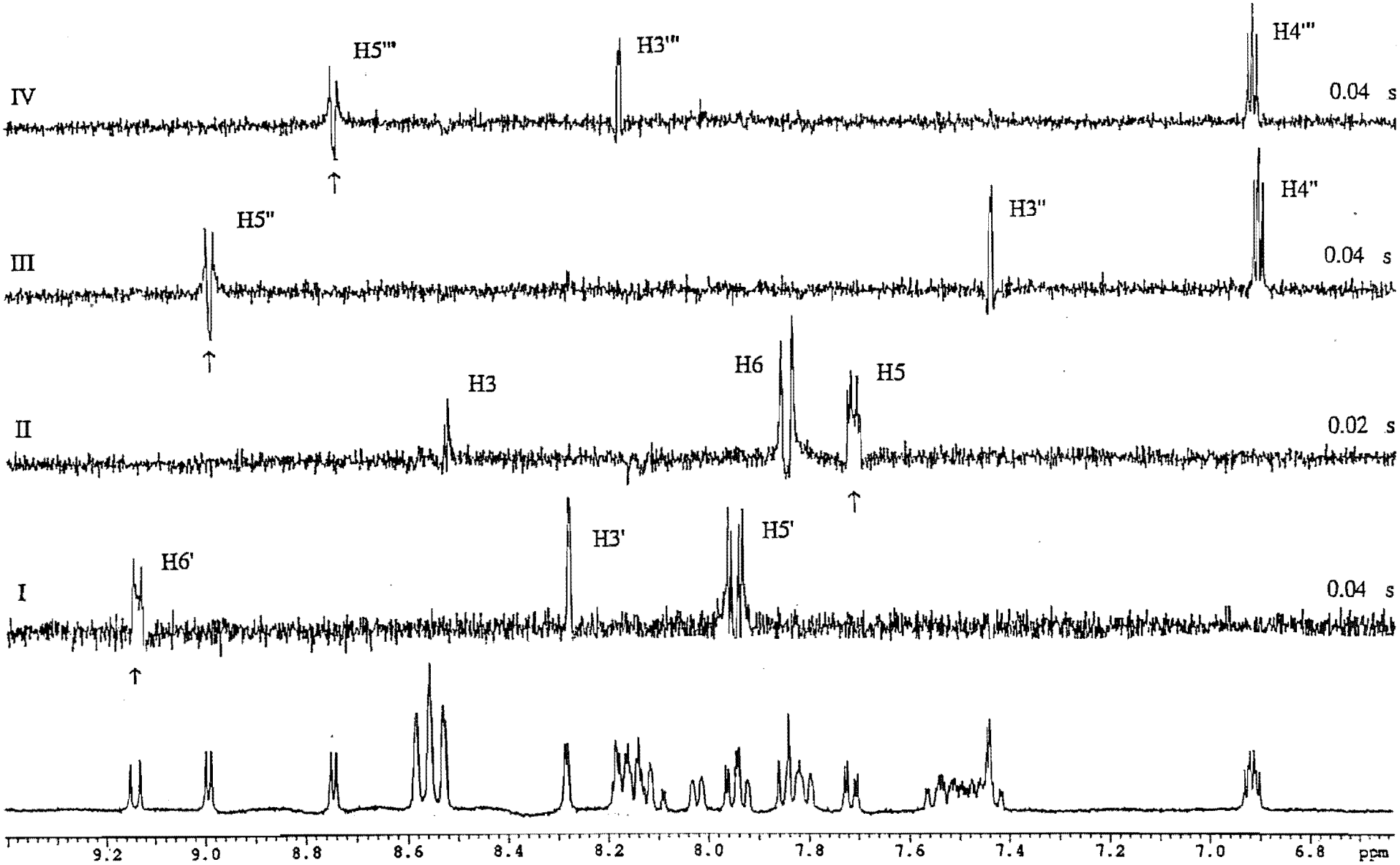

Figure 6.14 1D TOCSY Spectra of **162**

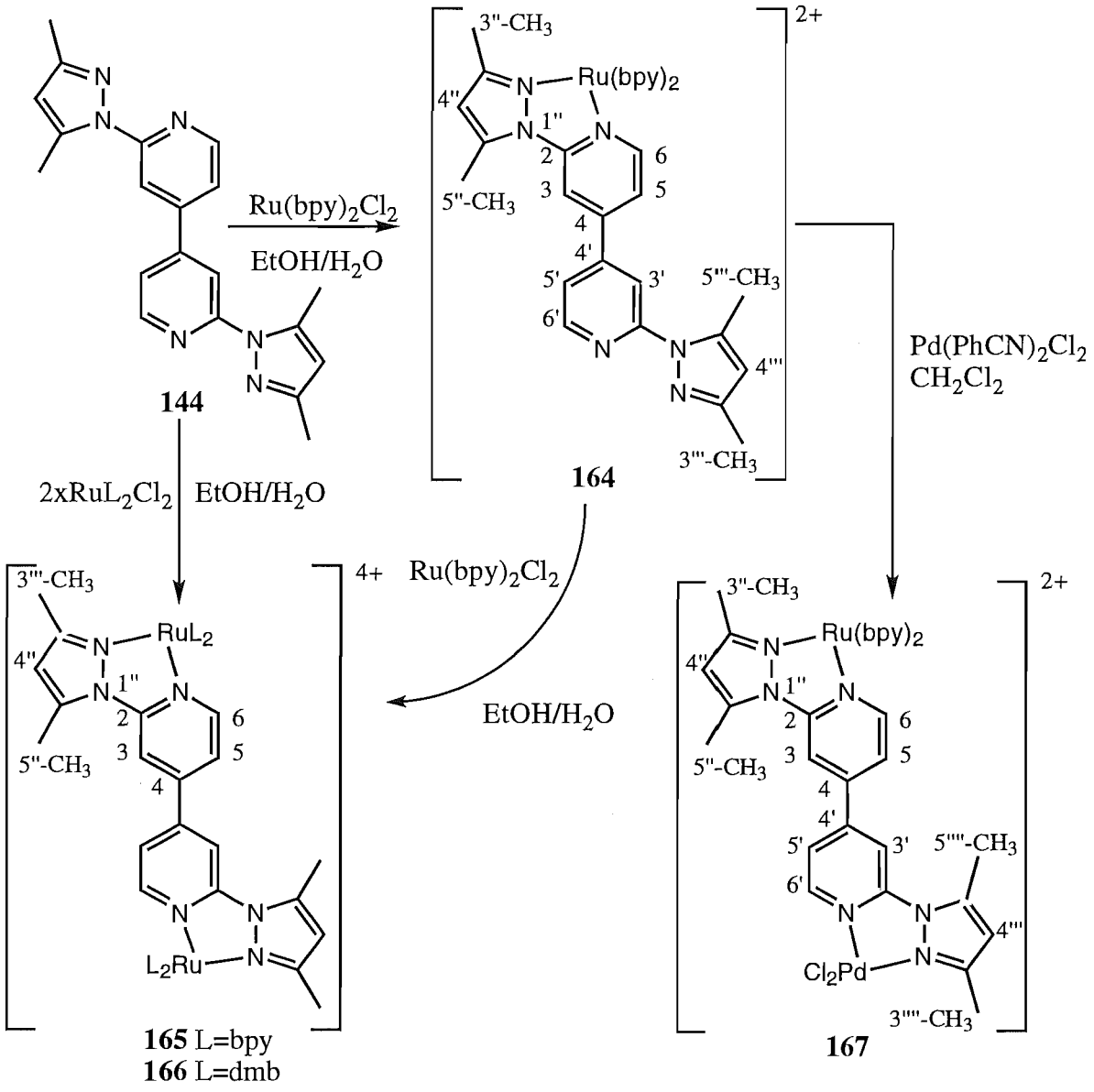

Scheme 6.5.

The ^{1}H NMR spectrum of **164** is similar to that of **157**, except that the pyrazole H3 and H5 protons are absent from the aromatic region. The spectrum comprises 36 non-equivalent signals (24 in the aromatic region). The methyl groups of **145** were readily distinguished on the basis of the broadening of the 5"-CH_3 (2.98ppm) and 5'''-CH_3 (2.71ppm) singlets, relative to the 3"-CH_3 (1.58ppm) and 3'''-CH_3 (2.29ppm) singlets. Furthermore, whilst 5"-CH_3 is deshielded (+0.27ppm) due to both the σ-donation of electron density from the π-excessive pyrazole to the metal, and the change in conformation about the C2-N1" bond, the 3"-CH_3 lies over a pyridine ring and is shielded (-0.74ppm). This bond is transoid, as shown in the crystal structure of the free ligand, but cisoid in **164**, as a consequence of metal chelation. The aromatic region of the spectrum was assigned using a 2D COSY spectrum. The most downfield doublet at 8.64ppm was assigned as H6' and was found to correlate with the doublet of doublets at 7.60ppm, thus

locating H5'. The coupling of the disubstituted pyridine ring differs from that of the bpy pyridine rings and allows the doublet H6 (7.71ppm) and doublet of doublets H5 (7.54ppm) to be distinguished from overlapping bpy protons. The COSY spectrum confirmed this assignment by an observed correlation between H5 and H6. Long-range correlation from H5' located H3' (8.20pp), which is overlapped by bpyH4 signals. Similarly, H3 (8.54ppm) was correlated to H5, whilst the spin systems of the bpy rings were also assigned by the COSY spectrum.

The chemical shifts and CIS values are summarised in Table 6.11. Coordination induced shifts for the methyl groups have already been explained. In general, the remaining protons exhibit shifts consistent with ligand to metal σ-donation and metal to ligand π-back-bonding of electron density, although ring current anisotropy accounts for the shielding of H6 and, to a lesser extent H5, whilst chelation induced conformational changes contribute to H5'' and H3.

Table 6.11 ^{1}H NMR Chemical Shifts[a] of **145** and **164**. Coordination Induced Shifts[b].of **164**

	Ligand **145**						Bpy Ligands			
	H3	H5	H6	3''-CH_3	H4''	5''-CH_3	H3	H4	H5	H6
145	8.20	7.63	8.59	2.32	6.15	2.71	-	-	-	-
164	8.54	7.54	7.71	1.58	6.46	2.98	8.56	8.06	7.44	7.70
CIS[b]	+0.34	-0.09	-0.88	-0.74	+0.31	+0.27	8.58	8.09	7.41	7.83
	H3'	H5'	H6'	H3'''	H4'''	H5'''	8.58	8.20	7.54	7.96
164	8.20	7.60	8.64	2.29	6.16	2.71	8.58	8.15	7.57	8.06
CIS[b]	+0.00	-0.03	+0.05	-0.03	+0.01	+0.00	-	-	-	

[a] For deuterated acetonitrile solutions. [b] CIS = $\delta_{complex}$-δ_{ligand}.

The ^{1}H NMR spectrum of the binuclear complex **165** is less complicated than that of **164**, since the ligand is symmetrical about the 4,4'-bond, when in the bridging mode. The bridging ligand protons were assigned by comparison with the spectrum of **164**. These assignments were confirmed by a 2D COSY spectrum, which was also used to locate the spin systems of the bpy rings. Similarly, the ^{1}H NMR spectrum of **166** was completely assigned by comparison with the spectrum of **164** and with the assistance of a 2D COSY spectrum. The ^{1}H NMR spectra of **165** and **166** are summarised in Table 6.12.

The diastereoisomers were not resolved in the spectra of the binuclear complexes. However, the multiplicities of the dmbH6 at 7.85ppm and the bpyH6 at 8.05ppm are not consistent with the normal doublet of the peripheral ligand. In fact the protons appear as two partially overlapping doublets. A similar effect was observed in the ^{1}H NMR spectrum of **131** and may imply some resolution of the two diastereoisomers. The effects which account for the

CIS values of the coordinated rings in **164** also account for the CIS values of the bridging ligand protons of **165** and **166**.

Table 6.12 ^{1}H NMR Chemical Shifts[a] of **145**, **165** and **166**. Coordination Induced Shifts[b].of **165** and **166**.

	Ligand **145**						Ligand=L			
	H3	H5	H6	3"-CH_3	H4"	5"-CH_3	H3	H4	H5	H6
145	8.20	7.63	8.59	2.32	6.15	2.71	-	-	-	-
165	8.15	7.49	7.72	1.58	6.47	2.96	8.56	8.12	7.43	7.69
CIS[b]	-0.05	-0.14	-0.87	-0.74	+0.32	+0.25	8.56	8.08	7.41	7.82
							8.58	8.17	7.52	7.93
							8.58	8.16	7.54	8.06
166	8.16	7.49	7.71	1.59	6.46	2.96	8.41	2.55[c]	7.27	7.49
CIS[b]	-0.04	-0.14	-0.88	-0.73	+0.31	+0.25	8.41	2.57[c]	7.24	7.61
							8.41	2.61[c]	7.33	7.73
							8.41	2.63[c]	7.38	7.85

[a] For deuterated acetonitrile solutions. [b] CIS = $\delta_{complex}$-δ_{ligand}. [c] Methyl group not assigned.

UV/VIS absorption spectroscopy and cyclic voltammetry can be used to probe the electronic properties of the complexes **164-166** (Table 6.13). In general, the UV/VIS spectra show LC (λ<400nm) and MLCT (λ>400nm) absorption bands. For the mononuclear complex **164** the MLCT occurs at 430nm and is symmetrical. Coordinating a second $Ru(bpy)_2^{2+}$ unit results in a slight red shift of the MLCT (448nm), by lowering the bridging ligand LUMO, thus indicating a weak metal-metal interaction.

The effect of the methyl groups of the pyrazoles can be seen in the oxidation potentials of **164-166** and is analogous to the effect of the methyl groups of dmb ligands, as previously described. For example, in **164**, the energy of the d orbital is raised relative to **157**, as shown by the greater ease of oxidation (by 0.06V) of complex. Similarly, **165** and **166** are easier to oxidise than **159** and **160** respectively. It has been previously noted for structurally related complexes that methyl groups decrease oxidation potentials by approximately 0.025V per methyl group.[180]

The mononuclear complex also exhibits four reversible one electron reductions, the first of which was assigned to reduction of **145**, whilst the second and third reductions are bpy centred. This assignment was based on the free ligand ligand reduction (-1.87V), which implies that **145** has low lying π^* orbitals relative to bpy (-2.18V). Analogous to **157** and **158**, the fourth reduction was assigned to **145**.

The binuclear complex **165** exhibits a reversible two electron oxidation centred at +1.18V (ΔE_p=85mV). For **166**, the process is similar, but is centred at +1.11V (ΔE_p=85mV), as

a consequence of the peripheral dmb ligands. Thus, as was shown for the binuclear complexes **147**, **159**, and **160** already described and which incorporate a 4,4'-bipyridine bridge, oxidation of this complex involves two individual one electron transfers with a value for $\Delta E_{1/2}$ of 56±3mV. Hence, a weak metal-metal interaction occurs via the π system of the bridge, with rotation about the 4,4'-bond disrupting overlap of the π systems of the subunits. Values shown for E_{ox1} and E_{ox2} were also calculated from the working curves of Richardson and Taube.[227] Molecular modelling studies (Chem 3D Plus) gave an estimate of the metal-metal distance as 11.1Å. This value was found to vary less than 0.1Å between the cisoid and transoid conformations of the bridge.

Table 6.13 Absorption Maxima[a] and Redox Potentials[b] for **164-166**.

	λ_{max}	E_{ox1}	E_{ox2}	E_{red1}	E_{red2}	E_{red3}	E_{red4}	E_{red5}	$\Delta E_{ox\text{-}red}$
$Ru(bpy)_3^{2+}$	451	+1.27		-1.31	-1.50	-1.77			2.58
157	434	+1.24		-1.40	-1.55	-1.77	-2.12		2.64
164	430	+1.18		-1.43	-1.57	-1.80	-2.17		2.61
159	444	+1.23	+1.29	-1.09	-1.52[c]	-1.63	-1.86[d]		2.32
160	448	+1.12	+1.18	-1.11	-1.56[c]	-1.71[c]	-1.91		2.23
165	448	+1.15	+1.21	-1.14	-1.52[c]	-1.71	-1.82[c]		2.29
166	452	+1.08	+1.14	-1.15	-1.54[c]	-1.68	-1.78	-1.93	2.22

[a] In nanometres. [b]In Volts versus SCE. [c]Two electron. [d]Irreversible.

Further evidence of the weak metal-metal interaction, can be seen in the shift to less negative potentials of the first reduction, which corresponds to reduction of the bridging ligand LUMO. Back-bonding to the second $Ru(L)_2^{2+}$ unit lowers the energy of the bridging ligand LUMO resulting in easier reduction of the complex and, as shown above, a red shift in the MLCT. Since the difference between the first and second reduction potentials correlates with the relationship of Cooper et. al.,[224] the two electron process, at -1.52V (ΔE_p=100mV) for **165** and -1.54V (ΔE_p=90mV) for **166**, probably includes the second reduction of the bridging ligand. Further reductions are most likely centred on the peripheral ligands.

Complex **167** was synthesised from **164** as shown in Scheme 6.5. The ^1H NMR spectrum of **167** was tentatively assigned, by comparison with the spectra of **162** and **164** and the CIS values for the bridging ligand protons were found to be similar to those of **162**.

Chapter 7

Conclusion

Conclusion

In this work the use of new and known heterocycles as bidentate ligands has been described, with particular emphasis on binucleating ligands. The majority of the complexes synthesised have been of ruthenium(II), although for some of the ligands molybdenum(0), palladium(II), copper(I), copper(II) and nickel(II) complexes have been synthesised.

The metal to ligand interactions in the complexes are governed by the specific metal and ligand involved. The ligands described here have quite different π-donor/acceptor properties compared with bpy. Hence the properties of their ruthenium complexes are significantly modified relative to those of $Ru(bpy)_3^{2+}$. These properties have been examined by UV/VIS absorption spectroscopy and cyclic voltammetry. Furthermore, the substituted bipyrimidines and 2,4-bis-(1-pyrazolyl)pyrimidine have demonstrated that ligand structure can limit both the selection of coordination sites available for metal chelation, and the coordination geometry of the metal.

^1H NMR spectroscopy has been shown to be a useful tool in the characterisation of ruthenium complexes, and as a means to probe the specific ligand-metal interactions and deduce the structure of such complexes. Proton Coordination Induced Shifts (CIS) due to coordination induced conformational changes, inter ligand through-space ring-current anisotropy and ligand to metal σ donation and metal to ligand π back-donation have been described for most of the complexes. Calculation of such values requires the unambiguous assignment of the ^1H NMR spectrum. For many of the complexes, the spectrum has been simplified by replacing the bpy ligands with dmb ligands, which removes any overlap of signals and coupling due to the bpyH4 proton. In some cases this has allowed complete assignment of the ligand protons, making this technique a much cheaper alternative to the use of d_8-bpy. More often than not, 1D TOCSY or 2D COSY spectra were required to assign, or confirm the assignment of, the ligands in the complexes. In this respect, the 1D TOCSY is particularly useful since the assignment of complete spin systems can be achieved if only one proton of that spin system is isolated in the spectrum. This was shown most clearly in the 1D TOCSY spectrum of **121** in which irradiating the two isolated protons of the bridging ligand **109** located the remaining protons amongst the mass of overlapping bpy signals.

By using a range of different bridging ligands this study has clearly shown the dependence of metal-metal interactions on the inter-metal separation in binuclear complexes.

For the binuclear complexes of the series of ligands **40**, **109**, **132**, **144**, **145**, **25** and **110**, the inter-metal separation increases in the order shown. The interaction in each case has been probed by UV/VIS absorption spectroscopy and cyclic voltammetry. In the absence of electronic coupling via the bridging ligand, the metal centres undergo oxidation at nearly the same potential, as was the case for the biruthenium complex, **131**, of the ligand **110**, in which the flexible bridge holds the two metals at a distance of 12.8-13.6Å. Any metal-metal interaction leads to asymmetry and the existence of discrete oxidation waves for each metal centre, with the splitting of the waves ($\Delta E_{1/2}$) and hence, the degree of metal-metal interaction, decreasing with increasing separation of the metals. Figure 7.1 shows the expansion of the oxidation waves for three of the biruthenium complexes included in this study. The inter-metal separation in the complexes increases from top to bottom in the figure. A similar trend has been observed in the magnitude of the red shift of the lowest energy MLCT ($d\pi$-π^*(BL)) for binuclear complexes.

Metal-metal interactions are not exclusively controlled by the distance between the interacting metals but also depend on a number of other factors which are significant to the complexes described in this study. For example, the weak interaction in the binuclear complexes of **25**, **110**, **144** and **145** is due in part to the disruption of bridging ligand conjugation by rotation about inter-ring bonds. Furthermore, the methyl groups of **40** increase the electron density of the bridge in the complex **64** and account for the greater stabilisation of the mixed valence state relative to the complex **38**, for which the inter-metal separation (5.8Å) is the same.

Mechanisms for metal-metal interactions, in the form of either an Electron-type Superexchange or a Hole-type Superexchange process, have been discussed in recent publications.[225,246,247] Which mechanism occurs depends on the relative energies of ligand LUMO, HOMO and metal d orbitals (Figure 7.2). Electron-type Superexchange, in which mixing between the ligand π^*-LUMO and the metal d orbitals is the major contribution to the metal-metal interaction, occurs when the bridging ligand has low-lying π^* orbitals. Where the low-lying π^* orbitals of the bridging ligand are replaced by electron-rich high-lying π^* orbitals, the mechanism occurs by Hole-type Superexchange, which is attributable to an electronic interaction of the ligand π-HOMO and metal d orbitals. Furthermore, within each mechanism the degree of metal-metal interaction depends on the relative energies of the mixing ligand and metal orbitals. Thus the metal-metal interaction in **121**, which occurs via Electron-type Superexchange, is smaller (160mV, 6.2Å) than in $(bpy)_2Ru(\mathbf{15})Ru(bpy)_2^{4+}$ (170mV, 6.7Å), due to the higher energy of the π^* orbitals of **109** relative to **15**.

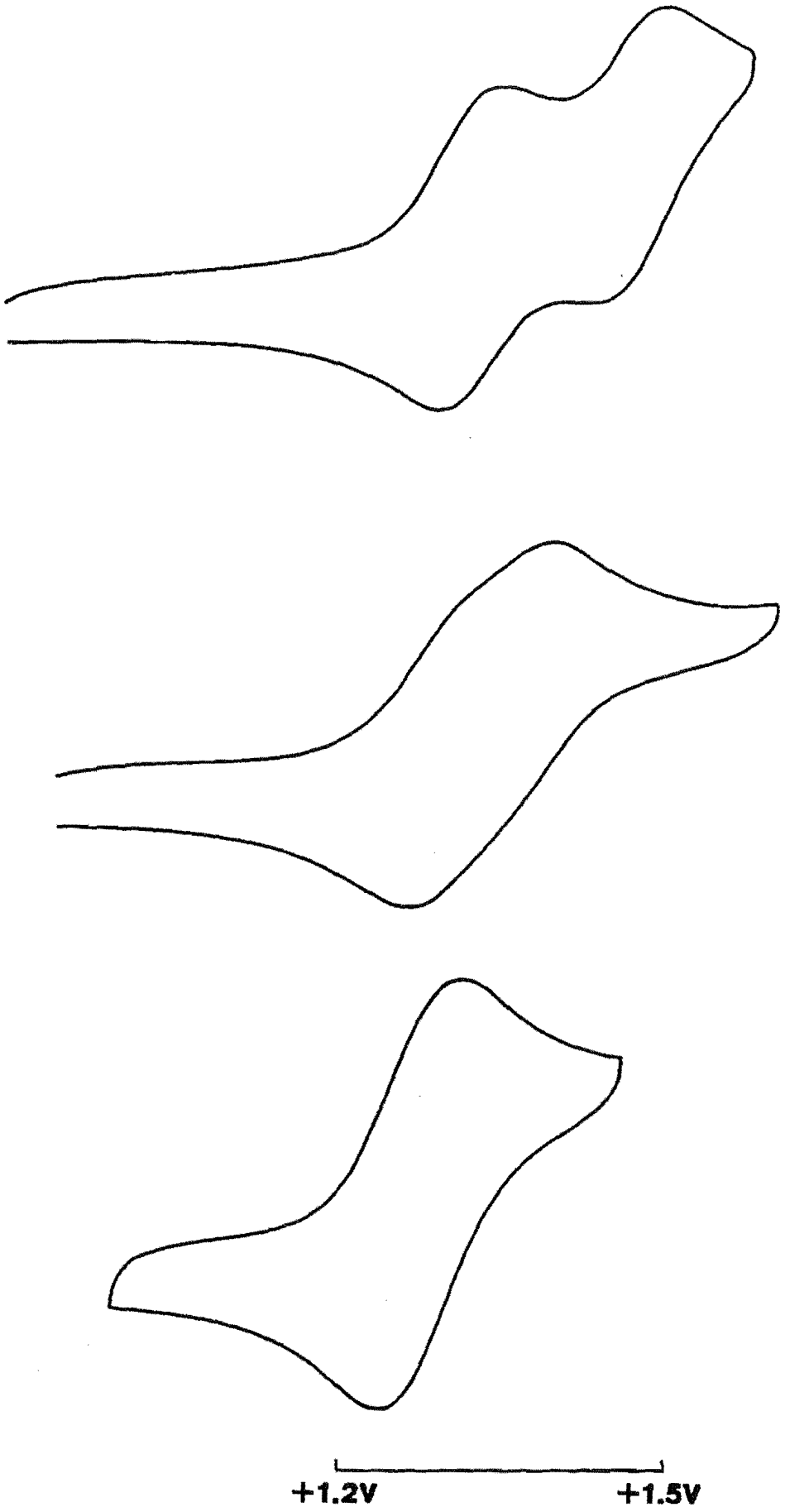

Figure 7.1 Oxidation Waves for **121** (top), **139** (middle) and **159** (bottom).

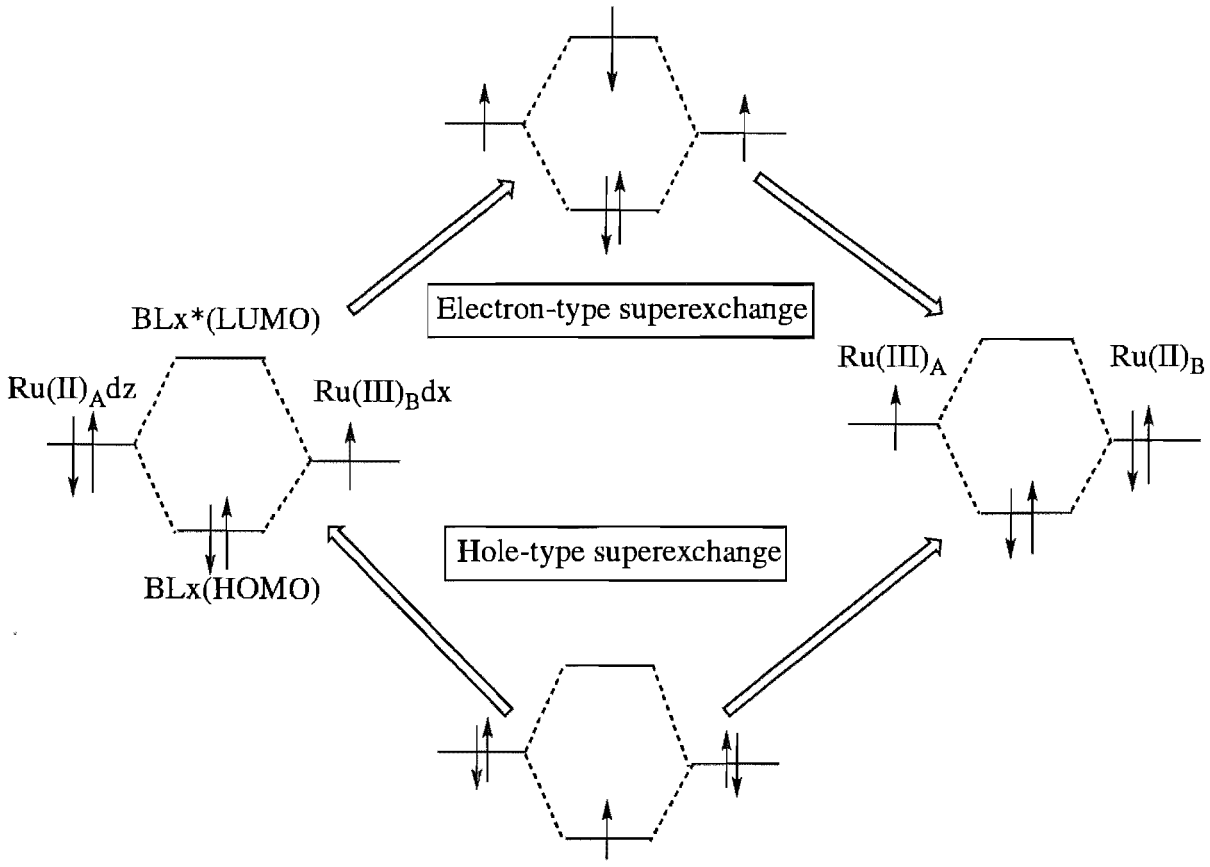

Figure 7.2

The type of spectator ligand that is used in binuclear complexes may also affect the metal-metal interaction. The unsymmetrical complexes $(bpy)_2Ru(BL)Ru(dmb)_2^{4+}$ (where BL=**25**, **109** and **144**) show a larger value for $\Delta E_{1/2}$ than the corresponding symmetrical complexes, since the $Ru(dmb)_2^{2+}$ unit is more readily oxidised than the $Ru(bpy)_2^{2+}$. This has highlighted the role that spectator ligands have to play in such systems as the degree of interaction can also be controlled by the appropriate choice of spectator ligand. A recent comprehensive review[225] has proposed that the strong modification of metal-metal interactions, by variation of the spectator ligands, may have important consequences for controlling such interactions in multinuclear compounds and for the design of systems featuring switchable electron and energy transfer processes.

In summary the degree of metal-metal interaction in bridged binuclear complexes depends on the distance between the metals, the ability of the ligand to delocalise the electronic charge, the relative energy of ligand HOMO/LUMO and metal d orbitals, the specific mechanism involved and identity of the spectator ligands. The present work has demonstrated that it is possible to modify or tune the metal-metal interactions in binuclear complexes, by the appropriate choice of bridging and spectator ligands and hence, in much the same way that the

properties of $Ru(bpy)_3^{2+}$ have been tuned, in recent years, by replacement of one or more of the bpy ligands by a different heterocyclic ligand.

Metal-metal interactions govern the rate of electron and energy transfer between the metal units and the electrochemical properties of the binuclear complexes. The complexes described here are potential building blocks for photochemical and electrochemical devices. These supramolecular assemblies are one of the greatest challenges facing modern chemistry[20] and control of metal-metal interactions is crucial to the design of such systems. The choice of bridging ligands, including those described here, is now extensive enough to allow the synthesis of polynuclear complexes with desired 'tailor-made' properties.

Chapter 8

Experimental

Experimental

8.1. General Experimental

NMR spectra were recorded on a Varian 300 Unity spectrometer with a 5mm or 3mm probe and operating at 300MHz and 75MHz for ^{1}H and ^{13}C, respectively. Spectra recorded in $CDCl_3$ were referenced relative to internal Me_4Si and those recorded in d_6-DMSO, $(CD_3)_2CO$ and CD_3CN were referenced against the solvent signals. When required, nOe, 1D TOCSY and two dimensional experiments (COSY, HMQC, HMBC) were performed using standard pulse sequences and parameters available with the Unity 300 system. UV/VIS absorption spectra were recorded using a Perkin Elmer Lambda 2 spectrometer for acetonitrile or acetone solutions.

Molecular modelling was performed on a Macintosh computer using the modelling package CHEM 3D Plus^{TM}. Ru-N bond distances were assigned an optimum value of 2.06Å.

Cyclic voltammetric measurements were made using either a Par Model 174A polarographic analyser coupled to a Par Model 175 universal programmer or a Par Model 173 potentiostat coupled to a home-built waveform generator. Measurements were made of solutions containing *ca* 1 mM complex in acetonitrile with 0.1 M tetrabutylammonium hexafluorophosphate as the supporting electrolyte, using a scan rate of 100 mV s^{-1} (unless otherwise stated) and a glassy carbon disk working electrode (area = 0.07 cm^2). Ferrocene was used as an internal standard and potentials are given versus the saturated calomel electrode ($E^{o'}(Fc^{+}/Fc)$ = 0.31 V vs SCE).

Melting points were determined using an Electrothermal melting point apparatus and are uncorrected. Mass spectra were recorded using a Kratos MS80RFA spectrometer with a Mac 3 data system. Electron Impact spectra were obtained at 70eV with a source temperature of 150°C. Fast Atom Bombardment (FAB) spectra were acquired in a nitrobenzyl alcohol matrix using an Iontech ZN11FW FAB gun operated at 8KV and 2mV. Elemental analyses were performed by the Chemistry Department, University of Otago, Dunedin.

Radial chromatography was performed on a Chromatotron (Harrison and Harrison) using Merck type 60 $P.F._{254}$ silica gel. Column chromatography was performed with silica gel (grade 923 100-200mesh), alumina (Grade H 100-200mesh , neutral 100-240 mesh, acidic 150mesh) or sephadex-SP C-25 ion exchange resin (40-120μ) Solvents were purified according to standard literature procedures.[248,249] Unless otherwise stated reagents were obtained from commercial sources. $Ru(bpy)_2Cl_2$,[250] $Ru(dmb)_2Cl_2$,[251] $Ru(DMSO)_4Cl_2$,[252] $Pd(PhCN)_2Cl_2$,[253] $Ni(PPh_3)_2Cl_2$[202] and $Mo(\eta^4\text{-}C_7H_8)(CO)_4$[191] were prepared by literature procedures. Formyl camphor[254] was prepared by Andrew Watson in this department.

8.2. Syntheses of Ligands.

4,4'-Dimethyl-2,2'-bipyrimidine (40).

Step 1.

2-Chloro-4-methylpyrimidine (**56**).

The method of Bennett *et al.*[188] for the diazotisation of **68** (see later) was applied to 2-amino-4-methylpyrimidine (**54**). Accordingly, **54** (5g, 46mMol) was added to concentrated hydrochloric acid (30ml) cooled below 0°C. Whilst maintaining the temperature at -10°C an aqueous solution (15ml) of sodium nitrite (4g, 58mMol) was added dropwise and the resulting mixture left to stir at -10°C for 3 hours. The mixture was neutralised with NaOH, allowed to warm to room temperature and extracted with chloroform (3x30ml). The chloroform extracts were combined, dried over magnesium sulphate and the chloroform removed *in vacuo*. The resultant yellow solid was dissolved in chloroform (1-2ml) and absorbed onto a silica gel chromatography plate. The chloroform fraction was evaporated to give **56** as a clear oil which solidified on standing. Yield 2.45g (41%) Mp 48-50°C. Lit. 48-50°C.[255] ^{1}H NMR ($CDCl_3$) δ: 2.55 (3H), 4-CH_3; 7.14, H5; 8.48, H6. ^{13}C NMR ($CDCl_3$) δ: 24.0, 4-CH3; 119.4, C5; 158.9, C6; 161.1, C2; 170.8, C4. The methanol/chloroform (1:10) fraction gave 2-hydroxy-4-methylpyrimidine (**55**) as a yellow solid. Yield 1.0g (20%). This solid (9mMol) was added slowly to $POCl_3$ cooled in ice. The resultant mixture was refluxed for 2 hours, cooled and the solvent removed *in vacuo*. The residue was carefully treated with ice, made alkaline with aqueous ammonia and extracted with chloroform. The chloroform fraction was purified by chromatography as described above to give additional **56**. Yield 0.8g (69%).

Step 2.

4,4'-Dimethyl-2,2'-bipyrimidine (**40**).

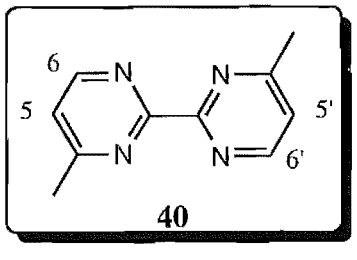

40

The complex $Ni^0(PPh_3)_2$ was generated *in situ* using the method of Nasielski *et al.*[189] A mixture of nickel chloride (0.92g, 3.9mMol), triphenylphosphine (4.03g, 15.6mMol) and zinc dust (0.36g, 5.55mMol), in dry dimethylformamide (20ml), was stirred at 50°C under an argon atmosphere. After 1 hour, a solution of **56** (0.5g, 3.9mMol) in dimethylformamide (5ml) was added under an argon atmosphere and the mixture left to stir at 50°C for a further 12 hours. The resultant brown mixture was poured into aqueous ammonia (80ml, 2M), filtered to remove the

precipitate of triphenylphosphine oxide, and the filtrate extracted with chloroform (4x60ml). The chloroform extracts were combined, dried over anhydrous potassium carbonate and concentrated (1-2ml), *in vacuo*. The solution was absorbed onto a silica gel radial chromatography plate and eluted with ethyl acetate/petroleum ether (3:1) to remove excess triphenylphosphine. Compound **40** was eluted with chloroform and the solvent removed *in vacuo* to give a white solid. Yield 163mg (45%). Mp 98-99°C. Calcd for $C_{10}H_{10}N_4$ C: 64.45, H: 5.41, N: 30.09. Found C: 63.69, H: 5.42, N: 30.09. Mass spectrum: $M^{+\cdot}$ calcd for $C_{10}H_{10}N_4$: 186.0905. Found: 186.0904. ^{1}H NMR ($CDCl_3$) δ: 2.74 (6H), 4-CH_3; 7.30 (2H), H5; 8.87 (2H), H6. ^{1}H NMR (CD_3CN) δ: 2.64 (6H), 4-CH_3; 7.42 (2H), H5; 8.83 (2H), H6. ^{1}H NMR (DMSO-d_6) δ: 2.66 (6H), 4-CH_3; 7.61 (2H), H5; 8.91 (2H), H6. ^{13}C NMR ($CDCl_3$) δ: 24.1 (2C), 4-CH_3; 121.0 (2C), C5; 157.5 (2C), C6; 162.4 (2C), C2; 168.5 (2C), C4. ^{13}C NMR (CD_3CN) δ: 23.7 (2C), 4-CH_3; 121.0 (2C), C5; 157.6 (2C), C6; 163.5 (2C), C2; 168.3 (2C), C4.

4,4'-Bis-t-butyl-2,2'-bipyrimidine (41).

Step 1.

Bis-(4,4-dimethylpentane-1,3-dionato)copper(II) (**67**).

This compound was prepared from pinacolone (**66**) by the method of Brown *et al.*[200]

Step 2.

2-Amino-4-t-butylpyrimidine (**68**).

This compound was prepared from **67** by the method of Clark *et al.*[201]

Step 3.

2-Chloro-4-t-butylpyrimidine (**70**).

As described by Bennett *et al.*,[188] 2-amino-4-t-butylpyrimidine (**67**) (0.91g, 6.0mMol) was added to concentrated hydrochloric acid (5ml) cooled below 0°C. Whilst maintaining the temperature at -10°C, an aqueous solution (2ml) of sodium nitrite (0.53g, 7.6mMol) was added dropwise and the resulting mixture left to stir at -10°C for 1.5 hours. The mixture was neutralised with NaOH, allowed to warm to room temperature and extracted with chloroform (3x10ml). The chloroform extracts were combined, dried over magnesium sulphate and the chloroform removed *in vacuo* to give an oil. The oil (in 1-2ml of chloroform) was absorbed onto a silica gel column (10x2cm) and the column eluted with chloroform. Evaporation of the chloroform fraction gave **41** as a clear oil. Yield 0.36g (35%). ^{1}H NMR ($CDCl_3$) δ: 1.35 (9H), CH_3; 7.26, H5; 8.52, H6. The chloroform/methanol (10:1) fraction gave 2-hydroxy-4-(t-butyl)pyrimidine (**69**) as a white solid. Yield 0.20g (22%). Mp 191-193°C. Lit. 194-195°C.[188] The compound **69**

(0.20g, 1.3mMol) was added to $POCl_3$ cooled in ice. The resultant mixture was refluxed for 2 hours, cooled and the solvent removed *in vacuo*. The residue was carefully treated with ice, made alkaline with aqueous ammonia and extracted with chloroform. The extract was dried over anhydrous $MgSO_4$, concentrated and chromatographed as described above. Evaporation of the chloroform fraction gave **70**. Yield 45mg (27%).

Step 4.

4,4'-Bis-t-butyl-2,2'-bipyrimidine (**41**).

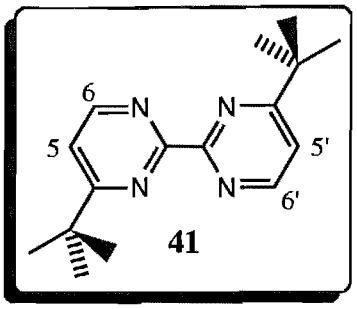

41

A blue solution of $Ni(PPh_3)_2Cl_2$ (750mg, 1.15mMol), PPh_3 (601mg, 2.30mMol), in dry dimethylformamide (20ml), was treated with zinc dust (77mg, 1.18mMol) and stirred for 1 hour, under a nitrogen atmosphere. During this time the colour changed to green, yellow and finally to red. 2-Chloro-4-t-butylpyrimidine (**70**) (196mg, 1.15mMol) was added to the red mixture which was stirred for 40 hours. The mixture was poured into water (35ml), boiled for 5 minutes and filtered. The filtrate was treated with ammonium hexafluorophosphate and the resultant white precipitate filtered and dissolved in 2:1 acetonitrile/water (15ml). Potassium cyanide (177mg) was added to the solution which was then refluxed briefly, cooled and extracted with chloroform (3x15ml). The extracts were combined and the chloroform removed *in vacuo*. The residue was dissolved in concentrated hydrochloric acid (5ml), extracted with chloroform (3x5ml) to remove triphenylphosphine, then made alkaline with aqueous NaOH (2M) and re-extracted with chloroform (3x10ml). The final extracts were combined, whereupon evaporation of the solvent gave **41** as an off-white solid, which was recrystallised from ethanol/ether. Yield 30mg (9.6%). Mp 114-115°C. Mass spectrum: $M^{+\cdot}$ calcd for $C_{16}H_{22}N_4$: 270.1844. Found: 270.1840. ^1H NMR ($CDCl_3$) δ: 1.48 (18H), CH_3; 7.45 (2H), H5; 8.91 (2H), H6. ^{13}C NMR ($CDCl_3$) δ: 29.8 (6C), CH_3; 38.6 (2C), $C(CH_3)_3$; 117.0 (2C), C5; 156.1 (2C), C6; 163.1 (2C), C2; 179.2 (2C), C4.

2,2'-Bi-(5S,8R)-5,6,7,8-tetrahydro-8,9,9-trimethyl-5,8-methanoquinazoline (42).

Step 1.

2-Amino-(5S,8R)-5,6,7,8-tetrahydro-8,9,9-trimethyl-5,8-methanoquinazoline (**74**).

A mixture of formyl camphor (**73**) (3.0g, 17mMol) and guanidine carbonate (1.5g, 12mMol) was heated for 1 hour at 120°C. The reaction melt was cooled and ethanol (20ml)

added to give a precipitate of crude **74**, which was filtered on a fine porosity funnel. Further extraction of the precipitate on the funnel with ethanol (3x20ml) gave **74** as a white solid. Yield 1.05g (89%).

Step 2.

2-Chloro-(5S,8R)-5,6,7,8-tetrahydro-8,9,9-trimethyl-5,8-methanoquinazoline (**76**).

The amine **74** (1.05g, 5.17mMol) was added to concentrated hydrochloric acid (5ml) cooled below 0°C. Whilst maintaining the temperature below -10°C, an aqueous solution (2ml) of sodium nitrite (0.46g, 6.67mMol) was added dropwise, and the resultant mixture left to stir at -10°C for 1.5 hours. The mixture was neutralised with NaOH, allowed to warm to room temperature and extracted with chloroform (3x10ml). The combined extracts were concentrated (1-2ml) *in vacuo* and absorbed onto a silica gel radial chromatography plate, which was eluted with chloroform to give two bands. The first band was collected, and the solvent removed *in vacuo* , to give **76** as a clear oil, which crystallised on standing. Yield 0.55g (48%). Mp 84-86°C. Mass spectrum: $M^{+\cdot}$ calcd for $C_{12}H_{15}N_2Cl$: 222.0924. Found: 222.0924. ^1H NMR ($CDCl_3$) δ: 0.60 (3H), syn-9-CH_3; 1.03 (3H), anti-9-CH_3; 1.17, endo-H6; 1.25, endo-H7; 1.30 (3H), 8-CH_3; 1.96, exo-H7; 2.19, exo-H6; 2.95, H5; 8.22, H4. The second band was collected and the solvent removed *in vacuo* to give 2-hydroxy-(5S,8R)-5,6,7,8-tetrahydro-8,9,9-trimethyl-5,8-methanoquinazoline (**75**). Yield 0.32g (30.3%). Mp 213-215°C. Mass spectrum: $M^{+\cdot}$ calcd for $C_{12}H_{16}N_2O$: 204.1263. Found: 204.1261. ^1H NMR ($CDCl_3$) δ: 0.70 (3H), syn-9-CH_3; 1.01 (3H), anti-9-CH_3; 1.16, endo-H6; 1.38, endo-H7; 1.24 (3H), 8-CH_3; 1.90, exo-H7; 2.12, exo-H6; 2.78, H5; 7.44, H4. Compound **75** (0.30g, 1.47mMol) was refluxed in $POCl_3$, as described above for **55** and **69**, to give additional **76**. Yield 185mg (57%).

Step 3.

2,2'-Bi-(5S,8R)-5,6,7,8-tetrahydro-8,9,9-trimethyl-5,8-methanoquinazoline (**42**).

A mixture of nickel chloride (0.32g, 2.47mMol), triphenylphosphine (1.41g, 5.38mMol) and zinc dust (0.13g, 2.0mMol), in dry dimethylformamide (10ml), was stirred at 50°C under an argon atmosphere. After 1 hour, during which time the colour of the mixture changed from blue to green and finally to red ($Ni^0(PPh_3)_2$[189]), a solution of **76** (0.3g, 1.35mMol), in dimethylformamide (3ml), was added under an argon atmosphere, and the mixture left to stir at 50°C for a further 12 hours. The

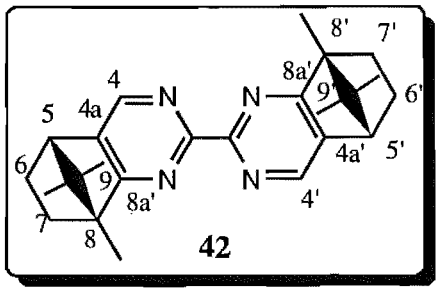

42

resultant brown mixture was poured into aqueous ammonia (50ml, 2M), filtered to remove the precipitate of triphenylphosphine oxide and the filtrate extracted with chloroform (3x40ml). The extracts were combined and the solvent removed *in vacuo*. The residue was redissolved in chloroform (1-2ml) and absorbed onto a silica gel radial chromatography plate. Excess triphenylphosphine was eluted with petroleum ether/ethyl acetate (1:1). Compound **42** was eluted with chloroform and the solvent removed *in vacuo* to give a white solid. Yield 0.11g (44%). Mp 186-188°C. Mass spectrum: $M^{+\cdot}$ calcd for $C_{24}H_{30}N_4$: 374.2471. Found: 374.2471. ^1H NMR ($CDCl_3$) δ: 0.63 (6H), syn-9-CH_3; 1.05 (6H), anti-9-CH_3; 1.25 (2H), endo-H6; 1.29 (2H), endo-H7; 1.47 (6H), 8-CH_3; 1.95 (2H), exo-H7; 2.23 (2H), exo-H6; 3.02 (2H), H5; 8.64 (2H), H4. ^1H NMR (CD_3CN) δ: 0.66 (6H), syn-9-CH_3; 1.11 (6H), anti-9-CH_3; 1.18 (2H), endo-H6; 1.35 (2H), endo-H7; 1.37 (6H), 8-CH_3; 2.03 (2H), exo-H7; 2.28 (2H), exo-H6; 3.11 (2H), H5; 8.58 (2H), H4. ^{13}C NMR (CD_3CN) δ: 9.7 (2C), 8-CH_3; 18.5 (2C), anti-9-CH_3; 19.5 (2C), syn-9-CH_3; 25.61 (2C), C6; 31.4 (2C), C7; 49.6 (2C), C5; 54.9 (2C), C9; 57.5 (2C), C8; 138.4 (2C), C4a; 147.4 (2C), C4; 162.0 (2C), C2; 179.6 (2C), C8a.

2,4-Bis-(1-pyrazolyl)pyrimidine (53).

Potassium pyrazolate was prepared by stirring pyrazole (0.46g, 6.7mMol) and potassium (0.26g, 6.7mMol) in dry diglyme (40ml) at 70°C for 2 hours under a nitrogen atmosphere. 2,4-Dichloropyrimidine (**81**) (1g, 6.7mMol) was added to the suspension of the pyrazolate salt and the mixture stirred at 120°C. After 3 days, the mixture was cooled to room temperature and filtered to remove KCl. The diglyme was then removed *in vacuo* and the resultant residue rigourously extracted with chloroform.

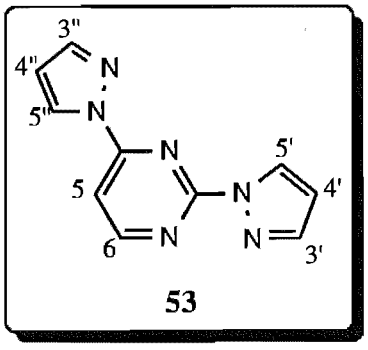

53

The chloroform was concentrated to give a yellow oil, the ^1H NMR spectrum of which indicated a complex mixture of substituted pyrimidines. The oil was redissolved in chloroform (1-2ml), absorbed onto silica gel, and purified by radial chromatography (4 mm plate). Elution with petroleum ether/chloroform (3:1) produced 2 bands, the first of which was found to contain **83** and unreacted **81** (200mg). By fractionating the band 6mg of pure **83** was obtained. The second band contained 80mg of **84**. The major product, **53**, was eluted with methanol/chloroform (1:50) and the solvent removed *in vacuo* to give a white solid. Yield 450mg (32%). Mp 143-144°C. Calcd for $C_{10}H_8N_6$ C: 56.6, H: 3.8, N: 39.6. Found C: 56.5, H: 3.6, N: 39.5. Mass spectrum: $M^{+\cdot}$ calcd for $C_{10}H_8N_6$: 212.0810. Found: 212.0813. ^1H NMR ($CDCl_3$) δ: 6.55,

H4'; 6.56, H4"; 7.82, H5; 7.84, H3'; 7.88, H3"; 8.64, H5'; 8.73, H5"; 8.78, H6. ^{1}H NMR (CD_3CN) δ: 6.62, H4'; 6.67, H4"; 7.84, H5; 7.88, H3'; 7.92, H3"; 8.77, H5'; 8.78, H5"; 8.83, H6. ^{13}C NMR (CD_3CN) 106.3, C5; 109.0, C4'; 109.9, C4"; 128.4, C5"; 130.1, C5'; 143.9, C3'; 144.7, C3"; 155.9, C2; 158.7, C4; 161.3, C6.

2-Chloro-4-(1-pyrazolyl)pyrimidine (83).

Preparation as above. White solid. Yield 6mg (0.5%). Due to the very low yield, further coupling reactions with **83** were not attempted. Mp 120-122°C. Mass spectrum: $M^{+\cdot}$ calcd for $C_7H_5N_4Cl$: 180.0203. Found: 180.0209. ^{1}H NMR ($CDCl_3$) δ: 6.54, H4'; 7.82, H3'; 7.87, H5; 8.59, H5'; 8.63, H6.

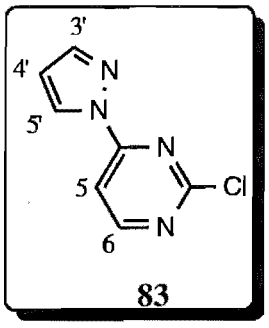

83

4-Chloro-2-(1-pyrazolyl)pyrimidine (84)

Preparation as above. White solid. Yield 80mg (6.6%). Due to the very low yield, further coupling reactions with **84** were not attempted. Mp 111-114°C. Mass spectrum: $M^{+\cdot}$ calcd for $C_7H_5N_4Cl$: 180.0203. Found: 180.0202. ^{1}H NMR ($CDCl_3$) δ: 6.53, H4'; 7.25, H5; 7.86, H3'; 8.59, H5'; 8.64, H6.

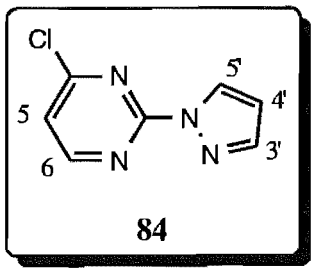

84

2,2'-Biperimidine (91).

The compound **91** was prepared from the method of Patshorcke and Reid.[209] A mixture of 1,8-diaminonaphthalene (1.0g, 6.3mMol) and diethyloxalate (0.47g, 3.16mMol) was heated (220°C), with stirring, in a 100ml round bottom flask and the ethanol and water produced was distilled. The reaction melt was cooled to room temperature, whereupon methanol (40ml) was added to the flask and the resulting mixture stirred for 15 minutes. The resultant red solid was filtered, washed with methanol and air dried. Yield 0.81g (77%). Mp >360°. Lit. >360°C.[209] ^{1}H NMR (DMSO-d_6) δ: 6.87 (2H), H9; 6.90 (2H), H4; 7.14 (2H), H7; 7.22 (2H), H6; 7.23 (2H), H8; 7.31 (2H), H5; 10.69 (2H), H1.

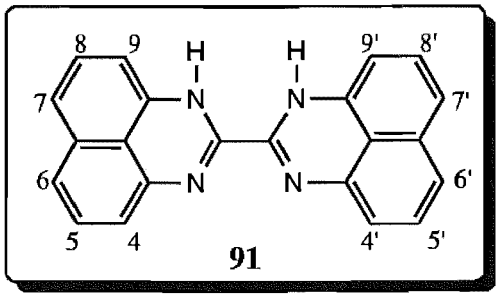

91

2-(2-Pyridinyl)perimidine (93).

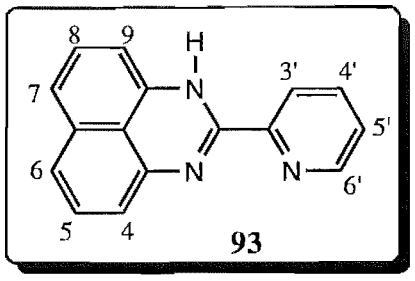

93

As described by Browne *et al.*,[212] a mixture of 2-cyanopyridine (3.39g, 37mMol) and sodium ethoxide (0.34g, 5mMol), in dry ethanol (80ml), was stirred at room temperature, in darkness, for 1 hour. Acetic acid (0.5g) was added followed by 1,8-diaminonaphthalene (4.7g, 30mMol). Additional acetic acid was added to maintain a pH of 5-7 and the mixture was stirred in darkness for 2 hours. The ethanol was removed *in vacuo* and the resultant residue extracted with benzene (5x40ml). The extracts were combined, treated with decolourising charcoal, filtered, and the benzene evaporated to leave a red solid. The solid was recrystallised from petroleum ether/chloroform to give deep red crystals of **93**. Yield 1.7g (23%). Mp 161-162°C. Lit. 162-163°C.[212] ^{1}H NMR ($CDCl_3$) δ: 6.35, H9; 6.90, H4; 7.06-7.22, H6, H7, H8; 7.25, H5; 7.45, H5'; 7.87, H4'; 8.43, H3'; 8.62, H6'; 9.39, H1. ^{1}H NMR (DMSO-d_6) δ: 6.81, H9; 6.88, H4; 7.12, H7; 7.18, H6; 7.21, H8; 7.29, H5; 7.74, H5'; 8.12, H4'; 8.41, H3'; 8.84, H6'; 11.09, H1. ^{1}H NMR (CD_3CN) δ: 6.61, H9; 6.84, H4; 7.12, H7; 7.19, H6; 7.19, H8; 7.28, H5; 7.60, H5'; 8.01, H4'; 8.39, H3'; 8.73, H6'; 9.78, H1. ^{13}C NMR (CD_3CN) δ: 103.2, C9; 115.2, C4; 118.6, C7; 118.8, C9b; 120.6, C8; 121.5, C3'; 126.3, C5'; 128.4, C6; 129.3, C5; 136.1, C6a; 137.8, C4'; 145.4, C9a; 148.8, C6'; C2 and C2'-not observed.

1-Methyl-2-(2-pyridinyl)perimidine (94).

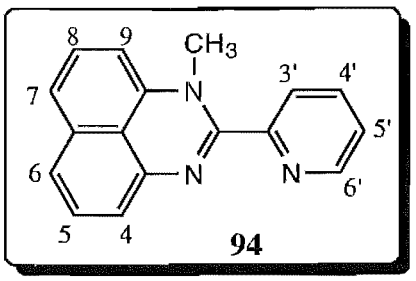

94

The following synthesis was derived from a procedure described by Paragamanian *et al.* for alkylating N1H perimidines.[211] To a solution of 2-(2-pyridinyl)perimidine (604mg,2.46mMol), in dry glyme (15ml), was added NaH (80mg,3.33mMol). Methyl iodide (400mg, 2.82mMol) was added and the solution stirred at room temperature for 8 hours. The glyme was removed *in vacuo* and the resultant residue extracted with hot dichloromethane (25ml). The extract was cooled to room temperature, diluted with petroleum ether and cooled at 0°C overnight. The resultant yellow crystals of **94** were filtered and air dried. Yield 477mg (75%). Mp 172-174°C. Mass spectrum: $M^{+\cdot}$ calcd for $C_{17}H_{13}N_3$: 259.1109. Found: 259.1105. ^{1}H NMR ($CDCl_3$) δ: 3.14, 1-CH_3; 6.32, H9; 6.94,

H4; 7.23, H6; 7.23, H7; 7.30, H5; 7.32, H8; 7.40, H5'; 7.79, H3'; 7.88, H4'; 8.69, H6'. ^{1}H NMR (DMSO-d_6) δ: 3.17, 1-CH_3; 6.56, H9; 6.86, H4; 7.30, H7; 7.35, H6; 7.37, H8; 7.38, H5; 7.66, H5'; 7.87, H3'; 8.11, H4'; 8.79, H6'. ^{1}H NMR (CD_3CN) δ: 3.15, 1-CH_3; 6.47, H9; 6.84, H4; 7.25, H7; 7.29, H6; 7.32, H8; 7.34, H5; 7.54, H5'; 7.76, H3'; 8.00, H4'; 8.73, H6'. ^{1}H NMR ($(CD_3)_2CO$) δ: 3.32, 1-CH_3; 6.57, H9; 6.92, H4; 7.31, H7; 7.34, H6; 7.37, H8; 7.40, H5; 7.65, H5'; 7.96, H3'; 8.12, H4'; 8.80, H6'. ^{13}C NMR (CD_3CN) δ: 36.4, 1-CH_3; 102.1, C9; 115.1, C4; 118.0, C9b; 119.4, C7; 120.4, C8; 124.5, 124.8, C3' and C5'; 128.3, C6; 129.0, C5; 135.6, C6a; 137.8, C4'; 141.0, C3a; 143.8, C9a; 149.1, C6'; 154.7, C2'; 155.8, C2.

2-(2-Pyrimidinyl)perimidine (95).

Step 1.

2-Cyanopyrimidine.

A solution of 2-chloropyrimidine (17.2g, 15mMol) and trimethylamine (19.9g, 37mMol) in benzene (120ml) was allowed to stand for 5 days, as described by Case *et al.*[256] The resultant yellow precipitate of 2-pyrimidinyltrimethylammonium chloride was filtered and dried in a vacuum desiccator. Yield 22.75g (87%). This solid (7g, 61mMol) was gradually added to, with stirring, a mixture of potassium cyanide (8.16g, 125mMol) and acetamide (14.3g) at 80°-90°C. The resultant brown liquid was heated until gas evolution ceased and cooled to room temperature. The cooled melt was dissolved in water (80ml) and extracted with ether. The ether extract was dried over magnesium sulphate, and the ether removed *in vacuo* to give a clear oil which solidified on standing. Yield 1.8g (28%). Mp 41°C. Lit. 41-42°C.[256] ^{1}H NMR ($CDCl_3$) δ: 7.55, H4; 8.88 (2H), H3 and H5.

Step 2.

2-(2-Pyrimidinyl)perimidine (**95**).

A mixture of 2-cyanopyrimidine (1.5g, 14mMol) and sodium ethoxide (0.136g, 2mMol), in dry ethanol (40ml), was stirred at room temperature, in darkness, for 1 hour. Acetic acid (0.22g) was added followed by 1,8-diaminonaphthalene (2.07g, 13mMol). Additional acetic acid was added to maintain a pH of 5-7 and the mixture was stirred in darkness for 2 hours. The ethanol was removed *in vacuo* and the resultant residue was firstly extracted with benzene (4x30ml). The extracts were combined,

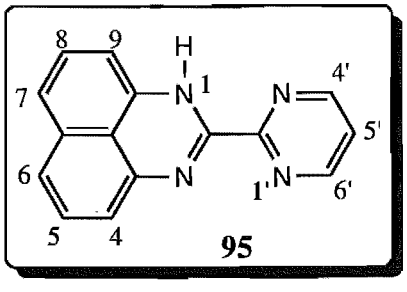

95

treated with decolourising charcoal, filtered and the benzene evaporated to leave a brown solid (1.2g) which was shown, by ^{1}H NMR spectroscopy, to contain approximately 220mg (6%) of the desired product. The residue remaining after extraction with benzene was extracted a second time with hot dichloromethane. Evaporation of the dichloromethane extract gave **95** as a red solid, which was recrystallised from petroleum ether/chloroform. Yield 585mg (16%). Mp 200-203°C-decomposition. Mass Spectrum: $M^{+\cdot}$ Calcd for $C_{15}H_{10}N_4$: 246.0905. Found: 246.0908. ^{1}H NMR ($CDCl_3$) δ: 6.73 (2H), H4 and H9; 7.13 (2H), H6 and H7; 7.18 (2H), H5 and H8; 7.46, H5'; 8.94 (2H), H4' and H6'; H1 not observed. ^{1}H NMR (CD_3CN) δ: 6.60, H9; 6.86, H4; 7.19 (4H), H5, H6, H7 and H8; 9.00 (2H), H4' and H6'; 9.71, H1.

4,6-Bis-(2-pyridinyl)pyrimidine (109).

Step 1.

1,3-Bis-(2-pyridinyl)-1,3-propanedione (**113**).

The method of Texidor *et al.* was used to prepare **113**.[220] Sodium ethoxide was prepared in a three-neck flask from dry ethanol (67ml) and sodium (2.25g, 100mMol) under a nitrogen atmosphere. The ethanol was removed *in vacuo* and 80 ml of dry toluene was transferred to the flask, followed by 2-methoxycarbonylpyridine (**111**) (13.44g,110mMol). 2-Acetylpyridine (**112**) (16.63g,110mMol) was slowly added to this mixture whilst maintaining the temperature at 43-50°C, during which time a colour change, from yellow to red, was observed. An off-white solid formed and stirring was continued for 1 hour, followed by heating on a steam bath for 45 minutes. The off-white solid was filtered, dried and added, with stirring, into a mixture containing water (100 ml), acetic acid (100 ml) and ice (336 g) to give a white solid (**113**), which was filtered and dried. Yield 13.9g (62%). ^{1}H NMR ($CDCl_3$) δ: 4.94 (2H), CH_2; 7.45 (2H), H5; 7.87 (2H), H4; 8.16 (2H), H3; 8.76 (2H), H6.

Step 2.

4,6-Bis-(2-pyridinyl)pyrimidine (**109**).

As described by Case *et al.*,[218] **113** (4.1g, 18mMol) was refluxed in formamide (50 g) for 6 hours. The mixture was concentrated to one half its volume and diluted with 100ml of water to give a precipitate. The precipitate was washed with water and extracted with ether. The extract was dried over magnesium sulphate and the solvent removed *in vacuo*. The residue was sublimed at 90°C (10mm Hg) and the sublimate

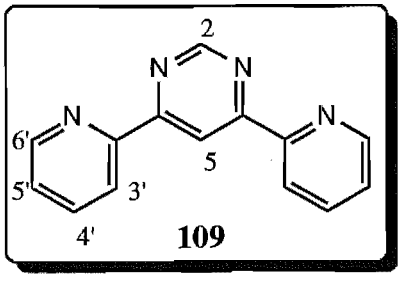

109

recrystallised from ether to give white crystals of **109**. Yield 0.8 g (20%). Mp 111-113°C. Lit.113-114°C.[218] ^{1}H NMR ($CDCl_3$) δ: 7.44 (2H), H5'; 7.90 (2H), H4'; 8.53 (2H), H3'; 8.80 (2H), H6'; 9.37, H2; 9.39, H5. ^{1}H NMR (CD_3CN) δ: 7.60 (2H), H5'; 8.05 (2H), H4'; 8.61 (2H), H3'; 8.86 (2H), H6'; 9.38, H2; 9.43, H5. ^{1}H NMR $(CD_3)_2CO$ δ: 7.71 (2H), H5'; 8.17 (2H), H4'; 8.73 (2H), H3'; 8.94 (2H), H6'; 9.47, H2; 9.64, H5. ^{1}H NMR (DMSO-d_6) δ: 7.73 (2H), H5'; 8.18 (2H), H4'; 8.63 (2H), H3'; 8.93 (2H), H6'; 9.45, H2; 9.53, H5. ^{13}C NMR (CD_3CN) δ: 113.2, C5; 121.7 (2C), C3'; 126.1 (2C), C5'; 137.8 (2C), C4'; 150.2 (2C), C6'; 154.1 (2C), C2'; 159.0, C2; 164.2, C4. ^{13}C NMR $(CD_3)_2CO$ δ: 113.1, C5; 121.6 (2C), C3'; 126.0 (2C), C5'; 137.6 (2C), C4'; 150.1 (2C), C6'; 154.2 (2C), C2'; 158.9, C2; 164.1, C4.

2,6-Bis-[6-(2-pyridinyl)-4-pyrimidinyl]pyridine (110).

Step 1.

2,6-Diethoxycarbonylpyridine (**128**).

2,6-Pyridine-dicarboxylic acid (12g, 72mMol) was refluxed in ethanol (60ml) in the presence of concentrated sulphuric acid (1.5 ml) for 8 hours. The resulting solution was poured into water (300ml), made alkaline with sodium carbonate then extracted with ether (4x100ml). The combined extracts were dried over magnesium sulphate and concentrated *in vacuo* to give **128** as a clear oil which crystallised on standing. Yield 8.5g (65%). Mp 42-43°C. Lit 42-43°C.[257] ^{1}H NMR ($CDCl_3$) δ: 1.47 (6H), CH_3; 4.50 (4H), CH_2; 8.02, H4; 8.30 (2H), H3 and H5.

Step 2.

2,6-Bis-[3-(2-pyridinyl)propane-1,3-dionato]pyridine (**129**).

Sodium ethoxide was prepared in a three-neck flask from sodium (0.82g) and dry ethanol (50ml). The ethanol was removed *in vacuo* and toluene (50ml), followed by the diester (4g, 17mMol) were added to the flask. Whilst stirring and maintaining the temperature of the mixture at 42°C, 2-acetylpyridine (**112**) (6.1g, 50mMol) was slowly added. The mixture was stirred for 30 minutes, cooled to room temperature and filtered. The resultant solid was dried and poured, with stirring, into a mixture of water (36ml), glacial acetic acid (46ml) and ice (120g). The yellow precipitate of **129** which formed was filtered, dried and recrystallised from ethanol. Yield 1.25g (20%). Mass spectrum: $M^{+\cdot}$ calcd for $C_{21}H_{15}N_3O_4$: 373.1063. Found: 373.1069. ^{1}H NMR ($CDCl_3$)-major tautomer-δ: 4.96, 7.49, 7.90, 8.06, 8.20, 8.32, 8.81.

Step 3.

2,6-Bis-[6-(2-pyridinyl)-4-pyrimidinyl]pyridine (**110**).

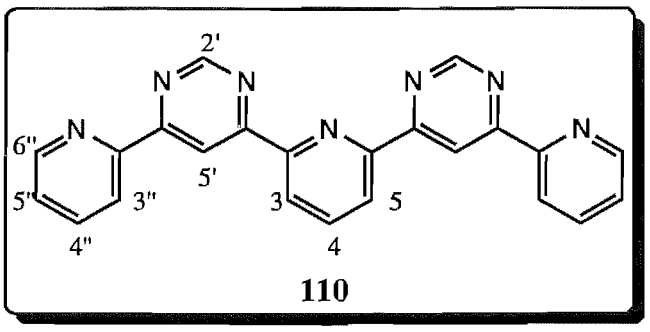

110

A mixture of **129** (0.5g, 1.34mMol) in formamide (30ml), was refluxed for 6 hours. After cooling to room temperature, a black precipitate formed and was filtered, washed with water and air dried. The brown formamide solution was concentrated *in vacuo* and diluted with water (40ml) to give additional product. The black solid was extracted with hot methanol and the extract cooled to give an off-white precipitate, which was filtered. Further recrystallisation from methanol gave an off-white solid (**110**). Yield 61mg (12%). Mp 190-195°C decomp. Mass spectrum: $M^{+\cdot}$ calcd for $C_{23}H_{15}N_7$: 389.1389. Found: 389.1392. ^1H NMR ($CDCl_3$) δ: 7.46 (2H), H5"; 7.92 (2H), H4"; 8.10, H4; 8.56 (2H), H3"; 8.67 (2H), H3 and H5; 8.84 (2H), H6"; 9.39 (2H), H2'; 9.62 (2H), H5'. ^1H NMR (CD_3CN) δ: 7.65 (2H), H5"; 8.09 (2H), H4"; 8.27, H4; 8.66 (2H), H3"; 8.76 (2H), H3 and H5; 8.95 (2H), H6"; 9.45 (2H), H2'; 9.64 (2H), H5'. In addition, the compound 2-[(2-pyridinyl)-4-pyrimidinyl]pyridine-6-carboxamide (**130**) was isolated from the methanol filtrate. Mass spectrum: $M^{+\cdot}$ calcd for $C_{15}H_{11}N_5O$: 277.0964. Found: 277.0968. ^1H NMR ($CDCl_3$) δ: 7.47, H5"; 7.93, H4"; 8.09, H4'; 8.38, H5'; 8.58, H3"; 8.73, H3'; 8.80, H6"; 9.35, H2; 9.39, H5.

2,6-Bis-(1-pyrazolyl)-1,5-naphthyridine (132).

Step 1.

1,5-Naphthyridine (**133**).

3-Aminopyridine (30g, 319mMol), sodium *m*-nitrobenzenesulphonate (140g), water (180ml), glycerol (100ml) and sulphuric acid (328g) were heated, with stirring, at 135°C for 20 hours.[229] Water (400ml) was added and the mixture made alkaline with NaOH and steam distilled. The distillate was made alkaline and continuously extracted with ether. The extract was dried over magnesium sulphate and the ether removed *in vacuo*. The resultant residue of **133** was recrystallised from petroleum ether. Yield 5g (12%). Mp 75°C. Lit. 75°C.[229] ^1H NMR ($CDCl_3$) δ: 7.67 (2H), H3; 8.44 (2H), H4; 9.00 (2H), H2.

Step 2.

1,5-Naphthyridine-di-N-oxide (**134**).

The method of Hart[231] was modified as follows. To a mixture of **133** (2.2g, 17mMol) in acetic acid (40ml) was added hydrogen peroxide (10ml, 30%v/v). The mixture was heated (70°-80°C) with stirring for 4 days and the resultant brown solution was cooled to room temperature and filtered. The acetic acid was evaporated *in vacuo* leaving a brown residue which was combined with water (20ml) and made alkaline with sodium carbonate. The resultant yellow precipitate of **134** was filtered and dried in a vacuum desiccator. Yield-0.95g (34%). Mp 297-300°C. Lit. 299-301°C.[231] ^{1}H NMR ($CDCl_3$) δ: 7.53 (2H), H3; 8.51 (2H), H4; 8.57 (2H), H2.

Step 3.

2,6-Dichloro-1,5-naphthyridine (**135**).

1,5-Naphthyridine-di-N-oxide (**134**) (600mg, 3.7mMol) was slowly added to $POCl_3$ cooled in an ice/water bath. The mixture was refluxed for 6 hours, cooled and the $POCl_3$ removed *in vacuo* leaving a brown residue. Ice was cautiously added to the residue, the resultant solution made alkaline with aqueous ammonia, and extracted with chloroform. The extract was dried over magnesium sulphate and the solvent removed *in vacuo*. The residue was found, by ^{1}H NMR spectroscopy to consist of predominantly **135** and other mono- and dichlorinated side-products. The residue was redissolved in chloroform (1-2ml), absorbed onto a column of silica (10x2.5cm) and the column eluted with chloroform. Evaporation of the first fraction gave **135** as an off-white solid. Yield 260mg (35%). Mp 234-236°C. Lit. 236-238°C.[231] ^{1}H NMR ($CDCl_3$) δ: 7.66 (2H), H3; 8.28 (2H), H4. Similarly, **136** was obtained from the second fraction as an off-white solid. Yield 44mg (6%). ^{1}H NMR ($CDCl_3$) δ: 7.70, H3; 7.78, H7; 8.38, H4; 8.85, H6. The other side products were not isolated.

Step 4.

2,6-Bis-(1-pyrazolyl)-1,5-naphthyridine (**132**)

Potassium pyrazolate was prepared by stirring pyrazole (204mg, 3.0mMol) and potassium (120mg, 3.0mMol), for 2 hours, in dry diglyme (10ml) (70°C), under a nitrogen atmosphere. 2,6-Dichloro-1,5-naphthyridine (**135**) (260mg, 1.3mMol) was added to the suspension of the pyrazolate salt and the mixture stirred at

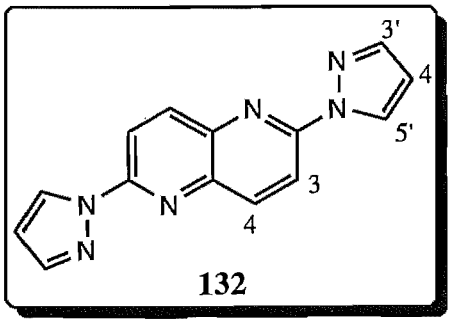

132

120°C. After 3 days, the mixture was filtered hot and the filtrate allowed to cool to room temperature. The resultant precipitate was filtered, extracted with chloroform (25ml) and the extract concentrated (3ml) and diluted with methanol. The white precipitate which formed was filtered and air dried. By diluting the diglyme filtrate with water (20ml), additional product was obtained as an off-white precipitate. The precipitates were combined and recrystallised from acetonitrile to give white needles of **132**. Yield-155mg (45%). Mp 232-233°C. Mass spectrum: $M^{+\cdot}$ calcd for $C_{12}H_{10}N_6$: 262.0967. Found: 262.0967. ^{1}H NMR ($CDCl_3$) δ: 6.56 (2H), H4'; 7.82 (2H), H3'; 8.40 (2H), 8.46 (2H), H3 and H4; 8.77 (2H), H5'. ^{1}H NMR (CD_3CN) δ: 6.67 (2H), H4'; 7.90 (2H), H3'; 8.49 (4H), H3 and H4; 8.84 (2H), H5'.

2,2'-Bis-(1-pyrazolyl)-4,4'-bipyridine (144).

Step 1.

4,4'-Bipyridine-di-N-oxide.(**152**)

The synthesis of 4,4'-bipyridine mono-N-oxide, as described by Moran *et al.*,[230] was modified as follows. Hydrogen peroxide (4ml, 50%) was added to a stirred solution of 4,4'-bipyridine (5g) in glacial acetic acid (25ml). The solution was heated (70°C) for 7 hours, treated with more hydrogen peroxide (4ml) and heated, with stirring, for a further 4 days. The solution was cooled to room temperature, poured into water (180ml) and made alkaline with sodium carbonate. The resultant yellow precipitate of **152** was filtered and dried in a vacuum desiccator. Yield 5g (81%). ^{1}H NMR (DMSO-d_6) δ: 7.99 (4H), H3 and H5; 8.40 (4H), H2 and H6.

Step 2.

2,2'-Dichloro-4,4'-bipyridine.(**153**)

4,4'-Bipyridine-di-N-oxide (**152**) (2.2g, 12.7mMol) was slowly added to $POCl_3$ (25ml), whilst cooling in an ice/water bath, analogous to the preparation of 2-chloro-4,4'-bipyridine, as described by Moran *et al.*[230] The mixture was refluxed for 7 days, cooled to room temperature, filtered and $POCl_3$ was removed *in vacuo*. The resultant residue was treated with ice (20g) and made alkaline with potassium carbonate to give a brown precipitate of **153**, which was filtered and dried in a vacuum desiccator. ^{1}H NMR (DMSO-d_6) δ: 8.01 (2H), H5; 8.17 (2H), H3; 8.67 (2H), H6.

Step 3.

2,2'-Bis-(1-pyrazolyl)-4,4'-bipyridine (**144**).

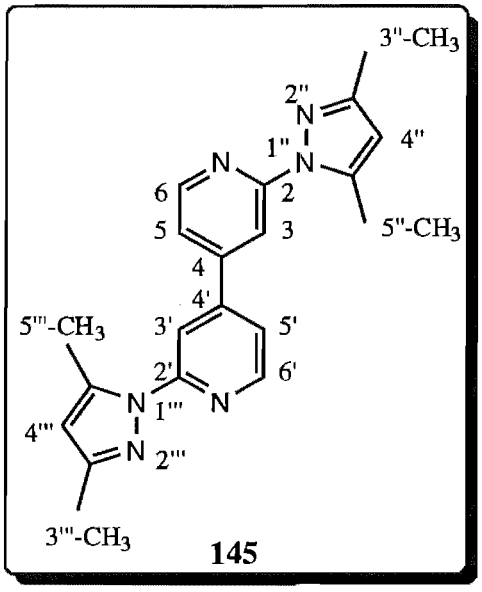

145

Potassium pyrazolate was prepared by stirring pyrazole (0.44g, 6.5mMol) and potassium (0.25g, 6.4mMol) in dry diglyme (30ml) (70°C), for 2 hours, under a nitrogen atmosphere. To the suspension of the pyrazolate salt was added **153** (0.7g, 3.1mMol) and the resultant mixture stirred at 120°C for 2 days. The mixture was cooled, filtered and the filtrate concentrated to 10ml *in vacuo*. Addition of methanol (25ml) to the diglyme produced yellow crystals of **144**. Recrystallisation from $CH_3CN/CHCl_3$ gave white needles suitable for X-ray analysis. Yield 0.127g (14.2%). Mp 186-187°C. Calcd for $C_{16}N_{12}N_6$ C: 66.66, H: 4.20, H: 29.15. Found C: 66.27, H: 3.88, N: 29.02. Mass spectrum: $M^{+\cdot}$ calcd for $C_{16}H_{12}N_6$: 288.1123. Found: 288.1121. ^1H NMR ($CDCl_3$) δ: 6.52 (2H), H4"; 7.53 (2H), H5; 7.79 (2H), H3"; 8.35 (2H), H3; 8.54 (2H), H6; 8.63 (2H), H5". ^1H NMR (CD_3CN) δ: 6.62 (2H), H4"; 7.73 (2H), H5; 7.87 (2H), H3"; 8.38 (2H), H3; 8.63 (2H), H6; 8.70 (2H), H5". ^{13}C NMR (CD_3CN-protonated carbons) δ: 108.5 (2C), C4"; 110.3 (2C), C3; 120.0 (2C), C5; 127.6 (2C), C5"; 142.7 (2C), C3"; 149.7 (2C), C6; 150.9 (2C), 154.8 (2C), C2 and C4.

2,2'-Bis-(3,5-dimethyl-1-pyrazolyl)-4,4'-bipyridine (145).

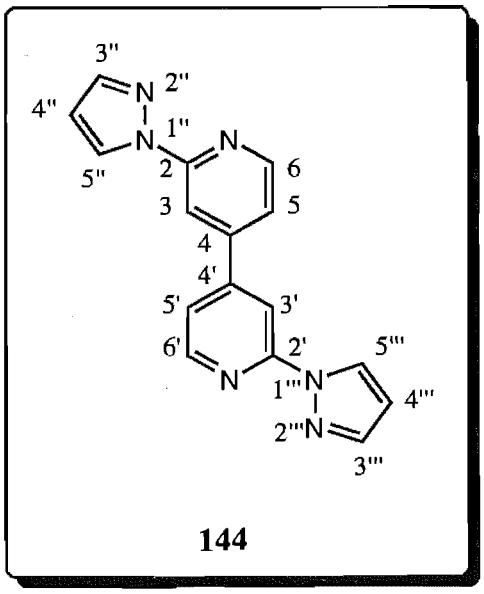

144

Potassium 3,5-dimethylpyrazolate was prepared by stirring 3,5-dimethylpyrazole (0.63g, 6.5mMol) and potassium (0.25g, 6.4mMol) in dry diglyme (30ml) (70°C), for 2 hours, under a nitrogen atmosphere. 2,2'-Dichloro-4,4'-bipyridine (**153**) (0.7g, 3.1mMol) was added to the suspension of the dimethylpyrazolate salt. The mixture was stirred at 120°C for 2 days, allowed to cool to room temperature, filtered and the filtrate concentrated to 5ml *in vacuo*. Methanol (35ml) was added and the solution was left to cool (0°C) overnight to give white crystals (30mg) of **145**. Additional **145**

(180mg) was obtained by the addition of water (20ml) to the filtrate. Recrystallisation from CH_3CN gave white needles suitable for X-ray analysis. Yield 216mg (20%). Mp 140-141°C. Calcd for $C_{20}H_{20}N_6$ C: 69.75, H: 5.85, N: 24.40. Found C: 69.52, H: 5.76, N: 24.51. Mass spectrum: $M^{+\cdot}$ calcd for $C_{20}H_{20}N_6$: 344.1749. Found: 344.1745. ^1H NMR ($CDCl_3$) δ: 2.32 (6H), 5"-CH_3; 2.68 (6H), 3"-CH_3; 6.03 (2H), H4"; 7.46 (2H), H5; 8.19 (2H), H3; 8.52 (2H), H6. ^1H NMR (CD_3CN) δ: 2.32 (6H), 5"-CH_3; 2.71 (6H), 3"-CH_3; 6.15 (2H), H4"; 7.63 (2H), H5; 8.20 (2H), H3; 8.59 (2H), H6. ^{13}C NMR (CD_3CN) δ: 13.1 (2C), 5"-CH_3; 14.3 (2C), 3"-CH_3; 109.6 (2C), C4"; 113.2 (2C), C3; 119.0 (2C), C5; 142.2 (2C), 148.1 (2C), C3", C5", C2 or C4; 148.94 (2C), C6; 150.38 (2C), 154.9 (2C), C3", C5", C2 or C4.

Attempted syntheses.

4,4'-Dichloro-2,2'-bipyrimidine (**82**)

A mixture of nickel chloride (1.57g, 12.1mMol), triphenylphosphine (6.95g, 26.9mMol) and zinc dust (0.618g, 9.53mMol), in dry dimethylformamide (35ml), was stirred at 50°C under an argon atmosphere.[189] After 1 hour, 2,4-dichloropyrimidine (**81**) (1g, 6.623mMol) was added to the red mixture, whilst maintaining an inert atmosphere, whereupon stirring was continued for a further 12 hours (50°C). The mixture was poured into aqueous ammonia (150 ml, 2M) and the resultant precipitate filtered. The filtrate was extracted with chloroform (4x80ml) and the extracts combined, dried over potassium carbonate and the solvent removed *in vacuo* to give a yellow oil. The aqueous phase was also refluxed in the presence of potassium cyanide and similarly extracted with chloroform to yield a brown oil. Analysis of both oils, by ^1H NMR spectroscopy, indicated that the reaction had failed to give the desired product **82**. Attempts to dimerize **81** with $Ni^0(PPh_3)_2$ generated from the precursor $Ni(PPh_3)_2Cl_2$ in a similar manner to syntheses described earlier, were also unsuccessful.

2-Chloro-4-(1-pyrazolyl)pyrimidine (**83**).

To a mixture of pyrazole (137mg, 2.01mMol) and NaH (50mg, 2.1mMol), in dry glyme, (30ml) was added **81** (300mg, 2.01mMol). Analysis of the crude reaction mixture, by ^1H NMR spectroscopy, indicated no formation of the desired product **83**, or its isomer **84**, after stirring at room temperature for 24 hours or refluxing the mixture for 24 hours. Alternative solvents THF and acetone also gave no reaction.

4,4'-Bis-(bromomethyl)-2,2'-bipyrimidine.

A mixture of 4,4'-dimethyl-2,2'-bipyrimidine (71mg, 0.38mMol) and N-bromosuccinimide (135mg, 0.76mMol) in carbon tetrachloride (10ml) was illuminated with a

tungsten bulb (100W) for 6 hours. The mixture was filtered and the carbon tetrachloride washed with aqueous sodium metabisulphate and dried over magnesium sulphate. Analysis of the organic layer by ^{1}H NMR indicated that the reaction had failed to give the desired product.

8.3 Syntheses of Complexes.

General preparation of ruthenium(II) complexes.

The compound $Ru(bpy)_2Cl_2.2H_2O$ or $Ru(dmb)_2Cl_2.2H_2O$ was refluxed in ethanol/water (3:1) for 1 hour. The ligand was added and the solution refluxed for 4-6 hours. The mixture was cooled to room temperature, filtered to remove unreacted ligand and concentrated to dryness *in vacuo*. The residue was dissolved in the minimum volume of water and the product precipitated by the addition of an aqueous solution of NH_4PF_6. Diruthenium complexes were prepared by using the monoruthenium complex as the ligand or by reacting one equivalent of the ligand with two equivalents of ruthenium. Formation of polynuclear complexes generally required reflux times of up to 24 hours, for dinuclear complexes, or 48 hours for complexes of higher nuclearity. Homoleptic complexes were prepared in a similar manner by refluxing three equivalents of the ligand with one equivalent of $Ru(DMSO)_4Cl_2$ in ethanol/water for 8-20 hours. Complexes were purified by chromatography, on either alumina or on sephadex-SP C-25 ion exchange gel, or by recrystallisation from either ethanol/water or by diffusing ether into a solution of the complex in acetonitrile, or by a combination of these methods.

Assignment of bpy/dmb ligands in the ^{1}H NMR spectra of Ru(II) complexes.

For some of the complexes an attempt has been made to assign some, or all, of the protons in each spin system of the bpy or dmb rings. In general, this was achieved using 1D TOCSY and/or 2D COSY experiments. The methyl groups are not included in the assignments of the dmb rings. Protons of the same spin system are denoted a, b, c, or d (eg: spin system a=bpyH3a, bpyH4a etc). All four bpyH6a-d, or dmbH6a-d, protons are usually well spread out in the spectra of the complexes. Hence, the spin systems are assigned on the basis of the chemical shift of the bpyH6 (dmbH6) proton; i.e. bpyH6a is assigned as the most shielded proton, with bpyH6b, bpyH6c and bpyH6d assigned in increasing order of chemical shift.

Tetrakis-(triphenylphosphine)-μ-(4,4'-dimethyl-2,2'-bipyrimidine-N1,N3'-N1',N3)-dicopper(I)-diperchlorate (57).

A mixture of **40** (18.6mg, 0.1mMol), Cu (9.0mg, 0.15mMol), $Cu(ClO_4)_2.6H_2O$ (35.0mg, 0.1mMol) and PPh_3 (100.0mg, 0.4mMol), in methanol (10ml), was refluxed for 1

hour. Yellow crystals of **57** were removed by filtration while the solvent was still hot. Additional crystals were obtained by cooling the filtrate. Yield 91.1mg (53%). Calcd for $C_{82}H_{70}N_4O_8P_4Cl_2Cu_2.3H_2O.HClO_4$ C: 57.40, H: 4.52, N: 3.27. Found C: 57.40, H: 4.41, N: 3.29. ^{1}H NMR (CD_3CN) δ: 2.61 (6H), 4-CH_3; 7.28 (24H), *o*-Ph; 7.37 (24H), *m*-Ph; 7.46 (2H), H5; 7.49 (12H), *p*-Ph; 8.63 (2H), H6. ^{1}H NMR (DMSO-d_6) δ: 2.63 (6H), 4-CH_3; 7.31 (24H), *o*-Ph; 7.46 (24H), *m*-Ph; 7.56 (12H), *p*-Ph; 7.74 (2H), H5; 8.86 (2H), H6.

Tetracarbonyl-(4,4'-dimethyl-2,2'-bipyrimidine-N1,N1')-molybdenum (58).

To a stirred solution of **40** (10mg, 0.05mMol) in dry THF (10ml) was added, dropwise, a green solution of $Mo(CO)_4C_7H_8$ (12mg, 0.04mMol) in dry THF (4ml). The solution rapidly became deep red and was stirred for 1 hour then diluted with ether (5ml) and cooled (0°C) overnight. The resultant red precipitate of **58** was filtered and dried. Yield 11mg (56%). ^{1}H NMR ($CDCl_3$) δ: 2.82 (6H), 4-CH_3; 7.35 (2H), H5; 9.08 (2H), H6. Repeating the reaction with $Mo(CO)_4C_7H_8$ (24mg, 0.08mMol) also gave **58**. Yield 14mg (71%).

Dichloro-(4,4'-dimethyl-2,2'-bipyrimidine-N1,N1')-palladium(II) (59).

Palladium chloride (20mg, 0.120mMol) was dissolved in hot HCl (5ml) and added dropwise to a hot solution of **40** (23mg, 0.124mMol) in methanol (5ml). The resultant precipitate of **59** was filtered and dried in a vacuum desiccator. Yield 34mg (78%). Similarly, a two fold excess of palladium chloride (46mg, 0.24mMol) gave **59**. Yield 35mg (80%). Calcd for $C_{10}H_{10}N_4Cl_2Pd$ C: 33.04, H: 2.77, N: 15.41. Found C: 32.91, H: 2.77, N: 15.70. ^{1}H NMR (DMSO-d_6) δ: 2.82 (6H), 4-CH_3; 7.95 (2H), H5; 9.24 (2H), H6.

Bis-(2,2'-bipyridine)-(4,4'-dimethyl-2,2'-bipyrimidine)-ruthenium(II)-bis-(hexafluorophosphate).

4,4'-Dimethyl-2,2'-bipyrimidine (**40**) (20mg, 0.107mMol) was reacted with $Ru(bpy)_2Cl_2.2H_2O$ (46mg, 0.090mMol) as described above. The product was obtained as a red solid. ^{1}H NMR analysis showed the product to be a 1:1 mixture of the symmetrical (N1,N1') (**60**) and unsymmetrical (N1,N3') (**61**) isomers. Yield 86mg (94%). FAB mass spectrum: calcd for $[C_{30}H_{26}N_8PF_6Ru]^+$: 745.097. Found: 745.098.

Bis-(2,2'-bipyridine)-(4,4'-dimethyl-2,2'-bipyrimidine-N1,N1')-ruthenium(II)-bis-(hexafluorophosphate) (**60**).

The symmetrical isomer **60** was obtained in pure form in the separation outlined for **64**. ^{1}H NMR (CD_3CN) δ: 2.77 (6H), 4-CH_3; 7.44 (2H), H5; 7.45 (2H), bpyH5a, 7.49 (2H),

bpyH5b; 7.75 (2H), bpyH6a; 7.87 (2H), H6; 7.93 (2H), bpyH6b; 8.11 (2H), 8.14 (2H), bpyH4a and bpyH4b; 8.55 (4H), bpyH3.

Bis-(2,2'-bipyridine)-(4,4'-dimethyl-2,2'-bipyrimidine-N1,N3')-ruthenium(II)-bis-(hexafluorophosphate) (**61**).

The unsymmetrical isomer **61** could not be isolated in pure form, but was assigned in the spectrum of the mixture **60/61**. ^{1}H NMR (CD_3CN) δ: 1.90 (3H), 4'-CH_3; 2.76 (3H), 4-CH_3; 7.39, bpyH5; 7.40 (2H), H5 and bpyH5; 7.41, bpyH5; 7.46, bpyH6; 7.51, bpyH5; 7.54 (2H), H5' and bpyH6; 7.70, H6; 7.81, 7.83, bpyH6; 8.05, 8.13, 8.16, 8.17, bpyH4; 8.53, 8.54, 8.58, 8.59, bpyH3; 8.99, H6'.

Bis-(4,4'-dimethyl-2,2'-bipyridine)-(4,4'-dimethyl-2,2'-bipyrimidine)-ruthenium(II)-bis-(hexafluorophosphate).

4,4'-Dimethyl-2,2'-bipyrimidine (**40**) (22mg, 0.12mMol) was reacted with $Ru(dmb)_2Cl_2.2H_2O$ (63mg, 0.11mMol) as described above. The desired product was obtained as a red solid. ^{1}H NMR analysis showed the product to be a 1:1 mixture of the symmetrical (N1,N1') (**62**) and unsymmetrical (N1,N3') (**63**) isomers. Yield 73mg (70%). Calcd for $C_{34}H_{34}N_8P_2F_{12}Ru.2H_2O$ C: 41.60, H: 3.90, N: 11.41. Found C: 41.92, H: 3.96, N: 11.62. FAB mass spectrum: calcd for $[C_{34}H_{34}N_8PF_6Ru]^+$: 801.1592. Found: 801.1593.

Bis-(4,4'-dimethyl-2,2'-bipyridine)-(4,4'-dimethyl-2,2'-bipyrimidine-N1,N1')-ruthenium(II)-bis-(hexafluorophosphate) (**62**).

The symmetrical isomer **62** was obtained in pure form in the separation outlined for **65**. ^{1}H NMR (CD_3CN) δ: 2.58 (6H), 2.59 (6H), dmb4-CH_3; 2.77 (6H), 4-CH_3; 7.29 (2H), dmbH5a; 7.31 (2H), dmbH5b; 7.42 (2H), H5; 7.55 (2H), dmbH6a; 7.72 (2H), dmbH6b; 7.86 (2H), H6; 8.39 (4H), dmbH3.

Bis-(4,4'-dimethyl-2,2'-bipyridine)-(4,4'-dimethyl-2,2'-bipyrimidine-N1,N3')-ruthenium(II)-bis-(hexafluorophosphate) (**63**).

The unsymmetrical isomer **63** could not be isolated in pure form, but was assigned in the spectrum of the mixture **62/63**. ^{1}H NMR (CD_3CN) δ: 1.90 (3H), 4'-CH_3; 2.54 (3H), 2.56 (3H), 2.60 (3H), 2.61 (3H), dmb4-CH_3; 2.76 (3H), 4-CH_3; 7.22 (2H), dmbH5a and dmbH5b; 7.33, dmbH5c; 7.34 (2H), dmbH5d and dmbH6a; 7.37, H5'; 7.52, H5; 7.60, dmbH6b; 7.62, dmbH6c; 7.68, H6; 7.90, dmbH6d; 8.37 (2H), dmbH3a and dmbH3b; 8.41 (2H), dmbH3c and dmbH3d; 8.97, H6'.

Tetrakis-(2,2'-bipyridine)-μ-(4,4'-dimethyl-2,2'-bipyrimidine-N1,N3'-N1',N3)-diruthenium(II)-tetrakis-(hexafluorophosphate) (64).

The 1:1 mixture **60/61** (20mg, 0.022mMol) was reacted with $Ru(bpy)_2Cl_2.2H_2O$ (6mg, 0.012mMol) as described above. The chloride salt of the product was absorbed onto a sephadex column. A purple band corresponding to unreacted $Ru(bpy)_2Cl_2.2H_2O$ was eluted first with water. The symmetrical complex **60** was eluted with 0.1M NaCl as an orange band. Yield 8mg (41%-rel. to **60/61**). The dinuclear complex **64** was eluted with 0.5M NaCl as a green band and both **60** and **64** were precipitated by the addition of aqueous NH_4PF_6. The ratio of the diastereoisomers in **64** varied from 4:1 to 5:1. Traces of the minor racemic isomer could not be removed from the mixture, despite attempts to purify the major meso isomer, by successive fractional recrystallisations (ether/acetonitrile). Yield 10mg (29%-rel. to **60/61**). Calcd for $C_{50}H_{42}N_{12}P_4F_{24}Ru_2$ C: 37.69, H: 2.66, N: 10.55. Found C: 37.64, H: 2.83, N: 10.94. FAB mass spectrum: calcd for $[C_{50}H_{42}N_{12}P_3F_{18}Ru_2]^+$: 1449.067. Found: 1449.065. Major diastereoisomer (ΛΔ) ^{1}H NMR (CD_3CN) δ: 1.95 (6H), 4-CH_3; 7.45 (2H), bpyH5a; 7.46 (2H), H5; 7.47 (2H), bpyH5b; 7.51 (2H), bpyH6a; 7.63 (2H), bpyH5c; 7.78 (2H), H6; 7.79 (2H), bpyH5d; 7.82 (2H), bpyH6b; 7.87 (2H), bpyH6c; 8.11 (2H), bpyH4a; 8.15 (2H), bpyH4b; 8.21 (2H), bpyH4c; 8.26 (2H), bpyH4d; 8.55 (4H), bpyH3c and bpyH3d; 8.58 (4H), bpyH3a and bpyH3b. Minor diastereoisomer (ΛΛ/ΔΔ)-tentative assignments-^{1}H NMR (CD_3CN) δ: 1.95 (6H), 4-CH_3; 7.43 (2H), bpyH5; 7.43-7.52 (6H), bpyH5; 7.45 (2H), bpyH6; 7.46 (2H), H5; 7.57 (2H), bpyH5; 7.73 (2H), bpyH6; 7.87 (2H), bpyH6; 7.91 (2H), bpyH6; 8.12 (2H), 8.14 (2H), 8.27 (2H) and 8.28 (2H), bpyH4; 8.58 (2H), 8.59 (2H), 8.63 (2H) and 8.67 (2H), bpyH3.

Tetrakis-(4,4'-dimethyl-2,2'-bipyridine)-μ-(4,4'-dimethyl-2,2'-bipyrimidine-N1,N3'-N1',N3)-diruthenium(II)-tetrakis-(hexafluorophosphate) (65).

The 1:1 mixture **62/63** (15mg, 0.016mMol) was reacted with $Ru(dmb)_2Cl_2.2H_2O$ (5mg, 0.009mMol) as described above. The product, as a chloride salt in aqueous solution, was absorbed onto a sephadex column. Excess $Ru(dmb)_2Cl_2.2H_2O$ was eluted with water as a purple band followed by an orange band corresponding to the symmetrical mononuclear complex **62**, the latter being eluted with 0.1M NaCl and precipitated by the addition aqueous NH_4PF_6. Yield 7mg (46%-rel. to **62/63**). Complex **65** was eluted with 0.5M NaCl as a green band and similarly precipitated with aqueous NH_4PF_6. The ^{1}H NMR spectrum of **65** indicated a 3:1 mixture of the meso and racemic diastereoisomers. Neither isomer could be separated by

successive fractional recrystallisations (ether/acetonitrile). Yield 8mg (29%). FAB mass spectrum: calcd for $[C_{58}H_{58}N_{12}P_3F_{18}Ru_2]^+$: 1561.192. Found: 1561.192. Major diastereoisomer ($\Lambda\Delta$) ^{1}H NMR (CD_3CN) δ: 1.94 (6H), 4-CH_3; 2.56 (3H), 2.58 (3H), 2.64 (3H) and 2.67 (3H), dmb4-CH_3; 7.28 (2H), dmbH5; 7.31 (4H), dmbH5 and dmbH6; 7.42 (2H), H5; 7.46 (2H), dmbH5; 7.62 (4H), dmbH5 and dmbH6; 7.66 (2H), dmbH6; 7.75 (2H), H6; 8.15 (2H), dmbH6; 8.39 (4H), 8.43 (4H), dmbH3. Minor diastereoisomer ($\Delta\Delta/\Lambda\Lambda$)-tentative assignment-^{1}H NMR (CD_3CN) δ: 1.94 (6H), 4-CH_3; 2.57 (3H), 2.58 (3H), 2.69 (3H) and 2.73 (3H), dmb4-CH_3; 7.27 (2H), dmbH5; 7.31 (4H), dmbH5 and dmbH6; 7.35 (2H) and 7.43 (2H), dmbH5; 7.54 (2H), 7.60 (2H) and 7.69 (2H), dmbH6; 7.79 (2H), H6; 8.39 (2H), 8.43 (2H), 8.49 (2H) and 8.51 (2H), dmbH3.

[4,4'-Bis-(t-butyl)-2,2'-bipyrimidine-N1,N1']-tetracarbonyl-molybdenum (71).

A green solution of $Mo(CO)_4C_7H_8$ (16.4mg, 0.037mMol or 32.8mg, 0.037mMol) in THF (2ml) was added dropwise to a stirred solution of **41** (10mg, 0.037mMol) in THF (5ml). The resultant deep red solution was stirred for 2 hours and a layer of petroleum ether was added. The solution was left to cool (0°C) overnight to give **71** as a red microcrystalline solid. Yield 15mg (85%). ^{1}H NMR ($CDCl_3$) δ: 1.48 (18H), CH_3; 7.45 (2H), H5; 9.08 (2H), H6.

Bis-(4,4'-dimethyl-2,2'-bipyridine)-[4,4'-bis-(t-butyl)-2,2'-bipyrimidine N1,N1']-ruthenium(II)-bis-(hexafluorophosphate) (72).

4,4'-Bis-t-butyl-2,2'-bipyrimidine (**41**) (18mg, 0.067mMol) was reacted with $Ru(dmb)_2Cl_2.2H_2O$ (34mg, 0.059mMol) as described above. Complex **72** was recrystallised from acetonitrile/ether to give a red microcrystalline solid. Yield 36mg (52%). FAB mass spectrum: calcd for $[C_{40}H_{46}N_8PF_6Ru]^+$: 885.2531. Found: 885.2535. ^{1}H NMR (CD_3CN) δ: 1.48 (18H), CH_3; 2.59 (6H), 2.60 (6H), dmb4-CH_3; 7.29 (2H), dmbH5a; 7.34 (2H), dmbH5b; 7.56 (2H), dmbH6a; 7.57, H5; 7.74 (2H), dmbH6b; 7.91 (2H), H6; 8.40 (4H), dmbH3. ^{13}C NMR (CD_3CN) δ: 20.6 (4C), dmb4-CH_3; 28.8 (6C), CH_3; 38.5 (2C), $C(CH_3)_3$; 120.6 (2C), C5; 125.2 (4C), dmbC3; 128.6 (2C), 128.8 (2C), dmbC5; 150.8 (2C), 150.9 (2C), dmbC4; 151.1 (2C), 151.6 (2C), dmbC6; 156.8 (2C), 157.0 (2C), dmbC2; 158.7 (2C), C6; 162.7 (2C), C2; 179.6 (2C), C4.

Dichloro-[2,2'-bi-(5S,8R)-5,6,7,8-tetrahydro-8,9,9-trimethyl-5,8-methanoquinazoline-N3,N3']-palladium(II) (77).

A hot solution of $PdCl_2$ (5mg) in HCl (3ml) was added dropwise to a hot solution of **42** (11mg, 0.06mMol) in methanol (8ml). The resultant pale yellow precipitate of **77** was filtered

and air dried. Yield 9mg (26%). Calcd for $C_{24}H_{30}N_4Cl_2Pd.1.5H_2O$ C: 49.80, H: 5.74, N: 9.68. Found C: 50.21, H: 5.46, N: 9.76.

[2,2'-bi-(5S,8R)-5,6,7,8-tetrahydro-8,9,9-trimethyl-5,8-methanoquinazoline-N3,N3']-tetracarbonyl-molybdenum (78).

A green solution of $Mo(CO)_4C_7H_8$ (12mg, 0.04mMol) in dry THF was added dropwise(4ml), with stirring, to a solution of **42** (20mg, 0.05mMol) in dry THF (10ml). The solution rapidly became deep red and was stirred for 1 hour then diluted with petroleum ether (6ml) and cooled (0°C) overnight. The resultant red precipitate of **78** was filtered and dried. Yield 10mg (43%). Similarly, a two-fold excess of $Mo(CO)_4C_7H_8$ (24mg, 0.08mMol) gave **78**. Yield 13mg (56%). ^{1}H NMR ($CDCl_3$) δ: 0.65 (6H), syn-9-CH_3; 1.09 (6H), anti-9-CH_3; 1.27 (2H), endo-H6; 1.42 (2H), endo-H7; 1.47 (6H), 8-CH_3; 2.04 (2H), exo-H7; 2.30 (2H), exo-H6; 3.07 (2H), H5; 8.81 (2H), H4.

Bis-(4,4'-dimethyl-2,2'-bipyridine)-[2,2'-bi-(5S,8R)-5,6,7,8-tetrahydro-8,9,9-trimethyl-5,8-methanoquinazoline-N3,N3']-ruthenium(II)-bis-(hexafluorophosphate) (79).

Ligand **42** (27.9mg, 0.074mMol) was reacted with $Ru(dmb)_2Cl_2.2H_2O$ (39mg, 0.068mMol) and the resultant solid recrystallised from acetonitrile/ether, as described above, to give orange crystals of **79**. Yield 75mg (91%). Calcd for $C_{52}H_{60}N_{10}P_2F_{12}Ru.2CH_3CN$ C: 51.36, H: 4.97, N: 11.52. Found C: 51.04, H: 5.06, N: 11.34. FAB mass spectrum: calcd for $[C_{48}H_{54}N_8PF_6Ru]^+$: 989.316. Found: 989.317. ^{1}H NMR showed the complex to exist as two diastereoisomers. ^{1}H NMR (CD_3CN) δ: 0.36 (6H), Δ-syn-9-CH_3; 0.77 (6H), Λ-syn-9-CH_3; 0.96 (2H), Δ-endo-H6, Λ-endo-H6, Δ-endo-H7 or Λ-endo-H7; 1.07 (6H), 1.12 (6H), Λ-anti-9-CH_3 and Δ-anti-9-CH_3; 1.22 (2H), Δ-endo-H6, Λ-endo-H6, Δ-endo-H7 or Λ-endo-H7; 1.34 (2H), Δ-endo-H6, Λ-endo-H6, Δ-endo-H7 or Λ-endo-H7; 1.41 (2H), 1.45 (2H), Δ-8-CH_3 and Λ-8-CH_3; 1.50 (2H), Δ-endo-H6, Λ-endo-H6, Δ-endo-H7 or Λ-endo-H7; 2.12-2.31 (8H), Δ-exo-H6, Λ-exo-H6, Δ-exo-H7 and Λ-exo-H7; 2.58 (24H), dmb4-CH_3; 2.98 (2H), 3.02 (2H), Λ-H5 and Δ-H5; 7.27 (8H), dmbH5; 7.51 (2H), 7.54 (4H), dmbH6; 7.65 (2H), 7.68 (2H), Λ-H4 and Δ-H4; 7.70 (2H), dmbH6; 8.39 (8H), dmbH3. ^{13}C NMR (CD_3CN) δ: 9.4 (2C), 9.5 (2C), Λ-8-CH_3 and Δ-8-CH_3; 18.2 (2C), 18.3 (2C), Λ-anti-9-CH_3 and Δ-anti-9-CH_3; 19.1 (2C), 19.8 (2C), Λ-syn-9-CH_3 and Δ-syn-9-CH_3; 20.6 (8C), dmb4-CH_3; 24.8 (2C), 24.9 (2C), Λ-C6 and Δ-C6; 31.0 (2C), 31.1 (2C), Λ-C7 and Δ-C7; 49.7 (2C), 49.8 (2C), Λ-C5 and Δ-C5; 55.5 (4C), Λ-C9 and Δ-C9; 58.1 (2C), 58.2 (2C), Λ-C8 and Δ-C8; 125.1_6 (4C), 125.2_3 (2C),

125.3 (2C), dmbC3; 128.5 (4C), 128.6 (2C), 128.7 (2C), dmbC5; 141.8 (4C), Λ-C4a and Δ-C4a; 148.7 (2C), 149.0 (2C), Λ-C4 and Δ-C4; 150.5 (2C), 150.6 (4C), 150.6_4 (2C), dmbC4; 151.0 (2C), 151.1 (2C), 151.4 (2C), 151.7 (2C), dmbC6; 156.8_5 (2C), 156.9_2 (2C), 157.0 (4C), dmbC2; 162.1 (4C), Λ-C2 and Δ-C2; 180.5 (2C), 180.6 (2C), Λ-C8a and Δ-C8a.

Dichloro-mercury(II)-bis-(4,4'-dimethyl-2,2'-bipyridine)-μ-[2,2'-bi-(5S,8R)-5,6,7,8-tetrahydro-8,9,9-trimethyl-5,8-methanoquinazoline-N1,N1'-N3,N3']-ruthenium(II)-bis-(hexafluorophosphate) (80).

A solution of $HgCl_2$ (4.8mg, 0.18mMol) in acetone (5ml) was added dropwise to a stirred solution of **42** (20mg, 0.018mMol) in dichloromethane (10ml). The resultant purple solution was concentrated to 5ml and ether (5ml) was added to give a purple precipitate of **80**, which was filtered and air dried. Yield 16mg (65%). ^{1}H NMR (CD_3CN) δ: 0.36 (6H), Δ-syn-9-CH_3; 0.77 (6H), Λ-syn-9-CH_3; 0.96 (2H), Δ-endo-H6, Δ-endo-H6, Λ-endo-H7 or Λ-endo-H7; 1.07 (6H), 1.12, Λ-anti-9-CH_3 and Δ-anti-9-CH_3; 1.22 (2H), Δ-endo-H6, Δ-endo-H6, Λ-endo-H7 or Λ-endo-H7; 1.34 (2H), Δ-endo-H6, Δ-endo-H6, Λ-endo-H7 or Λ-endo-H7; 1.48 (2H), 1.52 (2H), Δ-8-CH_3 and Λ-8-CH_3; 1.50 (2H), Δ-endo-H6, Δ-endo-H6, Λ-endo-H7 or Λ-endo-H7; 2.12-2.31 (8H), Δ-exo-H6, Λ-exo-H6, Δ-exo-H7 and Λ-exo-H7; 2.58 (24H), dmb4-CH_3; 2.99 (2H), 3.02 (2H), 3.06 (2H), Λ-H5 and Δ-H5; 7.28 (6H), 7.29 (2H), dmbH5; 7.50 (2H), 7.53 (4H), dmbH6; 7.70 (4H), dmbH6 and Λ-H4 or Δ-H4; 7.74 (2H), Λ-H4 or Δ-H4; 8.39 (8H), dmbH3.

Bis-(2,2'-bipyridine)-[2,4-bis-(1-pyrazolyl)pyrimidine-N1,N2']-ruthenium(II)-bis-(hexafluorophosphate) (87).

2,4-Bis-(1-pyrazolyl)pyrimidine (**53**) (15.7mg, 0.074mMol) was reacted with $Ru(bpy)_2Cl_2.2H_2O$ (35mg, 0.067mMol) as described above. Complex **87** was obtained as an orange solid. Yield 59mg (88%). FAB mass spectrum: calcd for $[C_{30}H_{24}N_{10}PF_6Ru]^+$: 771.0871. Found: 771.0869. ^{1}H NMR (CD_3CN) δ: 6.78, H4''; 6.89, H4'; 7.42, bpyH5a; 7.46, bpyH5b; 7.50, H3'; 7.55, bpyH5d; 7.57, bpyH5c; 7.79 (2H), H5 and bpyH6a; 7.83, bpyH6b; 7.86, H6; 8.01, H3''; 8.02, bpyH6c; 8.10, bpyH4a; 8.13, bpyH4b; 8.17 (2H); bpyH4c and bpyH4d; 8.24, bpyH6d; 8.53, bpyH3a; 8.56 (3H), bpyH3b, bpyH3c and bpyH3d; 8.90, H5''; 9.06, H5'.

Bis-(4,4'-dimethyl-2,2'-bipyridine)-[2,4-bis-(1-pyrazolyl)pyrimidine-N1,N2']-ruthenium(II)-bis-(hexafluorophosphate) (88).

2,4-Bis-(1-pyrazolyl)pyrimidine (**53**) (14mg, 0.066mMol) was reacted with $Ru(dmb)_2Cl_2.2H_2O$ (35mg, 0.061mMol) as described above. The resultant brown solid was

recrystallised form acetonitrile/ether to give **88** as a microcrystalline product. Yield 51mg (80%). FAB mass spectrum: calcd for $[C_{34}H_{32}N_{10}PF_6Ru]^+$: 827.1497. Found: 827.1494. ^1H NMR (CD_3CN) δ: 2.58 (3H), 2.59 (3H), 2.61 (3H), 2.62 (3H), dmb4-CH_3; 6.78, H4"; 6.88, H4'; 7.25, dmbH5a; 7.29, dmbH5b; 7.34, dmbH5c; 7.38, dmbH5d; 7.47, H3'; 7.59, dmbH6a; 7.62, dmbH6b; 7.79, H5; 7.82, dmbH6c; 7.87, H6; 8.00, H3"; 8.03, dmbH6d; 8.37, dmbH3a; 8.40 (3H), dmbH3b, dmbH3c and dmbH3d; 8.89, H5"; 9.04, H5'.

Tri-[2,4-bis-(1-pyrazolyl)pyrimidine-N1,N2']-ruthenium(II) -bis-(hexafluorophosphate) (89).

2,4-Bis-(1-pyrazolyl)pyrimidine (**53**) (20mg, 0.094mMol) was reacted with $Ru(DMSO)_4Cl_2$ (13.8mg, 0.029mMol) as described above. Complex **89** was obtained as a yellow solid and recrystallised from acetonitrile/ether. Yield 20mg (67%). FAB mass spectrum: calcd for $[C_{30}H_{24}N_{18}PF_6Ru]^+$: 883.1117. Found: 883.1115. ^1H NMR (CD_3CN) δ: 6.80 (4H), H4"; 6.93 (2H), 6.96 (2H), H4'; 7.67, 7.72, H3'; 7.83, 7.86 (3H), H5; 7.89, 7.91, H3'; 8.02 (2H), 8.03 (2H), H3"; 8.06, 8.09, 8.33, 8.35, H6; 8.91 (4H), H5"; 9.05, 9.07, 9.08, 9.09, H5'.

Dichloro-[2-(2-pyridinyl)perimidine-N3,N1']-palladium(II) (96).

A hot solution of **93** (29.4mg, 0.12mMol) in methanol (8ml) was added dropwise to a hot solution of palladium chloride (20mg, 0.11mMol) in HCl (7ml). The resultant brown precipitate of **96** was filtered and dried in a vacuum desiccator. Yield 35mg (75%). Calcd for $C_{16}H_{11}N_3Cl_2Pd$ C: 45.47, H: 2.62, N: 9.94. Found C: 45.70, H: 2.73. N: 9.68. ^1H NMR (DMSO-d_6)-tentative assignments-δ: 6.87, H9; 7.18, H4; 7.29 (4H), H5, H6, H7 and H8; 7.85, H5'; 8.22, H4'; 8.56, H3'; 8.87, H6; 11.95, H1.

Tetracarbonyl-[2-(2-pyridinyl)perimidine-N3,N1']-molybdenum (97).

A mixture of **93** (52mg, 0.21mMol) and $Mo(CO)_6$ (55mg, 0.21mMol) in argon purged toluene (5ml) was refluxed for 1.5 hours under an argon atmosphere. The solution was cooled to room temperature, diluted with ether (20ml) and cooled (0°C) overnight. Purification attempts by chromatography on alumina (eluent-acetone) or by recrystallisation (acetone/ether or THF/ether) resulted in dissociation of the complex. ^1H NMR (DMSO-d_6) δ: 6.89, H9; 7.35, H8; 7.37, H7; 7.41, H6; 7.46, H5; 7.62, H4; 7.89, H5'; 8.42, H4'; 8.71, H3'; 9.21, H6'; 11.53, H1.

Bis-(2,2'-bipyridine)-[2-(2-pyridinyl)perimidine-N3,N1']-ruthenium(II)-bis-(hexafluorophosphate) (98).

Ligand **93** (13.5mg, 0.055mMol) was reacted with $Ru(bpy)_2Cl_2.2H_2O$ (26mg, 0.050mMol) as described above. Complex **98** was obtained as a black solid. Yield 34mg (72%). ^1H NMR (CD_3CN) δ: 5.84, H4; 6.63, H5; 6.81, H9; 7.09, H6; 7.16, H7; 7.25, H8; 7.35, 7.43, bpyH5; 7.47, H5'; 7.57, bpyH5; 7.58, bpyH6; 7.63 (2H), H6' and bpyH5; 7.72, 7.85, bpyH6; 8.09, 8.11, 8.05, bpyH4; 8.17 (2H), H4' and bpyH4; 8.45, 8.48, 8.52, bpyH3; 8.56, H3'; 8.62, bpyH4; 8.85, bpyH6; H1 not observed.

Bis-(4,4'-dimethyl-2,2'-bipyridine)-[2-(2-pyridinyl)perimidine-N3,N1']-ruthenium(II)-bis-(hexafluorophosphate) (99).

Ligand **93** (13.5mg, 0.055mMol) was reacted with $Ru(dmb)_2Cl_2.2H_2O$ (28.8mg, 0.050mMol) as described above. Complex **99** was isolated as a black solid. Yield 43mg (86%). ^1H NMR (CD_3CN) δ: 2.56 (3H), 2.57 (3H), 2.58 (3H), 2.63 (3H), dmb4-CH_3; 5.96, H4; 6.70, H5; 6.89, H9; 7.17, H6; 7.19, dmbH5a; 7.22, H7; 7.27, dmbH5b; 7.29, H8; 7.38, dmbH5c; 7.40, dmbH5d; 7.41, dmbH6a; 7.47, H5'; 7.52, dmbH6b; 7.65, dmbH6c; 7.66, H6'; 8.16, H4'; 8.31, dmbH3b; 8.33, dmbH3c; 8.40, dmbH3a; 8.45, dmbH3d; 8.58, H3'; 8.61, dmbH6d; H1-not observed.

Dichloro-[1-methyl-2-(2-pyridinyl)perimidine]-palladium(II) (100).

Palladium chloride (21.2mg, 0.12mMol) was dissolved in hot HCl (5ml) and added dropwise to a hot solution of **94** (32.3mg, 0.13) in methanol (5ml). The resultant brown precipitate was filtered, dried in a vacuum desiccator and dissolved in the minimum volume of DMF. A layer of methanol was carefully added and after 2 days crystals suitable for x-ray were obtained. Yield 17mg (32%). ^1H NMR (DMSO-d_6) δ: 3.33 (3H), 1-CH_3; 7.05 (2H), H4 and H9; 7.54, 7.56, H5 and H8; 7.59, 7.64, H6 and H7; 7.89, H5'; 8.12, H3'; 8.30, H4'; 8.98, H6'.

Bis-(4,4'-dimethyl-2,2'-bipyridine)-[1-methyl-2-(2-pyridinyl)perimidine]-ruthenium(II)-bis-(hexafluorophoshate) (101).

1-Methyl-2-(2-pyridinyl)perimidine (**94**) (14.3mg, 0.055mMol) was reacted with $Ru(dmb)_2Cl_2.2H_2O$ (30mg, 0.052mMol), as described above, to give **101** as a brown solid. Yield 39mg (74%). FAB mass spectrum: calcd for $[C_{41}H_{37}N_7PF_6Ru]^+$: 874.180. Found: 874.182.^1H NMR (CD_3CN) δ: 2.54 (3H), 2.58 (6H), 2.64 (3H), dmb4-CH_3; 3.74, 1-CH_3; 6.13, H4; 6.71, H9; 6.77, H5; 7.19, dmb5Ha; 7.25, H6; 7.28, dmbH5b; 7.31, H7; 7.36,

dmbH5d; 7.39, H8; 7.40, H5'; 7.46, dmbH5c; 7.48, dmbH6a; 7.62, dmbH6b; 7.69, H6'; 7.92, dmbH6c; 8.08, H4'; 8.25, dmbH3b; 8.30, dmbH3c; 8.33, H3'; 8.41, dmbH6d; 8.46, dmbH3a; 8.51, dmbH3d. ^{13}C NMR (CD_3CN) δ: 20.5, 20.6 (2C), 20.7, dmb4-CH_3; 42.3, 1-CH_3; 106.2, C9; 114.8, C4; 120.7, C9b; 121.8, C7; 123.5, C8; 124.8_0, 124.8_3, 125.5_7, 125.6_3, dmbC3; 125.6, 128.0, C3' and C5'; 128.0, 128.5, 128.5_6,128.6_1, dmbC5; 128.9, C6; 129.6, C5; 134.7, C6a; 136.8, C4'; 142.1, C3a; 147.5, C9a; 150.5 (3C), dmbC6 and dmbC4; 150.6, 150.8, dmbC4; 151.7, 152.3, 152.7, dmbC6; 153.9, C6'; 155.7, C2'; 157.0, 157.1, 157.3, 157.8, dmbC2; 161.4, C2.

Chloro-tris-[1-methyl-2-(2-pyridinyl)perimidine-N3,N3,N1',N1',N1']-ruthenium(II)-hexafluorophoshate (102).

Ligand **94** (30mg, 0.116mMol) was reacted with $Ru(DMSO)_4Cl_2$ (17mg, 0.035mMol) as described above. The resultant solid was chromatographed on a column of alumina (8x2cm) and eluted with methanol/chloroform (1:50) as a purple band. The band was collected and the solvent removed *in vacuo* to give **102** as a purple solid. Yield 22mg (59%). FAB mass spectrum: calcd for $[C_{51}H_{39}N_9ClRu]^+$: 879.237. Found: 879.235. ^1H NMR ($(CD_3)_2CO$) δ: 2.91 (3H), 2.93 (3H), 1a-CH_3 and 1b-CH_3; 4.33 (3H), 1c-CH_3; 6.38, H4a; 6.46, H4b; 6.56 (2H), H9a and H9b; 6.97, H5c; 7.03 (2H), H5b and H9c; 7.07, H5a; 7.33, H4c; 7.47, H6c; 7.43 (2H), H8a and H8b; 7.47 (2H), H6a and H7c; 7.48, H6b; 7.55, H7a or H7b; 7.57, H8c; 7.58, H7a or H7b; 7.70, H5'c; 7.79, 7.81, H5'a and H5'b; 8.28 (2H), H4'a and H4'b; 8.37, H4'c; 8.38, 8.41, H3'a and H3'b; 8.76, H6'a or H6'b; 8.88, H6'c; 9.02, H3'c; 9.29, H6'a or H6'b. Notation a-c refers to spin systems of pyridine and perimidine rings.

Dichloro-2-(2-pyrimidinyl)perimidine-palladium(II) (105).

Palladium chloride (14.1mg, 0.08mMol) was dissolved in hot HCl (5ml) and added dropwise to a hot solution of **95** (20mg, 0.081mMol) in methanol (5ml). The resultant grey precipitate of **105** was filtered and dried. Elemental analyses of the complex were unsatisfactory. Yield 25mg (73%).

Bis-(4,4'-dimethyl-2,2'-bipyridine)-[2-(2-pyrimidinyl)perimidine]-ruthenium(II)-bis-(hexafluorophoshate) (106).

2-(2-Pyrimidinyl)perimidine (**95**) (11.4mg, 0.046mMol) was reacted with $Ru(dmb)_2Cl_2.2H_2O$ (25.0mg, 0.043mMol), as described above, to give **106** as a brown solid.

Yield 42 (97%). FAB mass spectrum: calcd for $[C_{39}H_{34}N_8PF_6Ru]^+$: 861.1592. Found: 861.1592. ^1H NMR (CD_3CN) δ: 2.57 (3H), 2.58 (3H), 2.60 (3H), 2.63 (3H), dmb4a-CH_3, dmb4b-CH_3, dmb4c-CH_3 and dmb4d-CH_3; 5.76, H4; 6.71, H5; 6.84, H9; 7.19, H6; 7.22 (2H), H7 and dmbH5a; 7.29, H8; 7.30, dmbH5b; 7.41 (2H), dmbH5c, dmbH6a; 7.44, dmbH5d; 7.52, H5'; 7.63, dmbH6b; 7.65, dmbH6c; 7.92, H6'; 8.36 (2H), dmbH3b, dmbH3c; 8.38, dmbH3a; 8.43, dmbH3d; 8.65, dmbH6d; 9.02, H4'.

4,6-Bis-(2-pyridinyl)pyrimidine-dichloro-palladium(II) (114).

Palladium chloride (15mg, 0.086mMol) was dissolved in hot HCl (5ml) and added dropwise to a hot solution of **109** (20mg, 0.086) in methanol (5ml). The resultant precipitate was filtered and dried in a vacuum desiccator. Yield 28mg. Elemental analysis indicated a mixture of monopalladium (**114**) and dipalladium complexes (**115**). Calcd for $C_{14}H_{10}N_4Cl_2Pd$ C: 40.86, H: 2.45, N:13.61. Found C: 30.45, H: 2.15, N: 10.17.

μ-(4,6-Bis-(2-pyridinyl)pyrimidine)-tetrachloro-dipalladium(II) (115).

A hot solution of **109** (10mg, 0.043) in methanol (5ml) was added dropwise to a hot solution of palladium chloride (15.2mg, 0.086mMol) in HCl (5ml). The resultant yellow precipitate of **115** was filtered and dried in a vacuum desiccator. Yield 20.9mg (83%). Calcd for $C_{14}H_{10}N_4Cl_2Pd_2.H_2O$ C: 27.77, H: 1.99, N: 9.23. Found C: 27.87, H: 1.55, N: 9.25.

4,6-Bis-(2-pyridinyl)pyrimidine-tetracarbonyl-molybdenum(0) (116).

A mixture of **109** (60mg, 0.256mMol) and $Mo(CO)_6$ (66mg, 0.250mMol), in toluene, (10ml) was degassed for 1 hour, then refluxed for 2 hours under an argon atmosphere. The resultant blue solution was cooled to room temperature, evaporated to dryness *in vacuo*, and the residue extracted with acetone. The acetone extract was filtered and the filtrate absorbed onto an alumina column (2.5x20cm). The mononuclear complex was eluted with acetone as a purple band, collected and concentrated *in vacuo* to a volume less than 1ml. The solution was diluted with ether (5ml) and petroleum ether (5ml) to give a purple precipitate of **116** which was filtered and air dried. Yield 80mg (72%). Calcd for $C_{18}H_{10}N_4O_4Mo$ C: 48.89, H: 2.28, N: 12.67. Found C: 49.09, H: 2.26, N: 13.02. ^1H NMR ($(CD_3)_2CO$) δ: 7.80, H5"; 7.95, H5'; 8.25, H4"; 8.46, H4'; 8.78, H3"; 8.98, H6"; 9.10, H3'; 9.36, H6'; 9.51, H5; 9.85, H2. ^1H NMR (DMSO-d_6) δ: 7.78, H5"; 7.96, H5'; 8.23, H4"; 8.46, H4'; 8.77, H3"; 8.97, H6"; 9.09, H3'; 9.36, H6'; 9.47, H5; 9.85, H2.

μ-4,6-Bis-(2-pyridinyl)pyrimidine-octacarbonyl–dimolybdenum(0) (117).

A mixture of **109** (40mg, 0.17mMol) and $Mo(CO)_6$ (212.2mg, 0.80mMol), in argon purged toluene (5ml), was refluxed for 6 hours under an argon atmosphere. The green solution was cooled to room temperature, diluted with ether (20ml) and cooled (0°C) overnight. The resultant blue precipitate was filtered and air dried. The product was dissolved in acetone and eluted down a column of alumina (2.5x20cm). The blue band, which separated from traces of the pink mononuclear complex, was collected and the acetone concentrated (20ml). Petroleum ether (5ml) was added and the solution cooled (0°C) to give **117** as a dark blue microcrystalline solid. Yield 62mg (56%). Calcd for $C_{22}H_{10}N_4O_8Mo_2$ C: 40.64, H: 1.55, N: 8.62. Found C: 40.30, H: 1.48, N: 8.82. ^1H NMR ($(CD_3)_2CO$) δ: 7.98 (2H), H5'; 8.47 (2H), H4'; 9.22 (2H), H3'; 9.38 (2H), H6'; 9.73, H5; 10.37, H2. ^1H NMR (DMSO-d_6) δ: 7.93 (2H), H5'; 8.50 (2H), H4'; 9.21 (2H), H6'; 9.26 (2H), H3'; 9.70, H5; 9.97, H2.

Reaction of 109 with copper(II) chloride.

To a solution of $CuCl_2.2H_2O$ (54.58mg, 0.320mMol) in methanol (5ml) was added **109** (25mg, 0.107mMol) in methanol (5ml). The resultant green precipitate was filtered and air dried. Yield 14mg (24%). Calcd for $C_{14}H_{10}N_4Cl_4Cu_2.2H_2O$ C: 31.19, H: 2.60, N: 10.39. Found C: 31.16, H: 2.02, N: 10.29.

Reaction of 109 with copper(II) perchlorate.

To a solution of $Cu(ClO_4)_2.6H_2O$ (52.4mg, 0.140mMol) in acetonitrile (2ml) was added **109** (16.6mg, 0.070mMol) in acetonitrile (2ml). After standing for 3 days, the blue solution deposited a blue solid which was filtered and air dried. Additional product precipitated from the filtrate when cooled (0°C) overnight. Yield 25mg (64%). Calcd for $C_{14}H_{14}N_4O_{10}Cl_2Cu$ C: 31.27, H: 2.62, N: 10.42. Found C: 30.65, H: 2.35, N: 10.31.

Reaction of 109 with nickel(II) perchlorate.

To a solution of $Ni(ClO_4)_2.6H_2O$ (34.37mg, 0.094mMol) in methanol (5ml) was added **109** (11mg, 0.047mMol) in methanol (5ml). The resultant pale yellow precipitate was filtered and air dried. Yield 21mg (85%). Calcd for $C_{14}H_{14}N_4O_{10}Cl_2Ni$ C: 31.87, H: 2.67, N: 10.61. Found C: 32.11, H: 2.79, N: 10.77.

Bis-(2,2'-bipyridine)-4,6-bis-(2-pyridinyl)pyrimidine-ruthenium(II)-bis-(hexafluorophosphate) (119).

4,6-Bis-(2-pyridinyl)pyrimidine (**109**) (40mg, 0.171mMol) was reacted with $Ru(bpy)_2Cl_2.2H_2O$ (80.8mg, 0.155mMol) as described above. The solid was chromatographed on a column of alumina (8x2.5cm). The product was eluted with dichloromethane/methanol (100:1) as a red band which was collected and the solvent removed *in vacuo* to give **119** as a red solid. Yield 101mg (69%). Calcd for $C_{34}H_{26}N_8P_2F_{12}Ru.H_2O$ C: 42.73, H: 2.95, N: 11.72. Found C: 42.86, H: 2.68, N: 11.72. FAB mass spectrum: calcd for $[C_{34}H_{26}N_8PF_6Ru]^+$: 793.0966. Found: 793.0968. ^1H NMR (CD_3CN) δ: 7.47, 7.48 (2H), 7.49, bpyH5; 7.59, H5'; 7.65, H5"; 7.78 (2H), 7.84, bpyH6; 7.90, H6'; 8.01, bpyH6; 8.06, H4"; 8.14 (4H), bpyH4; 8.20, H4'; 8.51, H3"; 8.54, H2; 8.58 (4H), bpyH3; 8.88, H6"; 8.89, H3'; 9.42, H5. ^{13}C NMR (CD_3CN) δ: 115.0, C5; 122.6 C3"; 124.7 (2C), 124.7_7, 124.8, bpyC3; 126.8, C3'; 127.3, C5"; 127.9, 128.0, 128.1 (2C) bpyC5; 129.8, C5'; 138.3 (2C), C4" and bpyC4; 138.4 (4C), C4' and bpyC4; 150.6, C6"; 151.9, C6'; 152.2, C2"; 152.3, 152.4, 152.6_7, 152.7_4, bpyC6; 155.8, C2'; 157.3 (2C), 157.4 (2C), bpyC2; 160.2, C2; 163.9, C6; 165.2, C4. In addition, the binuclear complex **121** was eluted with dichloromethane/methanol (10:1) as a purple band, which was collected and the solvent removed *in vacuo* to give a purple/black solid. Yield 20mg (7%).

Bis-(4,4'-dimethyl-2,2'-bipyridine)-4,6-bis-(2-pyridinyl)pyrimidine-ruthenium(II)-bis-(hexafluorophosphate).(120)

4,6-Bis-(2-pyridinyl)pyrimidine (**109**) (40mg, 0.171mMol) was reacted with $Ru(dmb)_2Cl_2.2H_2O$ (110mg, 0.155mMol) as described above. The resultant solid was chromatographed on a column of alumina (8x2.5cm). The product was eluted with dichloromethane/methanol (100:1) as a red band which was collected and solvent removed *in vacuo* to give **120** as a red solid. Yield 65mg (42%). Calcd for $C_{38}H_{34}N_8P_2F_{12}Ru.H_2O$ C: 45.93, H: 3.45, N: 11.28. Found C: 44.92, H: 3.43, N: 11.34. FAB mass spectrum: calcd for $[C_{38}H_{34}N_8PF_6Ru]^+$: 849.1592. Found: 849.1597. ^1H NMR (CD_3CN) δ: 2.58 (6H), dmb4-CH_3; 2.60 (6H), dmb4-CH_3; 7.28 (2H), 7.32 (2H), dmbH5; 7.57 (2H), dmbH6 and H5'; 7.59, 7.64, dmbH6; 7.65, H5"; 7.79, dmbH6; 7.90, H6'; 8.06, H4"; 8.17, H4'; 8.42 (4H), dmbH4; 8.51, H3"; 8.52, H2; 8.86, H3'; 8.88, H6"; 9.39, H5. ^{13}C NMR (CD_3CN) δ: 20.6 (4C), dmb4-CH_3; 114.9, C5; 122.5, C3"; 125.3 (2C), 125.4 (2C), dmbC3; 126.7, C3'; 127.2, C5";

128.5, 128.7 (3C), dmbC5; 129.6, C5'; 138.3, C4'; 140.0, C4"; 150.6, 150.8_6, 150.9_2, 150.9_6, 151.2_7, 151.3_4, 151.4, 151.8, C6", dmbC4 and dmbC6 or C6"; 152.3, C2"; 152.6, C6' or dmbC6; 156.0, C2'; 156.8 (2C), 156.9 (2C), dmbC2; 160.1, C2; 163.4, C6; 165.4, C4. In addition the binuclear complex **122** was eluted with dichloromethane/methanol (10:1) as a purple band which was collected and solvent removed *in vacuo* to give a purple solid. Yield 5mg (1.6%).

Tri-[4,6-bis-(2-pyridinyl)pyrimidine]-ruthenium(II)-bis-(hexafluorophosphate) (123).

4,6-Bis-(2-pyridinyl)pyrimidine (**109**) (50.0mg, 0.213mMol) was reacted with $Ru(DMSO)_4Cl_2$ (31.3mg, 0.065mMol) as described above. The resultant red solid was chromatographed on a column of alumina (8x2.5cm). The product **123** was eluted with dichloromethane/methanol (100:1) as a red band which was collected and solvent removed *in vacuo* to give a red solid. Yield 59mg (83%). FAB mass spectrum: calcd for $[C_{42}H_{30}N_{12}PF_6Ru]^+$: 949.1402. Found: 949.1401. The ^1H NMR spectrum of **123** indicated a 3:1 mixture of meridonal and facial isomers. Attempts to separate the two isomers on sephadex, using NaCl (0.01M-0.05M) eluent, were unsuccessful. ^1H NMR (CD_3CN) δ: 7.62 (4H), H5'; 7.70 (2H), 7.72 (2H), H5"; 7.83, 7.92, 8.10, H6'; 8.12 (4H), H4"; 8.16, H6'; 8.25 (4H), H4'; 8.51, H2; 8.54 (4H), H3"; 8.59, 8.82, 8.88, H2; 8.91 (4H), H6"; 8.95, 8.97 (3H), H3'; 9.57 (3H), 9.58, H5. ^1H NMR ($(CD_3)_2CO$) δ: 7.78 (4H), H5'; 7.90 (4H), H5"; 8.19 (4H), H4"; 8.34, 8.44, H6'; 8.50 (2H), 8.51 (2H), H4'; 8.61 (2H), 8.62 (2H), H3"; 8.66, 8.74, H6'; 8.88, 8.97, H2; 8.99 (4H), H6"; 9.25, 9.30, H2; 9.42 (3H), 9.43, H3'; 9.68, 9.69, 9.70, 9.71, H5. ^{13}C NMR (CD_3CN) δ: 115.5, 115.5_5, 115.6, 115.7, C5; 123.0 (4C), C3"; 127.1, 127.2 (2C), 127.3, C5"; 127.6 (4C), C3'; 129.9 (2C), 130.2 (2C), C5'; 139.0 (2C), 139.1 (4C), 139.2 (2C), C4' and C4"; 150.0_5, 150.1, 150.1_6, 150.2, C6"; 151.7 (4C), C2"; 152.9, 153.3, 153.4, 153.8, C6'; 155.6 (2C), 155.7 (2C), C2'; 160.2, 160.6, 160.7, 161.1, C2; 163.8 (4C), C6; 165.1 (2C), 165.2 (2C), C4.

Tetrakis-(2,2'-bipyridine)-μ-4,6-bis-(2-pyridinyl)pyrimidine-diruthenium(II)-tetrakis-(hexafluorophosphate) (121).

4,6-Bis-(2-pyridinyl)pyrimidine (**109**) (20mg, 0.0854mMol) was reacted with $Ru(bpy)_2Cl_2.2H_2O$ (82.7mg, 0.171mMol) and the product recrystallised from ether/acetonitrile, as described above. Complex **121** was obtained as a dark purple microcrystalline solid. Yield

115mg (82%). FAB mass spectrum: calcd for $[C_{54}H_{42}N_{12}P_3F_{18}Ru_2]^+$: 1497.0668. Found: 1497.0662. The ^1H NMR spectrum of **121** indicated a 7:6 mixture of two diastereoisomers, **121a** and **121b**. The binuclear complex (5mg) was dissolved in 2-3 drops of water/acetonitrile (2:1) and absorbed onto C-25 sephadex. The column was eluted with NaCl (0.1M), followed by NaCl (0.3-0.5M) to give a purple band which was split into five fractions. Each fraction was treated with aqueous NH_4PF_6 and the resultant purple precipitate filtered and air dried. ^1H NMR analysis showed that the first fraction was slightly enriched in diastereoisomer **121a**, whereas the fifth fraction was slightly enriched in diastereoisomer **121b**. Fractions two to four showed no enrichment. Recrystallisation of the first and fifth fractions from ether/acetonitrile failed to achieve a greater enrichment of either isomer. Racemic diastereoisomer ($\Delta\Delta/\Lambda\Lambda$) **121a**: ^1H NMR (CD_3CN) δ: 7.13 (2H), 7.23 (2H), 7.25 (2H), 7.39 (2H), bpyH5; 7.48 (2H), 7.52 (2H), 7.55 (4H), bpyH6; 7.59 (2H), H5'; 7.70, H2; 7.80 (2H), H6'; 7.99 (2H), 8.08 (2H), 8.11 (2H), 8.18 (2H), bpyH4; 8.26 (2H), H4'; 8.36 (2H), 8.44 (2H), 8.53 (2H), 8.55 (2H), bpyH3; 9.04 (2H), H3'; 9.33, H5. Meso diastereoisomer ($\Delta\Lambda$) **121b**: ^1H NMR (CD_3CN) δ: 7.22 (2H), 7.23 (2H), 7.27 (2H), 7.44 (2H), bpyH5; 7.60 (6H), bpyH6; 7.62 (2H), H5'; 7.66, H2; 7.82 (2H), bpyH6; 7.87 (2H), H6'; 7.97 (2H), 8.10 (2H), 8.12 (2H), 8.20 (2H), bpyH4; 8.30 (2H), H4'; 8.46 (2H), 8.49 (2H), 8.51 (2H), 8.52 (2H), bpyH3; 9.04 (2H), H3'; 9.35, H5.

Tetrakis-(4,4'-dimethyl-2,2'-bipyridine)-μ-4,6-bis-(2-pyridinyl)pyrimidine-diruthenium(II)-tetrakis-(hexafluorophosphate) (122).

4,6-Bis-(2-pyridinyl)pyrimidine (**109**) (10mg, 0.042mMol) was reacted with $Ru(dmb)_2Cl_2.2H_2O$ (54.2mg, 0.094mMol) and the product was recrystallised from acetonitrile/ether, as described above. Complex **122** was obtained as a dark purple microcrystalline solid. Yield 75mg (94%). FAB mass spectrum: calcd for $[C_{62}H_{58}N_{12}P_3F_{18}Ru_2]^+$: 1609.192. Found: 1609.194. The ^1H NMR spectrum of **122** indicated the presence of two diastereoisomers, **122a** and **122b**, in a ratio 5:3, although neither could be assigned to the meso or racemic form. ^1H NMR (CD_3CN) Bridging ligand isomer **122a** δ: 7.56 (2H), H5'; 7.78 (2H), H6'; 7.97, H2; 8.23 (2H), H4'; 9.01 (2H), H3'; 9.32, H5. Bridging ligand isomer **122b** δ: 7.58 (2H), H5'; 7.84 (2H), H6'; 8.26 (2H), H4'; 7.97, H2; 9.02 (2H), H3'; 9.33, H5. Dmb ligands of **122** δ: 2.53 (6H), 2.55 (12H), 2.57 (12H), 2.62 (12H), 2.65 (6H), dmb4-CH_3; 6.97 (2H), 6.99 (4H); dmbH5; 7.05 (2H), 7.06 (2H), dmbH6; 7.12 (2H), 7.23 (2H), dmbH5; 7.23 (2H), dmbH6; 7.25 (2H), dmbH5; 7.28 (2H), 7.37 (4H),

dmbH6; 7.42 (4H), dmbH5; 7.54 (2H), dmbH6; 8.03 (2H), dmbH6; 8.12 (2H), 8.17 (2H), 8.19 (2H), dmbH3; 8.35 (2H), 8.37 (2H), 8.38 (6H), dmbH3.

Bis-(2,2'-bipyridine)-bis-(4,4'-dimethyl-2,2'-bipyridine)-μ-4,6-bis-(2-pyridinyl)pyrimidine-diruthenium(II)-tetrakis-(hexafluorophosphate) (124).

Complex **120** (17mg, 0.0136mMol) was reacted with $Ru(bpy)_2Cl_2.2H_2O$ (4.4mg, 0.008mMol) as described above and the product recrystallised from acetonitrile/ether as described above. Complex **124** was obtained as a dark purple solid. Yield 22mg (95%). FAB mass spectrum: calcd for $[C_{58}H_{50}N_{12}P_3F_{18}Ru_2]^+$: 1553.1294. Found: 1553.1301. The ^1H NMR spectrum of **124** indicated the presence two diastereoisomers, **124a** and **124b**, in the ratio 7:6. The isomers were distinguished in the spectrum, but could not be assigned to either the meso or racemic forms. ^1H NMR (CD_3CN) Bridging ligand isomer **124a** δ: 7.56, H5"; 7.60, H5'; 7.75, H2; 7.77, H6"; 7.80, H6'; 8.24, H4"; 8.25, H4'; 9.04 (2H), H3' and H3"; 9.33, H5. Bridging ligand isomer **124b** δ: 7.58, H5"; 7.62, H5'; 7.81, H2; 7.85, H6"; 7.87, H6'; 8.26, H4"; 8.28, H4'; 9.04 (2H), H3' and H3"; 9.35, H5. Dmb and bpy ligands of **124** δ: 2.55 (3H), 2.56 (6H), 2.57 (3H), 2.61 (6H), 2.63 (3H), 2.65 (3H), dmb4-CH_3; 6.95 (2H), dmbH5; 7.02-7.09 (4H), dmbH5 and dmbH6; 7.13 (2H), bpyH5; 7.22-7.29 (8H), dmbH5, bpyH5 and dmbH6; 7.34-7.44 (6H), bpyH5, dmbH5 and dmbH6; 7.50-7.63 (8H), bpyH6, bpyH5; 7.84 (2H), bpyH6; 7.94 (2H) bpyH4; 8.05-8.13 (6H), bpyH4, dmbH6; 8.19-8.37 (10H), bpyH3, bpyH4, dmbH3; 8.50-8.56 (6H), bpyH3.

Dichloropalladium(II)-bis-(2,2'-bipyridine)-μ-[4,6-bis-(2-pyridinyl)pyrimidine]-ruthenium(II)-bis-(hexafluorophosphate) (125).

A solution of $Pd(PhCN)_2Cl_2$ (6.5mg, 0.017mMol) in dichloromethane was added dropwise to a solution of **119** (15.3mg, 0.016mMol) in dichloromethane. The resultant dark blue precipitate of **125** was filtered and air dried. Yield 16mg (88%). Calcd for $C_{34}H_{26}N_8P_2F_{12}C_{12}RuPd.H_2O$ C: 36.04, H: 2.49, N: 9.89. Found C: 35.48, H: 2.01, N: 10.12. FAB mass spectrum: calcd for $[C_{34}H_{26}N_8PF_6Cl_2RuPd]^+$: 968.9375. Found: 968.9372. ^1H NMR (CD_3CN) δ: 7.49, 7.51 (2H), 7.53, bpyH5; 7.71, H5'; 7.76, 7.78, 7.80, bpyH6; 7.90, H5"; 7.99, H6'; 8.04, bpyH6; 8.16, 8.19 (2H), 8.22, bpyH4; 8.29, H4'; 8.44, H4"; 8.59, 8.61 (3H), bpyH3; 8.70, H3"; 8.96, H3'; 9.05, H5; 9.10, H2; 9.26, H6". ^{13}C NMR (CD_3CN) δ: 116.5, C5; 124.8, 124.9 (3C), bpyC3; 126.1, C3" or C3'; 128.1, 128.2, 128.3, 128.4, bpyC5; 128.7, C3' or C3"; 130.23, 131.4, C5' and C5"; 138.8, C4'; 138.9, 139.0,

139.2, 139.3, bpyC4; 142.0, C4"; 151.7, 152.0, bpyC6; 152.4, C6'; 152.7, 153.0, bpyC6; 153.3, C6''; 153.8, 154.0, C2' and C2"; 156.9 (2C), 157.1 (2C), bpyC2; 159.8, C2; 161.8, C4; 167.9, C6.

Tri-[bis-2,2'-bipyridine-μ-4,6-bis-(2-pyridinyl)pyrimidine)-ruthenium(II)]-ruthenium(II)-octa-(hexafluorophosphate) (127).

Complex **123** (15mg, 0.014mMol) was reacted with $Ru(bpy)_2Cl_2.2H_2O$ (23.6mg, 0.045mMol) as described above. The resultant solid was recrystallised from acetonitrile/ether to give **127** as a black microcrystaline solid. Yield 35mg (78%).

Tetrakis-(2,2'bipyridine)-μ-2,6-bis-[6-(2-pyridinyl)-4-pyrimidinyl]pyridine-diruthenium(II)-tetrakis(hexafluorphosphate) (131).

Ligand **110** (10mg, 0.026mMol) was reacted with $Ru(bpy)_2Cl_2.2H_20$ (29.4mg, 0.057mMol) as described above. The chloride salt of **131** was absorbed onto C-25 sephadex column. Excess $Ru(bpy)_2Cl_2.2H_20$ was eluted as purple band with 0.1M NaCl. The product was eluted with 0.5M NaCl as a red band. This was collected, treated with aqueous NH_4PF_6 and the resultant red precipitate was filtered and air dried. Yield 42mg (90%). FAB mass spectrum: calcd for $[C_{63}H_{47}N_{15}P_3F_{18}Ru_2]^+$: 1652.115. Found: 1652.117. ^1H NMR(CD_3CN) δ: 7.48 (2H), 7.49 (4H), 7.50 (2H), bpyH5; 7.64 (2H), H5"; 7.79 (2H), 7.81 (2H), 7.86 (2H), bpyH6; 7.94 (2H), H6"; 8.05 (8.03) (2H), bpyH6; 8.16 (8H), bpyH4; 8.29, H4; 8.30 (2H), H4"; 8.60 (8H), bpyH3; 8.61 (2H), H2'; 8.71 (2H), H3 and H5; 9.14 (2H), H3"; 9.70 (2H), H5'.

Bis-(2,2'-bipyridine)-2,6-bis-(1-pyrazolyl)-1,5-naphthyridine-ruthenium(II)-bis-(hexafluorophosphate) (137).

Ligand **132** (15mg. 0.057mMol) was reacted with $Ru(bpy)_2Cl_2.2H_2O$ (26mg, 0.050mMol) as described above. Complex **137** was obtained as a yellow solid. Yield 44mg (91%). FAB mass spectrum: calcd for $[C_{34}H_{26}N_{10}PF_6Ru]^+$: 821.1027. Found: 821.1026. ^1H NMR (CD_3CN) δ: 6.66, H4"; 6.94, H4'; 7.32, H3'; 7.40, bpyH5b; 7.42, bpyH5d; 7.47, bpyH5a; 7.54, bpyH5c; 7.57, H8; 7.64, bpyH6a; 7.68, bpyH6b; 7.85, H3"; 8.02, H7; 8.03 (2H), bpyH4a and bpyH6c; 8.13, bpyH4b; 8.16, bpyH4c; 8.17, bpyH4d; 8.19, bpyH6d; 8.44, bpyH3a; 8.47, H3; 8.53, bpyH3c; 8.56, bpyH3b; 8.61, bpyH3d; 8.69, H4; 8.75, H5"; 9.01, H5'.

Bis-(4,4'-dimethyl-2,2'-bipyridine)-2,6-bis-(1-pyrazolyl)-1,5-naphthyridine-ruthenium(II)-bis-(hexafluorophosphate) (138).

2,6-Bis-(1-pyrazolyl)-1,5-naphthyridine (**132**) (15mg, 0.057mMol) was reacted with $Ru(dmb)_2Cl_2.2H_2O$ (29mg, 0.050mMol) as described above. The resultant solid was chromatographed on a column of alumina (2.5x8cm). Complex **138** was eluted with chloroform/methanol (25:1) as an orange band. Yield 45mg (88%). FAB mass spectrum: calcd for $[C_{38}H_{34}N_{10}PF_6Ru]^+$: 877.1653. Found: 877.1657. ^1H NMR (CD_3CN) δ: 2.52 (3H), 2.59 (3H), 2.61 (3H), 2.63 (3H), dmb4-CH_3; 6.66, H4''; 6.93, H4'; 7.22, dmbH5d; 7.24, dmbH5b; 7.27, dmbH5a; 7.29, H3'; 7.38, dmbH5c; 7.46, dmbH6a; 7,48, dmbH6b; 7.61, H8; 7.81, dmbH6c; 7.86, H3''; 7.96, dmbH6d; 8.06, H4; 8.31, dmbH3a; 8.39, dmbH3c; 8.40, dmbH3b; 8.44, dmbH3d; 8.46, H3; 8.67, H4; 8.76, H5''; 9.00, H5'.

Tetrakis-(2,2'-bipyridine)-μ-2,6-bis-(1-pyrazolyl)-1,5-naphthyridine-diruthenium(II)-tetrakis-(hexafluorophosphate) (139).

Ligand **132** (5mg. 0.019mMol) was reacted with $Ru(bpy)_2Cl_2.2H_2O$ (21mg, 0.040mMol) as described above. The product was recrystallised from acetonitrile/ether to give **139** as a red microcrystalline solid. The ^1H NMR spectrum of **139** indicated the formation of a single diastereoisomer as a major product, but also showed evidence of a minor product which may correspond to the other diastereoisomer. Yield 28mg (88%). FAB mass spectrum: calcd for $[C_{54}H_{42}N_{14}P_3F_{18}Ru_2]^+$: 1525.0729. Found: 1525.0734. ^1H NMR (CD_3CN) δ: 6.90 (2H), H4'; 7.30 (2H), H3'; 7.37 (2H), bpyH5a; 7.38 (2H) bpyH5b; 7.45 (2H), bpyH6a; 7.50 (2H), bpyH5d; 7.56 (2H), bpyH6b; 7.60 (2H), bpyH5c; 7.76 (2H), H4; 8.01 (2H), H3; 8.03 (2H), bpyH4a; 8.07 (2H), bpyH6c; 8.13 (2H), bpyH4b; 8.19 (2H), bpyH4c; 8.22 (2H), bpyH4d; 8.28 (2H), bpyH6d; 8.37 (2H), bpyH3a; 8.51 (2H), bpyH3c; 8.56 (2H), bpyH3b; 8.62 (2H), bpyH3d; 8.79 (2H), H5'.

Tetrakis-(4,4'-dimethyl-2,2'-bipyridine)-μ-2,6-bis-(1-pyrazolyl)-1,5-naphthyridine-diruthenium(II)-tetrakis-(hexafluorophosphate) (140).

2,6-Bis-(1-pyrazolyl)-1,5-naphthyridine (**132**) (5mg, 0.019mMol) was reacted with $Ru(dmb)_2Cl_2.2H_2O$ (23mg, 0.040mMol) as described above. Recrystallisation from acetonitrile/ether gave a red microcrystalline solid which was found, by ^1H NMR spectroscopy, to be a 3:2 mixture of a major and a minor isomer, corresponding to the two diastereoisomer

(meso and racemic). Ion-exchange chromatography on sephadex (0.1-0.5M NaCl eluent) failed to separate the isomers, neither of which could be unambiguously assigned to the meso or racemic diastereoisomers. Protons of the bridging ligand, but not the dmb ligands, were assigned to each isomer. Yield 23mg (68%). FAB mass spectrum: calcd for $[C_{62}H_{58}N_{14}P_3F_{18}Ru_2]^+$: 1637.198. Found: 1637.201. ^1H NMR (CD_3CN) bridging ligand-major isomer δ: 6.90 (2H), H4'; 7.27 (2H), H3'; 7.82 (2H), H4; 8.10 (2H), H3; 8.76 (2H), H5'. Minor isomer δ: 6.90 (2H), H4'; 7.27 (2H), H3'; 7.77 (2H), H4; 8.08 (2H), H3; 8.75 (2H), H5'. Dmb ligands δ: 2.51-2.65 (48H), 4-CH_3; 7.09-7.35 (18H), H5 and H6; 7.41 (3H), 7.44 (3H), H5; 7.73 (2H), 7.80 (2H), 7.86 (2H), 8.01 (2H), H6; 8.30- 8.45 (16H), H3.

Tetrakis-(2,2'-bipyridine)-μ-(2,2':4',4'':2'',2'''-quaterpyridine)-diruthenium(II)-tetrakis-(hexafluorophosphate) (141).

The ^1H NMR spectrum of **141**[153] was assigned unambiguously. ^1H NMR (CD_3CN) δ: 7.46 (4H), 7.48 (4H), bpyH5; 7.51 (2H), H5; 7.80 (2H), H5'; 7.81 (6H), 7.83 (2H), bpyH6; 7.84 (2H), H6; 7.95 (2H), H6'; 8.13 (4H), 8.14 (4H), bpyH4; 8.17 (2H), H4; 8.58 (8H), bpyH3; 8.77 (2H), H3; 8.89 (2H), H3'.

Bis-(4,4'-dimethyl-2,2'-bipyridine)-2,2':4',4'':2'',2'''-quaterpyridine-ruthenium(II)-bis-(hexafluorophosphate) (146).

$Ru(dmb)_2Cl_2.2H_2O$ (35.0mg, 0.061mMol) was reacted with **25** (19.2mg, 0.064mMol) as described above. The complex **146** was obtained as a red solid. Yield 58mg (96%). FAB mass spectrum: calcd for $[C_{44}H_{38}N_8PF_6Ru]^+$: 925.1905. Found: 925.1898. ^1H NMR (CD_3CN) δ: 2.58 (6H), 2.60 (6H), dmb4-CH_3; 7.29 (2H), 7.31 (2H), dmbH5; 7.48, H5; 7.52, H5'''; 7.59, 7.61 (2H), 7.66, dmbH6; 7.79, H5'; 7.83, H6; 7.87, H5''; 7.92, H6'; 8.02, H4'''; 8.13, H4; 8.42, dmbH3; 8.56, H3'''; 8.75, H3; 8.77, H6'''; 8.88, H3'; 8.90, H3''; 8.93, H6''.

Tetrakis-(4,4'-dimethyl-2,2'-bipyridine)-μ-(2,2':4',4'':2'',2'''-quaterpyridine)-diruthenium(II)-tetrakis-(hexafluorophosphate) (147).

The mononuclear complex **146** (35.4mg, 0.035mMol) was reacted with $Ru(dmb)_2Cl_2.2H_2O$ (20mg, 0.035mMol) as described above. The binuclear complex **147** was obtained as a red solid. Yield 51mg (80%). FAB mass spectrum: calcd for $[C_{68}H_{62}N_{12}P_3F_{18}Ru_2]^+$: 1685.223. Found: 1685.224. ^1H NMR (CD_3CN) δ: 2.58 (12H), 2.60 (12H), dmb4-CH_3; 7.29 (4H), 7.31 (4H), dmbH5; 7.50 (2H), H5; 7.59 (6H), 7.61 (2H),

dmbH6; 7.78 (2H), H5'; 7.84 (2H), H6; 7.95 (2H), H6'; 8.15 (2H), H4; 8.42 (8H), dmbH3; 8.75 (2H), H3; 8.87 (2H), H3'.

Bis-(2,2'-bipyridine)-bis-(4,4'-dimethyl-2,2'-bipyridine)-μ-(2,2':4',4'':2'',2'''-quaterpyridine)-diruthenium(II)-tetrakis-(hexafluorophosphate) (148).

$Ru(bpy)_2Cl_2.2H_2O$ (19.5mg, 0.037mMol) was reacted with **146** (40.0mg, 0.037mMol), as described above, to give **148** as a red solid. Yield 63mg (91%). FAB mass spectrum: calcd for $[C_{64}H_{54}N_{12}P_3F_{18}Ru_2]^+$: 1629.161. Found: 1629.162. ^1H NMR (CD_3CN) δ: 2.58 (6H), 2.60 (6H), dmb4-CH_3; 7.29 (2H), 7.31 (2H), dmbH5; 7.46 (2H), 7.48 (2H), bpyH5; 7.50, H5'''; 7.51, H5; 7.60 (3H), 7.61 (1H), dmbH6; 7.78, H5''; 7.80, H5'; 7.81 (2H), 7.83 (2H), bpyH6; 7.84 (2H), H6 and H6'''; 7.95 (2H), H6' and H6''; 8.13 (2H), 8.14 (2H), bpyH4; 8.15, H4'''; 8.17, H4; 8.42 (4H), dmbH3; 8.58 (4H), bpyH3; 8.80, H3'''; 8.82, H3; 8.91, H3''; 8.93, H3'.

Tris-(2,2':4',4'':2'',2'''-quaterpyridine)-ruthenium(II)-bis-(hexafluorophosphate) (149).

2,2':4',4'':2'',2'''-Quaterpyridine (**25**) (100mg, 0.32mMol) was reacted with $Ru(DMSO)_4Cl_2$ (47mg, 0.1mMol) and the resultant solid recrystallised from acetonitrile/ether, as described above. Complex **149** was obtained as a red microcrystalline solid. Yield 111mg (84%). FAB mass spectrum: calcd for $[C_{60}H_{42}N_{12}PF_6Ru]^+$: 1177.234. Found: 1177.233. The ^1H NMR spectrum was assigned by comparison with the spectrum of **146**. Proton signals were broadened due to the presence of meridonal and facial isomers, in a 3:1 ratio respectively. ^1H NMR (CD_3CN) δ: 7.55 (8H), H5 and H5'''; 7.84 (4H), H5'; 7.87 (4H), H6; 7.88-7.92 (8H), H6' and H5'; 8.04 (4H), H4'''; 8.20 (4H), H4; 8.53 (4H), H3'''; 8.76 (4H), H3; 8.83 (4H), H6'''; 8.92-8.95 (8H), H3', H3'' and H6''.

Tri-[bis-(2,2'-bipyridine)-μ-(2,2':4',4'':2'',2'''-quaterpyridine)-ruthenium(II)]-ruthenium(II)-octakis-(hexafluorophosphate) (150).

The homoleptic complex **149** 20mg (0.015mMol) was reacted with $Ru(bpy)_2Cl_2.2H_2O$ (25.2mg, 0.048mMol), as described above, to give the tetranuclear complex **150** as a red solid, which was recrystallised from acetonitrile/ether. Yield 48mg (93%). Calcd for $C_{120}H_{90}N_{24}P_8F_{48}Ru_4.8H_2O$ C: 40.30, H: 2.99, N: 9.40. Found C: 40.39, H: 3.01, N: 9.40.

Dichloropalladium(II)-bis-(2,2'-bipyridine)-μ-(2,2':4',4'':2'',2'''-quaterpyridine)-ruthenium(II)-bis-(hexafluorophosphate) (151).

A solution of $Pd(PhCN)_2Cl_2$ (10.8mg, 0.028mMol) in dichloromethane was added dropwise to a solution of **146** (30mg, 0.028mMol) in dichloromethane. The resultant brown precipitate of **151** was filtered and air dried. Yield 16mg (48%). FAB mass spectrum: calcd for $[C_{44}H_{38}N_8PF_6Cl_2RuPd]^+$: 1103.032. Found: 1103.034. ^1H NMR (CD_3CN) δ: 2.59 (6H), 2.61 (6H), dmb4-CH_3; 7.30 (2H), 7.32 (2H), dmbH5; 7.52, H5; 7.74, H5'''; 7.85 (2H), H6 and H5'; 8.01, H6'; 8.09, H5''; 8.18, H4; 8.31, H4'''; 8.43 (4H), dmbH3; 8.49, H3'''; 8.68, H3''; 8.82, H3; 8.99, H3'; 9.25, H6'''; 9.35, H6''.

Bis-(2,2'-bipyridine)-2,2'-bis-(1-pyrazolyl)-4,4'-bipyridine-ruthenium(II)-bis-(hexafluorophosphate) (157).

Ligand **144** (27mg, 0.094mMol) was reacted with $Ru(bpy)_2Cl_2.2H_2O$ (44mg, 0.085mMol) as described above. The resultant solid was chromatographed on a column of alumina (8x2.5cm), whereupon **157** was eluted with chloroform/ methanol (50:1) as a red band. The fraction was collected and the solvent removed *in vacuo* to give a red solid. Yield 37mg (44%). FAB mass spectrum: calcd for $[C_{36}H_{28}N_{10}PF_6Ru]^+$: 847.11837. Found: 847.11841. ^1H NMR (CD_3CN) δ: 6.63, H4'''; 6.88, H4''; 7.43, H3''; 7.44, bpyH5a; 7.48, bpyH5b; 7.50, bpyH5d; 7.55, bpyH5c; 7.67, H6; 7.71, H5'; 7.76, H6; 7.82, bpyH6a; 7.85, bpyH6b; 7.87, H3'''; 7.94, bpyH6c; 8.03, bpyH6d; 8.11, bpyH4a, 8.14, bpyH4b; 8.16 (2H), bpyH4c and bpyH4d; 8.44, H3'; 8.50, H3; 8.55, bpyH3d; 8.58 (3H), bpyH3a, bpyH3b and bpyH3c; 8.69, H6'; 8.70, H5'''; 9.01, H5''. The dinuclear complex **159** was eluted with chloroform/methanol (10:1) as a red band which was collected and the solvent removed *in vacuo* to give a red solid. Yield 34mg (28%).

Bis-(4,4'-dimethyl-2,2'-bipyridine)-2,2'-bis-(1-pyrazolyl)-4,4'-bipyridine-ruthenium(II)-bis-(hexafluorophosphate) (158).

Ligand **144** (27.5mg, 0.095mMol) was reacted with $Ru(dmb)_2Cl_2.2H_2O$ (49.9mg, 0.087mMol) as described above. The product **158** was recrystallised from ethanol/water to give an orange microcrystalline solid. Yield 85mg (83%). FAB mass spectrum: calcd for $[C_{40}H_{36}N_{10}PF_6Ru]^+$: 903.1801. Found: 903.1819. ^1H NMR (CD_3CN) δ: 2.59 (3H), 2.60 (3H), 2.61 (3H), 2.62 (3H), dmb4-CH_3; 6.61, H4'''; 6.87, H4''; 7.27, dmbH5a; 7.32, dmbH5b; 7.34, dmbH5d; 7.36, dmbH5c; 7.41, H3''; 7.63, dmbH6a; 7.65 (2H), H5 and

dmbH6b; 7.75, dmbH6c; 7.76, H5'; 7.83, dmbH6d; 7.77, H6; 7.86, H3'''; 8.41, dmbH3a; 8.42, H3'; 8.43 (3H), dmbH3b, dmbH3c and dmbH3d; 8.60, H3; 8.65, H6'; 8.67, H5'''; 9.06, H5''.

Tetrakis-(2,2'-bipyridine)-μ-[2,2'-bis-(1-pyrazolyl)-4,4'-bipyridine]-diruthenium(II)-tetrakis-(hexafluorophosphate) (159).

$Ru(bpy)_2Cl_2.2H_2O$ (57mg, 0.11mMol) was reacted with **144** (15.0mg, 0.052mMol), as described above, to give **159** as a red solid. Yield 46mg (52%). FAB mass spectrum: calcd for $[C_{56}H_{44}N_{14}P_3F_{18}Ru_2]^+$: 1551.089. Found: 1551.087. ^1H NMR (CD_3CN) δ: 6.90 (2H), H4''; 7.44 (4H), H3'' and bpyH5a; 7.47 (2H), bpyH5b; 7.49 (2H), bpyH5c; 7.53 (2H), bpyH5d; 7.67 (2H), H5; 7.81 (4H), H6 and bpyH6a; 7.83 (2H), bpyH6b; 7.93 (2H), bpyH6c; 7.99 (2H), bpyH6d; 8.11 (2H), bpyH4a; 8.14 (4H), bpyH4b and bpyH4c; 8.16 (2H), bpyH4d; 8.50 (2H), H3; 8.54 (2H), bpyH3a; 8.57 (6H), bpyH3b, bpyH3c and bpyH3d; 9.02 (2H), H5''. ^{13}C NMR (CD_3CN) δ: 111.1 (2C), C3; 112.4 (2C), C4''; 122.0 (2C), C5; 124.4 (C), 124.6 (4C), 124.7 (2C), bpyC3; 127.6 (2C), 127.8 (2C), 128.0 (2C), 128.1 (2C), bpyC5; 132.7 (2C), C5''; 138.3 (2C), 138.4 (2C), 138.4_6 (2C), 138.5_2 (2C), bpyC4; 145.6 (2C), C3''; 146.4 (2C), C4; 152.1 (2C), C6; 152.2 (2C), 152.3 (2C), 152.6 (4C), bpyC6; 157.3 (2C), 157.5 (2C), 157.6 (2C), 157.8 (2C), bpyC2; C2-not observed.

Tetrakis-(4,4'-dimethyl-2,2'-bipyridine)-μ-[2,2'-bis-(1-pyrazolyl)-4,4'-bipyridine]-diruthenium(II)-tetrakis-(hexafluorophosphate) (160).

Ligand **144** (14.0mg, 0.049mMol) was reacted with $Ru(dmb)_2Cl_2.2H_2O$ (56.5mg, 0.098mMol) as described above. Complex **160** was obtained as a red solid. Yield 58mg (65%). FAB mass spectrum: calcd for $[C_{64}H_{60}N_{14}P_3F_{18}Ru_2]^+$: 1663.2138. Found: 1663.2142. ^1H NMR (CD_3CN) δ: 2.59 (12H), 2.61 (12H), dmb4-CH_3; 6.89 (2H), H4''; 7.27 (2H), dmbH5a; 7.31 (4H), dmbH5b and dmbH5d; 7.35 (2H), dmbH5c; 7.42 (2H), H3''; 7.60 (2H), dmbH6a; 7.62 (2H), dmbH6b; 7.66 (2H), H5; 7.72 (2H), dmbH6c; 7.79 (2H), dmbH6d; 7.81 (2H), H6; 8.39 (2H), H3; 8.41 (8H), dmbH3a, dmbH3b, dmbH3c and dmbH3d; 8.91 (2H), H5''. ^{13}C NMR (CD_3CN) δ: 20.5_7, (2C), 20.6_2 (6C), dmb4-CH_3; 110.9 (2C), C3; 112.3 (2C), C4''; 121.9 (2C), C5; 125.0 (2C), 125.2 (4C), 125.3 (2C), dmbC3; 128.2 (2C), 128.4 (2C), 128.6 (4C), dmbC5; 132.3 (2C), C5''; 145.1 (2C), C3''; 146.0 (2C), C4; 150.7 (2C), dmbC4; 150.8_8 (2C), dmbC6; 150.9_4 (2C), 151.1 (2C), dmbC4; 151.2 (2C), 151.4 (4C), dmbC6; 152.0 (2C), C6; 152.1 (2C), dmbC4; 157.2 (2C), 157.3 (2C), 157.8 (2C), 157.9 (2C), dmbC2; C2-not observed.

Bis-(2,2'-bipyridine)-bis-(4,4'-dimethyl-2,2'-bipyridine)-μ-[2,2'-bis-(1-pyrazolyl)-4,4'-bipyridine]-diruthenium(II)-tetrakis-(hexafluorophosphate) (161).

Complex **158** (40mg, 0.038mMol) was reacted with $Ru(bpy)_2Cl_2.2H_2O$ (20mg, 0.038mMol) and the resultant product recrystallised from acetonitrile/ether, as described above, to give **161** as a red microcrystalline solid. Yield 56mg (84%). FAB mass spectrum: calcd for $[C_{60}H_{52}N_{14}P_3F_{18}Ru_2]^+$: 1607.151. Found: 1607.153. ^1H NMR (CD_3CN) δ: 6.89, H4'''; 6.90, H4''; 7.27, dmbH5a; 7.29, dmbH5b; 7.30, dmbH5d; 7,34, dmbH5c; 7.41, H3'''; 7.44 (2H), H3'' and bpyH5a; 7.48, bpyH5b; 7.50, bpyH5d; 7.54, bpyH5c; 7.61, dmbH6a; 7.63, dmbH6b; 7.66, H5'; 7.67, H5; 7.72, dmbH6c; 7.79, dmbH6d; 7.81 (3H), H6, H6' and bpyH6a; 7.83, bpyH6b; 7.93, bpyH6c; 8.00, bpyH6d; 8.11, 8.14, 8.15, 8.16, bpyH4; 8.39, H3'; 8.40, H3; 8.41 (4H), dmbH3; 8.57 (3H), 8.54, bpyH3; 8.92, H5'''; 8.94, H5''.

Dichloro-palladium(II)-bis-(2,2'-bipyridine)-μ-[2,2'-bis-(1-pyrazolyl)-4,4'-bipyridine]-ruthenium(II)-bis-(hexafluorophosphate) (162).

A solution of $Pd(PhCN)_2Cl_2$ (5.7mg, 0.015mMol) in dichloromethane was added dropwise to a solution of **157** (14.8mg, 0.015mMol) in dichloromethane. The resultant orange/red precipitate of **162** was filtered and air dried. Yield 15.3mg (87%). ^1H NMR (CD_3CN) δ: 6.91, H4''; 6.92, H4'''; 7.45 (2H), H3'' and bpyH5a; 7.48, bpyH5b; 7.52, bpyH5d; 7.54, bpyH5c; 7.72, H5; 7.81, bpyH6a; 7.83, bpyH6b; 7.85, H6; 7.93, bpyH6c; 7.96, H5'; 8.02, bpyH6d; 8.12, bpyH4a; 8.14 (2H), bpyH4b and bpyH4c; 8.16, bpyH4d; 8.19, H3'''; 8.29, H3'; 8.53, H3; 8.54, bpyH3a; 8.57 (3H), bpyH3b, bpyH3c and bpyH3d; 8.75, H5'''; 9.00, H5''; 9.14, H6'.

Dichloro-palladium(II)-bis-(4,4'-dimethyl-2,2'-bipyridine)-μ-[2,2'-bis-(1-pyrazolyl)-4,4'-bipyridine]-ruthenium(II)-bis-(hexafluorophosphate) (163).

A solution of $Pd(PhCN)_2Cl_2$ (9.5mg, 0.025mMol) in dichloromethane was added dropwise to a solution of **158** (25.3mg, 0.024mMol) in dichloromethane. The resultant red precipitate of **163** was filtered and air dried. Yield 16mg (52%). FAB mass spectrum: calcd for $[C_{40}H_{36}N_{10}PF_6Cl_2RuPd]^+$: 1079.022. Found: 1079.025. ^1H NMR (CD_3CN) δ: 2.59 (3H), 2.60 (6H), 2.62, dmb4-CH_3; 6.89, H4'''; 6.91, H4''; 7.28, dmbH5a; 7.31, dmbH5b; 7.38, dmbH5d; 7.39, dmbH5c; 7.42, H3''; 7.62, dmbH6a; 7.64' dmbH6b; 7.77, dmbH6c; 7.84, H5;

7.86 (2H), H6 and dmbH6d; 8.05, H5'; 8.08, H3'''; 8.40, dmbH3a; 8.43 (3H), dmbH3b, dmbH3c and dmbH3d; 8.60, H3'; 8.76, H3; 9.04, H6'; 9.12, H5'''; 9.31, H5''.

Bis-(2,2'-bipyridine)-[2,2'-bis-(3,5-dimethyl-1-pyrazolyl)-4,4'-bipyridine]-ruthenium(II)-bis-(hexafluorophosphate) (164).

Ligand **145** (33mg, 0.096mMol) was reacted with $Ru(bpy)_2Cl_2.2H_2O$ (45mg, 0.086mMol) as described above. The resultant solid was absorbed onto a column of alumina. Complex **164** was eluted with chloroform/methanol (25:1) as a red band. Evaporation of the fraction gave a red solid. Yield 50mg (50%). FAB mass spectrum: calcd for $[C_{40}H_{36}N_{10}PF_6Ru]^+$: 903.181. Found: 903.182. ^1H NMR (CD_3CN) δ: 1.58 (3H), 3''-CH_3; 2.29 (3H), 3'''-CH_3; 2.71 (3H), 5'''-CH_3; 2.98 (3H), 5''-CH_3; 6.16, H4'''; 6.46, H4''; 7.41, bpyH5b; 7.44, bpyH5a; 7.54 (2H), H5 and bpyH5c; 7.57, bpyH5d; 7.60, H5'; 7.70, bpyH6; 7.71, H6; 7.83, bpyH6b; 7.96, bpyH6c; 8.06 (2H), bpyH4a and bpyH6d; 8.09, bpyH4b; 8.15, bpyH4d; 8.20 (2H), H3' and bpyH4c; 8.54, H3; 8.57 (2H), bpyH3a and bpyH3b; 8.58 (2H), bpyH3c and bpyHd; 8.64, H6'. The binuclear complex **165** was eluted with chloroform/methanol (10:1) as a red band. Yield 18mg (11%).

Tetrakis-(2,2'-bipyridine)-μ-[2,2'-bis-(3,5-dimethyl-1-pyrazolyl)-4,4'-bipyridine]-diruthenium(II)-tetrakis-(hexafluorophosphate) (165).

Ligand **145** (10mg, 0.029mMol) was reacted with $Ru(bpy)_2Cl_2.2H_2O$ (35mg, 0.067mMol) and the product **165** recrystallised from acetonitrile/ether as described above to give a red solid. Yield 22mg (43%). FAB mass spectrum: calcd for $[C_{60}H_{52}N_{14}P_3F_{18}Ru_2]^+$: 1607.151. Found: 1607.154. ^1H NMR (CD_3CN) δ: 1.58 (6H), 3''-CH_3; 2.96 (6H), 5''-CH_3; 6.47 (2H), H4''; 7.41 (2H), bpyH5b; 7.43 (2H), bpyH5a; 7.49 (2H), H5; 7.52 (2H), bpyH5c; 7.54 (2H), bpyH5d; 7.69 (2H), bpyH6a; 7.72 (2H), H6; 7.82 (2H), bpyH6b; 7.93 (2H), bpyH6c; 8.06 (2H), bpyH6d; 8.08 (2H), bpyH4b; 8.12 (2H), bpyH4a; 8.15 (2H), H3; 8.16 (2H), bpyH4d; 8.17 (2H), bpyH4c; 8.56, bpyH3d; 8.57, bpyH3b; 8.58, bpyH3a; 8.59, bpyH3c; . ^{13}C NMR (CD_3CN) δ: 11.9 (2C), 3''-CH_3; 15.0 (2C), 5''-CH_3; 111.5 (2C), C4''; 114.5 (2C), C3; 121.3 (2C), C5; 124.7 (2C), 124.7_5 (2C), 124.7_9 (4C), bpyC3; 127.8 (2C), 127.9 (2C), 128.1 (2C), 128.2 (2C), bpyC5; 138.2 (2C), 138.2_8 (2C), 138.3_3 (2C), 138.5 (2C), bpyC4; 146.3 (2C), 146.5 (2C), C5'' and C4; 152.0 (2C), 152.1 (2C), 152.3 (2C), bpyC6; 152.4 (2C), C2 or C3''; 152.6 (2C), bpyC6; 152.7 (2C), C6; 153.1 (2C), C2 or C3''; 157.2_7 (2C), 157.2_3 (2C), 157.4 (2C), 157.5 (2C), bpyC2;

Tetrakis-(4,4'-dimethyl-2,2'-bipyridine)-μ-[2,2'-bis-(3,5-dimethyl-1-pyrazolyl)-4,4'-bipyridine]-diruthenium(II)-tetrakis-(hexafluorophosphate) (166).

$Ru(dmb)_2Cl_2.2H_2O$ (39mg, 0.067mMol) was reacted with 2,2'-bis-(3,5-dimethyl-1-pyrazolyl)-4,4'-bipyridine (10mg, 0.029mMol) and the resultant solid recrystallised from acetonitrile/ether as described above. The binuclear complex **166** was obtained as a red microcrystalline solid. Yield 35mg (65%) FAB mass spectrum: calcd for $[C_{68}H_{68}N_{14}P_3F_{18}Ru_2]^+$: 1719.276. Found: 1719.278. ^1H NMR (CD_3CN) δ: 1.59 (6H), 3"-CH_3; 2.55 (6H), 2.57 (6H), 2.61 (6H), 2.63 (6H), dmb4-CH_3; 2.96 (6H), 5"-CH_3; 6.46 (2H), H4"; 7.24 (2H), dmbH5b; 7.27 (2H), dmbH5a; 7.33 (2H), dmbH5c; 7.38 (2H), dmbH5d; 7.49 (4H), H5 and dmbH6a; 7.61 (2H), dmbH6b; 7.71 (2H), H6; 7.73 (2H), dmbH6c; 7.85 (2H) dmbH6d; 8.16 (2H), H3; 8.41 (8H), dmbH3a, dmbH3b, dmbH3c and dmbH3d.

Dichloropalladium(II)-bis-(2,2'-bipyridine)-μ-[2,2'-bis-(3,5-dimethyl-1-pyrazolyl)-4,4'-bipyridine]-ruthenium(II)-bis-(hexafluorophosphate) (167)

To a solution of **164** (14.7mg, 0.014mMol) in CH_2Cl_2 (3ml) was added, dropwise, a solution of $Pd(PhCN)_2Cl_2$ in CH_2Cl_2 (2ml). The red precipitate of **167** was filtered and air dried. Yield 15.5mg (90%). FAB mass spectrum: calcd for $[C_{40}H_{36}N_{10}PF_6Cl_2RuPd]^+$: 1081.019. Found: 1081.020. ^1H NMR (CD_3CN) δ: 1.58 (3H), 3"-CH_3; 2.64 (3H), 3'"-CH_3; 2.87 (3H), 5'"-CH_3; 3.00 (3H), 5"-CH_3; 6.45, H4'"; 6.48, H4"; 7.42 (2H), bpyH5; 7.57 (3H), H5 and bpyH5; 7.69, bpyH6; 7.78, H6; 7.80 (2H), H5' and bpyH6; 7.97, bpyH6; 8.00, H3'; 8.07, bpyH6; 8.08, 8.12, 8.18 (2H), bpyH4; 8.25, H3; 8.54, 8.55, 8.59 (2H), bpyH3; 9.24, H6'.

Attempted complex syntheses.

Reaction of **93** with $Ru(DMSO)_4Cl_2$.

2-(2-Pyridinyl)perimidine (**93**) (30mg, 0.122mMol) was reacted with $Ru(DMSO)_4Cl_2$ (18mg, 0.037mMol) as described above. The product was obtained as a black solid. Yield 36mg (89%). The ^1H NMR spectrum of the solid was too complicated to assign. Neither ^1H NMR spectroscopy nor elemental analysis could confirm the formation of the desired product.

Bis-(4,4'-dimethyl-2,2'-bipyridine)-(2-2'-biperimidine)ruthenium(II)-bis-(hexafluorphosphate) (**103**) and Tetrakis-(4,4'-dimethyl-2,2'-bipyridine)-μ-(2-2'-biperimidine)diruthenium(II)-tetrakis-(hexafluorphosphate) (**104**)

A mixture of **91** (20mg, 0.060mMol) and $Ru(dmb)_2Cl_2.2H_2O$ (32mg, 0.055mMol) in ethylene glycol was refluxed for 6 hours. The solution was cooled and treated with aqueous

NH_4PF_6. The resultant black precipitate was shown, by ^1H NMR spectroscopy, to be a mixture of monodentate complexes. Attempts to separate this mixture by chromatography on alumina were unsuccessful. Addition of one more equivalent of $Ru(dmb)_2Cl_2.2H_2O$ and K_2CO_3 (30mg) failed to give the dinuclear complex **104**, with a similar complicated mixture of monodentate complexes being obtained.

Tetrakis-(4,4'-dimethyl-2,2'-bipyridine)-μ-[2-(2-pyrimidinyl)perimidinate]-ruthenium(II)-tris-(hexafluorophoshate) (**107**).

The ligand **95** (11.4mg, 0.046mMol) was reacted with $Ru(dmb)_2Cl_2.2H_2O$ (50mg, 0.087mMol) as described above. The ^1H NMR spectrum of the resultant solid indicated a mixture of complexes. Although the mononuclear complex **106** could be distinguished in the spectrum, the dinuclear complex **107** could not. Chromatography of this mixture on a column of alumina succeeded in separating **106** by eluting with chloroform/methanol (25:1). Elution with chloroform/methanol (10:1), methanol and finally acetonitrile gave fractions which were found, by ^1H NMR spectroscopy, to contain mixtures of polynuclear complexes, but not **107**. Similarly, chromatography on sephadex was successful in separating **106**, by eluting with 0.2M NaCl. However, eluting with 0.5M-0.8M NaCl failed to give **107**. In both cases, a significant quantity of brown solid was irreversibly absorbed onto the column material.

Alternatively, **95** (10mg, 0.01mMol) was reacted with $Ru(dmb)_2Cl_2.2H_2O$ (6mg, 0.01mMol) as described above. As described above, attempts to purify the resultant solid on sephadex or alumina could isolate **106**, but not **107**.

The above reactions were repeated in the presence of a small quantity of K_2CO_3 (5mg) to deprotonate the ligand. Similarly, **107** could not be detected in the resultant mixture of products.

Bis-(2,2'-bipyridine)-4,6-di-(2-pyridinyl)pyrimidineruthenium(II)-tetrachloromolybdenum-bis-(hexafluorphosphate) (**126**).

To a solution of **119** (25mg, 0.027mMol) in dichloromethane (5ml) was added a solution of $Mo(CO)_4(\eta^4\text{-}C_7H_8)$ (10mg, 0.033mMol) in dichloromethane (5ml). The resultant red solution was stirred for 36 hours. ^1H NMR analysis indicated that only 3% of **119** had been converted to **126**.

A mixture of **119** (25mg, 0.027mMol) and $Mo(CO)_6$ (14mg, 0.053mMol) in argon purged toluene (20ml) was refluxed for 6 hours. No reaction was observed.

8.4. Crystallography

Intensity data were collected with a Nicolet P4s four-circle diffractometer using graphite-monochromatised Mo Kα radiation (λ 0.7107Å). Cell parameters were determined by least-squares refinement using the setting angles of at least 20 accurately centred reflections (2θ> 20°). Throughout data collections (ω scans) the intensities of three standard reflections were monitored and this showed no significant crystal decomposition. The intensities were corrected for Lorentz and polarisation effects but no corrections for absorption were deemed necessary.

All structures were solved by direct methods using SHELXS-90[258] and refined on F^2 by full-matrix least squares procedures using SHELXL-93.[259] All non-hydrogen atoms were refined with anisotropic displacement parameters. Hydrogens were included in calculated positions with the rotational orientations of the methyl groups deduced from circular Fourier syntheses. All hydrogens were assigned isotropic displacement parameters 1.3 times the isotropic equivalent of their carrier carbons. All data were used in the refinements; the functions minimised were $\Sigma w(F_o^2 - F_c^2)$, with $w = [\sigma^2(F_o^2) + aP^2]^{-1}$ where $P = [\max(F_0^2) + 2F_c^2]/3$. All calculations were performed on an IBM RISC 6000 computer. Final atomic coordinates and equivalent isotropic displacement parameters (defined as one third of the trace of the orthogonalised U_{ij} tensor) are given in Tables 8.1-8.7.

*Crystal Data for **100** at 185 K.* - $C_{17}H_{13}N_3Cl_2Pd$ *M* 436.6, triclinic, space group $P\bar{1}$, *a* 7.358(2), *b* 9.295(3), *c* 12.052(4)Å, α 99.88(2), β 94.16(3), γ 104.56(2)°, *V* 780.2(4)Å^3, *F*(000) 432, *Dc*(*Z*=2) 1.859gcm^{-1}, μ(Mo Kα) 15.3cm^{-1}, approximate crystal dimensions 0.28 by 0.11 by 0.01mm, $2\theta_{max}$ 50°, goodness of fit on F^2 1.04, *w*R (all 2743 data, a=0.0454) 0.101, conventional R [1862 data with $I > 2\sigma(I)$] 0.056 for 209 parameters.

*Crystal Data for **144** at 130 K.* - $C_{16}H_{12}N_6$, *M* 288.3, triclinic, space group $P\bar{1}$,*a* 8.061(1), *b* 9.024(1), *c* 10.680(1)Å, α 102.032(8), β 107.931(6), γ 107.355(7)°, *V* 665.8(1)Å^3, *F*(000) 300, *Dc*(*Z*=2) 1.438gcm^{-1}, μ(Mo Kα) 0.93cm^{-1}, approximate crystal dimensions 0.81 by 0.38 by 0.21mm, $2\theta_{max}$ 50°, goodness of fit on F^2 1.00, *w*R (all 2288 data, a=0.0258) 0.0787, conventional R [1847 data with $I > 2\sigma(I)$] 0.0288 for 200 parameters.

*Crystal Data for **145** at 130 K.* - $C_{20}H_{20}N_6$, *M* 344.4, orthorhombic, space group $P2_12_12_1$, *a* 7.077(2), *b* 13.906(4), *c* 16.697(5)Å, *V* 1643(1)Å^3, *F*(000) 728, *Dc*(*Z*=4) 1.392gcm^{-1}, μ(Mo Kα) 0.88cm^{-1}, approximate crystal dimensions 0.84 by 0.07 by 0.07mm, $2\theta_{max}$ 50°, goodness of fit on F^2 0.69, *w*R (all 1896 data, a=0.0207) 0.0762, conventional R [985 data with $I > 2\sigma(I)$] 0.0395 for 240 parameters.

Table 8.1. Atomic coordinates and equivalent isotropic displacement parameters ($Å^2$) for **100**.

Atom	10^4 x	10^4 y	10^4 z	10^3U_{eq}
Pd(1)	7707(1)	6290(1)	6329(1)	17(1)
Cl(1)	7293(3)	7062(2)	4638(2)	26(1)
Cl(2)	7752(4)	8678(2)	7249(2)	32(1)
C(1)	4877(12)	1523(10)	7820(8)	27(2)
N(1)	6255(10)	3004(8)	8204(6)	22(2)
C(2)	7109(12)	3855(9)	7469(7)	17(2)
N(3)	7980(10)	5343(8)	7759(6)	19(2)
C(3A)	8416(12)	6020(10)	8921(7)	20(2)
C(4)	9586(12)	7471(10)	9259(8)	25(2)
C(5)	9998(14)	8143(12)	10412(7)	33(2)
C(6)	9234(14)	7367(12)	11214(8)	40(3)
C(6A)	8060(14)	5848(12)	10897(7)	32(2)
C(7)	7169(15)	4972(14)	11679(9)	40(3)
C(8)	6098(15)	3557(14)	11348(8)	42(3)
C(9)	5740(13)	2839(11)	10180(8)	32(2)
C(9A)	6510(12)	3636(10)	9380(7)	23(2)
C(9B)	7630(13)	5163(11)	9731(7)	26(2)
N(1')	7505(10)	4134(8)	5556(6)	20(2)
C(2')	7237(12)	3149(10)	6282(7)	19(2)
C(3')	7328(11)	1658(9)	5928(7)	19(2)
C(4')	7611(12)	1176(10)	4835(7)	25(2)
C(5')	7752(12)	2157(10)	4088(7)	25(2)
C(6')	7727(12)	3655(10)	4485(7)	22(2)

Table 8.2. Atomic coordinates and equivalent isotropic displacement parameters ($Å^2$) for **144**.

Atom	10^4 x	10^4 y	10^4 z	10^3U_{eq}
N(1)	4744(1)	11375(1)	6628(1)	22(1)
C(2)	3363(2)	9975(1)	5741(1)	18(1)
C(3)	2000(2)	9820(1)	4504(1)	18(1)
C(4)	2083(2)	11216(1)	4145(1)	19(1)
C(5)	3518(2)	12699(1)	5070(1)	23(1)
C(6)	4787(2)	12717(2)	6278(1)	24(1)
N(1')	-1764(1)	10909(1)	227(1)	21(1)
C(2')	3(2)	12003(1)	839(1)	18(1)
C(3')	1274(2)	12190(1)	2122(1)	19(1)
C(4')	727(2)	11116(1)	2804(1)	19(1)
C(5')	-1107(2)	9932(1)	2165(1)	21(1)
C(6')	-2287(2)	9904(2)	916(1)	22(1)
N(1A)	3341(1)	8585(1)	6141(1)	19(1)
N(2A)	1905(1)	7098(1)	5366(1)	24(1)
C(3A)	2307(2)	6118(2)	6062(1)	25(1)
C(4A)	3964(2)	6940(2)	7265(1)	24(1)
C(5A)	4585(2)	8517(2)	7287(1)	22(1)
N(1B)	562(1)	12989(1)	62(1)	19(1)
N(2B)	2402(2)	14008(1)	511(1)	24(1)
C(3B)	2416(2)	14707(2)	-456(1)	26(1)
C(4B)	629(2)	14159(2)	-1514(1)	25(1)
C(5B)	-530(2)	13058(1)	-1151(1)	22(1)

Table 8.3. Atomic coordinates and equivalent isotropic displacement parameters ($Å^2$) for **145.**

Atom	10^4 x	10^4 y	10^4 z	10^3U_{eq}
N(1)	2520(6)	395(2)	2742(2)	21(1)
C(2)	2781(7)	1280(3)	2472(2)	21(1)
C(3)	2531(6)	2105(3)	2915(2)	19(1)
C(4)	1965(6)	2015(3)	3699(2)	17(1)
C(5)	1706(6)	1094(3)	4003(2)	21(1)
C(6)	2023(7)	332(3)	3517(2)	22(1)
N(1')	1028(5)	4457(3)	5195(2)	18(1)
C(2')	1685(7)	3637(3)	5475(2)	19(1)
C(3')	2014(6)	2833(3)	5017(2)	16(1)
C(4')	1654(6)	2865(3)	4206(2)	20(1)
C(5')	931(6)	3717(3)	3907(2)	19(1)
C(6')	684(6)	4489(3)	4409(2)	20(1)
N(1A)	3350(6)	1345(3)	1666(2)	23(1)
N(2A)	3389(5)	2256(2)	1334(2)	22(1)
C(3A)	4094(7)	2114(3)	612(2)	22(1)
C(4A)	4553(6)	1148(3)	481(2)	24(1)
C(5A)	4067(7)	669(3)	1164(2)	20(1)
C(6A)	4356(7)	2949(3)	53(2)	26(1)
C(7A)	4299(7)	-369(3)	1339(2)	25(1)
N(1B)	2034(5)	3599(2)	6294(2)	20(1)
N(2B)	2269(6)	2716(2)	6641(2)	21(1)
C(3B)	2681(7)	2893(3)	7393(2)	20(1)
C(4B)	2738(6)	3890(3)	7548(2)	22(1)
C(5B)	2324(7)	4328(3)	6848(2)	20(1)
C(6B)	3017(6)	2089(3)	7967(2)	25(1)
C(7B)	2237(7)	5374(3)	6666(2)	29(1)

Table 8.4. Anisotropic displacement parameters ($Å^2$) for **144**.

Atom	$10^3 U_{11}$	$10^3 U_{22}$	$10^3 U_{33}$	$10^3 U_{23}$	$10^3 U_{13}$	$10^3 U_{12}$
N(1)	20(1)	22(1)	18(1)	5(1)	4(1)	5(1)
C(2)	17(1)	20(1)	17(1)	6(1)	8(1)	6(1)
C(3)	17(1)	19(1)	16(1)	4(1)	6(1)	5(1)
C(4)	20(1)	22(1)	17(1)	6(1)	9(1)	9(1)
C(5)	25(1)	19(1)	22(1)	6(1)	7(1)	6(1)
C(6)	25(1)	18(1)	21(1)	4(1)	4(1)	2(1)
N(1')	19(1)	21(1)	20(1)	5(1)	5(1)	7(1)
C(2')	21(1)	17(1)	19(1)	5(1)	8(1)	9(1)
C(3')	18(1)	18(1)	19(1)	4(1)	5(1)	6(1)
C(4')	20(1)	18(1)	18(1)	4(1)	8(1)	9(1)
C(5')	22(1)	21(1)	21(1)	7(1)	10(1)	9(1)
C(6')	17(1)	21(1)	23(1)	5(1)	5(1)	5(1)
N(1A)	16(1)	18(1)	18(1)	6(1)	4(1)	3(1)
N(2A)	19(1)	19(1)	25(1)	7(1)	4(1)	2(1)
C(3A)	22(1)	22(1)	30(1)	13(1)	8(1)	6(1)
C(4A)	22(1)	29(1)	24(1)	15(1)	8(1)	11(1)
C(5A)	18(1)	28(1)	17(1)	9(1)	5(1)	7(1)
N(1B)	18(1)	19(1)	18(1)	5(1)	4(1)	6(1)
N(2B)	21(1)	23(1)	24(1)	9(1)	6(1)	6(1)
C(3B)	27(1)	25(1)	27(1)	12(1)	11(1)	9(1)
C(4B)	32(1)	26(1)	19(1)	10(1)	9(1)	13(1)
C(5B)	23(1)	23(1)	16(1)	5(1)	3(1)	11(1)

Table 8.5. Anisotropic displacement parameters ($Å^2$) for **145**.

Atom	$10^3 U_{11}$	$10^3 U_{22}$	$10^3 U_{33}$	$10^3 U_{23}$	$10^3 U_{13}$	$10^3 U_{12}$
N(1)	31(3)	18(2)	13(2)	-1(2)	6(2)	0(2)
C(2)	27(3)	25(3)	10(2)	3(2)	-1(2)	1(3)
C(3)	27(3)	11(2)	18(2)	0(2)	-2(2)	0(3)
C(4)	20(3)	18(2)	12(2)	-1(2)	1(2)	1(2)
C(5)	24(3)	24(3)	13(2)	3(2)	-1(2)	-3(3)
C(6)	29(3)	22(2)	14(2)	1(2)	2(2)	3(3)
N(1')	27(2)	15(2)	13(2)	-1(2)	3(2)	1(2)
C(2')	21(3)	19(3)	19(2)	-2(2)	5(2)	1(2)
C(3')	18(2)	13(2)	16(2)	1(2)	0(2)	2(2)
C(4')	25(3)	17(3)	18(2)	-3(2)	-1(2)	0(2)
C(5')	18(3)	23(3)	17(2)	1(2)	-4(2)	1(3)
C(6')	23(3)	19(3)	17(2)	3(2)	-3(2)	1(2)
N(1A)	35(3)	18(2)	15(2)	-2(2)	5(2)	-2(2)
N(2A)	33(3)	15(2)	18(2)	4(2)	1(2)	4(2)
C(3A)	31(3)	20(3)	15(2)	2(2)	0(2)	5(3)
C(4A)	30(3)	27(3)	14(2)	-4(2)	6(2)	3(3)
C(5A)	21(3)	23(3)	17(2)	0(2)	3(2)	3(3)
C(6A)	29(3)	26(3)	21(3)	0(2)	7(2)	0(3)
C(7A)	33(3)	19(2)	24(2)	-4(2)	0(3)	5(2)
N(1B)	32(3)	16(2)	13(2)	1(2)	-1(2)	0(2)
N(2B)	35(3)	13(2)	16(2)	3(2)	3(2)	2(2)
C(3B)	27(3)	17(2)	16(2)	0(2)	4(2)	7(3)
C(4B)	32(3)	15(2)	18(2)	-9(2)	0(2)	-3(3)
C(5B)	25(3)	15(2)	19(2)	-2(2)	-3(2)	0(3)
C(6B)	34(3)	25(3)	17(2)	5(2)	5(2)	1(3)
C(7B)	41(3)	25(3)	21(2)	-5(2)	1(3)	0(3)

Table 8.6. Hydrogen atom coordinates and isotropic displacement parameters ($Å^2$) for **144**.

Atom	10^4 x	10^4 y	10^4 z	10^3U_{eq}
H(3)	1031(2)	8779(1)	3915(1)	24
H(5)	3620(2)	13692(1)	4868(1)	30
H(6)	5753(2)	13745(2)	6902(1)	32
H(3')	2503(2)	13042(1)	2529(1)	25
H(5')	-1539(2)	9153(1)	2588(1)	27
H(6')	-3556(2)	9120(2)	515(1)	29
H(3A)	1552(2)	4978(2)	5775(1)	32
H(4A)	4533(2)	6492(2)	7925(1)	31
H(5A)	5688(2)	9407(2)	7977(1)	28
H(3B)	3522(2)	15496(2)	-432(1)	34
H(4B)	293(2)	14486(2)	-2316(1)	32
H(5B)	-1854(2)	12453(1)	-1654(1)	28

Table 8.7. Hydrogen atom coordinates and isotropic displacement parameters ($Å^2$) for **145**.

Atom	10^4 x	10^4 y	10^4 z	10^3U_{eq}
H(3)	2744(6)	2720(3)	2685(2)	24
H(5)	1314(6)	1001(3)	4542(2)	27
H(6)	1883(7)	-293(3)	3739(2)	28
H(3')	2485(6)	2261(3)	5256(2)	21
H(5')	608(6)	3768(3)	3357(2)	25
H(6')	246(6)	5076(3)	4185(2)	26
H(4A)	5094(6)	879(3)	11(2)	31
H(6A1)	3129(9)	3137(11)	-170(11)	33
H(6A2)	5208(28)	2763(6)	-383(8)	33
H(6A3)	4901(31)	3492(6)	347(4)	33
H(7A1)	4966(31)	-680(4)	894(7)	33
H(7A2)	3053(7)	-666(5)	1405(14)	33
H(7A3)	5030(30)	-448(3)	1833(9)	33
H(4B)	3013(6)	4193(3)	8045(2)	28
H(6B1)	2102(24)	2128(11)	8406(9)	33
H(6B2)	4301(14)	2137(11)	8184(11)	33
H(6B3)	2870(36)	1473(3)	7689(4)	33
H(7B1)	921(8)	5562(4)	6571(13)	38
H(7B2)	2989(26)	5509(4)	6186(8)	38
H(7B3)	2743(30)	5739(3)	7119(6)	38

Chapter 9

References

References.

1 J. Reedijk, in G. Wilkinson, R.D. Gillard and J.A. McCleverty (Eds.), Comprehensive Coordination Chemistry, Vol. 2, Pergamon, Oxford, 1987, p.73.

2 E.C. Constable and P.J. Steel, *Coord. Chem. Rev.*, 93 (1989) 205.

3 P.J. Steel, *Coord. Chem. Rev.*, 106 (1990) 227 and references therein.

4 F. Blau. *Ber. Dtsch. Chem. Ges.*, 27 (1888) 1077.

5 E.C. Constable, Adv. *Inorg. Chem.*, 34 (1989) 1.

6 A. Juris, V. Balzani, F. Barigelletti, S. Campagna, P. Belser and A. von Zelewsky, *Coord. Chem. Rev.*, 84 (1988) 85 and references therein.

7 K.R. Seddon, 'The Chemistry of Ruthenium,' Elsevier, New York, 984.

8 T.J. Meyer, *Pure Appl. Chem.*, 58 (1986) 1193.

9 K. Kalyanasundaram, M. Gratzel, and E. Pelizzetti, *Coord. Chem. Rev.*, 69 (1986) 57.

10 Y. Kawanishi, N. Kitamura and S. Tazuke, *Inorg. Chem.* 28 (1989) 2968.

11 P.J. Steel and E.C. Constable, *J. Chem. Soc., Dalton Trans.*, (1990) 1389.

12 P.J. Steel, F. Lahousse, D. Lerner and C. Marzin, *Inorg. Chem.*, 22 (1983) 1488.

13 R. Haga, R. Prins, J.G. Haasnoot, J. Reedijk and J.G. Vos, *J. Chem. Soc., Dalton Trans.*, (1987) 1389.

14 J.D. Petersen, W.R. Murphy, R. Sahai, K.J. Brewer and R.R. Ruminski, *Coord. Chem. Rev.*, 64 (1985) 261.

15 V. Balzani, S. Campagna, G. Denti, M. Marcaccio, F. Paolucci, C. Paradisi, S. Roffia and S. Scolastica, *Inorg. Chem.*, 32 (1993) 3003 and ref therein.

16 N. Sabbatini, V. Balzani, F. Bolleta, R. Ballardini, M.T.Gandolfi, A. Junis, M. Maestri, M.F. Manfrin and L. Moggi, *Coord. Chem. Rev.*, 125 (1993) 75.

17 C. Creutz, *Prog. Inorg. Chem.*, 30 (1983) 1.

18 D.E. Richardson and H. Taube, *Coord. Chem. Rev.*, 60 (1984) 107.

19 R.R. Ruminski, C. DeGroff and S.J. Smith, *Inorg. Chem.*, 31 (1992) 3325.

20 V. Balzani, F. Barigelletti, J.-P. Collins, A.M.W. Cargill-Thompson, E.C. Constable, L. Flamigni, J.-P. Sauvage and A. Sour, *J. Am. Chem. Soc.*, 116 (1994) 7692 and references therein.

21 M.P. Garcia, J.L. Millan, M.A. Esteruelas and L.A. Oro, *Polyhedron*, 6 (1987) 1427.

22 N.C. Thomas and J. Cox, *Polyhedron*, 7 (1988) 731.

23 K.J. Brewer, W.R. Murphy and J.D. Petersen, *Inorg. Chem.*, 26 (1987) 3376.

24 J.D. Scott and R.J. Puddephatt, *Organometallics*, 5 (1986) 2522.

25 D.P. Rillema and K.B. Mack, *Inorg. Chem.*, 21 (1982) 3849.

26 R. Sahai, L. Morgan and D.P. Rillema, *Inorg. Chem.*, 27 (1988) 3495.

27 R. Sahai, D.P. Rillema, R. Shaver, S. Van Wallendael, D.C. Jackman and M. Boldaji, *Inorg. Chem.*, 28 (1989) 1022.

28 K. Praefcke, B. Kohne, T. Kohlschreiber and F. Korinth, *Liebigs Ann. Chem.*, (1988) 609.

29 W. Kaim and S. Kohlmann, *Inorg. Chem.*, 25 (1986) 3306.

30 W. Kaim and S. Kohlmann, *Inorg. Chem.*, 26 (1987) 68.

31 E.C. Alyea, J. Malito, S.D. Ernst, W. Kaim and S.J. Kohlmann, *Polyhedron*, 8 (1989) 921.

32 S. Ernst, V. Kasack and W. Kaim, *Inorg. Chem.*, 27 (1988) 1146.

33 S.D. Ernst and W. Kaim, *Inorg. Chem.*, 28 (1989) 1520.

34 Q. Jaradat, K. Barqawi and T.S. Akasheh, *Inorg. Chim. Acta*, 116 (1986) 63.

35 M. Hunziker and A. Ludi, *J. Am. Chem. Soc.*, 99 (1977) 7370.

36 E.V. Dose and L.J. Wilson, *Inorg. Chem.*, 17 (1978) 2660.

37 R.R. Ruminski and J.D. Petersen, *Inorg. Chim. Acta*, 65 (1982) L177.

38 N.C. Thomas, *Inorg. Chim. Acta*, 131 (1987) 151.

39 K.J. Moore and J.D. Petersen, *Polyhedron*, 2 (1983) 279.

40 M. Bochmann, G. Wilkinson and G.B. Young, *J. Chem. Soc., Dalton Trans.*, 44 (1980) 1879.

41 P.M. Kiernan and A. Ludi, *J. Chem. Soc., Dalton Trans.*, (1978) 1127.

42 V.F. Sutcliffe and G.B. Young, *Polyhedron*, 3 (1984) 87.

43 J.D. Scott and R.J. Puddephatt, *Organometallics*, 5 (1986) 1538.

44 C. Overton and J.A. Connor, *Polyhedron*, 1 (1982) 53.

45 S. Lanza, *Inorg. Chim. Acta*, 75 (1983) 131.

46 K.A. Goldsby and T.J. Meyer, *Inorg. Chem.*, 23 (1984) 3002.

47 A. Vogler and J. Kisslinger, *Inorg. Chim. Acta*, 115 (1986) 193.

48 R. Sahai and D.P. Rillema, *Inorg. Chim. Acta*, 118 (1986) L35.

49 K.J. Brewer, W.R. Murphy and J.D. Petersen, *Inorg. Chim. Acta*, 159 (1989) 93.

50 G. Brewer and E. Sinn, *Inorg. Chem.*, 24 (1985) 4580.

51 A. Real, J. Zarembowitch, O. Kahn and X. Solans, *Inorg. Chem.*, 26 (1987) 2939.

52 N.S. Hosmane, J.S. Fagner, H. Zhu, U. Siriwardane, J.A. Maguire, G. Zhang and B.S. Pinkston, *Organometallics*, 8 (1989) 1769.

53 G. De Munno and G. Bruno, *Acta Crystallogr., Sect. C*, 40 (1984) 2030.

54 M. Julve, G. De Munno, G. Bruno and M. Verdaguer, *J. Chem. Research (S)*, (1987) 152.

55 M. Julve, G. De Munno, G. Bruno and M. Verdaguer, *Inorg. Chem.*, 27 (1988) 3160.

56 W. Matheis and W. Kaim, *Inorg. Chim. Acta*, 181 (1991) 15.

57 W. Matheis and W. Kaim, *Z. Anorg. Allg. Chem.* 593 (1991) 147.

58 P.S. Braterman, J.-I, Song, S. Kohlmann, C. Vogler and W. Kaim, *J. Organomet. Chem.*, 411 (1991) 207.

59 G. De Munno, J.A. Real, M. Julve and M.C. Muñoz, *Inorg. Chim. Acta*, 211 (1993) 227.

60 D.P. Matthews, J.P. Whitten and J.R. McCarthy, *Synthesis*, (1986) 336.

61 A.S. Abushamleh and H.A Goodwin, *Aust. J. Chem.*, 32 (1979) 513.

62 B.F. Fieselmann, D.N. Hendrickson and G.D. Stucky, *Inorg. Chem.*, 17 (1978) 2078.

63 M.S. Haddad and D.N. Hendrickson, *Inorg. Chem.*, 17 (1978) 2622.

64 L.A. Oro, M.T. Pinillos, C. Tejel, C. Foces-Foces and F.H. Cano, *J. Chem. Soc., Dalton Trans.*, (1986) 2193.

65 M. Haga, *Inorg. Chim. Acta*, 45 (1980) L183.

66 R. Usón, J. Gimeno,. J. Fornies and F. Martinez, *Inorg. Chim. Acta*, 50 (1981) 173.

67 R. Usón, J. Gimeno, J. Fornies, F. Martinez and C. Fernandez, *Inorg. Chim. Acta*, 54 (1981) L95.

68 R. Usón, J. Vicente and M.T. Chicote, *J. Organomet. Chem.*, 209 (1981) 271.

69 R. Usón and J. Gimeno, *J. Organomet. Chem.*, 220 (1981) 173.

70 R. Usón, L.A. Oro, M.A. Ciriano, M.M. Naval, M.C. Apreda, C. Foces-Foces, F.H. Cano and S. Garcia-Blanco, *J. Organomet. Chem.*, 256 (1983) 331.

71 A.J. Canty, K. Mills, B.W. Skelton and A.H. White, *J. Chem. Soc., Dalton Trans.*, (1986) 939.

72 M. Haga, T. Matsumura-Inoue and S. Yamabe, *Inorg. Chem.*, 26 (1987) 4148.

73 J. Diez, S. Falagan, P. Gamasa and J. Gimeno, *Polyhedron*, 7 (1988) 37.

74 S.W. Kaiser, R.B. Saillant, W.M. Butler and P.G. Rasmussen, *Inorg. Chem.*, 15 (1976) 2681.

75 M.S. Haddad, E.N. Duesler and D.N. Hendrickson, *Inorg. Chem.*, 18 (1979) 141.

76 M. Haga and A.M. Bond, *Inorg. Chem.*, 30 (1991) 475.

77 D.P. Rillema, R. Sahai, P. Matthews, A.K. Edwards, R.J. Shaver and L. Morgan, *Inorg. Chem.*, 30 (1990) 167.

78 R. Uson, J. Gimeno, J. Fornies, F. Martinez and C. Fernandez, *Inorg. Chim. Acta*, 63 (1982) 91.

79 R. Usón, L.A. Oro, J. Gimeno, M.A. Ciriano, J.A. Cabeca, A. Tiripicchio and M. Tiripicchio Camellini, *J. Chem. Soc., Dalton Trans.*, (1983) 323, and references therein.

80 R. Usón, J. Gimeno, L.A. Oro, M.A. Aznar and J.A. Cabeza, *Polyhedron*, 2 (1983) 163.

81 L.A. Oro, D. Carmona, M.P. Lamata, A. Tiripicchio and F.J. Lahoz, *J. Chem. Soc., Dalton Trans.*, (1986) 15.

82 P.W. Ball and A.B. Blake, *J. Chem. Soc. A*, (1969) 1415.

83 M. Ghedini, G. De Munno, G. Denti, A.M. Manotti Lanfredi and A. Tiripicchio, *Inorg. Chim. Acta*, 57 (1982) 87.

84 P. Dapporto, G. De Munno, G. Bruno and M. Romeo, *Acta Crystallogr., Sect. C*, 39 (1983) 718.

85 G. De Munno and G. Denti, *Acta Crystallogr., Sect. C*, 40 (1984) 616.

86 G. De Munno, G. Denti and P. Dapporto, *Inorg. Chim. Acta*, 74 (1983) 199.

87 P. Dapporto, G. De Munno, A. Sega and L. Mealli, *Inorg. Chim. Acta*, 83 (1984) 171.

88 G. De Munno and G. Bruno, *Acta Crystallogr., Sect. C*, 40 (1984) 2022.

89 M. Ghedini and F. Neve, *J. Chem. Soc., Dalton Trans.*, (1984) 1417.

90 M. Ghedini, F. Neve, F. Morazzoni and C. Oliva, *Polyhedron*, 4 (1985) 497.

91 A. Tiripicchio, A.M. Manotti Lanfredi, M. Ghedini and F. Neve, *J. Chem. Soc., Chem. Commun.*, (1983) 97.

92 M-T. Youinou, N. Rahmouni, J. Fischer and J. A. Osborn, *Angew. Chem. Int. Ed. Engl.*, 31(1992) 733.

93 L. Rosenberg, L.K. Thompson, E.J. Gabe and F.L. Lee, *J. Chem. Soc., Dalton Trans.*, (1986) 625.

94 L.K. Thompson, S.K. Mandal, E.J. Gabe, F.L. Lee and A.W. Addison, *Inorg. Chem.*, 26 (1987) 657.

95 L.K. Thompson, T.C. Woon, D.B. Murphy, E.J. Gabe, F.L. Lee and Y. Le Page, *Inorg. Chem.*, 24 (1985) 4719.

96 R. Uson, L.A. Oro, M. Esteban, D. Carmona, R.M. Claramunt and J. Elguero, *Polyhedron*, 2 (1984) 213.

97 L.K. Thompson, F.L. Lee and E.J. Gabe, *Inorg. Chem.*, 27 (1988) 39.

98 S.K. Mandal, L.K. Thompson, M.J. Newlands, F.L. Lee, Y. Le Page, J.-P. Charland and E.J. Gabe, *Inorg. Chim. Acta*, 122 (1986) 199.

99 S.K. Mandal, L.K. Thompson, E.J. Gabe, F.L. Lee and J.-P. Charland, *Inorg. Chem.*, 26 (1987) 2384.

100 S.K. Mandal, L.K. Thompson, E.J. Gabe, J.-P. Charland and F.L. Lee, *Inorg. Chem.*, 27 (1988) 855.

101 T.C. Woon, R. McDonald, S.K. Mandal, L.K. Thompson, S.P. Connors and A.W. Addison, *J. Chem. Soc., Dalton Trans.*, (1986) 2381.

102 L.K. Thompson, S.K. Mandal, L. Rosenberg, F.L. Lee and E.J. Gabe, *Inorg. Chim. Acta*, 133 (1987) 81.

103 J. Casabo, J. Pons, K.S. Siddiqi, F. Teixidor, E. Molins and C. Miravitlles, *J. Chem. Soc., Dalton Trans.*, (1989) 1401.

104 F.S. Keij, R.A.G. de Graaff, J.G. Haasnoot and J. Reedijk, *J. Chem. Soc., Dalton Trans.*, (1984) 2093.

105 R. Prins, P.J.M.W.L. Birker, J.G. Haasnoot, G.C. Verschoor and J. Reedijk, *Inorg. Chem.*, 24 (1985) 4128.

106 J. Pons, F. J. Sánchez, A. Labarta, J. Casabó, F. Texidor and A. Caubet, *Inorg. Chim. Acta*, 208 (1993) 167.

107 R. Hage, A.H.J. Dijkhuis, J.G. Haasnoot, R. Prins, J. Reedijk, B.E. Buchanan and J.G. Vos, *Inorg. Chem.*, 27 (1988) 2185.

108 R. Hage, J.G. Haasnoot, D.J. Stufkens, T.L. Snoeck, J.G. Vos and J. Reedijk, *Inorg. Chem.*, 28 (1989) 1413.

109 F. Barigelletti, L. De Cola, V. Balzani, R. Hage, J.G. Haasnoot, J. Reedijk and J.G. Vos, *Inorg. Chem.*, 28 (1989) 4344.

110 F. Barigelletti, R. Hage, V. Balzani, L. De Cola, J. G. Haasnoot, J. Reedijk and J.G. Vos, *Inorg. Chem.*, 30 (1991) 641.

111 M. Martin, M.P. Garcia and L.A. Oro, *Inorg. Chim. Acta*, 191 (1992) 221.

112 J.H, van Dieman, R. Hage, J.G. Haasnoot, H.E.B. Lempers, J. Reedijk, J.G. Vos, L. De Cola, F. Barigelletti and V. Balzani, *Inorg. Chem.*, 31 (1992) 3518.

113 H.P. Hughes, S. Bell, D. Martin, J.J. McGarvey and J.G. Vos, *Inorg. Chem.*, 32 (1993) 4402.

114 H.A. Goodwin and F. Lions, *J. Am. Chem. Soc.*, 81 (1959) 6415.

115 F.H. Case and E.J. Loft, *J. Am. Chem. Soc.*, 81 (1959) 905.

116 C.H. Braunstein, A.D. Baker, T.C. Strekas and H.D. Gafney, *Inorg. Chem.*, 23 (1984) 857.

117 Y. Fuchs, S. Lofters, T. Dieter, W. Shi, R. Morgan, T.C. Strekas, H.D. Gafney and A.D. Baker, *J. Am. Chem. Soc.*, 109 (1987) 2691.

118 R.R. Ruminski, T. Cockroft and M. Shoup, *Inorg. Chem.*, 27 (1988) 4026.

119 S. Campagna, G. Denti, G. De Rosa, L. Sabatino, M. Ciano and V. Balzani, *Inorg. Chem.*, 28 (1989) 2565.

120 R.R. Ruminski and J.O. Johnson, *Inorg. Chem.*, 26 (1987) 210.

121 R.R. Ruminski and I. Wallace, *Polyhedron*, 6 (1987) 1673.

122 E.M. Armstrong and P.K. Baker, *Synth. React. Inorg. Met.-Org. Chem.*, 18 (1988) 1.

123 M. Shoup, B. Hall and R.R. Ruminski, *Inorg. Chem.*, 27 (1988) 200.

124 W.R. Murphy, K.J. Brewer, G. Gettliffe and J.D. Petersen, *Inorg. Chem.*, 28 (1989) 81.

125 S. Campagna, G. Denti, L. Sabatino, S. Serroni, M. Ciano and V. Balzani, *J. Chem. Soc., Chem. Commun.*, (1989) 1500.

126 V. Balzani, S, Campagna, M. Ciano, G. Denti, L. Sabatino and S. Serroni, *Inorg. Chem.*, 29 (1990) 4750.

127 G. Di Marco, A. Bartolotta, V. Ricevuto, S. Campagna, G. Denti, L. Sabatino and G. De Rosa, *Inorg. Chem.*, 30 (1991) 270.

128 K. Kalyanasundaram, M. Grützel and Md.K. Nazeeruddin, *J. Chem. Soc., Dalton Trans.*, (1991) 343.

129 M.M. Richter and K.J. Brewer, *Inorg. Chim. Acta*, 180 (1991) 125.

130 A. Escuer, R. Vicente, T. Comas, J. Ribas, M. Gomez, X. Solans, D. Gatteschis and C. Zanchini, *Inorg. Chim. Acta*, 181 (1991) 51.

131 G. Denti, S. Serroni, S. Campagna, V. Ricevuto and V. Balzani, *Inorg. Chim. Acta*, 182 (1991) 127.

132 G. Denti, S. Serroni, S. Campagna, M. Ciano and V. Balzani, *J. Chem. Soc., Chem. Commun.*, (1991) 944.

133 G. Denti, S. Serroni, S. Campagna, M. Ciano and V. Balzani, *Inorg. Chem.*, 30 (1991) 3728.

134 J.A. Baiano and W.R. Murphy Jr, *Inorg. Chem.*, 30 (1991) 4594.

135 M.M. Richter and K.J. Brewer, *Inorg. Chem.*, 31 (1992) 1594.

136 A. Juris, S. Serroni, S. Campagna, M. Ciano and V. Balzani, *Inorg. Chem.*, 31 (1992) 2982.

137 S. Serroni and G. Denti, *Inorg. Chem.*, 31 (1992) 4251.

138 K. Kalyanasundaram, M. Grützel and Md. K. Nazeeruddin, *J. Phys. Chem.*, 96 (1992) 5865.

139 K.J. Brewer and M.M. Richter, *Inorg. Chem.*, 32 (1993) 2827.

140 A.D. Baker, H.D. Gafney, W. Hosek, T.C. Stretkas and S.A. Tysoe, *Inorg. Chem.*, 28, (1989), 1228.

141 D.P. Rillema, D.G. Taghdiri, D.S. Jones, C.D. Keller, L.A. Worl, T.J. Meyer and H.A. Levy, *Inorg. Chem.*, 26 (1987) 578.

142 R. Sahai and D.P. Rillema, *J. Chem. Soc., Chem. Commun.*, (1986) 1133.

143 F.R. Pfeiffer and F.H. Case, *J. Org. Chem.*, 31 (1966) 3384.

144 J.E.B. Johnson and R.R. Ruminski, *Inorg. Chim. Acta*, 208 (1993) 231.

145 D. Freiheit, J.E.B. Johnson, R.R. Ruminski, D. Serveiss and B. Synder, *Inorg. Chim. Acta*, 224 (1994) 27.

146 S. Kohlmann, S. Ernst and W. Kaim, *Angew. Chem. Int. Ed. Engl.*, 24 (1985) 684.

147 W. Kaim, S. Ernst and S. Kohlmann, *Polyhedron*, 5 (1986) 445.

148 W. Kaim and S. Kohlmann, *Inorg. Chem.*, 26 (1987) 1469.

149 J.E.B. Johnson, C. de Groff and R.R. Ruminski, *Inorg. Chim. Acta*, 187 (1991) 73.

150 J. Poppe, W. Kaim, A.B. Altabef and N.E. Katz, *J. Chem. Soc., Perkin Trans. 2*, (1993) 2105.

151 P.J. Steel and D.J. Vaughan, unpublished results, 1989.

152 M. Haga, K. Nozaki and T. Ohno, *Inorg. Chem.*, 31 (1992) 4256.

153 A.J. Downard, G.E. Honey, L.F. Phillips and P. J. Steel, *Inorg. Chem.*, 30 (1991) 2260.

154 M. Haga, T. Ano, K. Kano and S. Yamabe, *Inorg. Chem.*, 30 (1991) 3843.

155 T. Ohno, K. Nozaki and M. Haga, *Inorg. Chem.*, 31 (1992) 548.

156 T. Ano, M. Haga, T. Ishizaki. K. Kano, K. Nozaki and T. Ohno, *J. Chem. Soc., Dalton Trans.*, (1994) 263.

157 R.P. Thummel, C. Hery, D. Williamson and F. Lefoulon, *J. Am. Chem. Soc.*, 110 (1988) 7894.

158 R.P. Thummel, C. Hery, D. Williamson and F. Lefoulon, *Inorg. Chem.*, 32 (1993) 1587.

159 E.C. Constable, *Angew. Chem. Int. Ed. Engl.*, 30 (1991) 1450 and references therein.

160 G. Bernardinelli, C. Piguet and A.F. Williams, *Angew. Chem. Int. Ed. Engl.*, 30 (1991) 1450.

161 C.O. Dietrich-Buchecker, J. Guilhem and C. Pascard, *Angew. Chem.*, 102 (1990) 1202.

162 C.O. Dietrich-Buchecker, J. Guilhem and C. Pascard, *Angew. Chem. Int. Ed. Engl.*, 29 (1990) 1154.

163 C.O. Dietrich-Buchecker, and J.-P. Sauvage, *Angew. Chem.*, 101 (1989) 192.

164 C.O. Dietrich-Buchecker and J.-P. Sauvage, *Angew. Chem. Int. Ed. Engl.*, 28 (1989) 189.

165 B. Bocquet, G. Hopfgartner, C. Piguet, O. Schaad and A.F. Williams, *J. Am. Chem. Soc.*, 116 (1994), 9092.

166 X. Hua and A. von Zelewsky, *Inorg. Chem.*, 30 (1991) 3796.

167 F.R. Keene and D.A. Reitsma, *J. Chem. Soc., Dalton Trans.*, (1993) 2859.

168 C.R. Arana and H.D. Abruna, *Inorg. Chem.*, 32 (1993) 194.

169 M. Beley, J.-P Collins and J.-P Sauvage, *Inorg. Chem.*, 32 (1993) 4539.

170 V. Grosshenny and R. Ziessel, *J. Organomet. Chem.*, 453 (1993) C19;

171 J.-P Collins, P. Laine, J.-P. Launay, J.-P Sauvage and A. Sour, *J. Chem. Soc., Chem. Commun.*, (1993) 434.

172 J.N. Gex, W. Brewer, K. Bergmann, C.D. Tait, M.K. DeArmond, K.W. Hanck and D. W. Wertz, *J. Phys. Chem.*, 91 (1987) 4776.

173 W. Kaim, S. Ernst and V.J. Kasack, *J. Am. Chem. Soc.*, 112 (1990) 173.

174 K. Kalyanasundaram and Md.K. Nazearuddin, *Inorg. Chem.*, 29 (1990) 1880.

175 M. Krejcik and A.A. Vlcek, *Inorg. Chem.*, 31 (1992) 2390.

176 A.J. Downard, J. Steenwijk and P.J. Steel, *Aust. J. Chem.*, in press and references therein.

177 J. Reedijk, R. Hage, H.A. Nieuwenhuis, J.G. Haasnoot, R. Wang and J.G. Vos, *J. Chem. Soc. Dalton Trans.*, (1991) 3271.

178 P. Degn, R.A. Howie, R. Hage, B.E. Buchanan, J.H. van Dieman, J.G. Haasnoot, J.M.P Velasco, H. Hughes, B.S. Creaven, C. Long, J.G. Vos and J. Reedijk, *J. Chem. Soc., Dalton Trans.*, (1992) 1177.

179 A.J. Downard, G.E. Honey and P.J. Steel, *Inorg. Chem.*, 30 (1991) 3733.

180 D.L. Jameson, J.K. Blaho, K.T. Kruger and K.A. Goldsby, *Inorg. Chem.*, 28 (1989) 4312.

181 D.L. Jameson and K.A Goldsby, *J. Org. Chem.*, 55 (1990) 4992.

182 D.A. House, P.J. Steel and A. A. Watson, *Aust. J. Chem.*, 39 (1986) 1525.

183 P.K. Byers, A.J. Canty, R.T. Honeyman and A.A. Watson, *J. Organomet. Chem.*, 385 (1990) 429.

184 D.A. House, P.J. Steel and A. A. Watson, *Inorg. Chim. Acta*, 130 (1987) 167.

185 S. Mahapatra and R. Mukherjee, *J. Chem. Soc., Dalton Trans.*, (1992) 2337.

186 S. Mahapatra, N. Gupta and R. Mukerjee, *J. Chem. Soc., Dalton Trans.*, (1991) 2911.

187 V.S. Joshi, A. Sarkar and P.R. Rajamohanan, *J. Organomet. Chem.*, 409 (1991) 341 and references therein.

188 G.B. Bennett, R.B. Mason, L.J. Alden and J.B. Roach Jr, *J. Med. Chem.*, 21 (1978) 623.

189 J. Nasielski, A. Standaert and R. Nasielski-Hinkens, *Synthetic Commun.*, 21 (1991) 901.

190 C. Vogler, H.-D. Hausen, W. Kaim, S. Kohlmann, H.E.A. Kramer and J. Rieker, *Angew. Chem. Int. Ed. Engl.*, 28 (1989) 1659.

191 M.A. Bennett, L. Pratt and G.J. Wilkinson, *J. Chem. Soc.*, (1961) 2037.

192 P.W. Baxter, J. A. Conner, J.D. Wallis and D.C. Povey, *J. Organomet. Chem.*, 426 (1992) 187.

193 G. Orellana and C.A. Ibarra and J. Santoro, *Inorg. Chem.*, 27 (1988) 1025.

194 E.C. Constable and A.M.W. Cargill-Thompson, *J. Chem. Soc., Dalton Trans.*, (1992) 3467.

195 S. Chirayil and R.P. Thummel, *Inorg. Chem.*, 29 (1989) 813.

196 L. Braunschweiler and R.R. Ernst, *J. Magn. Reson.*, 53 (1983) 521.

197 D.G. Davis and A. Bax, *J. Am. Chem. Soc.*, 107 (1987) 7197.

198 T. Kanthimathi, Y.V.S. Narayana Moorthy, S. Subramanian and C.N. Pillai, *Magn. Reson. Chem.*, 32 (1994) 452.

199 P.C. Ford, D.F.P. Rudd, R. Gaunder and H. Taube, *J. Am. Chem. Soc.*, 90 (1968) 1187.

200 D.J. Brown and M.N. Paddon-Row, *J. Chem. Soc (C)*, (1967) 1928.

201 J.H. Clark, J.P. English, P.S. Winner, H.W. Marson, Q.P. Cole and J.W. Clapp, *J. Am. Chem. Soc.*, 68 (1946) 98.

202 J. Venanzi, *J. Am. Chem. Soc.*, 80 (1958) 719.

203 M. Iyoda, H. Otsuka, K. Sato, N. Nisato and M. Oda, *Bull. Chem. Soc. Jpn.*, 63 (1990) 808.

204 A.A. Watson, D.A. House and P.J. Steel, *J. Org. Chem.*, 56 (1991) 4072.

205 P.J. Steel and E.C. Constable, *J. Chem. Res.*, (1989) (S)-189 (M)-1601.

206 J.-M. Lehn and J.-B.R. de Vains, *Helv. Chim. Acta*, 75 (1992) 1221.

207 P. Belser and A. von Zelewsky, *Helv. Chim. Acta*, 63 (1980) 1675.

208 F. Sachs, *Justus Liebigs Ann. Chem.*, 365 (1909) 53.

209 W. Reid and J. Patshorke, *Justus Liebigs Ann. Chem.*, 616 (1958) 87.

210 L. Denivelle and K.C. Singhal, *Compt. Rend.*, 260 (1965) 5812.

211 V. Paragamian, M.B. Baker, B.M. Puma and J. Reale Jr, *J. Heterocycl. Chem.*, 5 (1968) 591.

212 E.J. Browne, *Aust. J. Chem.*, 26 (1973) 449.

213 P.D. Woodgate, J.M. Herbert and W.A. Denny, *Magn. Reson. Chem.*, 26 (1988) 191.

214 R.M. Claramunt, J. Doctor, D. Sanz, C. Foces-Foces, A.L. Llamas-Siaz, J. Elguero, R. Flammang, J.-P. Morizur, E. Chapon and J. Tortajada, *Helv. Chim. Acta,* 77 (1994) 121.

215 T.J. Rutherford, D.A. Reitsma and F.R. Keene, *J. Chem. Soc., Dalton Trans.*, (1994) 3659.

216 P.J. Steel and G.B. Caygill, *J. Organomet. Chem.*, Sect. C, 395 (1990) 359.

217 N.T. Huang, W.T. Pennington and J.D. Petersen, *Acta Chryst.*, 47 (1991) 2011.

218 J.J. Lafferty and F.H. Case, *J. Org. Chem.,* 32 (1967) 1591.

219 C.B. Caygill, R.M. Hartshorn and P.J. Steel., *J. Organomet. Chem.*, 382 (1990) 455.

220 F. Teixidor, R. Garcia, J. Pons and J. Casabó, *Tetrahedron*, 7 (1988) 43.

221 L. Chen, J.N. Bridson and L.K. Thompson, *Inorg. Chim. Acta*, 210 (1993) 215.

222 C.R. Johnston and R.E. Sheperd, *Inorg. Chem.*, 22 (1983) 2439.

223 K.B. Wiberg, D. Nakaji and C.M. Breneman, *J. Am. Chem. Soc.*, 111 (1989) 4178.

224 J.B. Cooper, D.B. Macqueen, J.D. Petersen and D.W. Wertz., *Inorg. Chem.*, (1990), 29, 3701.

225 G. Giuffrida and S. Campagna, *Coord. Chem. Rev.*, 135/136 (1994) 517.

226 J.B. Flanagan, S. Margel, A.J. Bard and F.C. Anson, *J. Am. Chem. Soc.*, 100 (1978) 4248.

227 D.E. Richardson and H. Taube, *Inorg. Chem.*, 20 (1981) 1278.

228 R.L. Myers and I. Shain, *Anal. Chem.*, 41 (1969) 980.

229 A. Albert, *J. Org. Chem.*, 25 (1960) 1790.

230 D.B. Moran, G.O. Mortan and J.D. Albright, *J. Heterocycl. Chem.*, 23 (1986) 1071.

231 E.P. Hart, *J. Chem. Soc.*, 157 (1954) 1879

232 E.V. Brown and A.C. Plasz, *J. Org. Chem.*, 32 (1967) 241.

233 D. Polcyn and I. Shain, *Anal. Chem.*, 38 (1966) 376.

234 J.-P. Gisselbrecht, M. Gross, J.-M. Lehn, J.-P. Sauvage, R. Ziessel, C. Piccini-Leopardi, J.M. Arrieta, G. Germain and M. Van Meerssche, *Nouv. J. Chim.*, 8 (1984) 661.

235 R. Sahai, D.A. Baucom and D.P. Rillema, *Inorg. Chem.*, 25 (1986) 3843.

236 M. Furue, N. Kuroda and S. Nozakura, *Chem. Lett.*, (1986) 1209.

237 J.-M. Lehn and R.J. Ziessel, *J. Chem. Soc., Chem. Commun*, (1987) 1292.

238 G.E. Honey, M.Sc Thesis, University of Canterbury (1990).

239 M. Haga, Md.M. Ali, H. Maegaua, K. Nozaki, A. Yoshimura and T. Ohno, *Coord. Chem. Rev.*, 132 (1994) 99.

240 G.E. Honey and P.J. Steel, *Acta Crystallogr., Sect. C.*, 47 (1991) 2247.

241 F. Bonati and B.J. Bovio, *Crystallogr. Spectrosc. Res.*, 20 (1990) 233.

242 W.A. Hallows, G.B. Carpenter, K.A. Pevear and D.A. Sweigart, *J. Heterocycl. Chem.*, 31 (1994) 899.

243 C. Avendano, M. Espada, B. Ocana, S. Garcia-Granda, M.R. Diaz, B. Tejerina, F. Gomez-Beltran, A. Martinez and J. Elguero, *J. Chem. Soc., Perkin 2,* (1993) 1547.

244 C.A. Bessel, R.F. See, D.L. Jameson, M.R. Churchill and K.J. Takeuchi, *J. Chem. Soc., Dalton Trans.*, (1992) 3223.

245 A.L. Llamas-Saiz, C. Foces-Foces and J. Elguero, *J. Mol. Struct.*, 319 (1994) 231 and references therein.

246 K. Kalyanasundaram and Md.K. Nazeeruddin, *Inorg. Chim. Acta*, 226 (1994) 213.

247 M. Haga, Md.M. Ali, S. Koseki, K. Nozaki, A. Yoshimura and T. Ohno, *Inorg. Chim. Acta*, 226 (1994) 17.

248 B.S. Ferris. A.J. Hannaford, P.W.G. Smith and A.R. Tatchell, Vogel's Textbook of Practical Organic Chemistry (Fifth Ed.), Longman Scientific and Technical, Essex, 1989, 5.

249 H.J.E. Lowenthal, Guide for the Perplexed Organic Chemist, Heyden and Son, London, 1978.

250 B.P. Sullivan, D.J. Salmon and T.J. Meyer, *Inorg. Chem.*, 17 (1978) 3334.

251 P.A. Mabrouk and M.S. Wrighton, *Inorg. Chem.*, 25 (1986) 526.

252 I.P. Evans, A. Spencer and G. Wilkinson, *J. Chem. Soc., Dalton Trans.*, (1973) 204.

253 M.S. Kharasch, R.C. Seyler and F. M. Mayo, *J. Am. Chem. Soc.* 60 (1938) 882.

254 A.W. Bishop, W. Sinclair and L. Claissen, *Liebigs Ann. Chem.*, 281 (1984) 314.

255 J.R. Marshall and J. Walker, *J. Chem. Soc.*, 154 (1951) 1013.

256 F.H. Case and E. Koft, *J. Am. Chem. Soc.*, 81 (1959) 906.

257 R. Lukes and M. Pergal, *Chem. Listy.*, 52 (1958) 68.

258 G.M. Sheldrick, *Acta Crystallogr.*, Sect. A, 46 (1990) 467.

259 G.M. Sheldrick, SHELXL-93, University of Gottingen, 1993.